

**The Physico-chemical and Biological
Analysis of Microbial Biosurfactants (BSs)
for Applications Towards Cancer
Therapies, Wound Healing Dressings and
Drug Delivery**

OLUFUNKE AJOKE AKIYODE

**A thesis submitted in partial fulfilment of the
requirements of the University of Greenwich for the
Degree of Doctor of Philosophy**

September 2017



DECLARATION

“I certify that the work contained in this thesis, or any part of it, has not been accepted in substance for any previous degree awarded to me, and is not concurrently being submitted for any degree other than that of Doctor of Philosophy) being studied at the University of Greenwich. I also declare that this work is the result of my own investigations, except where otherwise identified by references and that the contents are not the outcome of any form of research misconduct.”

_____ Miss O.A. Akiyode (Candidate)

_____ Dr J.S. Boateng (First supervisor)

ACKNOWLEDGEMENTS

Above and beyond all, I give glory to God the Father, God the Son and God the Holy Ghost for being my personal tutors as well as preparing me beforehand for the obstacles I've faced as well as helping me to keep my peace against all odds. He also gave me the most wonderful parents in this world with whom I have shared my triumphs and losses, and through it all they have stood by me. Each time I hit a wall and fell, I remembered the strength and courage of my brother Bayo and it pushed me up again. To my practical brother Shola who has taught, guided and financially supported me, I will always be thankful.

I don't even know how to begin to thank my first supervisor, Dr Joshua Boateng who first changed the course of my life during my MSc degree. Thank you for not giving up on me Sir, I hope someday I can teach, help and support someone, the way you've done during my research studies. I will also like to appreciate, Dr Giulia Getti, and Dr Daliya George for their supervisory contributions to my professional development.

When I look back at this time in my life, I will remember the empathy of Jonathan Payne and Dr. Alan Staple. I am grateful to all the technical staff for their help, but I would particularly like to appreciate Rachel Nice, Attiya Raza, Cris Laphorn, Iain Goodall, Mark Allen and Sam Lewis. Words are not enough to thank Andy Hurt, whose technical help has contributed immensely to the completion of my research studies. I would also like to thank Dami and Asif for their help in furthering my research. Dr Bruce Alexander has unknowingly rescued me at different times over the past few years, and for this I am thankful.

The teasing banter and jolly spirits of Uttam Roy made me laugh and considerably lightened my spirits. Heartfelt thank you to Alessandra for her unhesitant assistance with thermogravimetric analysis as well as to Khairul for giving me some of his SEM grids. I would like to thank Lara for showing me how to operate the manifold freeze-dryer. I am indebted to Tibiebi for the delicious meals she cooked as well as the water she bought which sustained my energy just when it was needed while I was writing.

I would especially like to acknowledge Dr Isaac Ayensu for his mock Vivas and listening to my presentation. The kindness, prayers and moral support I have received from, Brother Meadows & Sister Biola, Aunt Ludy, Aunt Cynthia, Uncle Roy and Aunt Jane, Aunt Hilary and Uncle Trevor and Kamilah have been priceless. I would also like to acknowledge the caring text messages Mummy Alade always sent to me. Finally I am obliged to appreciate all my colleagues who contributed directly or indirectly to my research.

Above all, once again I give glory to my Father, King and the source of my strength, the almighty God, without whom I am nothing.

ABSTRACT

Microbial biosurfactants (BSs) are secondary metabolites with a broad-spectrum of therapeutic applications including possible cancer therapy, chronic wound healing and nanoparticulate drug delivery systems. However, due to their individual complexities, there is limited physico-chemical analysis relevant to their drug delivery applications. The aims of this research are the systematic investigation of free BSs in cancer therapy as well as the formulation of free BSs and niosomes encapsulating BSs incorporated into lyophilised composite polymeric wound dressings for potential chronic wound healings. The physico-chemical characteristics of four selected BSs 95Dd rhamnolipids (BS1a), 95/90 rhamnolipids (BS1b), surfactin (BS2) and 1', 4''-sophorolactone 6', 6''-diacetate (BS3) were investigated through LC-MS, ATR-FTIR and surface tension analysis. This was followed by examination of cytotoxic activities determined via MTT assay following cell line-specific optimisation at intervals of 24, 48 and 72 h treatment on non-cancerous human embryo kidney (HEK 293), human Caucasian breast adenocarcinoma (MCF-7) and human leukaemia monocyte (THP-1) cell lines. The BSs were subsequently formulated in the form of niosomes initially in deionised water, which was followed by formulation of R-90 rhamnolipids (BS1c), REWOFERM SL ONE (BS4a), REWOFERM SL 446 (BS4b) and BS2 in PBS buffer and characterised for size, size distribution, zeta potential, ATR-FTIR, XRD and SEM in transmission mode. Once optimised, free BSs and BSs based niosomes were loaded into composite lyophilised wafer dressings comprising k-carrageenan (CARR) and sodium alginate (SA) as bioactive (medicated) wound dressings to potentially target the inflammatory phase of wound healing. Both wafer formulations were functionally characterised for hardness, ATR-FTIR, XRD, mucoadhesion and exudate handling properties. Anticancer activity was successfully detected and compared in all BSs selected for investigation in cancerous cells, additionally, all BSs had higher selectivity index than doxorubicin (DOX) and therefore have potential application as anticancer agents.

Novel, durable, porous, composite advanced wound dressings incorporating free BSs and niosome encapsulated BSs were developed for potential delivery of microbial BSs in chronic wounds.

CONTENTS

DECLARATION	ii
ACKNOWLEDGEMENTS	iii
ABSTRACT	iv
CONTENTS	v
LIST OF FIGURES	xi
LIST OF TABLES	xiv
ABBREVIATIONS	xviii
1 GENERAL INTRODUCTION	1
1.1 Surfactants	1
1.2 Biosurfactants	1
1.2.1 Microbial biosurfactants	1
1.3 Biological and biopharmaceutical applications of selected biosurfactants (BSs)	4
1.3.1 Drug delivery applications	4
1.3.1.1 Niosomes	5
1.3.1.2 Methods of preparation	6
1.3.1.2.1 Thin film hydration (TFH) method	6
1.3.1.2.2 Hand-shaking method (HSM)	7
1.3.1.2.3 The bubble method	7
1.3.1.2.4 Ether injection method	7
1.3.1.2.5 Reverse phase evaporation method	7
1.3.1.2.6 Sonication method	8
1.3.1.2.7 Microfluidation method	8
1.3.1.2.8 Heating method (HM)	8
1.3.1.2.9 Freeze and thaw method (FAT)	8
1.3.1.2.10 Dehydration rehydration method (DRM)	8
1.3.1.2.11 Proniosome technology (PT)	8
1.3.2 Cancer	9
1.3.2.1 Cancer therapy	10
1.3.2.1.1 Biosurfactants (BSs) in cancer therapy	12
1.3.3 Wounds and wound healing	15
1.3.3.1 Background	15
1.3.3.2 Wound healing	15
1.3.3.3 Types of wounds	16
1.3.3.2.1 Factors affecting wound healing	17
1.3.3.4 Wound management	18
1.3.3.4.1 Wound dressings	18

1.3.3.4.1.1 Traditional dressings	18
1.3.3.4.1.2 Modern wound dressings	19
1.3.3.4.1.2.1 Hydrocolloid dressings	19
1.3.3.4.1.2.2 Carrageenan (CARR)	19
1.3.3.4.1.2.3 Alginate dressings	20
1.3.3.4.1.2.4 Hydrogel dressings	20
1.3.4 Advanced therapeutic dressings	21
1.3.4.1 Medicated dressings	21
1.3.4.2 Biological dressings	21
1.3.4.3 Tissue engineered skin substitutes	22
1.3.5 Applications of BSs in wound healing	22
1.4 Aims and objectives	23
1.4.1 Hypothesis	23
1.4.2 Aims	23
1.4.3 Objectives	23
2 INSTRUMENTATION AND THEORY OF EXPERIMENTAL TECHNIQUES	25
2.1 Key analytical/ experimental techniques	25
2.1.1 Attenuated total reflectance Fourier transform infrared spectroscopy (ATR-FTIR)	25
2.1.1.1 Instrumentation	25
2.1.1.2 Applications in material and formulation characterisation	26
2.1.2 High performance liquid chromatography (HPLC)	27
2.1.2.1 Instrumentation	28
2.1.2.2 Liquid chromatography mass spectrometer (LC-MS)	28
3 SYSTEMATIC COMPARISON OF THE FUNCTIONAL PHYSICO-CHEMICAL CHARACTERISTICS AND BIOCIDAL ACTIVITY OF MICROBIAL DERIVED BIOSURFACTANTS ON BLOOD-DERIVED AND BREAST CANCER CELLS	30
3.1 Introduction	30
3.2 Materials and methods	31
3.2.1 Chemicals and reagents	31
3.3 Physico-chemical characterisation of BSs	31
3.3.1 Attenuated total reflectance Fourier transform infrared spectroscopy (ATR-FTIR)	31
3.3.2 High performance liquid chromatography (HPLC)	32
3.3.3 Liquid chromatography mass spectrometry (LC-MS)	32
3.3.3.1 HPLC/ESI-MS of rhamnolipids	32
3.3.3.2 HPLC/ESI-MS/MS of surfactin	32
3.3.3.3 HPLC/ESI-MS of sophorolipids	33
3.3.4 Measurement of critical micelle concentration (CMC) and minimum surface tension (ST)	33

3.4	Cell-growth curves	34
3.4.1	Trypan blue growth curve for THP-1, MCF-7 and HEK 293 cells	34
3.4.2	MTT growth curve for MCF-7 and HEK 293 cells	34
3.5	Cytotoxicity studies	34
3.5.1	Cytotoxicity against THP-1 cells	34
3.5.2	Cytotoxicity against MCF-7 and HEK 293 cells	35
3.5.3	Statistical analysis	35
3.6	Results and discussion	36
3.6.1	Physico-chemical characterisation	36
3.6.1.1	ATR-FTIR spectroscopy	36
3.6.1.1.1	ATR-FTIR spectrum of 95% and 90% rhamnolipids	36
3.6.1.1.2	ATR-FTIR spectrum of surfactin	36
3.6.1.1.3	ATR-FTIR spectrum of sophorolipids	37
3.6.1.1.4	Comparison of IR spectra between the different BSs	37
3.6.2	High performance liquid chromatography (HPLC)	38
3.6.2.1	HPLC of surfactin	38
3.6.2.2	HPLC of sophorolipids	38
3.6.3	Liquid chromatography mass spectrometer (LC-MS)	39
3.6.3.1	LC-MS of 95% and 90% rhamnolipids	39
3.6.3.2	LC-MS of surfactin	43
3.6.3.3	LC-MS of sophorolipids	43
3.6.4	Critical micelle concentration and surface tension (ST)	45
3.7	Cytotoxicity of biosurfactants (BSs)	46
3.7.1	Growth curves	46
3.7.2	Dose response curve of biosurfactants on THP-1, MCF-7 and HEK 293 cells	46
3.7.2.1	Rhamnolipids (BS1a and BS1b)	46
3.7.2.2	Surfactin (BS2)	47
3.7.2.3	Sophorolipids (BS3)	51
3.7.2.4	Doxorubicin (DOX)	51
3.7.2.5	Selectivity index	51
3.8	Conclusions	52
4	FORMULATION AND FUNCTIONAL CHARACTERISATION OF BIOSURFACTANT AND SPAN 60 BASED NIOSOMES	53
4.1	Introduction	53
4.2	Materials and methods	54
4.2.1	Materials	54
4.3	Formulation development	54

4.4	Lyophilisation of niosomes	58
4.5	Analytical characterisation	58
4.5.1	pH	58
4.5.2	Conductivity	58
4.5.3	Dynamic laser scattering (DLS)	59
4.5.4	Attenuated total reflectance Fourier transform infrared spectroscopy (ATR-FTIR)	59
4.5.5	X-ray diffraction (XRD)	59
4.5.6	Scanning electron microscopy in transmission mode (STEM)	60
4.5.7	Statistical analysis of data	60
4.6	Results and discussion	60
4.6.1	Preliminary investigations	60
4.6.2	Dynamic laser scattering (DLS)	62
4.6.2.1	Particle size, intensity and polydispersity index (PDI)	62
4.6.2.2	Zeta potential	70
4.6.3	Analytical characterisation	76
4.6.3.1	Attenuated total reflectance Fourier transform infrared spectroscopy (ATR-FTIR)	76
4.6.3.2	X-ray diffraction (XRD)	83
4.6.3.3	Scanning electron microscopy in transmission mode (STEM)	88
4.7	Conclusion	97
5	COMPOSITE BIOSURFACTANT LOADED LYOPHILISED WAFER DRESSINGS FOR POTENTIAL CHRONIC WOUND HEALING	99
5.1	Introduction	99
5.2	Materials	100
5.3	Methods	100
5.3.1	Formulation development	100
5.3.2	Scanning electron microscopy	102
5.3.3	X-Ray diffraction	102
5.3.4	Attenuated total reflectance Fourier transform infrared spectroscopy (ATR-FTIR)	103
5.3.5	Mechanical strength ('hardness')	103
5.3.6	Swelling studies	103
5.3.7	Porosity measurements	104
5.3.8	Water absorption (A_w), equilibrium water content, water reabsorption (ReA_w) and reversibility of equilibrium water content ($ReEWC$)	104
5.3.9	Evaporative water loss	105
5.3.10	Water vapour transmission rate (WVTR)	105
5.3.11	Thermogravimetric analysis (TGA)	105
5.3.12	<i>In vitro</i> adhesion studies	106

5.3.13	Statistical analysis of data	106
5.4	Results and discussion	106
5.4.1	Preliminary formulation development and optimisation	106
5.4.2	Scanning electron microscopy (SEM)	108
5.4.3	Mechanical strength ('hardness')	113
5.4.4	X-ray diffraction (XRD)	117
5.4.5	Attenuated total reflectance Fourier transform infrared spectroscopy (ATR-FTIR)	122
5.4.6	Fluid handling properties	125
5.4.6.1	Swelling	125
5.4.6.2	Pore analysis	128
5.4.6.3	Water absorption (A_w), equilibrium water content (EWC), water reabsorption ($Re A_w$) and reversibility of equilibrium content (ReEWC)	129
5.4.6.4	Evaporative water loss (EWL)	130
5.4.6.5	Water vapour transmission rate (WVTR)	132
5.4.6.6	Thermogravimetric analysis (TGA)	134
5.4.6.6	Mucoadhesion	134
5.5	Conclusions	137
6	LYOPHILISED WAFER DRESSINGS LOADED WITH BIOSURFACTANT BASED NIOSOMES FOR POTENTIAL CHRONIC WOUND HEALING	138
6.1	Introduction	138
6.2	Materials and methods	139
6.3	Methods	139
6.3.1	Formulation of BSs loaded niosomes	139
6.3.2	Formulation of composite gels	139
6.3.3	Formulation of wafers loaded with BSs based niosomes	139
6.3.4	Scanning electron microscopy (SEM)	141
6.3.5	X-Ray diffraction (XRD)	141
6.3.6	Attenuated total reflectance–Fourier transform infrared spectroscopy (ATR-FTIR)	141
6.3.7	Mechanical strength ('hardness')	141
6.3.8	Swelling studies	141
6.3.9	Porosity measurements	141
6.3.10	Water absorption (A_w), equilibrium water content (EWC), water reabsorption ($Re A_w$), reversibility of equilibrium water content (ReEWC) and stability of water absorption	141
6.3.11	Evaporative water loss	142
6.3.12	Water vapour transmission rate (WVTR)	142
6.3.13	Statistical analysis of data	142
6.4	Results & discussion	142

6.4.1	Formulation of composite wafers dressings loaded with BSs based niosomes	142
6.4.2	Scanning electron microscopy (SEM)	143
6.4.3	Mechanical strength ('hardness')	146
6.4.4	X-ray diffraction (XRD)	148
6.4.5	Attenuated total reflectance Fourier transform infrared spectroscopy (ATR-FTIR)	149
6.4.6	Fluid handling properties	152
6.4.6.1	Swelling	152
6.4.6.2	Pore analysis	155
6.4.6.3	Water absorption (A_w), equilibrium water content (EWC), water reabsorption (Re A_w) and reversibility of equilibrium content (ReEWC)	156
6.4.6.4	Evaporative water loss (EWL)	159
6.4.6.5	Water vapour transmission rate (WVTR)	161
6.7	Conclusions	163
7	SUMMARY COMMENTS AND FUTURE WORK	164
7.1	Summary comments	164
7.2	Future work	166
8	REFERENCES	167
9	APPENDIX	187
9.1	Supplementary information	187
9.2	Manuscripts	219
9.3	Conference abstracts and posters	220

FIGURES

Figure 1.1. Representative chemical structures of the four selected biosurfactants: (A) mono-rhamnolipid (anionic, MW 378.41; (B) di-rhamnolipid congeners (anionic; MW 510.60); (C) Surfactin congener (zwitterionic, MW 1036.34) and (D) 1', 4''- Sophorolactone 6', 6''-diacetate (non-ionic, MW 688.80).

Figure 1.2. Examples of novel nanostructured drug delivery systems (NDDS).

Figure 1.3. Therapeutic targeting of the hallmarks of cancer, (Hanahan, 2011).

Figure 1.4. Structure of daunorubicin (DNR) hydrochloride. The empirical formula and molecular weight are $C_{27}H_{29}NO_{10} \cdot HCl$ and 563.98 g/mol respectively.

Figure 1.5. Structure of doxorubicin (DOX) hydrochloride. The empirical formula and molecular weight of Dox are $C_{27}H_{29}NO_{11} \cdot HCl$ and 579.98 g/mol respectively.

Figure 1.6. Stages of wound healing adapted from (Beanes *et al.*, 2003).

Figure 2.1. A multiple reflection ATR system. A classic method for structure analysis is IR spectroscopy. Irradiation of molecules with IR light induces an oscillation of chemical bonds at characteristic frequencies and thus energy is absorbed.

Figure 3.1. ATR-FTIR spectra of 95% rhamnolipid (BS1a), 90% rhamnolipids (BS1b), surfactin (BS2) and sophorolipids (BS3).

Figure 3.2. Representative HPLC chromatogram of (a) surfactin (b) sophorolipids.

Figure 3.3. Total ion chromatograms of BS1a and BS1b (A & B respectively) and corresponding mass spectra (C & D respectively).

Figure 3.4. Representative LC-MS spectrum of sophorolipid (BS3) sample analysed.

Figure 3.5. Cytotoxicity of BSs and DOX on THP-1 cells after (A). 24 h (B). 48 h (C). 72 h (D). 24-72 h ($n = 3, \pm SD$).

Figure 3.6. Plots showing the cytotoxicity of BS3 on MCF-7 cells after (A). 24 h (B). 48 h (C). 72 h ($n = 4, \pm SD$).

Figure 4.1. Representative graph of percentage intensity of (A) rhamnolipid niosomes (TLH) peaks 1, 2 and 3 represent unimodal, bimodal and trimodal distributions respectively.

Figure 4.2. XRD diffractogram of pure span 60 (S60) standard.

Figure 4.3. XRD diffractogram of pure cholesterol (CHL) standard.

Figure 4.4. XRD diffractogram of pure dicetyl phosphate (DCP) standard.

Figure 4.5. XRD diffractogram of pure 1', 4''-sophorolactone 6', 6''-diacetate (BS3) standard.

Figure 4.6. XRD diffractogram of pure rhamnolipid standard.

Figure 4.7. XRD diffractogram of pure surfactin standard.

Figure 4.8. Representative XRD diffractograms showing effect of temperature on BS3:S60:CHL in 7.8:2.5:10 mM loaded niosomes.

Figure 4.9. Representative XRD diffractograms showing effect of temperature on 100.0×10^{-3} mg/l BS1c and BS4a loaded niosomes.

Figure 4.10. SEM of pure: (a) Span 60 (b) Cholesterol (c) Dicapryl phosphate standards.

Figure 4.11. Representative STEM images of BS:S60:CHL 0:10:10 mM (blank) niosomes at different temperatures.

Figure 4.12. STEM images of unsonicated BS3(0):S60(10):CHL(0) mM blank niosomes formulated at 70°C visualised and at different angles.

Figure 4.13. STEM images of sonicated (40 min) BS3(0):S60(10):CHL(0) mM blank niosomes formulated at 70°C and visualised at different angles.

Figure 4.14. Representative STEM image of BS:S60:CHL in (a), 5:5:10 (b), 7.8:2.5:10 (c) 10:0:10 mM formulations at different temperatures.

Figure 4.15. Effect of osmotic shock: (a) Rhamnolipids (BS1c) in PBS (b) Rhamnolipids (BS1c) in RPMI (c) Rhamnolipids (BS1c) in DMEM (d) Rewoferm SL ONE (BS4a) in PBS (e) Rewoferm SL ONE (BS4a) in RPMI (f) Rewoferm SL ONE (BS4a) in DMEM.

Figure 4.16. STEM images of 1.0×10^{-1} mg/l rhamnolipid niosomes and vesicles prepared by TLH and HSM at different magnifications (a) Rhamnolipid niosomes, (b) rhamnolipid vesicles (c) rhamnolipid niosomes, (d) rhamnolipid vesicles.

Figure 4.17. The effect of DCP on blank niosomes composed of (a) span 60, CHL and DCP, (b) S60 and CHL only.

Figure 4.18. Effect of CHL on 1.0 mg/l SL ONE (a) niosome vehicle formulated with S60 and CHL only, (b) Niosome vehicle formulated with S60 and DCP only.

Figure 4.19. Comparison of the initiation of mono and bilayer self-assembly in 2.0×10^{-1} mg/l (a) rhamnolipids and (b) SL ONE.

Figure 4.20. Comparison of rhamnolipid and surfactin loaded niosomes.

Figure 4.21. Surfactin loaded niosome at 1.65×10^{-1} mg/l.

Figure 4.22. 4.0×10^{-1} mg/l, 1', 4''-sophorolactone 6', 6''-diacetate (BS3) loaded niosomes.

Figure 5.1. SEM comparison of selected single polymer wafers prepared from pure CARR (ai) 1%(1:0) (aii) 1.5%(1:0) (aiii) 2%(1:0) pure SA (bi) 1%(0:1) (bii) 1.5%(0:1) (biii) 2%(0:1) and higher total polymer weight pure CARR gels (ci) 2.5%(1:0) (cii) 3%(1:0).

Figure 5.2. SEM images of composite wafers obtained from 1.0, 1.5 and 2.0 % (total polymer weight) CARR:SA gels at ratios of 1:0, 0:1, 1:1, 1:2 and 1:3 respectively.

Figure 5.3. Comparison of (ai) 1%(2:1) (aii) 1.5%(2:1) (aiii) 2%(2:1) (bi) 1%(3:1) (bii) 1.5%(3:1) (biii) 2%(3:1) CARR:SA wafers.

Figure 5.4. Comparison of 1.5%(1:3) and 2%(1:2) BSs loaded wafers.

Figure 5.5. XRD diffractogram of 2%(1:0)CARR:SA wafers.

Figure 5.6. XRD diffractogram of 1.5%(0:1)CARR:SA wafers.

Figure 5.7. XRD diffractogram of optimised selected 1.5%(1:3)CARR:SA wafers.

Figure 5.8. XRD diffractogram of optimised selected 2%(1:2)CARR:SA wafers.

Figure 5.9. XRD diffractograms of 1.5%(1:3)CARR:SA wafers loaded with 0.1% BS1c and 1.5%(1:3)CARR:SA wafers loaded with 0.1% BS4a.

Figure 5.10. XRD diffractograms of 2%(1:2)CARR:SA wafers loaded with 0.2% BS1c.

Figure 5.11. XRD diffractograms of 2%(1:2)CARR:SA loaded with 0.1% BS1c and 2%(1:2)CARR:SA wafers loaded with 0.1% BS4a.

Figure 5.12. XRD diffractograms of 1.5%(1:3)CARR:SA loaded with 5% BS4a and 2%(1:2)CARR:SA wafers loaded with 5% BS4a.

Figure 5.13. XRD diffractogram of 2%(1:2)CARR:SA wafers loaded with 0.1% BS2.

Figure 5.14. Swelling profiles (% swelling index against time of BLK CARR:SA wafers (1:1 and 1:2 ratios) of 1.5 and 2% total polymer weight, and 1:3 ratio of 1.5% total polymer weight in the presence of normal SWF.

Figure 5.15. Swelling profiles (% swelling index against time of CARR:SA 1.5%(1:3) wafers loaded with 0.1% BS1c, 0.2% BS1c, 0.1% BS4a and 5% BS4a in normal SWF.

Figure 5.16. Swelling profiles (% swelling index against time of CARR:SA 2%(1:2) wafers loaded with 0.1% BS1c, 0.2% BS1c, 0.1% BS4a and 5% BS4a in normal SWF.

Figure 6.1. Comparison of BLK and CARR:SA:BSs-NIO-DCP wafers. Unmarked and BS*** equals 100 and 600 µg/ml BSs loaded in niosomes.

Figure 6.2. Comparison of BLK and CARR:SA:BSs-NIO. Unmarked and BS*** equals 100 and 600 µg/ml BSs loaded in niosomes. Several SEM images were taken of each sample, and all discernible pores on each image were measured and averaged.

Figure 6.3. Representative XRD diffractograms of CARR-SA (1:2) wafers obtained from 2% w/w total polymer gels loaded with BLK niosomes (CARR:SA:BLK/BSs-NIO).

Figure 6.4. Swelling index of CARR:SA:BLK-NIO-DCP, CARR:SA:BS1c-NIO-DCP, CARR:SA:BS4a-NIO-DCP and CARR:SA:BS BS2***-NIO-DCP wafers. Unmarked and BS*** equals 100 and 600 µg/ml BSs loaded in niosomes.

Figure 6.5. Swelling index of CARR:SA:BLK-NIO, CARR:SA:BS1c-NIO, CARR:SA:BS4a-NIO and CARR:SA: BS2***-NIO wafers. Unmarked and BS*** equals 100 and 600 µg/ml BSs loaded in niosomes.

Figure 6.6. Swelling index of CARR:SA:BS2 and CARR:SA:BS1c*** wafers. Unmarked and BS*** equals 100 and 600 µg/ml BSs loaded in niosomes.

TABLES

Table 1.1. Cytotoxic activities of rhamnolipids reported in the literature

Table 1.2. Cytotoxic activities of surfactin reported in the literature

Table 1.3. Cytotoxic activities of sophorolipids reported in the literature

Table 3.1. CMC and minimum ST Values of the four selected BSs

Table 3.2. IC₅₀ of BSs and DOX on THP-1, MCF-7 and HEK 293 cells (n = 3, ±SD)

Table 3.3. SI of BSs and DOX on THP-1 and MCF-7 cell lines relative to that of the normal cells HEK 293 at different time points

Table 4.1. Optimisation of amount of cholesterol (CHL) on blank span 60 (S60) and lactonic sophorolipids (BS3) only niosomes using thin film hydration method (TFH)

Table 4.2. Optimisation of amount of cholesterol (CHL) on different concentrations of lactonic sophorolipids (BS3) loaded niosomes

Table 4.3. Optimisation of different concentrations of R-90 rhamnolipids (BS1c) on four component niosomes using thin film hydration method (TFH)

Table 4.4. Optimisation of different concentrations of R-90 rhamnolipids (BS1c) on one component vesicles using direct dissolution (DD)

Table 4.5. Optimisation of different concentrations of lactonic sophorolipids (BS3), Rewoferm SL ONE (BS4a) & SL 446 (BS4b) sophorolipids on four component niosomes using thin film hydration method (TFH)

Table 4.6. Optimisation of different concentrations of surfactin (BS2) on four component niosomes using thin film hydration method (TFH)

Table 4.7. Optimisation of different concentrations of R-90 rhamnolipids (BS1c), Rewoferm SL ONE (BS4a) & SL 446 (BS4b) sophorolipids and surfactin (BS2) on three component niosomes using thin film hydration method (TFH)

Table 4.8. Effect of temperature on size of 1', 4''-sophorolactone 6', 6''-diacetate loaded niosomes

Table 4.9. Effect of temperature on PDI of 1', 4''-sophorolactone 6', 6''-diacetate loaded niosomes

Table 4.10. Particle size and intensities of niosomes loaded with different concentrations of rhamnolipids

Table 4.11. Particle size and intensities of different concentrations of rhamnolipid loaded vesicles

Table 4.12. Particle size and intensities of different concentrations of Rewoferm SL ONE loaded niosomes

Table 4.13. Particle size and intensities of different concentrations of Rewoferm SL 446 loaded niosomes

Table 4.14. Particle size and intensities of different concentrations of surfactin loaded niosomes

Table 4.15. Comparison of the polydispersity index (PDI) of biosurfactant loaded niosomes and vesicles $n = 3$

Table 4.16. Effect of temperature on zeta potential of 1', 4''-sophorolactone 6', 6''-diacetate loaded niosomes

Table 4.17. Effect of temperature on pH of 1', 4''-sophorolactone 6', 6''-diacetate loaded niosomes

Table 4.18. Assignment of wavenumbers (cm^{-1}) present in pure span 60, cholesterol and dicetyl phosphate standards based on possible intermolecular/intramolecular interactions analysed by ATR-FTIR analysis

Table 4.19. Effect of temperature on wavenumbers (cm^{-1}) present in BS3(0):S60(10.0):CHL(10.0/20) blank niosomes at 10 and 20 mM CHL analysed by ATR-FTIR analysis

Table 4.20. Effect of temperature on wavenumbers present in two different concentrations of 1, 6-diacetate 6, 6''-sophorolactone loaded in BS3(5):S60(5):CHL(10) and BS3(7.8):S60(2.5):CHL(10) mM loaded niosomes analysed by ATR-FTIR analysis

Table 4.21. Effect of temperature on wavenumbers present in BS3(10):S60(0):CHL(0) mM loaded niosomes analysed by ATR-FTIR analysis

Table 4.22. Comparison of components (BS, S60, CHL DCP) effect on 1.0×10^{-1} mg/l rhamnolipid standards loaded in niosomes formulated with and without DCP (using thin film hydration method) as well as rhamnolipid vesicles formulated (using direct dissolution) and blank niosomes analysed by ATR-FTIR

Table 4.23. Comparison of components (BS, S60, CHL, DCP) effect on 1.0×10^{-1} mg/l Rewoferm SL ONE standards loaded in four component (4CN) (BS:S60:CHL:DCP) and three component (BS:S60:CHL) niosomes (3CN) analysed by ATR-FTIR

Table 4.24. Comparison of components (BS, S60, CHL, DCP) effect on 6.0×10^{-1} mg/l surfactin standards loaded in four component (4CN) (BS:S60:CHL:DCP) and three component (BS:S60:CHL) niosomes (3CN) analysed by ATR-FTIR

Table 5.1. Composition of single polymers used in preliminary optimisation of freeze-dried wafers from 1 -3% w/w total polymer gels

Table 5.2. Composition of polymers and BSs used in selected optimised freeze-dried wafers obtained from 1.5% w/w total polymer gels

Table 5.3. Composition of polymers and BSs used in selected optimised freeze-dried wafers obtained from 2.0% w/w total polymer gels

Table 5.4. Lyophilised wafers prepared from different gels containing different ratio combinations of CARR and SA, used to analyse surface morphology

Table 5.5. Comparison of the mean pore sizes (\pm SD) (μm) of single, composite and optimised selected BSs loaded wafers

Table 5.6. Reproducibility in 'hardness' of (a) four BLK freeze-dried wafers from 1 – 3% (1:0) CARR:SA, 1 - 2%(0:1), 1 – 2%(1:1, 1:2, 1:3) CARR:SA and (b) BSs loaded wafers from optimised selected 1.5%(1: 3) and 2%(1:2) CARR:SA

Table 5.7. Wavenumbers of various polymer and BSs starting materials and representative single CARR and SA wafers based on possible intermolecular/intramolecular interactions analysed by ATR-FTIR analysis

Table 5.8. Comparison of wavenumbers present in selected optimised CARR:SA:BLKs and representative CARR:SA:BSs loaded wafers based on ATR-FTIR analysis

Table 5.9. Comparison of the porosities of single, composite and BSs loaded wafers

Table 5.10. Comparison of the water absorption (A_w), equilibrium water content (EWC), water reabsorption (Re A_w) and reversibility of equilibrium content (ReEWC)

Table 5.11. Comparison of the evaporative water loss (EWL) of 1.5%(1:3) CARR:SA:BSs and 2%(1:2) CARR:SA:BSs wafers

Table 5.12. Comparison of the water vapour transmission rate (WVTR) of BLK 1.5 and 2%(0:1, 1:1, 1:2, 1:3, 3:1) CARR:SA wafers

Table 5.13. Comparison of the water vapour transmission rate (WVTR) of BSs loaded 1.5%(1:3) and 2%(1:2)CARR:SA wafers

Table 5.14. Residual moisture of optimised formulations analysed by TGA

Table 5.15. Comparison of the mucoadhesive stickiness of single, composite BLK and drug loaded wafers

Table 5.16. Comparison of the mucosal work of adhesion of single, composite and drug loaded wafers

Table 5.17. Comparison of the mucoadhesive cohesiveness of single, composite and drug loaded wafers

Table 6.1. Composition of composite wafers comprising BSs and DCP based niosomes including (CARR:SA:BSs-NIO-DCP) loaded into selected optimised freeze-dried wafers obtained from 2% w/w total polymer gels

Table 6.2. Composition of composite wafers comprising BSs based niosomes without DCP (CARR:SA:BSs-NIO) loaded into selected optimised freeze-dried wafers obtained from 2% w/w composite gels

Table 6.3. Lyophilised composite wafers with BSs based niosomes wafers prepared from 2% w/w total polymer gels, used to analyse surface morphology

Table 6.4. Comparison of the mean pore sizes (\pm SD) of wafers CARR:SA:BSs-NIO-DCP, CARR:SA:BSs-NIO and CARR:SA:BSs

Table 6.5. Reproducibility in 'hardness' of selected optimised niosome loaded freeze dried wafers compressed at five different locations to a depth of 2 mm at a speed of 1 mm/s, using 6 mm diameter stainless steel probe (standard deviations given in parenthesis)

Table 6.6. Composition of crystalline and amorphous phases of CARR:SA:BSs-NIO-DCP, CARR:SA:BSs-NIO and CARR:SA:BSs lyophilised wafers

Table 6.7. Assignment of various functional groups present in CARR:SA:BSs-NIO-DCP, CARR:SA:BSs-NIO and CARR:SA:BSs lyophilised wafers based on possible intermolecular interactions as analysed by ATR-FTIR analysis

Table 6.8. Comparison of the porosities of CARR:SA:BSs-NIO-DCP, CARR:SA:BSs-NIO and reference CARR:SA:BSs wafers

Table 6.9. Comparison of the water absorption (A_w), equilibrium water content (EWC) and water reabsorption ($Re A_w$) of CARR:SA:BSs-NIO-DCP, CARR:SA:BSs-NIO and CARR:SA:BSs wafers

Table 6.10. Comparison of the evaporative water loss (EWL) of CARR:SA:BSs-NIO-DCP, CARR:SA:BSs-NIO and CARR:SA:BSs wafers

Table 6.11. Comparison of the water vapour transmission rate (WVTR) of CARR:SA:BSs-NIO-DCP, CARR:SA:BSs-NIO and CARR:SA:BSs wafers

ABBREVIATIONS

ABS - Absorbance
ACN – Acetonitrile
ALL – Acute lymphocytic leukaemia
AML – Acute myelogenous leukaemia
APCI - Atmospheric-pressure chemical ionisation
ASP – Asparagine
ATCC - American Tissue and Cell Culture
ATR-FTIR - Attenuated total reflectance-Fourier transform infrared
Aw - Water absorption
BLK - Blank
BSA – Bovine serum albumin
B. subtilis – Bacteria subtilis
BS1a – 95Dd rhamnolipids
BS1b – 95/90 rhamnolipids
BS1c – R-90 rhamnolipids
BS2 – Surfactin
BS3 - 1', 4''-Sophorolactone 6', 6''-diacetate
BS4a – Rewoferm SL One sophorolipid
BS4b – Rewoferm SL 446 sophorolipid
BSs - Biosurfactants
BV-173 - B leukemic cell line
Candida. spp – Candida species
C. bombicola – Candida bombicola
CARR - Carrageenan
CARR:SA:BLK - Composite wafers with no biosurfactant based niosomes
CARR:SA:BS1c-NIO - Composite wafers containing rhamnolipid based niosomes
CARR:SA:BS2-NIO - Composite wafers containing surfactin based niosomes
CARR:SA:BS4a-NIO - Composite wafers containing rewoferm SL One sophorolipid based niosomes
CARR:SA:BS4b-NIO - Composite wafers containing rewoferm SL 446 sophorolipid based niosomes
CHL – Cholesterol
CI - Chemical ionisation
CLL – Chronic lymphocytic leukaemia
CMC - critical micelle concentration
CML – Chronic myelogenous leukaemia
CPP - critical packing parameter
Cu - Copper

CYP450 - Cytochrome P450
DCP – Dicyetyl phosphate
DI – Deionised water
DL – Drug loaded
DLS – Dynamic light scattering
DLVO - Deryaguin- Landau-Verwey-Overbeek
DMEM – Dulbecco’s minimal essential medium
DMSO – Dimethyl sulfoxide
DOX – Doxorubicin hydrochloride
DT - doubling time
EBV - Epstein-Barr virus
ECM - Extracellular matrix
EDL – Electrical double layer
EGF - epidermal growth factor
EI - Electron ionisation
ELSD - Evaporative light scattering detector
ESI - Electrospray ionisation
EWC - Equilibrium water content
EWL - Evaporative water loss
FAB - Fast atom bombardment
FGF - fibroblast growth factor
Fig - Figure
GLU - Glutamic acid
h – Hour
HCl – Hydrochloric acid
HEK 293 - Human embryo kidney cell line
HBV - Hepatitis B virus
HCV - Hepatitis C virus
HHV4 - Human herpesvirus 4
HHV8 - Human herpesvirus 8
HLB - Hydrophilic–lipophilic balance
HL-60 - Human promyelocytic leukaemia cell line
HTLV-I - Human T-lymphotropic virus-1
HPV 16 and HPV 18 - High-risk human papillomaviruses
HPLC – High performance liquid chromatography
IEP – Isoelectric point
IRE - Internal reflection elements

JNK – c-Jun N terminal protein
KSHV - Kaposi's sarcoma herpesvirus
K562 - Human chronic myelogenous leukaemia cells
LC-MS – High performance liquid chromatography mass spectrometry
LEU – Leucine
MCF-7 - Human Caucasian breast adenocarcinoma cell line
MCV - Merkel cell polyomavirus
Min – Minute/s
MS - Mass spectrometry
MTD – Maximum tolerable dose
MTT – [3-(4, 5-Dimethylthiazol-2-yl)-2, 5-Diphenyltetrazolium Bromide]
 m/z – Mass to charge
NF – Nuclear factor
NIO – Niosomes
NISV – non-ionic surfactant vesicles
NK – Natural killer
nm – Nanometre
OD – Optical density
OH - Hydroxyl radicals
PAF – Peak adhesive force
P. aeruginosa – Pseudomonas aeruginosa
PBS – Phosphate buffer saline
PCD – Programmed cell death
PCS - photon correlation spectroscopy
PDI – Polydispersity index
PEG – Polyethylene glycol
PGDF - platelet-derived growth factor
PHA's – poly (3-hydroxyalkanoates)
P13K – Phosphatidylinositol 3 Kinase
RDS – Respiratory distress syndrome
Re A_w - Water reabsorption
ReEWC - Reversibility of equilibrium water content
Rha – Mono-rhamnolipids
Rha₂ – Di-rhamnolipids
ROS – Reactive oxygen species
RPMI 1640 – Roswell Park Memorial Institute

R1 – Mono-rhamnolipids
R2 – Di-rhamnolipids
rpm – Revolutions per minute
SA – Sodium alginate
SD – Standard deviation
SEM – Scanning electron microscopy
RPMI 1640 - Roswell Park Memorial Institute medium
SI - selectivity index
SIM - Selected-ion monitoring
SKW-3 - T-cell chronic lymphocytic leukaemia cell line
SLN - Solid lipid nanoparticles
ST – Surface tension
STD – Standards
STEM – Scanning electron microscopy in transmission mode
SWF – Simulated wound fluid
S60 – Span 60
TA - Texture Analyser
TB - Trypan blue
TFA – Trifluoroacetic acid
TGA - Thermogravimetric analysis
TGF- β - Transforming growth factor
TIC - Total ion current
THP-1 - Human leukemic monocyte
TNF – Tumour necrosis factor
TSP – Thermospray
UPLC – Ultra performance liquid chromatography
UV – Ultra-violet
V/V – Volume per volume
WHO – World health organisation
WVTR - Water vapour transmission rate
W/W – Weight per weight
XRD - X-ray diffraction

CHAPTER 1 GENERAL INTRODUCTION

1.1 Surfactants

Surfactants are amphiphilic compounds that consist of one hydrophilic head and one hydrophobic tail and have surface activity (Hu, 2010). The hydrophilic part can be a charged polar group (*e.g.* sulphate), a zwitterionic group (*e.g.* glycine) or a non-charged polar group (*e.g.* poloxamers), whereas the hydrophobic part can be a non-polar group, comprising a single carbon chain or up to four alkyl chains (Tonova and Lazaravo, 2008). Based on the nature of their polar head group, surfactants can therefore be classified as anionic, non-ionic, zwitterionic and cationic, (Holmberg *et al.*, 2003; Pashley and Karaman, 2004; Rosen, 1978). They are synthesised from petrochemical sources such as sodium lauryl sulphate BP, polyoxyethylene glycol octylphenol ethers, phospholipids and alkyltrimethylammonium salts (Scarlat, 2015) and used in the formulation of detergents, personal care products and cleansing agents, (Scarlat, 2015) and this is possible through their surface active and interfacial properties.

1.2 Biosurfactants

Surfactants are also secreted by mammals (pulmonary surfactants) such as dipalmitoylphosphatidyl choline (DPPC), plants (lecithin), and microorganisms and these are referred to as biosurfactants to differentiate them from the chemically synthesised ones.

1.2.1 Microbial biosurfactants

Microbial biosurfactants (BSs) exist as low and high molecular weight compounds such as rhamnolipids, sophorolipids, surfactin, trehalose lipids and emulsan. They are further sub-divided into glycolipids (rhamnolipids, sophorolipids), lipopeptides, (surfactin) and polymeric BSs (emulsan). Due to their natural origins, BSs are recognised as non-toxic or of low toxicity, being biodegradable and therefore potential alternatives to synthetic surfactants (Harshada, 2014). In addition, BSs are multifunctional compounds that also have biotechnological and biomedical applications. The BSs investigated in this study (rhamnolipids, surfactin and sophorolipids) were selected on the basis of their therapeutic and biophysical properties as well as their ready availability. Rhamnolipids and sophorolipids are members of the same glycolipid sub-class while surfactin is a macrolide lipopeptide (Kakinuma *et al.*, 1969) and are amongst the most widely characterised biosurfactants and also used in several applications.

Rhamnolipids are synthesised from *Pseudomonas aeruginosa* (Bergstrom *et al.*, 1946) and exist as a family of congeners, some of which have isomers. The most prominent congeners are mono-rhamnolipids and di-rhamnolipids with molecular formulas Rha-C₁₀-C₁₀ and Rha-Rha-C₁₀-C₁₀ respectively. The structural units were further elucidated as being composed of two β -hydroxydecanoic acids linked through an ester bond to two rhamnose moieties via a 1,3 glycosidic linkage. The ratio of

mono to di-rhamnolipids produced by bacteria depends on the carbon sources utilised during biosynthesis (Lotfabad *et al.*, 2010). The di-rhamnolipid congener Rha-Rha-C₁₀-C₁₀ is considered to be the most common of its class (Abdel-Mawgoud *et al.*, 2011) and a higher percentage of di-rhamnolipids is produced when hydrophilic substrates are used during synthesis.

Surfactin, is predominantly secreted by *Bacillus subtilis* and its chemical structure consists of a cyclic lactone ring surrounded by seven amino acid residues interlinked with a β -hydroxyl fatty acid with a chain length that varies from 12 to 16 carbon atoms. Surfactin adopts a β turn, and forms a β helical sheet and the amino acid sequence is expressed as LLDLLDL and surrounded by a heptapeptide (leucine (L), aspartic acid (D), glutamic acid (E) and valine (V) ELLVDLL (Kakinuma *et al.*, 1969). There are 4 leucine residues which exist in equal pairs of D and L conformations. Additionally, the hydrophobic amino acid residues are situated at positions 2, 3, 4, 6 and 7 while negatively charged amino acid residues are situated at positions 1 and 5 respectively (Hue *et al.*, 2001; Tang *et al.*, 2010).

Gorin *et al.*, (1961) identified the yeast fungi, *Candida apicola* as a producer of sophorolipids. Since then sophorolipids have been found to be secreted extracellularly from several other non-pathogenic yeasts however, *Candida bombicola* has been the subject of many investigations. Sophorolipids exist as acidic or lactonic forms, with the latter resulting from internal esterification of the carboxylic acid group to a lactone ring. Additionally, structural variations could exist as a result of differences in hydroxylation of the terminal carbon atom via acetylation of the hydroxyl sophorose sugar at C6', C6'' or C4'' which may be diacetylated, monoacetylated or deacetylated. Structural variation could also be due to the possession of one or more saturation bonds. Lactonic sophorolipids are non-ionic BSs, however, the acidic forms can be converted into anionic, cationic, or zwitterionic forms by coupling the carboxylic end with di-carbodiimide. Sophorolipid isoforms exhibit different biological and chemical behaviours. For example, lactonic sophorolipids have better surface tension with cytotoxic, biocidal, spermicidal and hydrophobic properties while acidic sophorolipids have better foaming, detergent, solubility, cosmetic and bio-remediation properties.

Lipopeptides, glycolipids and other BSs, owing to their structural novelty and diverse biophysical properties, have recently emerged as possible broad-spectrum agents for cancer chemotherapy (Gudiña *et al.*, 2013). The cytotoxic activity of the selected BSs on cancer cells has been reported by a number of studies (Zhao *et al.*, 2013; Thanomsub *et al.*, 2006; Christova *et al.*, 2010; Cao *et al.*, 2011; Cao *et al.*, 2009a; Cao *et al.*, 2009b; Duarte *et al.*, 2014; Rashad *et al.*, 2014; Ribiero *et al.*, 2015; Chen *et al.*, 2006). However, the pharmacological effects of BSs on blood derived monocytic cancer cells has not been reported. In this study, the biological (*e.g.* anti-cancer) activities of these BSs is of particular interest. Furthermore, this research sheds new light on the action of lactonic sophorolipids on breast cancer cells. In addition, the work explores the potential of using the selected biosurfactants in dressings to potentially target the inflammatory phase of wound healing, especially in hard to heal wounds.

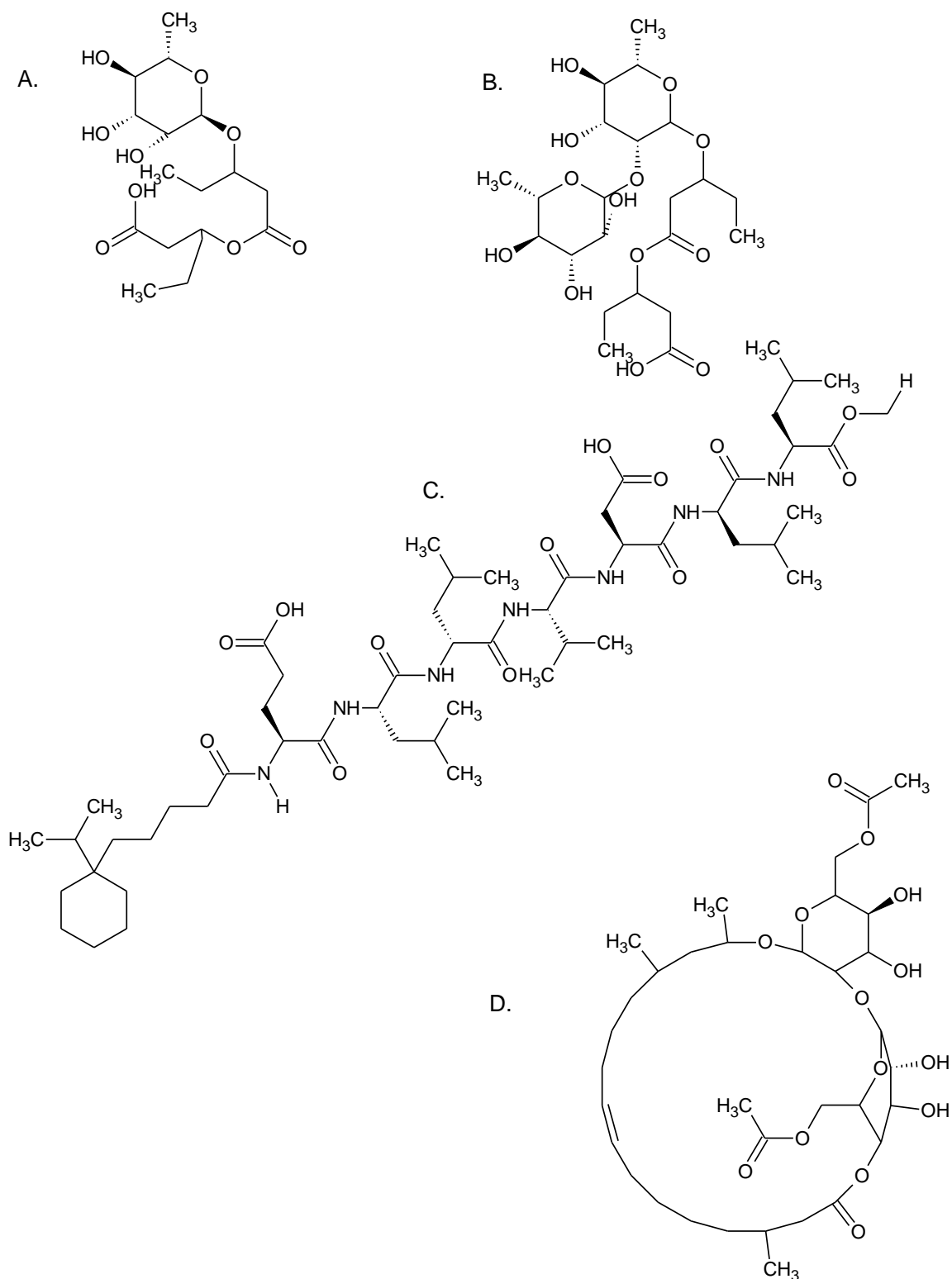


Figure 1.1. Representative chemical structures of the four selected biosurfactants: (A) mono-rhamnolipid (anionic, MW 378.41; (B) di-rhamnolipid congeners (anionic; MW 510.60); (C) Surfactin congener (zwitterionic, MW 1036.34) and (D) 1', 4''- Sophorolactone 6', 6''-diacetate (non-ionic, MW 688.80).

1.3 Biological and biopharmaceutical applications of selected biosurfactants (BSs)

BSs are multifunctional compounds that have bioremediation, biotechnology, and biomedical applications. However of further interest to this research is the field of pharmaceutical formulations and biopharmaceutical (drug delivery applications) including anti-cancer and wound healing. Lipopeptides, glycolipids and other BSs have recently emerged as possible broad-spectrum agents for cancer chemotherapy/biotherapy and also as safe vehicles in drug delivery formulations owing to their structural novelty and diverse biophysical properties (Gudina *et al.*, 2013).

1.3.1 Drug delivery applications

The surface active, interfacial tension and critical micelle concentration (CMC) characteristics of BSs make them good candidates for drug delivery. Drug delivery refers to the transportation of drugs to targeted sites and at regulated intervals in the body, which reduces toxicity to normal tissues.

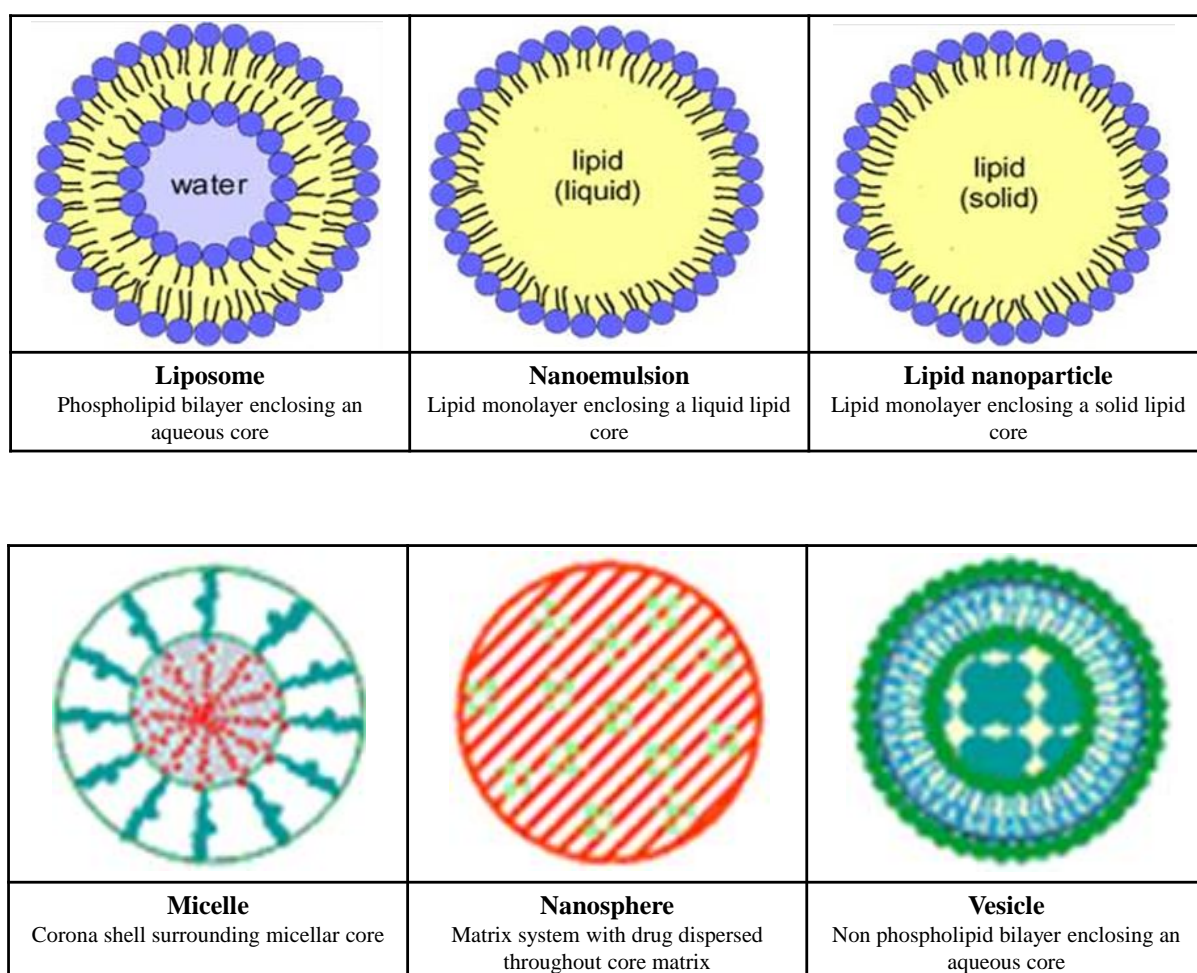


Figure 1.2. Examples of novel nanostructured drug delivery systems (NDDS) Uchechi *et al.*, 2014; Reddy and Swarnalatha 2010.

In recent years, there has been significant efforts at developing advanced novel drug delivery systems that are more efficient at targeting the drug to the required site of action, whilst also reducing unwanted side effects. Such novel drug delivery systems include micelles, microemulsions, vesicles (*e.g.* niosomes), liposomes and nanoparticles (Fig 1.2). BSs have been used for drug-delivery such as cationic surfactin in liposomes for siRNA delivery, cellular transfection of DNA delivery using mannosyl erythriol lipids (MEL) (Inoh *et al.*, 2001) and conjugated with gellan gold-plated nanoparticles, (Dhar *et al.*, 2011). However, their encapsulation into niosomes for targeting is a novel concept and will be one of the key objectives in the current study.

1.3.1.1 Niosomes

Niosomes are microscopic vesicles composed mainly of hydrated non-ionic surfactants with or without cholesterol (CHL) or its derivatives and vesicle size ranging from 20 nm - 50 μ m (Fathalla *et al.*, 2014). Niosomes are osmotically active, chemically stable and offer longer storage time in comparison to liposomes. When subjected to osmotic gradients, (Arunothayanun *et al.*, 1999) reported a higher rate of release for spherical vs polyhedral niosomes in hypotonic (water) and isotonic medium (2 M NaCl). The stability of niosomes is due to the use of synthetic non-ionic surfactants in place of biological phospholipids.

Their surface formation and modification are easy as a result of their functional head-group, they are biodegradable and non-immunogenic as well as being highly compatible with biological systems due to their non-ionic natures (Tangri and Khurana, 2011). Niosomes can be divided into three categories according to size: small unilamellar vesicles (SUV) (10 - 100 nm), large unilamellar vesicles (100 - 3000 nm) and multi-lamellar vesicles (MLV) where more than one bilayer is present (Shilpa *et al.*, 2011). Most niosomes are in the nano size range and therefore of the SUV type. Other specialised niosomes reported in literature include proniosome, surfactant ethosomes, elastic niosomes, polyhedral niosomes, discomes (disk-shaped vesicles) and aspasome (ascorbyl palmitate vesicle) (Kumar and Rajeshwarrao, 2011; Biswal *et al.*, 2008).

Non-ionic surfactants are the most common surface active agents used in preparing vesicles due to their superior benefits with respect to stability, compatibility and toxicity compared to their anionic, amphoteric or cationic counterparts. Examples used in niosome preparations include alkyl esters, alkyl amides, alkyl ethers and esters of fatty acids *e.g.* span 60, tween 60 and brij 52. Surfactant selection depends on the hydrophilic-lipophilic balance (HLB) and critical packing parameter (CPP). HLB ranges from 0-20 for non-ionic surfactants, whereas ionic surfactants have higher HLB's as a result of their hydrophilicity *e.g.* the HLB of sodium dodecyl sulphate (SDS) is 40. A low HLB (< 9) enables an oil soluble (lipophilic) surfactant while a high HLB (> 11) enables a water soluble (hydrophilic) surfactant. HLBs that fall within the range of 3-8 engender oil in water emulsions (W/O) while those that fall within 9-20 facilitate water in oil emulsions (O/W). CPP is a measure of the surfactants ability to form spherical micelles ($CPP < 1/3$), non-spherical micelles ($1/3 < CPP < 1/2$),

bilayer vesicles ($1/2 < CPP < 1$) or inverted micelles ($CPP \geq 1$) (Kumar and Rajeshwarrao, 2011; Pardakhty *et al.*, 2007).

In addition to surfactant properties, the cholesterol content tends to affect the vesicular properties such as entrapment efficiency, storage time, release and stability of proteins, biologicals anti-cancer, anti-infective and anti-inflammatory agents (Shilpa *et al.*, 2011; Biswal *et al.*, 2008). For surfactants with $HLB > 6$, cholesterol must be added to form bilayers and for lower HLB values, cholesterol enhances the stability of vesicles. Vesicle aggregation of niosomes may be prevented by the inclusion of compounds that introduce repulsive steric or electrostatic forces. Steric stabilisation can be imparted by the inclusion of Solulan C24 (a cholesteryl poly-24-oxyethylene ether) while dicetyl phosphate (DCP) is a common additive that acts as a charge inducer and is usually used to impart a negative charge on the surface of niosomes to stabilise the bilayers or to achieve electrophoretic mobility (Kumar and Rajeshwarrao, 2011). Generally, charged niosomes are more stable against aggregation and fusion than uncharged vesicles. Negative zeta potential values ranging between -42 and -58 mV are sufficiently high for electrostatic stabilisation and both surfactant type and encapsulation efficiencies may affect the zeta potential values (Bayindir and Yuksel, 2010).

1.3.1.2 Methods of preparation

Some of the methods for preparing niosomes include thin film hydration (TFH), reversed phase evaporation method (RPM), ether injection method (EIM), hand-shaking method (HM), sonication (SM), proniosome technology (PT), dehydration rehydration (DRM), freeze and thaw (FAT) method and the bubble method. These are briefly described below.

1.3.1.2.1 Thin film hydration (TFH) method

The thin-film hydration method is a simple preparation approach that is widely used for the formulation of MLVs. In this method, the surfactants and additives such as cholesterol (CHL), and dicetyl phosphate (DCP) are dissolved in an organic solvent inside a round-bottomed flask. The organic solvent is then evaporated using a rotary vacuum evaporator. A thin film formed on the side of the round-bottomed flask may be further dried and purified in a vacuum desiccator after which the film is hydrated with an aqueous solution such as water or PBS above the transition temperature of the surfactant. The transition temperature (T_c) is the melting point of the acyl chains and all lipids have a characteristic T_c , which is contingent upon the nature of the polar head group and on the length and degree of unsaturation of the acyl chains. Above the T_c , lipids form a liquid-crystalline phase that constitutes increased mobility of the acyl chains. A reduction in temperature below the T_c creates a transition to a more rigid state.

The mixture is subjected to mechanical shaking for about an hour to form milky niosomal dispersions. MLVs are usually formed during the hydration step (Tangri and Khurana, 2011; Baillie *et al.*, 1986). Balakrishnan *et al.*, (2009) used TFH to prepare minoxidil MLVs composed of cholesterol

and various non-ionic surfactants to target the skin of hairless mouse. They found that particular types of non-ionic surfactants and vesicle size determined transdermal bioavailability and concluded that these niosomal formulations have great potential for cutaneous targeting and the topical delivery of minoxidil in skin diseases such as hair loss.

1.3.1.2.2 Hand-shaking method (HSM)

The hand-shaking method is another technique for synthesising MLVs and is usually categorised together with the thin-film hydration method due to similar formulation protocol (Tangri and Khurana, 2011; Baillie *et al.*, 1986). The effect of sorbitan surfactants such as span 40, 60 and 80 for the delivery of cefuroxime axetil-a broad spectrum, second generation cephalosporin antibiotic, using the handshaking method, was investigated (Sambhakar *et al.*, 2011) due to its simplicity, scalability and cost-effectiveness.

1.3.1.2.3 The bubble method

In the bubble method, organic solvents are not used. The surfactant and additives in PBS (pH 7.4) are transferred into a glass reactor with three necks. The reactor is placed in a water bath to control the temperature with a thermometer positioned in the first neck, nitrogen is supplied through the second neck and water-cooled reflux delivered through the third neck. The niosome components are dispersed at 70°, then mixed with high shear homogeniser for 15 sec and immediately followed by the bubbling of nitrogen gas at 70°C to produce stable niosome dispersions with mean particle size generally ranging between 200 - 500 nm (Talsma *et al.*, 1994).

1.3.1.2.4 Ether injection method

The surfactants with additives are dissolved in an organic solvent such as diethyl ether and then injected slowly through a needle into the drug containing aqueous solution which is maintained at a constant temperature of about 60°C. The organic solvent is then evaporated through a rotary evaporator (Marwa *et al.*, 2013). In the process of the evaporation, surfactants are added, resulting in the formation of single layered vesicles. SUVs and LUVs produced by solvent injection technique have relatively high entrapped aqueous volume, which depending upon conditions, may range from 50 - 1000 nm (Shilpa *et al.*, 2011).

1.3.1.2.5 Reverse phase evaporation method

LUVs are usually prepared by reverse phase evaporation method whereby the surfactants and additives are dissolved in an organic solvent (Marwa *et al.*, 2013; Abdelkader *et al.*, 2011). However, after addition of the aqueous solvent containing the drug, the mixture is sonicated to form an emulsion, which is followed by the slow removal of the organic solvent using a rotary evaporator at about 40 - 60°C.

1.3.1.2.6 Sonication method

The aqueous phase containing the drug is added to the surfactant and additive mixture. The final mixture is probe sonicated at 60°C for 3 min to yield niosomes (Alam *et al.*, 2013).

1.3.1.2.7 Microfluidation method

This method can be used to synthesise unilamellar vesicles with smaller size, greater uniformity with high reproducibility. This method utilises the submerged jet principle through which two fluidised streams interact at ultra-high velocities in precisely defined micro channels within the interaction chamber. The impingement of a thin liquid sheet along a common front is arranged in such a way that the energy supplied to the system remains within the area of niosome formation (Kazi *et al.*, 2010).

1.3.1.2.8 Heating method (HM)

In this method, surfactants and additives are separately hydrated in PBS (pH 7.4) under a nitrogen atmosphere for an hour at room temperature. After 15 - 20 min, the solution is heated to about 120°C on a hot-plate stirrer to dissolve the CHL. The temperature is then reduced to 60°C, followed by addition of the surfactant and additives to the buffer-CHL mixture and stirred for a further 15 min. Synthesised niosomes are left to stand at room temperature for 30 min and then stored at 4 - 5°C under nitrogen atmosphere (Mozafari *et al.*, 2007).

1.3.1.2.9 Freeze and thaw method (FAT)

Niosomal suspensions are prepared using TFH by first freezing in liquid nitrogen for about 1 min and thawed in a water bath at 60°C for another min (Abdelkader *et al.*, 2011). The niosomal dispersions formed are called frozen and thawed multilamellar vesicles (FAT-MLVs).

1.3.1.2.10 Dehydration rehydration method (DRM)

The niosomal dispersions called dehydration rehydration vesicles (DRVs) are frozen in liquid nitrogen and then freeze-dried overnight. The resulting powder is then hydrated with PBS (pH = 7.4) at 60°C to obtain the niosomal suspension (Kirby and Gregoriadis, 1984).

1.3.1.2.11 Proniosome technology (PT)

The proniosome technique can be used as a precursor method to prepare stable niosomes by converting MLVs into SUVs using sonication (bath or probe) or high pressure homogenisation (a microfluidiser) or extrusion under high pressure (using French pressure cell). The application of energy breaks down the MLV structure into SUVs with high radius curvatures (Ibrahim *et al.*, 2008; Mokhtar *et al.*, 2008). Physico-chemical characterisation and analyses of niosomes include vesicle size, size distribution and zeta potential, morphology, entrapment efficiency, *in vitro* drug release, lamellarity, rigidity, stability, viscosity, conductivity and homogeneity.

1.3.2 Cancer

Cancer is a major cause of morbidity and mortality and runs in the top three causes of death worldwide (Stewart and Wild, 2014). It is a collection of over 100 diseases afflicting all body organs and it has increasingly become evident that cancer presents itself differently among different individuals (Levitzki and Klein, 2010). Cancer is a group of diseases characterised by unregulated cell growth and the invasion and spread of cells from the site of origin or primary site to other sites in the body. Cancer is a genomic disease at the cellular level (Pecorino *et al.*, 2016) and the key genes that are involved in its development are oncogenes and tumour suppressor genes. Mutation of proto-oncogenes results in uncontrolled growth and division, however, majority of cancers are not inherited. Cancer can also be triggered by physical (ultraviolet and ionising radiation), chemical (aflatoxin, arsenic from tobacco, food and drinking water respectively), biological carcinogens (infections from certain viruses, bacteria or parasites) and ageing (WHO, 2016). It has become very evident over the last three decades, that several viruses play significant roles in the multistage development of human neoplasms. Approximately 15 - 20% of cancers are associated with viral infections (McLaughlin-Drubin and Munger, 2008) and it is probably the 2nd most important factor after tobacco (Almeida and Barry, 2010). Tumorigenic retroviruses have been central to cancer biology and have led to the identification of more than 20 cellular oncogenes and the discovery of reverse transcriptase by Francis Peyton Rous (Moore and Chuang, 2010). Retroviruses are RNA tumour viruses that encode reverse transcriptase, an enzyme that is involved in the complex process that converts RNA into DNA. The WHO's international Agency for Research on Cancer estimates that one in five cancer cases worldwide are caused by infection with most caused by viruses (Parkin, 2006). However for some viruses, it is not entirely clear if specific viral products sustain mature tumour cells, promote a precancerous cell phenotype or unilaterally contribute to cancer through prolonged infection and chronic inflammation (Tsai and Chung, 2010).

The hallmarks of cancer (Fig 1.3) include growth signal autonomy, evasion of cell death, evasion of growth inhibitory signals, unlimited replicative potential, angiogenesis and invasion & metastasis. Additionally, there are two enabling characteristics which are tumour promoting inflammation and genomic instability. . However, progress in the last decade has added two emerging hallmarks to this list which are; reprogramming of energy metabolism and evading immune destruction (Pecorino, 2016). In addition to cancer cells, tumours exhibit another dimension of complexity in that they contain a repertoire of recruited, ostensibly normal cells that contribute to the acquisition of hallmark traits by creating the “tumour microenvironment,” (Hanahan, 2011).

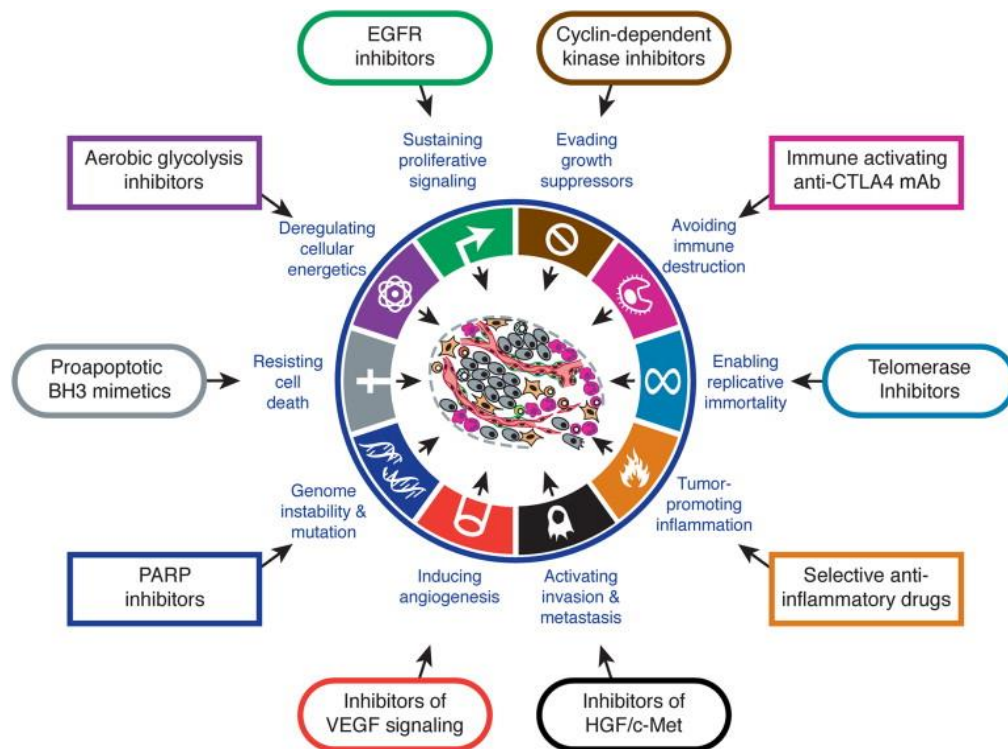


Figure 1.3. Therapeutic targeting of the hallmarks of cancer, (Hanahan, 2011).

Drugs that interfere with each of the acquired abilities of tumour growth and progression have been developed and are in clinical trials or in some cases approved for clinical use in treating certain forms of human cancer. Additionally, the investigational drugs are being developed to target each of the enabling characteristics and emerging hallmarks which also hold promise as cancer therapeutics.

1.3.2.1 Cancer therapy

Applications of tumour biology, molecular biology and genetics together with a greater understanding of pharmacological mechanisms of drug action have opened up the field of medical oncology (Fig 1.3). Cancer therapy includes surgery, radiation, hormone therapy, immunotherapy, chemotherapy and targeted therapy. Surgery and radiotherapy dominated the field of oncology till the 1960s when metastasis responded better to combination chemotherapy in the treatment of cancers (DeVita and Chu 2008). Almost 60% of anticancer drugs are of natural origin, such as plants (*e.g.* vincristine, irinotecan, camptothecines) and microorganisms (*e.g.* daunorubicin, doxorubicin, dactinomycines, mitomycin and bleomycin) (Grever, 2001). Cancer cells are normally highly-specialised cells which have regressed to a much simpler, more primitive stage and which unlike the normal parent, divide continuously, although inefficiently. Because a much higher proportion of cancer cells are undergoing division, they are more vulnerable than most normal cells to anti-cancer drugs. Both in normal and in neoplastic proliferating tissues, the toxicity of many of these drugs appears to be related to effects on the mitotic spindle and replicating DNA. The selective toxicity on tumours observed for some of the chemotherapeutic agents,

depends more on pharmacokinetic and metabolic factors in target cells than on the direct proximal action of the agent. In many cases, the selectivity of action of these agents depends mainly on the fact that normal proliferating tissues have distinctive physiological or biochemical characteristics that affect drug actions (Schartz and Mihic, 1973).

The anthracycline antibiotics daunorubicine (DNR) and doxorubicin (DOX) have been in clinical use for more than 30 years for the treatment of a wide variety of cancers such as acute myeloid leukaemia and in the case of doxorubicin, a wide diversity of solid tumours and is broadly considered the most active single agent available for the treatment of breast cancer (Tsang *et al.*, 2003). The existence of DNR (Fig 1.4) preceded that of DOX (Fig 1.5), however, it was found to be severely toxic and hence was used as a precursor to produce DOX. Despite their extensive clinical utilisation, their exact mechanism of action is not entirely clear. Doxorubicin's mechanism of action has been proposed to involve the synthesis of ceramide followed by activation of a transcription factor called CREB3L1 (Denard *et al.*, 2012), topoisomerase II inhibition, DNA intercalation, free radical generation and regulated intramembrane proteolysis (Thorn *et al.*, 2011). However, both DNR and DOX have cardiovascular side-effects and are limited to maximum recommended cumulative doses of 500 and 450 - 600 mg/m² respectively. This limitation combined with the development of spontaneous resistance, limits the optimal effectiveness of DNR and DOX (Monneret, 2001). Therefore, more effective but safe alternatives are required which this research seeks to investigate using the naturally obtained microbial BSs.

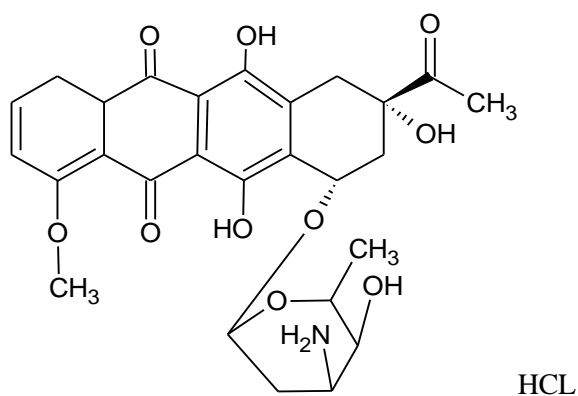


Figure 1.4. Structure of daunorubicin (DNR) hydrochloride. The empirical formula and molecular weight are C₂₇H₂₉NO₁₀ · HCl and 563.98 g/mol respectively.

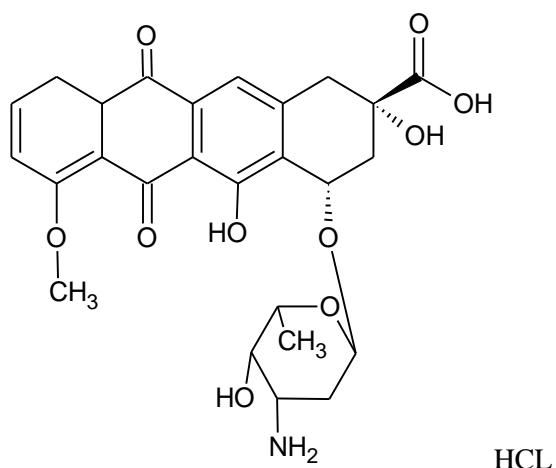


Figure 1.5. Structure of doxorubicin (DOX) hydrochloride. The empirical formula and molecular weight of Dox are $C_{27}H_{29}NO_{11} \cdot HCl$ and 579.98 g/mol respectively.

1.3.2.1.1 Biosurfactants (BSs) in cancer therapy

Lipopeptides, glycolipids and other surfactants have recently emerged as possible broad-spectrum agents for cancer therapy owing to their structural novelty and diverse biophysical properties (Gudina *et al.*, 2013). Cytotoxic activity of these BSs on cancer cells has been reported by a number of authors (Zhao *et al.*, 2013); Thanomsub *et al.*, 2007; Christova *et al.*, 2010; Cao *et al.*, 2011; Cao *et al.*, 2009a; Cao *et al.*, 2009b; Lee *et al.*, 2012; Duarte *et al.*, 2014; Rashad *et al.*, 2014; Shao *et al.*, 2012; Ribiero *et al.*, 2015; Chen *et al.*, 2006). Details of cancer studies reported using the four selected BSs being investigated in this research are provided in (Tables 1 - 3). However, the pharmacological effects of BSs on blood derived monocytic cancer cells (THP-1) has not been reported and therefore forms a key part of the objectives of this study. Furthermore, this research sheds new light on the action of lactonic sophorolipids on breast cancer cells. This will involve simultaneously comparing the surface properties, emulsification capability and cytotoxicity of the selected BSs.

Table 1.1. Cytotoxic activities of rhamnolipids reported in the literature

Rhamnolipids concentration	Cancer cells	Reference
0, 5, 10, 20, 40, 60, 80, 100 (mg) (di-rhamnolipids congeners)	MCF-7 (1 µg/mL) after 48 h	Zhao <i>et al.</i> , 2013
0, 5, 10, 20, 40, 60, 80, 100 (mg) (di-rhamnolipids congeners)	H460 (5 µg/mL) after 48 h	Zhao <i>et al.</i> , 2013
5, 10, 20, 30, 40 or 50 (µg/ml) (di- rhamnolipids congeners)	MCF-7 (IC ₅₀ of 6.25 µg/mL) after 48 h	Thanomsub <i>et al.</i> , 2007
25, 50, 100 and 200 (µM) (mono- rhamnolipids congeners)	BV-173 (IC ₅₀ of 50 µM) after 72 h	Christova <i>et al.</i> , 2010
25, 50, 100 and 200 (µM) (mono- rhamnolipids congeners)	SKW-3 (IC ₅₀ of 54 µM) after 72 h	Christova <i>et al.</i> , 2010
25, 50, 100 and 200 (µM) (mono- rhamnolipids congeners)	JMSU1 (IC ₅₀ of 60 µM) after 72 h	Christova <i>et al.</i> , 2010
25, 50, 100 and 200 (µM) (mono- rhamnolipids congeners)	HL-60 (IC ₅₀ of 67 µM) after 72 h	Christova <i>et al.</i> , 2010

Rhamnolipids exist as a family of congeners, some of which have isomers. The most prominent congeners are mono-rhamnolipids and di-rhamnolipids with molecular formulas Rha-C₁₀-C₁₀ and Rha-Rha-C₁₀-C₁₀ respectively. Human pre-B leukemic line (BV-173), T-cell chronic lymphocytic leukaemia (SKW-3), poorly differentiated transitional cell carcinoma of the urinary bladder line (JMSU1) and human promyelocytic leukemia (HL-60).

Table 1.2. Cytotoxic activities of surfactin reported in the literature

Surfactin concentration	Cancer cells	Reference
0, 20, 40, 60, 80, 100 (µg/ml) 24, 48 (h)	MCF-7 (IC ₅₀ of 30 µg/ml) (48 h)	Cao <i>et al.</i> , 2011
0, 5, 10, 20, 40, 80, 100 (mg/l) 24, 48 (h)	MCF-7 (IC ₁₀ of 24.8 mg/l) (48 h)	Cao <i>et al.</i> , 2009b
5, 10, 20, 30, 40 or 50 (µg/ml) (24 h)	MCF-7 (IC ₅₀ of 10 µg/ml) (24 h)	Lee <i>et al.</i> , 2012
0.05, 0.1, 0.2, 0.5 and 1 (g I ⁻¹) 24, 48, 72 (h)	MDA-MB-231 (IC ₅₀ of 0.5 g I ⁻¹) (4 h)	Duarte <i>et al.</i> , 2014
0.05, 0.1, 0.2, 0.5 and 1 (g I ⁻¹) 24, 48, 72 (h)	T47D (IC ₅₀ of 0.5 g I ⁻¹) after 24 h	Duarte <i>et al.</i> , 2014
5, 10, 20, 40, 80, 100 (mg/L)	K562 (IC ₅₀ of 19.1mg/L) after 48 hr	Cao <i>et al.</i> , 2009a
0, 10, 20, 40, 80, 160, 200, 240) (mg/L)	HEK 293 (IC ₅₀ of 105.6 mg/L) after 48 h	Cao <i>et al.</i> , 2011

Surfactin has been found to exist as a family of isoforms with peptidic variants and about 13-15 carbon length fatty acid chain. Non-aggressive human adenocarcinoma breast cancer cell line (MCF-7), aggressive human adenocarcinoma breast cancer cell line (MDA-MB-231), ductal carcinoma human breast cancer cell line (T47D) and human chronic myelogenous leukaemia cells (K562) and human embryonic kidney cells (HEK 293).

Table 1.3. Cytotoxic activities of sophorolipids reported in the literature

Sophorolipids Concentration	Cancer cells	References
0, 50, 100, 150, 200 mg (mixture of acidic and lactonic SLs (EI, EII, EIII, EIV))	MCF-7 (No effect)	Rashad <i>et al.</i> , 2014
0, 50, 100, 150, 200 mg (mixture of acidic and lactonic SLs (EI, EII, EIII, EIV))	HEPG2 (IC ₅₀) of 47.00±4.20, 36.00±3.50, 23.70±2.63, 19.00±1.80	Rashad <i>et al.</i> , 2014
0, 50, 100, 150, 200 mg (mixture of acidic and lactonic SLs (EI, EII, EIII, EIV))	A549 (IC ₅₀) of 46.60±4.30, 41.20±4.60, 29.00±2.80, 25.77±2.20	Rashad <i>et al.</i> , 2014
0, 50, 100, 150, 200 mg (mixture of acidic and lactonic SLs (EI, EII, EIII, EIV))	HCT116 (No effect)	Rashad <i>et al.</i> , 2014
0 to 60 microgram/mL (lactonic SLs)	KYSE 109 and KYSE 450	Shao <i>et al.</i> , 2012
0 to 100 C18:3, C18:1, and C18:0 mg L ⁻¹ (diacetylated SLs)	MDA-MB-231 (IC ₅₀) of 30 mg 11 (43.9 µM), 15 µg/ml (21.8 µM), and 15 µg/ml (21.7 µM)	Ribiero <i>et al.</i> , 2015
0, 5, 10, 20, 30, 60, 120 (µg/ml) (lactonic SLs)	H7402, A549, HL-60 and K562 (IC ₅₀ of ≤ 62.50 µg/ml after 24-48 h)	Chen <i>et al.</i> , 2006

Sophorolipids exists as acidic or lactonic forms, the latter of which is as a result of an internal esterification of the carboxylic acid group to a lactone ring. Sophorolipid isoforms exhibit different biological and chemical behaviours. The acidic to lactonic ratio is to a great extent determined by yeast strain, medium cultivation or type of carbon sources. Monoacetylated lactonic sophorolipid (MASL), diacetylated lactonic (DASL); human oesophageal cells (KYSE 109 and KYSE 450), human adenocarcinoma cells (MCF-7), MDA-MB-231, liver cancer line (H7402), lung cancer line A549), leukaemia lines (HL-60), human chronic myelogenous leukaemia cells (K562). Extraction by methanol (EI), followed by ethyl acetate (EII), purified with hexane (EIII), mixture of E1 & EIII (EIV).

1.3.3 Wounds and wound healing

1.3.3.1 Background

The skin is the largest organ of the human body with numerous complex but important functions which enables it to function as the first line of defense against trauma, pathogenic organisms or toxins (Nemoto *et al.*, 2012). The human adult skin is made up of an upper keratinised stratified epidermis beneath which lies a thick layer of collagen-rich dermal connective tissue that provides support and nourishment. The exposure of the skin tissues to the external environment makes it vulnerable to damage and physical trauma. In order to restore its homeostatic balance, a rapid and efficient recovery of any break in its structure must be effectively restored to avoid any complications, (Rosique *et al.*, 2015).

1.3.3.2 Wound healing

A wound may be defined as a disruption in the continuity of the epithelial lining of the skin or mucosa which could arise from physical or thermal damage or an underlying medical condition. (Dhivya *et al.*, 2015). Wound healing is a dynamic process of tissue regeneration and growth through four overlapping phases, which are haemostasis and inflammation, migration, proliferation and maturation phases (Fig 1.6), (Beanes *et al.*, 2003).

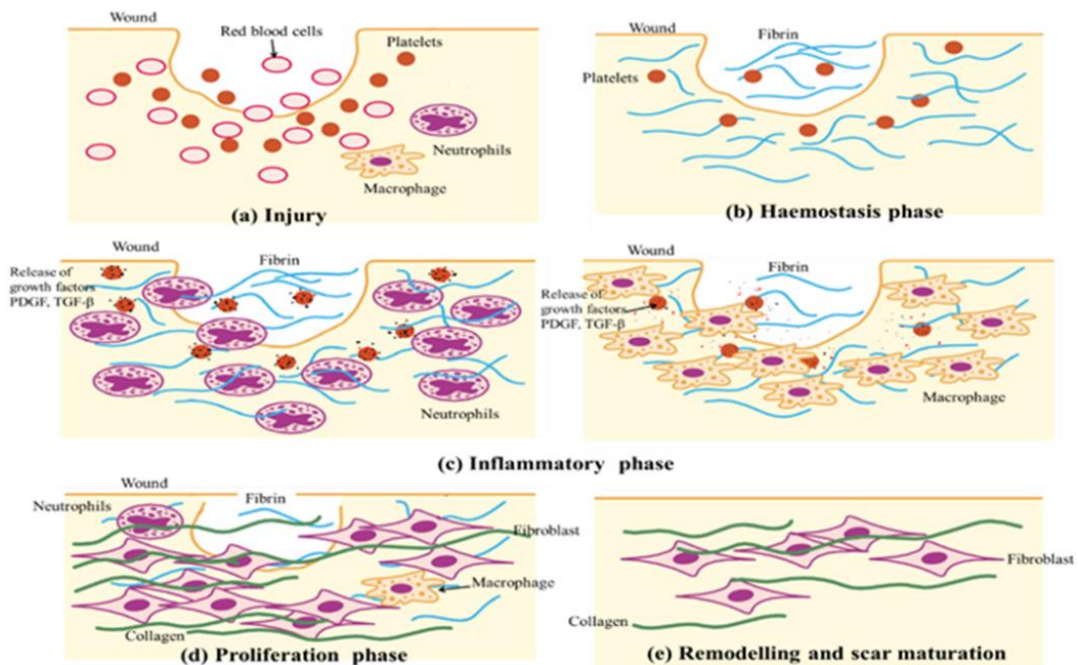


Figure 1.6. Stages of wound healing adapted from (Beanes *et al.*, 2003).

These phases and their biochemical and physiological functions must occur in the proper sequence, at a specific time, and continue for a specific duration at an optimal intensity (Mathieu *et al.*,

2006). There are many factors that can affect wound healing which interfere with one or more phases in this process, thus causing improper or impaired tissue repair. Bleeding usually occurs when the skin is injured and serves to flush out bacteria and/or antigens from the wound (Jameson and Havran, 2007; Mills *et al.*, 2008). The first phase, haemostasis begins immediately after wounding, with vascular constriction and fibrin clot formation. The clot surrounding wound tissue releases pro-inflammatory cytokines and growth factors such as transforming growth factor (TGF)- β , platelet-derived growth factor (PDGF), fibroblast growth factor (FGF), and epidermal growth factor (EGF).

Following haemostasis, neutrophils enter the wound site and begin the critical task of phagocytosis to remove foreign materials, bacteria and damaged tissue. The inflammatory phase occurs almost simultaneously with haemostasis, sometimes from within a few min to 24 h and lasts for about 3 days. It involves both cellular and vascular responses of macrophages which appear and continue the process of phagocytosis as well as releasing more PDGF and TGF- β . Once the wound site is cleaned out, fibroblasts migrate in to begin the proliferative phase and deposit new extracellular matrix (ECM). During the proliferative phase, vascular integrity is restored, the soft tissue defect is filled with new connective tissue produced by fibroblasts and the wound surface is covered with the new epithelium. The migratory and proliferative phases are inter-dependent *.i.e.* collagen synthesis and angiogenesis occur simultaneously, thus forming the granulation tissue which consists of capillary loops; fibroblasts, inflammatory cells and extracellular matrix (Campos *et al.*, 2008). The maturation phase also called the 'remodelling phase' involves the formation of cellular connective tissue and strengthening of the new epithelium which determines the nature of the final scar. Cellular granular tissue is changed to an acellular mass from several months up to about two years. In this phase, regression of many of the newly formed capillaries occurs, so that vascular density of the wound returns to normal. One critical feature of the remodelling phase is ECM remodelling to an architecture that approaches that of the normal tissue. The wound also undergoes physical contraction throughout the entire wound healing process, which is believed to be mediated by contractile fibroblasts (myofibroblasts) that appear in the wound (Gosain and DiPietro, 2004; Campos *et al.*, 2008).

1.3.3.3 Types of wounds

On the basis of duration and nature of the repair process, wounds can be classified as acute or chronic. An acute wound is an injury to the skin that occurs suddenly due to accidents, burns or chemical or mechanical injuries and usually heals in a predictable timeframe usually within 8 - 12 weeks depending on depth of the damage (Dhivya *et al.*, 2015). Chronic wounds are those that usually fail to heal within the expected time frame of 12 weeks and often reoccur due to disruptions in the orderly sequence of wound healing stages (Dhivya *et al.*, 2015). Such wounds fail to heal because of repeated tissue insults or underlying physiological conditions (Moore and Gray, 2008) such as diabetes and malignancies, persistent infections, poor primary treatment and other patient related factors. Chronic wounds include

diabetic foot ulcers, decubitus ulcers (bedsores or pressure sores) and leg ulcers (venous, ischaemic or of traumatic origin).

Wounds are also categorised based on the number of skin layers and area of skin affected (Boateng *et al.*, 2008). Injury that affects the epidermal skin surface alone is referred to as a superficial wound while injury involving both the epidermis and the deeper dermal layers including the blood vessels, sweat glands and hair follicles is referred to as partial thickness wound. Full thickness wounds by definition involve total loss of the epidermal and dermal layers, extending at least to the subcutaneous fat tissue layer and possibly as deep as the fascia muscle layer and the bone, (Boateng *et al.*, 2008).

Chronic wounds that produce liquid, fistulae or other more acute injuries following haemostasis have been described as exuding wounds. Exudate is essentially blood from which most of the red cells and platelets have been removed and forms a key component in all stages of wound healing, keeping wounds moist by continuous irrigation (Watson, 2012). Additionally exudate supplies the wound with leucocytes which helps to control bacteria and reduce the incidence of infection at the wound surface. The smell and staining of excessive exudate can have a negative impact on the patients overall health, psychological well-being and quality of life (Hareendran *et al.*, 2005) and it is therefore an important objective in clinical wound management.

1.3.3.3.1 Factors affecting wound healing

Foreign bodies introduced deep into the wound at time of injury can cause chronic inflammatory responses delaying healing and sometimes leading to granuloma or abscess formation. Other problems associated with wound healing are the formation of hypertrophic scars or keloid (raised) scars resulting from excess collagen production if the cells persist at the site in the latter part of the wound healing process (Mendonca and Coutinho-Netto, 2009). Pathogenic bacteria such as *Staphylococcus aureus*, *Pseudomonas aeruginosa*, *Streptococcus pyogenes* and some *Proteus*, *Clostridium* and *Coliform* species can be detrimental to the healing process. Inadequate control measures to manage infected wounds can lead to cellulitis (cell inflammation) and consequently bacteraemia and septicaemia, both of which can be fatal. Poor nutritional status and old age (Lee *et al.*, 2006) also reduce the ability to fight infection. Protein, vitamin (*e.g.* vitamin C) and mineral deficiencies impair the inflammatory phase and collagen synthesis, leading to prolonged healing times (Regan, 2007).

Pre-existing conditions such as diabetes (Falanga, 2005) and anaemia delay wound healing because compromised circulation results in the delivery of inadequate nutrients, blood cells and oxygen to the wound. Cancer can give rise to wounds in the form of multiple skin lesions or fungating wounds that frequently have associated symptoms. Malignant wounds may occur in up to 5% of patients with cancer and in 10% of patients with metastatic disease (Seaman, 2006). Fungating wounds are normally described when malignant tumours infiltrate and erode through the skin. Breast cancer, melanoma, bladder, colon, kidney, ovary, uterus, stomach, head and neck and lung cancers can all potentially cause fungating wounds, with fungating breast wounds being the most common. Fungating wounds frequently

have many associated symptoms including exudate, infection, slough/necrosis, bleeding, pain at wound site, itching and irritation and malodour. Exudate is considered the most common problem of fungating wounds and commonly causes leakage unto clothing (Regan, 2007).

1.3.3.4 Wound management

1.3.3.4.1 Wound dressings

Application of various dressings with varied functional characteristics is the most common means of managing wounds. More than 3000 products with varied functional characteristics have been introduced to treat different types of wounds by targeting various aspects of the wound healing process. Other factors which have contributed to the wide range of wound dressings include the different type of wound (*e.g.* acute, chronic, exuding, dry wounds *etc.*), however no single dressing is suitable for the management of all wounds (Dhivya *et al.*, 2015). Historically, wet-to-dry dressings have been used extensively for wounds requiring debridement (Shah, 2011) which is the removal of necrotic tissue or foreign material from areas around the wound to increase the chances of wound healing. This removal is important because the open wound bed cannot be observed and assessed effectively with necrotic tissue. The presence of necrotic tissue in a wound also increases the chances of infection and sepsis and consequently prolongs the inflammatory phase (Nigam *et al.*, 2006). Dressings are classified in different categories based on their function in the wound, type of material employed to produce the dressing and the physical form of the dressing (Falabella, 2006). Dressings are further classified into primary, secondary and island dressings (Van Rijswijk, 2006). Dressings which make direct physical contact with the wound surface are referred to as primary dressings while secondary dressings cover the primary dressing. Island dressings possess a central absorbent region that is surrounded by an adhesive portion (Boateng *et al.*, 2008). Other classification criteria include traditional dressings, modern and advanced dressings, skin replacement products and wound healing devices. However many dressing fit under multiple classifications.

1.3.3.4.1.1 Traditional dressings

These include topical liquid and semi-solid formulations as well as dry traditional dressings. Traditional dressings such as natural or synthetic bandages, cotton wool, lint and gauzes with varying degrees of absorbency were used for the management of wounds. Their primary functions were to keep wounds dry by facilitating evaporation of wound exudates and preventing entry of harmful bacteria into the wound. Topical formulations are prepared as liquid (solutions, suspensions and emulsions) and semi-solid (ointments, pastes, gels and creams) preparations and their use is widespread. However liquid dosage forms have short residence times on the wound site, especially where there is a measurable degree of suppuration (exuding) of wound fluid, while semi-solid preparations are not very effective on

the wound area of highly exuding wounds as they rapidly absorb fluid, lose their rheological characteristics and become mobile and messy.

1.3.3.4.1.2 Modern wound dressings

Due to the limitations of traditional dressings, modern dressings are based on the concept of creating an optimum environment to allow epithelial cells to move unimpeded, for the treatment of wounds. Such optimum conditions include a moist environment around the wound, effective oxygen circulation to aid regenerating cells and tissues and a low bacterial load. Modern wound dressings have been developed to facilitate the process of wound healing rather than just to cover the wound. Based on the cause and type of wound, numerous products are available in the market making the selection a very difficult task. Modern wound dressings are usually based on synthetic polymers and are classified as passive, interactive and bioactive products. Passive products are non-occlusive such as gauze and tulle dressings used to cover the wound to restore its function underneath. Interactive dressings are semi-occlusive or occlusive available in the forms of films, foams, hydrogel and hydrocolloids. These dressings act as a barrier against penetration of bacteria in the wound environment and are mainly classified on the basis of their functional material which includes hydrocolloids, alginates and hydrogels and generally occur in the form of gels, thin films and foam sheets.

1.3.3.4.1.2.1 Hydrocolloid dressings

Hydrocolloids are a family of interactive dressings obtained from colloidal (gel forming) materials such as carboxymethylcellulose combined with other materials such as elastomers and adhesives. Hydrocolloid dressings are useful because they adhere to both dry and moist wound sites and do not cause pain on removal (Boateng *et al.*, 2008). They are used for light to moderately exuding wounds such as pressure sores, minor burns and traumatic injuries. They are permeable to water vapour, impermeable to bacteria and used to manage leg ulcers where in addition to debriding properties, appear to be superior in the treatment of wounds that fail to respond to compression therapy alone (Koksal and Bozkurt, 2003). In their intact state hydrocolloids are impermeable to water vapour but on absorption of wound exudate, a change in physical state occurs with the formation of a gel covering the wound and become more permeable to water as the gel forms. As they do not cause pain on removal they are particularly useful in paediatric wound care management of both acute and chronic wounds (Dhivya *et al.*, 2015).

1.3.3.4.1.2.2 Carrageenan (CARR)

CARR's are a family of highly sulphated galactans which are strongly anionic polymers due to their half-ester sulphate moieties. CARR is linear, water-soluble, high molecular weight material with a high degree of polydispersity which typically forms highly viscous aqueous solutions from 70-90°C.

Commercially, CARR is available as stable sodium potassium and calcium salts or, most commonly, as a mixture of these. It comes in three types such as kappa, Iota and Lambda depending upon the position of the ester sulphate group (Nono, *et al.*, 2012).

1.3.3.4.1.2.3 Alginate dressings

These are produced from the calcium and sodium salts of alginic acid, a polysaccharide comprising mannuronic and guluronic acid units. Alginate dressings can occur either in the form of freeze-dried porous sheets (foams) or as flexible fibres, the latter indicated for packing cavity wounds. The use of alginates as dressings stems primarily from their ability to form gels upon contact with wound exudates (high absorbency). The high absorption occurs through strong hydrophilic gel formation, which limits wound secretions and minimises bacterial contamination (Dhivya *et al.*, 2015). Alginates rich in mannuronate form soft flexible gels upon hydration whereas those rich in guluronic acid form firmer gels upon absorbing wound exudate. When applied to wounds, ions present in the alginate fibre are exchanged with those present in exudate and blood to form a protective film of gel (Thomas, 2000).

1.3.3.4.1.2.4 Hydrogel dressings

Hydrogels are insoluble hydrophilic materials made from synthetic polymers such as poly (methacrylates) and poly-vinyl pyrrolidone. The high water content of hydrogels (70 - 90 %) helps granulation tissues and epithelium in a moist environment. Soft elastic property of hydrogels provides easy application and removal after the wound is healed without any damage. Temperature of cutaneous wounds is decreased by hydrogels providing soothing and cooling effect. Hydrogels are used for dry chronic wounds, necrotic wounds, pressure ulcers and burn wounds. It has been reported (Thomson, 2006) that with the exception of infected and heavily exuding wounds, hydrogel dressings are suitable for all four stages of wound healing. Hydrogel dressings are non-irritant, non-reactive with biological tissue and permeable to metabolites. Many researchers have reported that hydrogel dressings are used to treat chronic leg ulcers which can be difficult to heal. Limitations of hydrogel dressings include exudate accumulation which leads to maceration and bacterial proliferation that produces foul smell in wounds. In addition, they possess low mechanical strength making them difficult to handle (Dhivya *et al.*, 2015).

1.3.4 Advanced therapeutic dressings

In addition to protecting the wound bed from contamination, wound dressings can be exploited as platforms to deliver bioactive agents to wound sites or to take active part in the wound healing process.

1.3.4.1 Medicated dressings

The use of topical bioactive agents in the form of solutions, creams, and ointments for drug delivery to the wound is not very effective as they rapidly absorb fluid and in the process lose their rheological characteristics and become mobile (Boateng *et al.*, 2008). For this reason, the use of secondary wound dressings is preferred in the case of exudative wounds as they provide better exudate management and prolonged residence at the wound site. Advanced medicated dressings are designed to have biological activity either on its own or the release of bioactive constituents (drugs) incorporated within the dressing (Dhivya *et al.*, 2015). The incorporated drugs can play an active role in the wound healing process either directly as cleansing or debriding agents for removing necrotic tissues or indirectly as antimicrobial drugs which prevent or treat infection or growth agents (growth factors) to aid tissue regeneration (Momoh *et al.*, 2015, Boateng *et al.*, 2015). In chronic wound management where patients usually undergo long treatments and frequent dressing changes, a system that delivers drugs to a wound site in a controlled fashion can improve patient compliance and therapeutic outcomes. Bioadhesive, polymeric (synthetic, semisynthetic, or naturally derived) dressings are potentially useful in the treatment of local infections where it may be beneficial to achieve increased local concentrations of antibiotics while avoiding high-systemic doses, thus reducing patient exposure to an excess of drug beyond that required at the wound site (Boateng and Cantazano, 2015).

By controlling the degree of swelling, cross-linking density and degradation rate, delivery kinetics can be tailored according to the desired drug release schedule. Drug release from polymeric formulations is controlled by one or more physical processes including (1) hydration of the polymer by fluids (2) swelling to form a gel (3) diffusion of drug through the polymer matrix and (4) eventual degradation/erosion of the polymeric system (Pawar *et al.*, 2014). Upon contact of a dry polymeric dressing with a moist wound surface, wound exudate penetrates into the polymer matrix. This causes hydration and eventually swelling of the dressing to form a release system over the wound surface. In certain wound dressings, the mechanism for drug release has been explained by the hydrolytic activity of enzymes present in the wound exudates or from bacteria in the case of infected wounds (Dhivya *et al.*, 2015).

1.3.4.2 Biological dressings

Biological dressings are produced from biomaterials which play an important role in the healing process. These dressings are known for their biocompatibility, biodegradability and non-toxic nature and are derived generally from natural tissues or artificial sources such as collagen, hyaluronic acid, chitosan, alginate and elastin (Boateng *et al.*, 2008; Boateng and Cantazano, 2015). These materials are

used alone or in combination depending on the nature and type of wound. Biological dressings are sometimes incorporated with growth factors and antimicrobials to enhance wound healing process. Collagen a major structural protein has been reported by many researchers for their active role in natural healing process. Collagen initiates fibroblast formation and accelerates endothelial migration upon contact with wound tissue. Hyaluronic acid (HA) is a glycosaminoglycan component of extracellular matrix (ECM) with unique biological and physico-chemical features. Similar to collagen, HA is biocompatible, biodegradable and lacks immunogenicity. Chitosan promotes the formation of granulation tissue during the proliferative stage of wound healing. When compared to other dressings, biological dressings are reported to be more superior to other types of dressings (Dhivya *et al.*, 2015).

1.3.4.3 Tissue engineered skin substitutes

Human skin or dermal equivalent (HSE) has two types of tissue engineered substitutes available. The first one mimics the layer of skin composed of keratinocytes and fibroblast on collagen matrix (cell containing matrix), while the second contains only the dermal elements with fibroblast on collagen matrix (acellular matrix). Major mechanism of HSE is to secrete and stimulate wound growth factors by which epithelisation is achieved. Bioengineered skin substitutes are capable of adapting to their environment so that they are able to release growth factors and cytokines incorporated in dressings. Bioengineered dressings are suitable for diabetic foot ulcer and substitute consists of keratinocytes and fibroblast-seeded collagen for venous ulcers (Dhivya *et al.*, 2015).

1.3.5 Applications of BSs in wound healing

Inflammation is one of the main phases of wound healing in which tissue monocytes are activated and transform into macrophages, which are probably the main cells involved in control of the repair process (Van der Veer *et al.* 2011). Macrophage activation has implications for various aspects of wound healing, including phagocytosis of cellular debris, synthesis of extracellular matrix and release of cytokines that stimulate increased vascular permeability, angiogenesis and epithelialisation. The release of factors from platelets is the main stimulus for migration and macrophage activation, while the phagocytosis of cellular components such as fibronectin or collagen also contributes towards the healing process (Henderson *et al.* 2011).

BSs are known to have anti-inflammatory activities (Seydlova and Svobova, 2008) and therefore potential wound healing effect. Rhamnolipids have been reported for the re-epithelisation of mucous membrane tissues, particularly for the treatment and prevention of gum disease and promote periodontal regeneration (Stipcevic *et al.*, 2006). Additionally, low concentrations of rhamnolipids are able to inhibit the phagocytic actions of macrophages (McClure and Schiller, 1996) and therefore control the inflammatory phase. Stipcevic *et al.*, (2006) investigated the wound healing properties of di-rhamnolipid BAC-3 formulated as an ointment and applied topically on full thickness burn wounds in normal Spague-Dawley rats covering 5% of the total body surface area. At higher concentrations (\geq

500 µg/ml), the di-rhamnolipid BAC-3 was found to be toxic and caused necrosis due to haemolytic action arising from its detergent property. This appeared to be associated with the insertion of two apolar fatty acid residues into the phospholipid bilayer of the cell membrane. However, the di-rhamnolipid BAC-3 was generally well tolerated when administered subcutaneously, once daily for 7 days to female Swiss-Webster mice in doses up to 120 mg/ (kg day) (Stipcevic *et al.*, 2006). Byeon *et al.*, (2008) observed that surfactin was able to downregulate LPS-induced nitrous oxide production in RAW264.7 cells and primary macrophages by inhibiting NF-kB, MAPK, and Akt pathways. Sophorolipids have acted as desquamating and depigmenting agents by eliminating the surface portion of the protective layer of the epidermis as part of the wound healing process. Additionally sophorolipids are stimulators of skin fibroblast metabolism contributing to skin restructuring, repair and protection (Concaix *et al.*, 2003).

1.4 Aims and objectives

The overall aim of the study is to investigate the pharmacological and biopharmaceutical properties of four selected BSs on cancer cells and wound healing activity. This involves establishing the potential biocidal, anti-microbial and anti-inflammatory activities of BSs to determine which of their structural characteristics may be tuned for greater efficacy.

1.4.1 Hypothesis

1. The cytotoxicity of BSs is linked to the composition of their hydrophilic head and hydrophobic tails as well as the presence of congeners and isomers. BSs can form mixed micelles which exert a detergent-like effect that disrupts the plasma membrane.
2. BSs are known to have anti-inflammatory activities and therefore potential wound healing effect. Incorporation of free BSs and BSs based niosomes in composite CARR/SA gels may affect the functional properties of lyophilised wafer wound dressings.

1.4.2 Aims

1. Testing of the anti-proliferative activity for several BSs on THP-1, MCF-7 and control HEK 293 cell lines.
2. Formulation & testing of free BSs and BSs based niosomes within lyophilised composite polymeric wafers.

1.4.3 Objectives

1. The structures, functional groups, and compositions of the selected BSs will be analysed using attenuated Fourier transform infra-red spectroscopy (ATR-FTIR), high performance chromatography (HPLC) and liquid chromatography coupled mass spectrometer (LC-MS).
2. Growth curves will be produced for three cell lines (MCF-7, THP-1, HEK 293) in order to identify log phase and ideal culturing conditions.

3. Cytotoxicity will be detected following cell line-specific optimisation at 24, 48, and 72 h. By testing types of BSs at the three time intervals, effect of association on three cell lines will be investigated. Cell viability will be determined by MTT assay measured with microplate photometer.
4. Pre-formulation studies to identify and characterise biocompatible and biodegradable polymeric systems, with potential for targeting wound healing and deliver BSs, will be carried out, which will range from basic formulation (such as polymer gel preparation to identifying optimum compositions that will ensure wafer stability.
5. Investigation of the physico-chemical and bioanalytical properties of BSs from lyophilised composite wafers.
6. Investigation of the physico-chemical and bioanalytical properties of BSs based niosome loaded wafers and comparison with pure BSs loaded wafers.

CHAPTER 2 INSTRUMENTATION AND THEORY OF EXPERIMENTAL TECHNIQUES

2.1 Key analytical/ experimental techniques

Compounds from natural resources require analytical techniques to characterise their physico-chemical properties to confirm identity and purity of the compounds and their stability under real life and stressed storage conditions, such as solid state form, polymorphisms, hydrates or solvates. The main analytical tools employed to characterise the BSs are briefly discussed below.

2.1.1 Attenuated total reflectance Fourier transform infrared spectroscopy (ATR-FTIR)

Infrared spectroscopy is a standard method of analytical pharmacy and chemistry which provides the images of vibration of atoms within compounds. Therefore it is also referred to as vibrational spectroscopy. IR spectrum is obtained by passing infrared radiation through the sample and determining what fraction of the incident radiation is absorbed at a particular frequency. IR is a fingerprint technique which can be used to confirm structural confirmation as well as for quality control in pharmaceutical industries (Dole *et al.*, 2011).

2.1.1.1 Instrumentation

The two types of instruments customarily used for IR are dispersive and Fourier transform. The dispersive instrument uses a monochromator while the Fourier transform uses an interferometer. The term Fourier transformation originated from a mathematical operation demonstrated by 'Jean Fourier' which converts frequency into time domain (Dole *et al.*, 2011). Fourier transform infrared (FTIR) spectrometers have almost entirely replaced dispersive instruments because of their better performance in terms of speed and efficiency. The instrument consists of an interferometer, fixed mirror, a movable mirror, beam splitter. The IR region of the electromagnetic spectrum has dimension of wavenumbers extending from $\sim 13000\text{ cm}^{-1}$ to $\sim 10\text{ cm}^{-1}$. The 3 main infrared regions; near, middle and far regions span from $\sim 13000\text{ cm}^{-1}$ to 4000 cm^{-1} , 4000 cm^{-1} to 400 cm^{-1} , and 400 cm^{-1} to 10 cm^{-1} wavenumbers, respectively (Bellisola and Sorio, 2012). To enable, electromagnetic absorption a bond must have a dipole moment and the intensity of radiation depends on the dipole moments as well as the electronegativity of the atoms in the molecule.

ATR-FTIR operates by the same electromagnetic principle that governs basic IR spectroscopy which absorbs molecular bonds ranging from $400 - 4000\text{ cm}^{-1}$. ATR is used for qualitative and quantitative analysis and it exploits the characteristic of molecular bonds which have regions of absorption (Bellisola and Sorio, 2012). Solid and liquid samples with no preparation can be analysed through ATR crystals (Zn selenide, germanium, or diamond) (Fig 2.1). ATR has revolutionised IR spectroscopy in terms of faster sampling, sample preparation, reproducibility and minimal user

variation. A minimum amount of sample is required for analysis, however to obtain accurate results, a background test must first be run to reduce the incidence of noise. In ATR-FTIR spectroscopy, wavelength of the incident radiation affects the depth of penetration of IR radiation into the sample. The infrared spectrum is formed as a consequence of the absorption of electromagnetic radiation at frequencies that correlate to the vibration of specific sets of chemical bonds from within a molecule (Bellisola and Sorio, 2012). The results are analysed by asymmetrical and symmetrical stretching and bending movements of characteristic frequencies or wavelength with different vibrational energies peaking at a particular energy. In the case of FTIR, strong infrared light on the sample is absorbed by vibrational energy and monitoring what's left after light passes through potassium bromide (KBr) discs, while in ATR, the light passes from underneath, bounces above and then travels back through the sample again to elicit the required spectroscopic output.

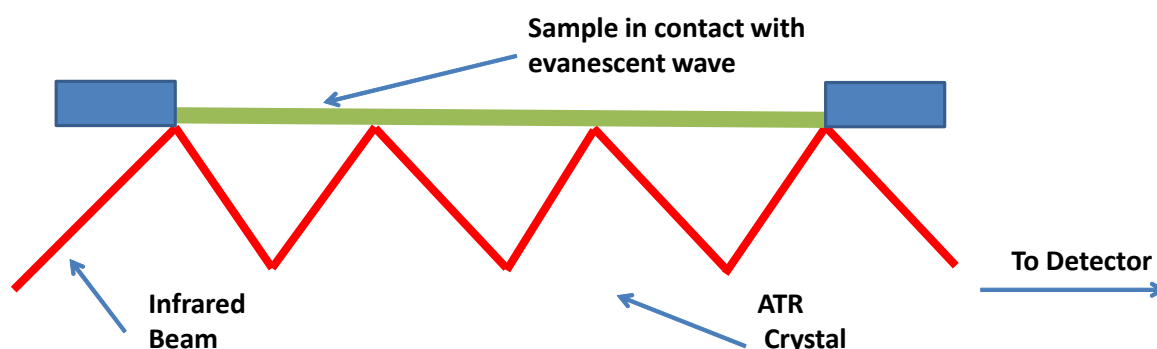


Figure 2.1. A multiple reflection ATR system. A classic method for structure analysis is IR spectroscopy. Irradiation of molecules with IR light induces an oscillation of chemical bonds at characteristic frequencies and thus energy is absorbed.

2.1.1.2 Applications in material and formulation characterisation

Fourier transform infrared spectroscopy is a versatile tool in pharmaceutical science research, with a wide field of applications ranging from characterisation of formulations to elucidation of kinetic processes in drug delivery. Recent new applications of these methods include study of drug delivery systems and in particular topical drug delivery system. ATR-FTIR method is used to study drug penetration, and influence of penetration modifiers and also in *in vivo* studies.

ATR-FTIR has also been used widely in biological studies where it has been used to analyse adsorbed species on solid/ liquid interphases. With the use of single or multiple internal reflection elements (IRE), the exact penetration depths of samples are determined by the angle of incidence and refractive indices of both ATR crystal and sample, and the wavelength of light, (Watson, 2005). Pawar *et al.*, (2014) used wafers combining drug-loaded biological dressings to improve chronic wound healing and used ATR-FTIR analysis to demonstrate intermolecular interactions responsible for the physical stabilities of the wafers. The release patterns of ketoconazole using dodecanol-collodion

membrane as an acceptor membrane and vaseline as an ointment base were studied with the help of ATR-FTIR (Wartewig *et al.*, 2005; Kazarian and Chan 2006). Boateng *et al.*, (2015) compared the mucoadhesive performance of antimicrobial solvent cast film and freeze-dried wafer dressings using ATR-FTIR spectroscopy by monitoring the diffusion of mucin solution [2% w/w in phosphate buffered saline (PBS) pH 7.4] through the formulations. ATR-FTIR spectroscopy showed that mucin diffused independently through the solvent and across the films and wafers.

2.1.2 High performance liquid chromatography (HPLC)

Chromatography is an analytical technique based on the separation of molecules due to differences in their structure and/or composition. In general, chromatography involves moving a sample through the system over a stationary phase. The molecules in the sample will have different affinities and interactions with the stationary support, leading to separation of its constituent molecules. Sample components that display stronger interactions with the stationary phase will move more slowly through the column than components with weaker interactions. Chromatographic separations can be carried out using a variety of stationary phases, including immobilised silica on glass plates (thin-layer chromatography), volatile gases (gas chromatography), paper (paper chromatography) and liquids (liquid chromatography). A mobile phase is described as a fluid which percolates through or along a stationary bed in a definite direction and may be a liquid, gas or a supercritical fluid, (Ardrey, 2003).

High-performance liquid chromatography (HPLC) is the most widely used analytical technique used in pharmaceutical industries and is used for qualitative as well as quantitative analysis (Kupiec, 2004) because it results in highly efficient separations and in most cases provides high detection sensitivity (Bhardwaj *et al.*, 2015). It can be used to analyse the various components of mixtures using normal and reverse phase mechanisms with a stationary (sorbent) and mobile phase. The most widely used components of stationary phases are silica gel particles of varying pore sizes, while the mobile phase which is further divided into A (weak) and B (strong) solvents, can be individual or combinations of hexane, dichloromethane, isopropanol or methanol (normal phase) and methanol or acetonitrile, modified with aqueous acid *e.g.* trifluoroacetic acid and tetrahydrofuran (for reverse phase). Majority of HPLC separations utilise reverse phase chromatography in which the mobile phase is more polar than the stationary phase which results in the faster elution of the more polar analytes. It is not always possible to achieve adequate separation by using isocratic elution which may lead to longer retention times especially for non-polar analytes. Therefore combinations of solvents that accelerate longer retaining compounds are juxtaposed during gradient elution. The boiling point, surface tension and conductivity of mobile phase affects the performance of an interface and therefore degassing the solvents to prevent bubble formation is vital. The results are analysed based on retention time, area under the peak and flow rate.

2.1.2.1 Instrumentation

The major components of a typical HPLC system includes a mobile phase reservoir, pump, injector, column and a detector. HPLC employs various detectors such as UV/Vis spectrophotometer, diode array spectrophotometer, within a wavelength of 280 - 546 nm, however for mixtures which lack chromophores evaporative light scattering detectors (ELSD) and mass spectrometers can be used, (Watson, 2005).

The selectivity of a detector is its ability to determine an analyte of interest without interference from other materials present in the analytical system. Data analysis is through a digital microprocessor and specialist software and depending on the type of detector data such as the retention time, the peak areas, molecular weight, mass to charge, concentration are obtained. These results are matched to reference libraries and used to identify components of mixtures (congeners, structural isomers, proteins and/or lipids). Most of the drugs in multi component dosage forms can be analysed by HPLC method because of several advantages like rapidity, specificity, accuracy, precision and ease of automation in this method. HPLC methods development and validation play important roles in new discovery, development, manufacture of pharmaceutical drugs and various other studies related to humans and animals (Bhardwaj *et al.*, 2015).

2.1.2.2 Liquid chromatography mass spectrometer (LC-MS)

Mass spectrometry is the determination of a mass-to charge ratio of an analyte either on its own or within a mixture. The major components of a mass spectrometer must include methods of sample introduction, ion production, ion separation and ion detection & data manipulation

The multidimensional applications of mass spectrometry (MS) enables molecular, qualitative and quantitative analysis, which has accelerated the drug discovery process from clinical trials to regulatory approval. Mass spectrometry detection is superior to other chromatography detectors because it can provide specific identity based on the molecular weight and structure of the unknown when compared to a spectral library. A full scan spectrum can be obtained from picogram (pg) amounts of analytes. The main limitation of chromatography is the inability to completely identify an unknown compound based on its retention times which may be similar for other compounds. The mass spectrometer inlet system for liquid chromatography also called the interface between the two components must remove as much unwanted mobile phase as possible while transferring the maximum amount of analyte into the mass spectrometer and generate all available analytical information (Ardrey, 2003). Buffers are used to control the rate of ionisation. The incompatibilities of the mobile phase and pressure make the coupling of the two systems challenging, because the mobile phase of HPLC is in liquid form. Further, analytes separated by HPLC are relatively volatile and sometimes thermally labile and therefore not amenable to harsh ionisation by certain mass spectrometers. However, the introduction of electrospray ionisation (ESI) placed mass spectrometry in a leading position in biopolymer structure bioanalysis, (Deziel, 1999).

Ionisation methods that may be utilised in LC-MS include electron ionisation (EI), chemical ionisation (CI), fast atom bombardment (FAB), thermospray (TSP), electrospray (ESI) and atmospheric-pressure chemical ionisation (APCI). A mass spectrum may be considered to be a plot of the number of ions of each m/z ratio produced by an analyte upon ionisation. The quadrupole mass analyser, (quadrupole) ion-trap, double-focusing and tri-sector, time-of-flight mass analysers may be used to separate ions of different m/z ratios, determine m/z values and measure the relative intensities of each group of ions. Sensitivity of the system increases when a partial scan which covers a small number of m/z ratios is obtained in a technique known as selected-ion monitoring (SIM). The total ion current (TIC) shows the sum of the intensity of each of the chromatographic separation by giving peaks. The retention changes with column length and flow rate (Ardrey, 2003). The multidimensional applications of mass spectrometry (MS) enables molecular, qualitative and quantitative analysis, which has accelerated the drug discovery process from clinical trials to regulatory approval.

CHAPTER 3 SYSTEMATIC COMPARISON OF THE FUNCTIONAL PHYSICO-CHEMICAL CHARACTERISTICS AND BIOCIDAL ACTIVITY OF MICROBIAL DERIVED BIOSURFACTANTS ON BLOOD-DERIVED AND BREAST CANCER CELLS

3.1 Introduction

Different types of cancers; (*e.g.* carcinomas, hybridomas, haematological or solid tumours) may give variable responses to drugs. Differences in responses to treatment may also be due to enzymes, proteins and lipids which are peculiar to these malignancies.

Cell culture allows the study of the relationship between host cells and intracellular microorganisms, the analysis of immunological parameters such as cytokines and other proteins, the evaluation of antimicrobial effectiveness, and the performance of cytotoxic assays (evaluation of the effects of drugs or other agents on cancer cells) including measurement of viability and proliferation in cell cultures. These methods can be used as monitoring tools to determine if a sample stimulates, inhibits and/or affects cell growth and viability. The cell-line growth curves are applied in the evaluation of the characteristics of cell growth, which shows a lag-phase immediately after reseeding. This is the time required for a cell to recover from trypsinisation, to rebuild its cytoskeleton, and to secrete an extracellular matrix that facilitates the linkage between the cells and their propagation along the substrate. The duration of this phase could range from a few h up to 48 h. Subsequently, the cell enters into exponential growth referred to as the log-phase, in which the cell population doubles at a characteristic rate defined as doubling time (DT) (characteristic for each cell line). Therefore, the effects of drugs and chemical agents that stimulate or inhibit cell growth can be studied. Finally, when the cell population is very dense and all the substrate has been metabolised, the cells enter into a stationary phase, where the rate of growth drops to almost zero (Freshney, 2006).

Due to their structural novelty and diverse biophysical properties, lipopeptides, glycolipids and other BSs have recently emerged as possible broad-spectrum agents for cancer chemotherapy (Gudiña *et al.*, 2013). The cytotoxic activity of the selected BSs on cancer cells has been reported by a number of authors (Zhao *et al.*, 2013; Thanomsub *et al.*, 2006; Christova *et al.*, 2010; Cao *et al.*, 2011; Cao *et al.*, 2009a; Cao *et al.*, 2009b; Duarte *et al.*, 2014; Rashad *et al.*, 2014; Ribiero *et al.*, 2015; Jing *et al.*, 2006). However, the pharmacological effects of BSs on blood derived monocytic cancer cells has not been reported. In this study, the biological (*e.g.* anti-cancer) activities of these BSs is of particular interest. Furthermore, this research sheds new light on the action of lactonic sphorolipids on breast cancer cells.

Some metabolic enzymes such as cytochrome P450 (CYP450) and glutathione S-transferase activate certain anti-cancer drugs. The presence of CYP450 shows inter-individual variation and

therefore its detection, identification and quantification prior to starting treatment is essential (Alfarouk *et al.*, 2015). As a result, optimisation of ideal culturing conditions would create a means of interpreting dose response curves. Growth curves for 3 cell lines (THP-1, MCF-7 and HEK 293) were studied to identify optimal log phase for drug testing. The growth curves for MCF-7 and HEK 293 were determined using trypan blue (TB) and MTT assays, while THP-1 was observed using trypan blue only. In these studies MTT assay was optimised under various conditions before the commencement of dose and time dependent studies.

The aim of this work therefore was to functionally characterise the physico-chemical properties and systematically compare the surface active properties and cytotoxicity of the four selected biosurfactants (R-95TM rhamnolipid (BS1a), R-90TM rhamnolipid (BS1b), surfactin (BS2) and 1', 4''-sophorolactone 6', 6''-diacetate from yeast (BS3)) against blood derived and breast cancer cell lines using MTT assay. Pre-formulation characterisation of selected microbial BSs and a positive control are important in order to recognise changes in the character of the drug during and after formulation (Narang and Desai, 2009). Therefore in this study, attenuated total reflectance Fourier transform infrared spectroscopy (ATR-FTIR), liquid chromatography mass spectrometer (LC-MS), and surface tension were used to analyse and characterise the four selected BSs used in this research. These analytical techniques were used to confirm their structural characteristics, which are essential for confirming their identity and functional activity.

3.2 Materials and methods

3.2.1 Chemicals and reagents

R-95TM rhamnolipid (BS1a), R-90TM rhamnolipid (BS1b), surfactin (BS2) and 1', 4''-sophorolactone 6', 6''-diacetate (BS3) from yeast, doxorubicin hydrochloride, penicillin/streptomycin and MTT (3-[4,5-dimethyl-2-thiazolyl]-2,5-diphenyl-2H-tetrazolium bromide) were purchased from Sigma Aldrich (Gillingham, UK). Dulbecco's modified eagles medium (DMEM), supplemented with 10% heat inactivated foetal bovine serum [Origin: EU approved (South American)] in PET bottle (Gibco). All other reagents were of analytical grade and used as received.

3.3 Physico-chemical characterisation of BSs

3.3.1 Attenuated total reflectance Fourier transform infrared spectroscopy (ATR-FTIR)

Before ATR-FTIR analysis the diamond crystal surface was cleaned and background spectra were collected. Samples were individually placed with just enough material to cover the crystal area. The pressure arm was positioned over the sample area and the arm of a Spectrum 100 series universal ATR accessory was locked into a precise position above the diamond crystal. This allowed force to be applied to the sample to ensure proper contact with the diamond crystal. IR spectra were collected

between 400 and 4000 wave numbers (cm^{-1}) at a scan rate of 0.2 using a Perkin Elmer UATR Two infrared spectrometer.

3.3.2 High performance liquid chromatography (HPLC)

HPLC analysis was carried out for surfactin (BS2) and sophorolipid (BS3), both of which possess a UV chromophore, using an Agilent 1200 HPLC system composed of vacuum degasser, auto sampler, quaternary pump, UV-detector and an electronic integrator (HP Chemstation software rev A.09). An aliquot (20 μl) of the standard BS2 solution was injected onto a reversed-phase Gemini C18 column (250 x 4.6mm internal diameter; 5 μm particle size) (110A S/N 267789-48) held at room temperature. The mobile phase was flushed through the system for 10 min before beginning each run, and the samples were then eluted using an isocratic mobile phase composed of acetonitrile (0.1%) : trifluoroacetic acid (TFA) in deionised water (70:30, v/v) at a flow rate of 0.7 ml/min. The eluted components were detected using UV at 210 nm. The BS3 solutions were analysed using the same column and mobile phase as for BS2 but with mobile phase flow rate of 0.5 ml/min and detection of 205 nm.

3.3.3 Liquid chromatography mass spectrometry (LC-MS)

3.3.3.1 HPLC/ESI-MS of rhamnolipids

Compositional analysis of 95 (BS1a) and 90% (BS1b) rhamnolipids were performed by modifying (Dézuel *et al.*, 1999) HPLC/ESI-MS method. Briefly, 0.1 mg/ml of BS1a and BS1b were prepared in methanol and 1 μl was injected onto Micromass Quattro Ultima (Waters, Wilmslow, UK) triple quadrupole mass spectrometer system using a 10 cm x 2.1 mm Supelco Ascentis Express (Supelco, Bellefonte, PA, USA) C18 reverse phase column (particle size 2.7 μm) in a mobile phase reverse phase gradient composition of A: water + 0.1% (v/v) formic acid and B: acetonitrile + 0.1% (v/v) formic acid. The gradient conditions were set as follows: initial composition of A : B (75 : 25), A : B (50 : 50) at 30 min, A : B (10 : 90) at 45 min, A : B (10 : 90) at 50 min, A : B (75 : 25) at 70 min and a re-equilibration of A : B (75 : 25) for 20 min. The mobile phase flow rate was 0.25 ml/min which was not split. Experiments were conducted using an electrospray ionisation (ESI) source operated in negative ion mode with a capillary voltage of 3.2 kV, 15 V cone voltage, a source and probe temperatures at 150°C and desolvation temperature of 400°C while the scanning mass range was from 50 - 900 m/z units.

3.3.3.2 HPLC/ESI-MS/MS of surfactin

Compositional analysis of BS2 was performed by modifying a previously reported HPLC/ESI-MS/MS method (Pecci *et al.*, 2010). Briefly, 0.1 mg/ml of BS2 was prepared in a mobile phase (see below) and 1 μl was injected on to a Waters (Manchester, UK) ACQUITY UPLC® BEH C18 column (particle size: 1.7 μm). A mobile phase gradient was employed with composition of A: water + 0.1% (v/v) formic acid and B: acetonitrile + 0.1% (v/v) formic acid. The flow rate was 0.5 ml/min to the electrospray source. The gradient conditions were an initial composition of A : B (50 : 50) , A : B (50 : 50) at 0.34

min, A : B (0 : 100) at 2.38 min, A : B (0 : 100) at 2.95 min, A : B (50 : 50) at 3.00 min and a re-equilibration of A : B (50 : 50) at 5 min. No splitter was used, so the entire flow was introduced to the electrospray source and the UPLC column temperature was maintained at 40°C throughout the run. Experiments were conducted using an electrospray ionisation (ESI) source operated in positive ion mode with a capillary voltage of 1.5 kV. Initially, 15 V cone voltage was used to generate typical MS data confirming elution order, approximate purity profile and mass analysis. Consequently an elevated cone voltage of 100 V was used to generate pseudo MS/MS spectra on a Waters QDA single quadrupole mass spectrometer. The source and probe temperatures were at 120°C and 600°C respectively while the scanning mass range was from 100 - 1250 m/z units.

3.3.3.3 HPLC/ESI-MS of sophorolipids

Compositional analysis of BS3 was performed by modifying a previously HPLC/ESI-MS and HPLC/ESI-MS/MS method (Ribeiro *et al.*, 2015). Briefly, 5 mg/ml of BS3 was prepared in a mobile phase (see below) and 1 μ l was injected on to a Waters (Manchester, UK) Acquity reverse phase chromatography system using an ACQUITY UPLC® BEH C18 column (particle size: 1.7 μ m) in a mobile phase reverse phase gradient composition of A: water + 0.1% (v/v) formic acid and B: Acetonitrile + 0.1% (v/v) formic acid. The flow rate was 0.25 ml/min to the electrospray source and the gradient conditions were an initial composition of A : B (50 : 50), A : B (50 : 50) at 0.6 min, then A : B (40 : 60) at 3.2 min, A : B (0 : 100) at 5.7 min, A : B (0 : 100) at 6.9 min, A : B (50 : 50) at 8.2 min and a re-equilibration of A : B (50 : 50) at 10 min. No splitter was used, so the entire flow was introduced to the electrospray source and the UPLC column temperature was maintained at 40°C throughout the run. Experiments were conducted using an electrospray ionization (ESI) source operated in positive and negative ion mode with a capillary voltage of 1.5 kV and 15 V cone on Waters QDA UPLC single quadrupole. The source and probe temperatures were set at 120°C and 600°C respectively while the scanning mass range was from 100 - 800 m/z units.

For all LC-MS analyses, nitrogen was used as both nebulizer and cone gas and supplied at a pressure of approximately 6 bars.

3.3.4 Measurement of critical micelle concentration (CMC) and minimum surface tension

The surface tension and critical micelle concentration (CMC) of BS1a, BS1b, BS2 and BS3 were measured. These biosurfactants have chain lengths of 12-18 carbon atoms, a range over which only BS1a and BS1b are soluble at room temperature, while BS2 and BS3 were soluble in Tris HCl buffer at pH 8.5. The surface tension measurements were undertaken at a temperature of $25 \pm 1^\circ\text{C}$ using a bubble pressure tensiometer (SITA Science on-line t60, Germany), calibrated by reference to de-ionised water (Mansour *et al.*, 2015). Surface tension was recorded at a bubble life time value of 10,000 sec.

Their surface tensions decrease with increasing concentrations until their CMC's are reached above which their plateau surface tensions are as low as 26.9 mN/m indicating excellent surface activities.

3.4 Cell-growth curves

3.4.1 Trypan blue growth curve for THP-1, MCF-7 and HEK 293 cells

Once the cell lines reached 80 to 90% of confluence, Cell were seeded in 96 well plates (100 μ l/well) at concentrations of 2.5×10^5 cells/ml, 1×10^5 cells/ml and 5×10^4 cells/ml for THP-1, MCF-7 and HEK 293 respectively. Plates were incubated at 37°C in a CO₂ incubator over a period of 10 days. Samples from each cell lines were collected after 4 h and daily thereafter. Adherent cells were first detached via trypsin, then stained with trypan blue (SIGMA) at a 1:2 dilution and counted in a Neubauer hemocytometer. Non adherent cells were directly stained with trypan blue (SIGMA) at a 1:2 dilution and counted in a Neubauer hemocytometer. Each experiment was carried out in triplicates and repeated three times.

3.4.2 MTT growth curve for MCF-7 and HEK 293 cells

Cells were plated as above and after 4 h incubation and daily thereafter, 10 μ l of 3-[4, 5-dimethyl-2-thiazolyl]-2, 5-diphenyl-2H- tetrazolium bromide (MTT) reagent was added to the wells and incubated for a further 4 h. Subsequently, 75 μ l of supernatant media was discarded from each of the wells after which 50 μ l of DMSO was added to solubilise the formazan formed in the treated wells. The plate was incubated for 10 min and analysed on a plate reader at 540 nm. Each experiment was repeated three times.

3.5 Cytotoxicity studies

3.5.1 Cytotoxicity against THP-1 cells

Cytotoxicity of BS1a, BS1b, BS2 and BS3 and DOX against human leukemic monocyte (THP-1), ECACC number 88081201) cell lines obtained from American Tissue and Cell Culture (ATCC), was also determined by MTT assay according to the optimised protocol below. THP-1 cells were grown in RPMI 1640 medium (Sigma Aldrich, UK) supplemented with 10% foetal bovine serum (heat inactivated) (Gibco, UK and 1% penicillin/streptomycin (Sigma Aldrich, UK)). The THP-1 cells suspended in 50 μ l RPMI 1640 medium were seeded in 96 well plates at a concentration of 5×10^5 cells/ml and treated with 50 μ l each of the four BSs and DOX at different concentrations using RPMI 1640 as diluting agent. After 24, 48 and 72 h incubation at 37°C in 5% CO₂ respectively, 10 μ l of 5 mg/ml MTT in PBS were added to the wells, and the cells were incubated for another 4 h at 37°C. After the 4 h of incubation with MTT reagent, the THP-1 cells were spun down at 600 g for 5 min. Finally, 50 μ l of DMSO was added after 75 μ l of media supernatant had been withdrawn. The formation of

formazan was measured using multiscan EX microplate photometer at 540 nm. Cell viability was calculated according to the following equation:

$$\text{Cell viability (\%)} = (A_{Tr} / A_{UTr}) \quad \text{Equation 3.1}$$

where A_{Tr} is the absorbance of cells treated with BSs and DOX and A_{UTr} is the absorbance of untreated cells. IC_{50} value was calculated from dose-response curves of the cell viability versus concentration graphs, plotted using GraphPad Prism 5.

3.5.2 Cytotoxicity against MCF-7 and HEK 293 cells

Cytotoxicity of BS1a, BS1b, BS2 and BS3 and doxorubicin hydrochloride (DOX) (Sigma Aldrich, UK) against human Caucasian breast adenocarcinoma (MCF-7 ECACC number 86012803) and non-cancerous human embryo kidney (HEK 293, ECACC 85120602) cell lines obtained from American Tissue and Cell Culture (ATCC), were determined by MTT (Sigma Aldrich, UK) assay according to the optimised protocol below. MCF-7 and HEK 293 were sub-cultured in Dulbecco's modified eagles medium (DMEM), and all were supplemented with 10% heat inactivated foetal bovine serum (Gibco, UK) and 1% penicillin/streptomycin (Sigma Aldrich, UK). MCF-7 and HEK 293 cells suspended in 100 μ l DMEM medium were seeded in 96 well plates at a concentration of 10^5 cells/ml and incubated at 37°C in 5% CO_2 for 24 h. Both cells were then treated with the BSs and DOX at different concentrations using DMEM as diluting solution. After 24, 48 and 72 h respectively, 10 μ l of 5 mg/ml MTT in PBS solution was added to the wells and the cells were incubated for another 4 h at 37°C. The positive and negative controls (untreated cells and cell treated with BSs and DOX) were included in the assay. The formation of formazan was measured using multiscan EX microplate photometer at 540 nm as described above and cell viability calculated using equation 3.1 described previously.

3.5.3 Statistical analysis

All numerical data was analysed using GraphPad Prism 5. IC_{50} values were extrapolated from dose-response curves using the sigmoidal-dose response (variable) model. To obtain the IC_{50} values, dose-response curves of the % viability were generated using a four-parameter nonlinear regression with either variable or fixed slope (Prism, GraphPad). Using a constrained or fixed Hill slope of -1, bottom and top plateaus of 0 and 100 respectively, BSs and DOX concentrations were log transformed and the % viability was plotted using nonlinear regression. This analysis with a fixed Hill slope provided the parameter of potency (IC_{50}) but without the index of cooperativity as the Hill slope was standardised.

3.6 Results and discussion

3.6.1 Physico-chemical characterisation

The physico-chemical properties of the four BSs were characterised using various analytical techniques to confirm their structural characteristics, which are essential for confirming their identity and functional activity.

3.6.1.1 ATR-FTIR spectroscopy

3.6.1.1.1 ATR-FTIR spectrum of 95% and 90% rhamnolipids

The dominant absorbance bands of the two rhamnolipids (BS1a and BS1b) are shown in (Fig 3.1). The strong, broad bands around $3331\text{-}3335\text{ cm}^{-1}$ are attributed to hydrogen bonding and O-H stretching of the hydroxyl groups. The double bands centred at $2925\text{-}2928$ are assigned to asymmetric stretches for CH (in CH_2 groups) whilst those centred at $2855\text{-}2856\text{ cm}^{-1}$ are derived from symmetric C-H stretching vibrations of aliphatic groups such as those represented in the hydroxydecanoic acid chain tails. A C=O stretching band at 1731 cm^{-1} is characteristic of ester bonds and carboxylic acid groups. In the fingerprint region of the spectrum, the area between $1445\text{-}1380\text{ cm}^{-1}$ represents C-H and O-H deformation vibration, typical for carbohydrates as in the rhamnose units of the molecule. The lower range of the fingerprint region below 1200 cm^{-1} represents different kinds of C-H, C-O and CH_3 vibrations which cannot be allocated more specifically (Zhao *et al.*, 2013). It should be noted that all the above reference used rhamnolipids obtained from different model organisms, culture and purification conditions and this accounts for the slight differences in the IR spectra of samples used in this study and those reported in the reference.

3.6.1.1.2 ATR-FTIR spectrum of surfactin

The IR spectrum of surfactin (BS2) (Fig 3.1) were evaluated with focus on the main bands. The absorption band with a maximum of 3300 cm^{-1} corresponding to the N-H stretch can be attributed to peptide residues. Another intense band with maxima of 2957 cm^{-1} and 2927 cm^{-1} , corresponding to the C-H (CH_3) and (CH_2) stretch, can be associated with the lipopeptide portion of the molecule. At 1719 cm^{-1} , a medium intensity band is observed that can be related to the absorption of C=O groups from lactonisation. At 1643 cm^{-1} a CO-N stretch is attributed to the amide group while bands at 1467 cm^{-1} and 1387 cm^{-1} indicate aliphatic chains ($-\text{CH}_3\text{-CH}_2$). These results agree with the analysis of Sousa and co-workers (2014) and suggest that the surfactin employed in this study was of the expected standard.

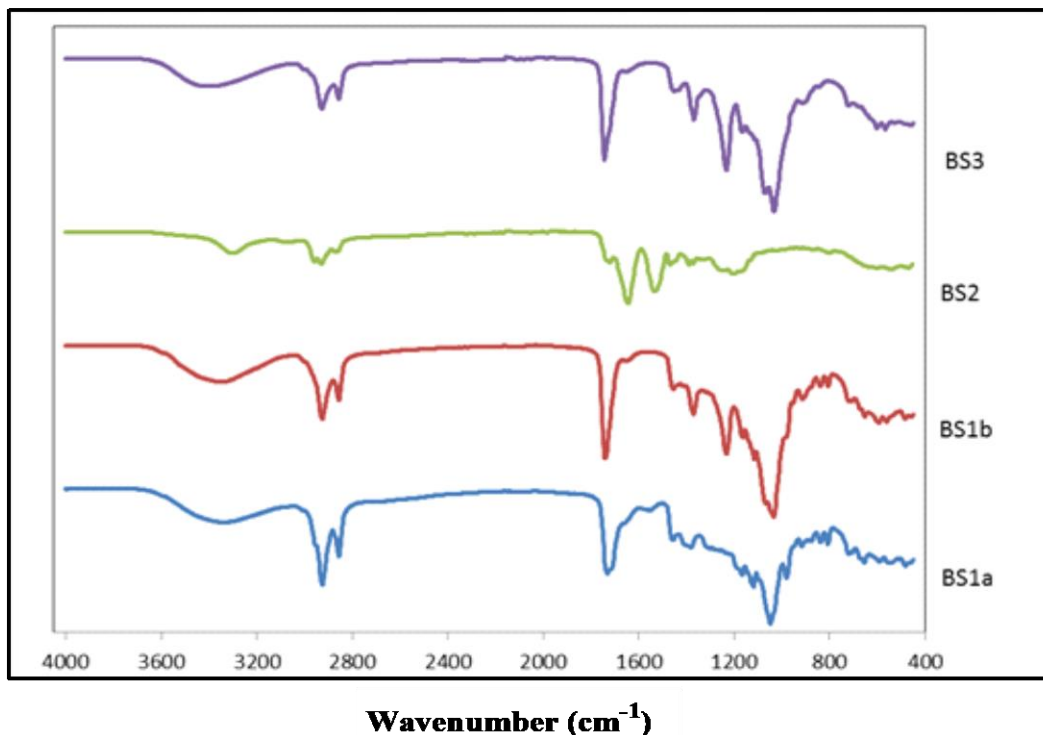


Figure 3.1. ATR-FTIR spectra of 95% rhamnolipid (BS1a), 90% rhamnolipids (BS1b), surfactin (BS2) and sophorolipids (BS3).

3.6.1.1.3 ATR-FTIR spectrum of sophorolipids

The dominant absorbance bands for sophorolipids (BS3) are shown in (Fig 3.1). The spectra revealed broad bands at 3406 cm^{-1} which correspond to O-H stretching, while asymmetrical and symmetrical stretching of methylene occurred at 2927 cm^{-1} and 2856 cm^{-1} respectively. The absorption band at 1744 cm^{-1} was attributed to C=O stretching from lactone esters or acids. The bands at 1451 cm^{-1} corresponded to the C-O-H in the plane binding of carboxylic acids (-COOH). The C=O absorption band from acetyl esters was observed at 1232 cm^{-1} , while the stretch of C-O band of C (-O)-O-C in lactone groups can be observed at 1166 cm^{-1} . The C-O stretch from C-O-H groups of sugar (sophorose moiety) was observed at 1071 cm^{-1} . Finally the IR spectra revealed the absorption band for C=C at 721 cm^{-1} . With the exception of 3406 cm^{-1} which corresponded to the O-H stretch, all structural details analysed were found to be similar to those reported by (Rashad *et al.*, 2014).

3.6.1.1.4 Comparison of IR spectra between the different BSs

As a result of different chemical structures (Fig 3.1), the BSs showed different FTIR fingerprints; BS2 showed very distinct pattern between $400\text{-}1600\text{ cm}^{-1}$ which may be due to the lack of sugar residues and the presence of amide (-CO-N stretch) at 1643 cm^{-1} and an unassigned shoulder at $1467\text{-}1387\text{ cm}^{-1}$. BS1a and BS1b (representing both rhamnolipids) had bending of O-H bands in the carboxylic acid group at $1445\text{-}1370\text{ cm}^{-1}$, (C-O-C stretching of rhamnose sugars with a shoulder and pyranyl 1 sorption

band 1232-1034 cm^{-1} (shoulder) (C-O-C stretching in the rhamnose), (pyranyl I sorption band) & (α -pyranyl II sorption band at 916 cm^{-1} and 806-838 cm^{-1} respectively). On the other hand, BS3 had [(C-O-H in plane binding of carboxylic acids at 1451 cm^{-1} , C=O absorption band due to acetyl esters at 1232 cm^{-1} , (C-O band of C (-O)-O-C due to lactones) at 1166 cm^{-1} , (C-O stretch from C-O-H sophorose sugars at 1071 and 721 cm^{-1} (C=C)]. Details of the differences in the FTIR profiles of the four selected biosurfactants, are summarised in Tables 1 and 2 in the supplementary data in the appendix section.

3.6.2 High performance liquid chromatography (HPLC)

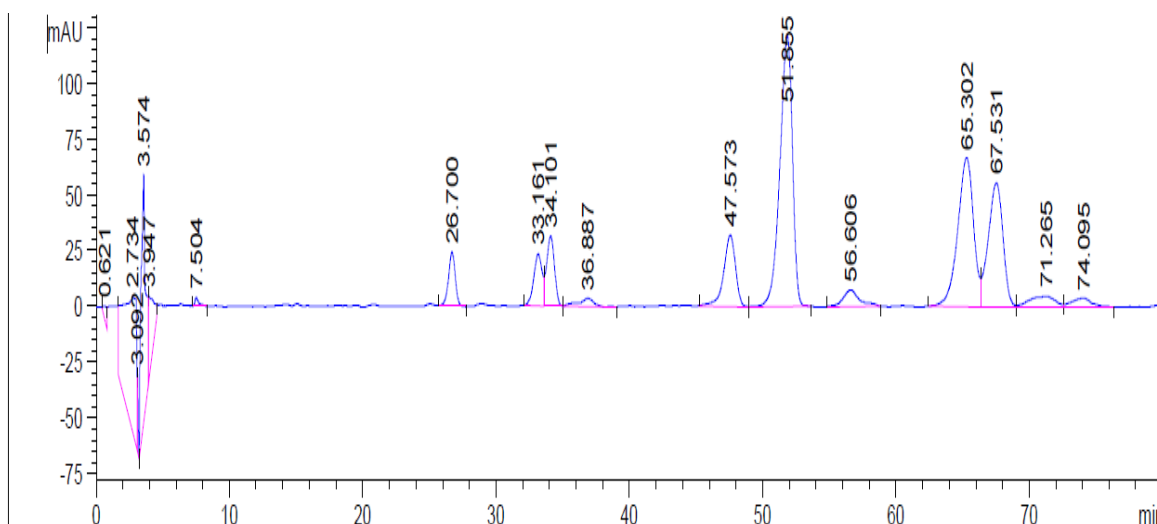
As the selected BSs will be incorporated into novel drug delivery systems to test their release for biological activity, HPLC was used to analyse surfactin and sophorolipids since they possessed chromophores which allowed UV detection during the HPLC run.

3.6.2.1 HPLC of surfactin

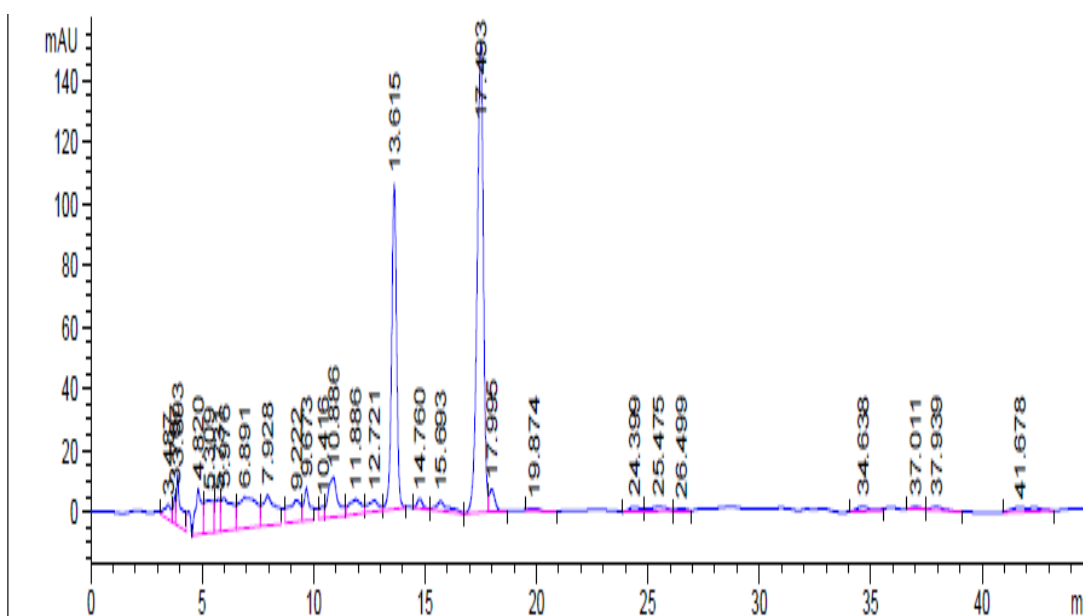
As will be expected of a microbial derived biosurfactants, the standard surfactin showed a complex mix of different isoforms and Fig 3.2a shows that the sample contained nine isoforms, which eluted between 26 and 67 min. Of these isoforms, seven were major namely, peaks 1, 2, 3, 4, 5, 7, 8, and two were minor namely, peaks 6, and 9. In addition, the Fig 3.2a shows that the peaks were well separated except isoform peaks 2 and 3, which differed in their retention times by less than 1 min. Once the conditions had been optimised, HPLC was repeated 10 times for the purpose of reproducibility and the standard deviation between the 10 runs was 0.94. This result was in accordance with that obtained by (Abdel-Mawgoud *et al.*, 2008), and therefore deemed acceptable.

3.6.2.2. HPLC of sophorolipids

Standard sophorolipid (Fig 3.2b) contained two major isoform peaks, which eluted between 13 and 17 min. The Fig shows that the peaks were well separated and differed in their retention times by about 4 min. Once the conditions had been optimised, HPLC was repeated 10 times for the purpose of reproducibility with a standard deviation of 0.03 which was deemed acceptable.



(a)



(b)

Figure 3.2. Representative HPLC chromatogram of (a) surfactin (b) sophorolipids.

3.6.3 Liquid chromatography mass spectrometer (LC-MS)

LC-MS was used to characterise the selected biosurfactants, which was particularly useful for the two rhamnolipids (BS1a and BS1b) due to their lack of a functional chromophore, which meant that it was not possible to analyse them using HPLC with UV detection.

3.6.3.1 LC-MS of 95% and 90% rhamnolipids

Seven main peaks were obtained from the LC-MS spectra of BS1a (Fig 3.3A & C) at m/z values of 175.1, 233.4, 621.8, 649.9, 503.6, 677, and 175.1 respectively. However, the peaks at m/z 175 which

occurred at retention times of 0.74 and 63 min could not be assigned and did not correspond to any congeners found in literature and therefore suspected to be noise. The most abundant ions were found at m/z 649.9 and 503.6 which have been identified as the (Rha₂-C₁₀-C₁₀), and (Rha-C₁₀-C₁₀) congeners respectively (Déziel *et al.*, 1999; 2000). On the other hand, nine main peaks were obtained from the LC-MS spectra of BS1b (Fig 3.4B & 4D) at m/z values 181.1, 621.7, 475.7, 650.0, 649.9, 503.7, 677.8, 531.7, 191.1 respectively. However, as was the case for BS1a, the peaks at m/z 181 and 191 which occurred at 0.74 and 63 min were not assigned and did not correspond to any congeners found in literature. Further, the most abundant ion was an unassigned peak at m/z 650.0 with a relative abundance of 23%. This was followed by m/z 677 which was identified as the isomeric pair Rha₂-C₁₂-C₁₀/ Rha₂-C₁₀-C₁₂ with a relative abundance of 19.3%. The peaks at m/z 503.7 and 649.9 were identified as (Rha-C₁₀-C₁₀) and Rha₂-C₁₀-C₁₀ with elution times of 40 and 37 min respectively. However, unequivocal identification would only be possible if tandem-MS/mode is employed.

The most predominant components for 95% and 90% rhamnolipids correlated with the results from Zhao *et al.*, 2013, which were obtained from crude extracts analysed by ESI-MS. In their study, the mass spectrum of mono-rhamnolipid (R₁) showed intense molecular ions at m/z 333, 475, 503 and 529 with molecular ion at m/z 503 as the predominant component, which corresponded with the known structure of mono-rhamnolipids. On the other hand, their mass spectrum of di-rhamnolipid (R₂) samples showed the presence of signals at m/z 479, 621, 649, 677 and 685 with predominant ion at m/z 649 corresponding to di-rhamnolipids. Tandem-MS/mode was used to unequivocally identify the predominant R₁ ion as Rha-C₁₀-C₁₀ which showed daughter ions at m/z 333 corresponding to a ruptured ester link, m/z 169 corresponding to breaking of fatty acid chain and m/z 163 corresponding to the fragmented link in the rhamnose-alkyl chain. In the case of R₂, the major molecular ion with m/z 649 was identified as Rha₂-C₁₀-C₁₀ which gave daughter ions at m/z 479 corresponding to a rupturing of the ester link to give Rha-C₁₀ and hydroxyl decanoate (m/z 169) as well as another daughter ion at m/z 163 corresponding to a single rhamnose.

The congeners in this research were further confirmed on the basis of (Deziel *et al.*, 1999) who reported the synthesis of rhamnolipids from 2 separate cultures grown on mannitol and naphthalene. For the mannitol culture, 28 congeners were identified although most were in trace amounts. However, the pseudo molecular ion at m/z 475 was the base peak but some fragment ions were observed at m/z 305, 311 and 333. Further, collision induced fragmentation in their study revealed that the pseudo molecular ion at m/z 475 were the isomers Rha-C₈-C₁₀ and Rha-C₁₀-C₈ which co-eluted under negative electrospray ionisation. Additionally, m/z 305 and 333 ions were cleaved at the 3-carbon-oxygen bond to give corresponding daughter ions at m/z 141 and 169. Furthermore m/z 163 produced by the cleavage of the rhamnose moiety was common to both BS1a and BS1b. The predominant ion was identified as Rha-Rha-C₁₀-C₁₀ with a relative abundance of 56.9%. While the most abundant 3-hydroxy fatty acids were C₈, C₁₀, and C₁₂; unsaturated C_{12:1} and C_{14:1} rhamnolipids were also observed.

In a further study (Deziel *et al.*, 2000) comparing LC-MS with direct infusion which did not require prior chromatographic separation, 23 congeners were identified, with Rha-Rha-C₁₀-C₁₀, Rha-C₁₀-C₁₀, Rha-C₈-C₁₀, Rha₂-C₁₀-C₁₂ and Rha-C₁₀-C_{12:1} and Rha₂-C₁₀-C₈ being the most abundant congeners. Chistova *et al.*, (2011) detected mono- and di-rhamnolipid congeners as anions at m/z values of 503 and 649, which corresponded to the deprotonated molecules of Rha-C₁₀-C₁₀ (mono-rhamnolipid) and Rha₂-C₁₀-C₁₀ (di-rhamnolipid) respectively. When both congeners were subjected to further tandem-MS mode, the pseudo molecular ion at m/z 503 produced two major fragment peaks at m/z 333 and 339 corresponding to ruptured ester links as well as m/z 169 corresponding to released fatty acid. However, the fragmentation of the main pseudo molecular ion at m/z 649 produced daughter ions at m/z 479 corresponding to the rupture of the ester bond between the two alkyl chains in di-rhamnolipid. The other characteristic ions they detected were m/z 339 representing the cleavage of the link between the rhamnose and alkyl moiety as well as a daughter ion at m/z 163 corresponding to the single rhamnose detected.

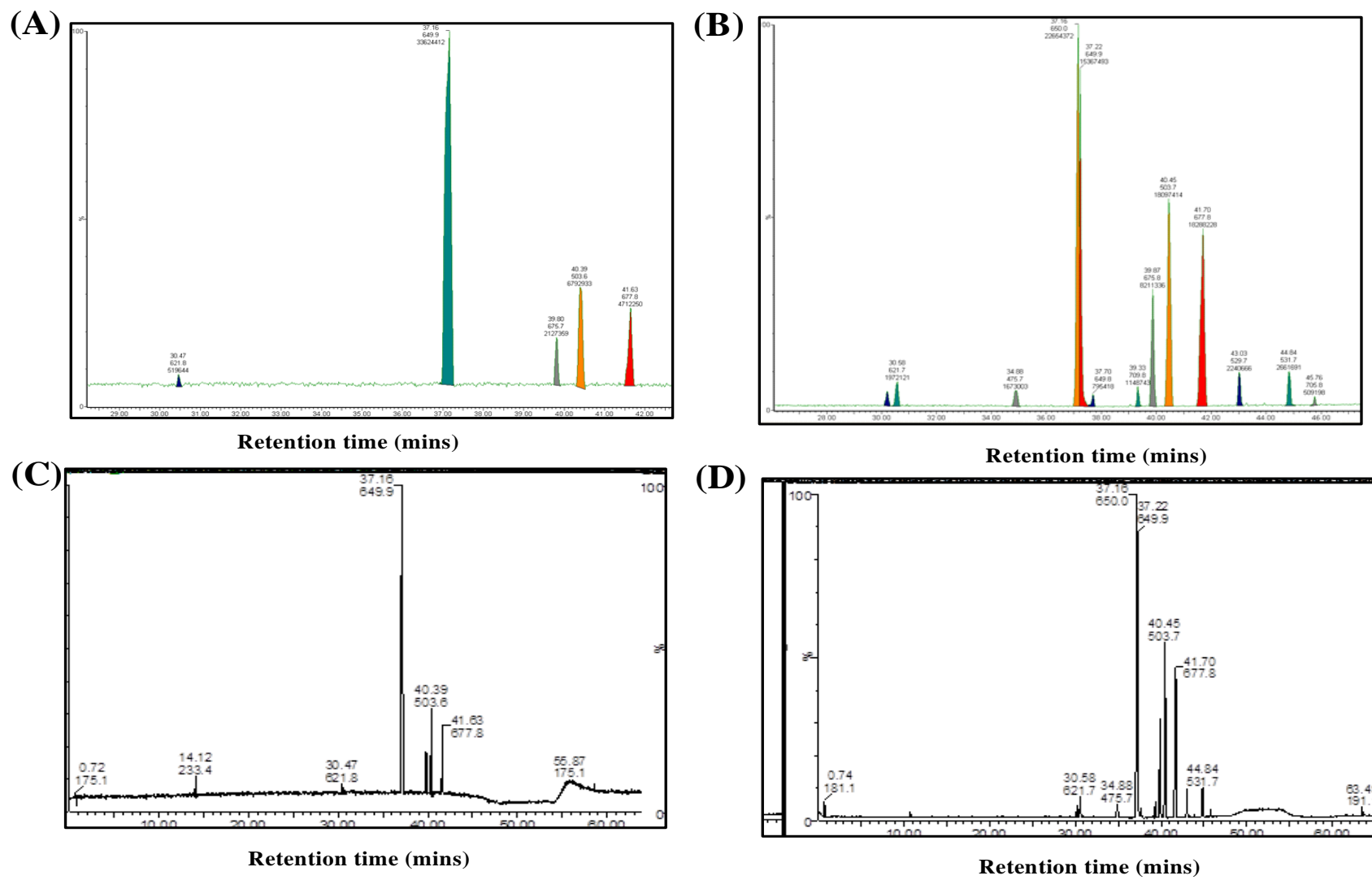


Figure 3.3. Total ion chromatograms of BS1a and BS1b (A & B respectively) and corresponding mass spectra (C & D respectively).

3.6.3.2 LC-MS of surfactin

The sample provided was nominally of 98% purity with a given molar mass of 1036.34 g/mol. Multiple peaks were observed in the extracted ion chromatogram, suggesting that several structural isomers are present. These peaks were independently resolved into 8 mass spectra. The structural isomers resolved from each mass spectra were putatively assigned to members of surfactin family based on literature as summarised in Table A3 of the appendix. The heterogeneity in the Leu/Ile at the 2nd and 7th position respectively of the peptide sequence of surfactin is well established. However, resolution of Leu and Ile using LC-MS is quite challenging. Therefore, surfactin was further characterised by tandem mass spectrometry at higher cone voltage of 100 V, however, the fragmentation pattern was observed to predominantly match the results obtained at lower voltage. The peaks at m/z 995, 1009, 1023, 1037, 1051 may represent the $[M + H]^+$ ions of the same surfactin basic structure but with difference in mass of 14 Da, suggesting that the metabolites produced during microbial synthesis differ only in the length of the fatty acid chain component. Alkali metal ion (*e.g.* Na^+) adducts are a common feature in the mass spectra of surfactin, by binding of the metal ion to free carboxylic acid groups in the biosurfactant. The sodium and potassium adducts of surfactin are the most common, as these metal ions are ubiquitously present in nature (Hue *et al.*, 2001; Vater *et al.*, 2002). The addition of chloride salts of these metals to surfactin samples, greatly enhance the relative intensity of corresponding metal ion species in the mass spectra (Hue *et al.* 2001; Williams and Brodbelt, 2004). The precursor ions m/z 1017, 1031, 1045, 1059 and 1073 can be attributed to sodium ion adducts of surfactin homologues with m/z 995, 1009, 1023, 1037 and 1051, (Figs A1 and A2). The precursor ion m/z 1061 in the mass spectra (data not shown) can be attributed to potassium adduct of surfactin homologue with m/z of 1023. The absence of any strong basic amino acids in surfactins preferentially make peptide bonds and ester groups to be protonated, and thus making them susceptible targets for intra-molecular nucleophilic cleavage reactions mediated by $-C=O$ groups adjacent to these protonated sites.

3.6.3.3 LC-MS of sophorolipids

The sophorolipid sample provided was nominally of 70% purity with a given molar mass of 688 g/mol thus providing a protonated ion of m/z of 689. Fig A3 in appendix shows the total ion chromatograms and Fig 3.4 shows a representative mass spectrum of the sophorolipid sample analysed. Multiple peaks, 1 – 7, containing m/z 689 were observed in the extracted ion chromatogram, with the sodiated adduct at m/z 711, suggesting the presence of several structural isomers. In the 0-100% ion chromatogram, seven peaks were eluted, with most showing overlapping signals. The second chromatographic peak at retention time of 2.34 min had a shoulder on the left side of the peak resulting from a co-eluted peak at 2.26 min. These peaks were independently resolved into seven mass spectra all of which showed other masses not observed in the ion chromatogram, however, individual identification of each m/z peak was beyond the scope of the current study.

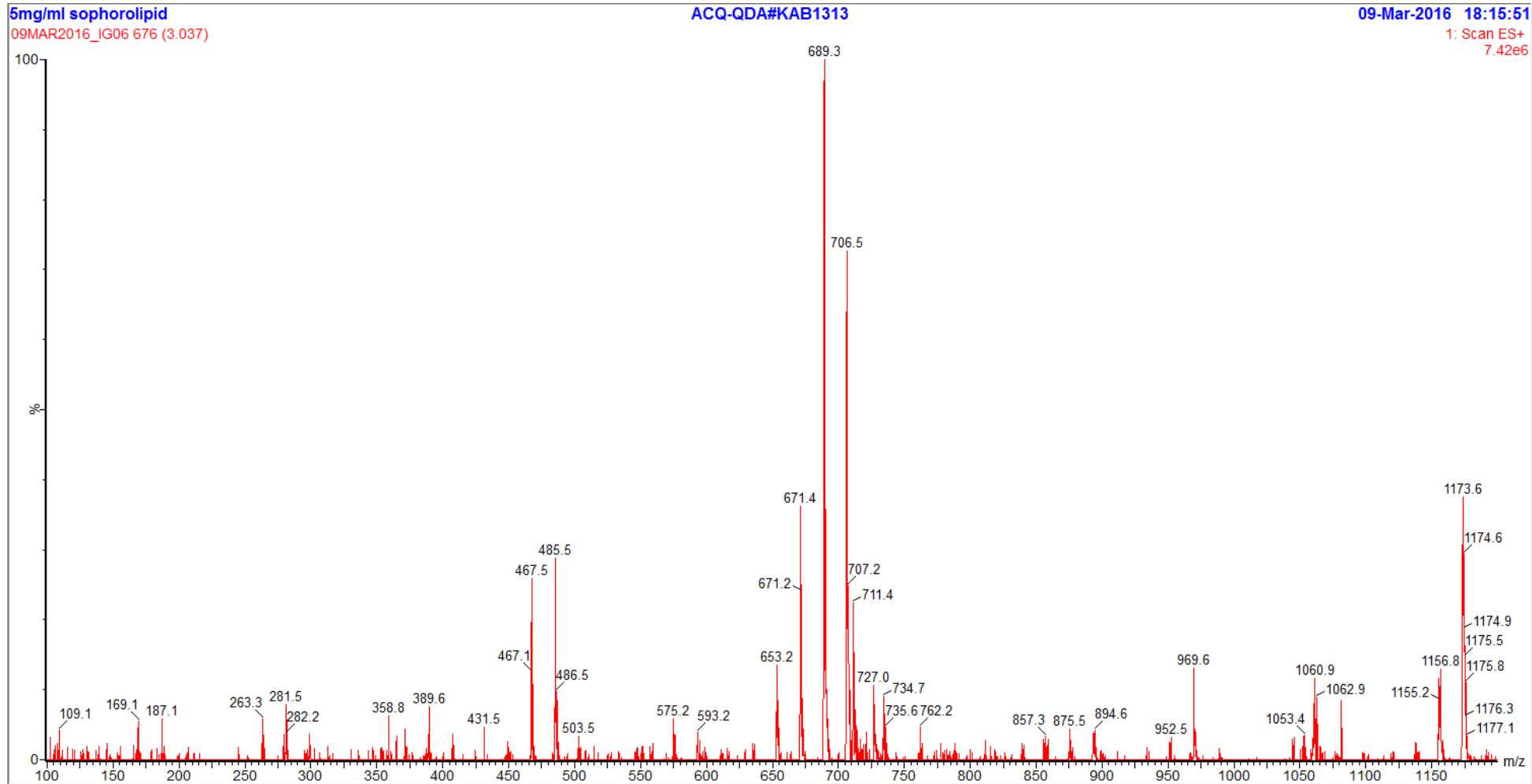


Figure 3.4. Representative LC-MS spectrum of sophorolipid (BS3) sample analysed.

3.6.4 Critical micelle concentration and surface tension (ST)

The critical micelle concentration (CMC) is the point at which the amount of surfactant added to solutions begins to form micelles whilst surface tension (ST) is a measure of the work required to bring a molecule from the bulk phase to the surface (Rosen, 1978). Table 3.1 shows comparative CMC and minimum ST data of the four BSs analysed. The CMC values of the BSs were significantly lower in comparison with chemical surfactants such as sodium carboxylate which has a CMC value of 1805 mg/L (Stanley *et al.*, 2009). The surface tension of water is 72.75 mN/m (at 20°C) and good BSs can reduce surface tension of water to 35 mN/m, (Manivasgan *et al.*, 2014). This is interesting and suggests that the BSs used in this study possessed excellent surface lowering properties with surface tension ranging between 26.00 – 32.96 mN/m. Rhamnolipids have been found to reduce the surface tension of water to 26.90 mN/m at a CMC of 51.50 mg/L (Nitschke *et al.*, 2005), surfactin to 27.00 nN/M at a CMC of 10 mg/L (Yeh *et al.*, 2005) and sophorolipids to 33.50 mN/m at CMC of 9.50 mg/L (Joshi-Navare *et al.*, 2013) and all these reported values correspond to the data obtained in this research as shown in (Table 3.1). The CMC of ionic detergents is determined by the combined effect of the repulsive and hydrophobic interaction effect on membrane proteins and lipids by their head and tail groups respectively. A detergent is a small amphiphilic molecule which when added to the solution surrounding a lipid bilayer, interacts with the hydrophobic tails of the lipids. As a result of this the detergent tends to disrupt the bilayer. If the interacting membrane contains proteins, (*e.g.* cell membrane), the hydrophobic tails of the detergent molecules also interact with the hydrophobic parts of the membrane proteins.

Table 3.1. CMC and minimum ST Values of the four selected BSs ($n = 3$, \pm SD)

Surfactants	CMC (μ g/ml)	Minimum S.T. (mN/m)
BS1a	4.78	27.20 (\pm 0.06)
BS1b	6.01	26.00 (\pm 0.17)
BS2	16.90	26.90 (\pm 0.10)
BS3	7.68	32.96 (\pm 0.05)

Consequently, the detergent molecules confer biocidal properties by displacing cell membrane phospholipids and end up forming water-soluble detergent-protein complexes. Ortiz *et al.*, (2006), described the molecular interaction between the phospholipid acyl chains of a phosphatidyl choline membrane and produced di-rhamnolipid molecule as a consequence of the intercalation between the di-rhamnolipids and phospholipids. The alignment of the hydrocarbon chains of the di-rhamnolipid with the phospholipids acyl chains can disrupt the phospholipid packing, reduce cooperativity of the transition and shift the phase transition temperature to lower values.

Rhamnose is a deoxy sugar, sophorose is a disaccharide while leucine, asparagine and glutamic acid are amino acids present in surfactin, as opposed to the amino sugar in doxorubicin. It is

hypothesised that their amphiphilic parts fuse with the phospholipid bilayer of the cell membrane via passive diffusion to exert a detergent-like effect that disrupts the plasma membrane. The double bonds and length of hydrocarbon chain contained in microbial biosurfactants may reduce the strength of hydrophobic interactions and disrupt the phospholipid packing of the membrane bilayer. In this research, the four biosurfactants had hydrocarbon tails in the order of BS3 > BS2 > BS1b/ BS1a (elucidated by MS data). The sophorolipids tested in this study has a chain length of 18 carbon atoms followed by surfactin which varied in chain length from 12-16 carbon atoms and rhamnolipids with 2 double chains of 12 carbon atoms. It is hypothesised that these hydrocarbon chains forms mixed micelles with the phospholipid bilayer to exert a detergent-like effect that disrupts the plasma membrane. This is consistent with the CMC of BSs recorded in (Table 3.1).

3.7 Cytotoxicity of biosurfactants (BSs)

3.7.1 Growth curves

The aim of this section was to determine the growth curves for the cell lines to identify optimal log phase for testing with the BSs. It was important to analyse the behaviours of the individual cell-lines, to inform the subsequent evaluation of the anti-proliferative effects of the selected BSs. The growth curves for MCF-7 and HEK 293 cells were determined using trypan blue (TB) and MTT assays, while the non-adherent cancerous THP-1 cell was observed using trypan blue only. Further discussion can be found in the supplementary data (section A3.1) of the appendix.

3.7.2 Dose response curve of biosurfactants on THP-1, MCF-7 and HEK 293

MTT assay was carried out on three cell lines following 24, 48 and 72 h of exposure to the BSs and showed significant changes in cell proliferation at the different time points as outlined below. The chemotherapy agent DOX employed as positive control showed IC₅₀ values higher than all the BSs which is to be expected. The cytotoxicity profiles of BS1a, BS1b, BS2, BS3 and DOX against THP-1 are shown in Fig 3.5 whilst the profiles of the most potent BSs (BS3) against MCF-7 are shown in Fig 3.6. The corresponding IC₅₀ values of all the BSs and DOX against the three cell lines are summarised in Table 3.2. More detailed discussion for activity of the BSs and DOX against the two cancerous cell lines (THP-1 and MCF-7) is provided below.

3.7.2.1 Rhamnolipids (BS1a and BS1b)

THP-1 showed sensitivity to BS1a at concentration of 48.71 µg/ml after 72 h, (Table 3.2) but a much greater effect was observed with BS1b after 48 and 72 h with IC₅₀ of 14.47 and 8.10 µg/ml respectively. These results differ from a previous study (Christova *et al.*, 2013) on human pre-B leukemic line BV-173, T-cell chronic lymphocytic leukaemia SKW-3 and human promyelocytic leukaemia HL-60 cell lines. The IC₅₀ they obtained for mono-(Rha-C₁₀-C₁₀) and di-(Rha₂-C₁₀-C₁₀) rhamnolipid congeners after 72 h exposure were (50, 54, 67) µM and (82, 108, 77) µM respectively

indicating greater potency of mono-rhamnolipids in comparison to di-rhamnolipids. This may be due to the differences in composition of the different congeners, or cell line differentiations. Dose-response curves showed that BS1a had an IC_{50} of 33.08 $\mu\text{g/ml}$ on MCF-7 cells after 72 h (Table 3.2). This was a much lower cytotoxic effect compared to that obtained by (Zhao *et al.*, 2013; Thanomsub *et al.*, 2006), who reported values at 1 $\mu\text{g/ml}$ and 6.25 $\mu\text{g/ml}$ respectively after 48 h. This may be due to the fact that BS1a is a mixture of both di-rhamnolipids and mono-rhamnolipids. Zhao *et al.*, (2013) reported no activity when mono-rhamnolipids congeners and the crude extract were tested on MCF-7. However, BS1b showed greater sensitivity on MCF-7 cells which may be due to the activity of the predominant congener which was unassigned from the LC-MS data. Cytotoxicity may also be due to the presence of the second most abundant congener which was the isomeric pair Rha₂-C₁₂-C₁₀/ Rha₂-C₁₀-C₁₂. This contradicts (Thanomsub *et al.*, 2006) report that no activity was detected and therefore requires further investigation. BS1b appeared to be toxic to normal cells (Table 3.2) after 24 h but this cytotoxicity decreased after 48 and 72 h. The anticancer action of rhamnolipids (BS1a & BS1b) may be due to the capacity of their amphiphilic parts to fuse with the phospholipid bilayer to exert a detergent-like effect that disrupts the cell/ plasma membrane.

3.7.2.2 Surfactin (BS2)

THP-1 showed greater sensitivity to BS2 with IC_{50} of 24.42, 17.76 and 11.29 $\mu\text{g/ml}$ after 24, 48 and 72 h respectively, (Table 3.2) in comparison to that reported (Cao *et al.*, 2009a) with a value of 19.1 $\mu\text{g/ml}$ after 48 h on human chronic myelogenous leukaemia (K562) cells. This may be due to culture conditions, or cell line differentiations. Dose-response curves showed that BS2 had an IC_{50} of 21.17 $\mu\text{g/ml}$ on MCF-7 cells after 72 h (Table 3.2). This was a much lower cytotoxic effect compared to that obtained by (Cao *et al.*, 2011; Lee *et al.*, 2012) who reported cytotoxicity at 30 $\mu\text{g/ml}$ and 10 $\mu\text{g/ml}$ respectively after 48 h. This may be due to differences in potency because of different sources with the surfactin used by Cao *et al.*, 2011; obtained from *Bacillus natto*, whilst that used (BS2) in the current study was an industry standard. Further, BS2 appeared to be toxic to normal cells (Table 3.2) after 24 and 72 h but this cytotoxicity decreased after 48 h which may indicate a lag phase of the cells disrupted by external stimuli. Surfactins are characterised by the presence of four amino acids; leucine, valine, glutamic acid and aspartic acid in repeating d and l conformations to form a seven membered peptide ring attached to a lactone fatty acid chain. According to (McClements, 2006) the force of electrical charges decreases with increasing ionic strength. Ionic interactions refer to the electrostatic forces between synergistic and repulsively charged groups. The exposure of numerous side chains may lead to cellular lysis by increasing the permeability of the membrane and metabolite flow. This is due to changes in the physical structure of the membrane though the alteration of its protein conformation which alters functions such as transport and generation of energy.

Table 3.2. IC₅₀ of BSs and DOX on THP-1, MCF-7 and HEK 293 cells (*n* = 3, ±SD)

Drugs	THP-1			MCF-7			HEK 293		
	IC ₅₀ (µg/ml)								
	24	48	72	24	48	72	24	48	72
BS1a	176.20 (±0.12)	59.52 (±6.12)	48.71 (±0.12)	153.40 (±0.12)	98.27 (±0.13)	33.08 (±0.90)	61.65 (±7.47)	209.40 (±0.10)	83.91 (±4.07)
BS1b	61.97 (±0.10)	14.47 (±0.24)	8.10 (±0.36)	168.50 (±0.17)	42.85 (±0.16)	30.05 (±0.16)	30.98 (±4.31)	63.51 (±0.13)	57.03 (±0.15)
BS2	24.42 (±0.23)	17.76 (±0.24)	11.29 (±0.28)	111.70 (±0.12)	119.40 (±0.17)	21.17 (±0.20)	29.53 (±0.18)	76.61 (±14.48)	46.52 (±0.14)
BS3	10.52 (±0.18)	5.58 (±0.26)	6.78 (±0.24)	51.46 (±0.16)	33.49 (±0.15)	10.75 (±0.23)	21.53 (±0.20)	40.57 (±8.11)	27.53 (±1.03)
DOX	15.68 (±1.16)	6.49 (±0.63)	2.95 (±0.36)	11.12 (±0.77)	8.35 (±0.64)	4.60 (±0.49)	16.70 (±0.66)	6.08 (±0.54)	0.54 (±0.43)

The table above shows comparative IC₅₀ data and confidence intervals of BSs and DOX on THP-1, MCF-7 and HEK 293 cells at different time points. Values were derived from the graph of percentage cell viability against drug concentration (µg/ml) from MTT assay. Data represent the mean ± S.D. of three (*n* = 3, ± SD) independent experiments.

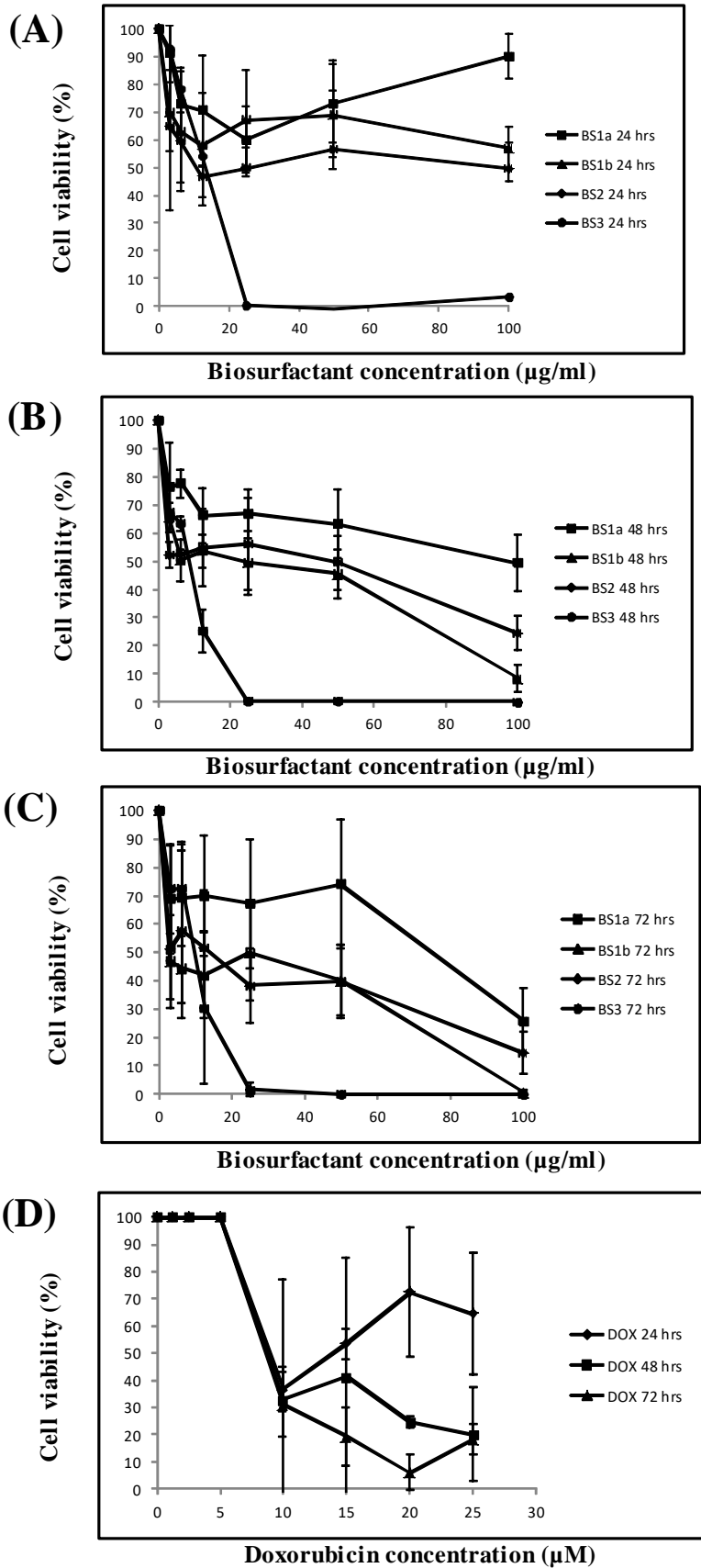


Figure 3.5. Cytotoxicity of BSs on THP-1 cells after (A). 24 h (B). 48 h (C). 72 h (D). 24-72 h Dox ($n = 3, \pm SD$).

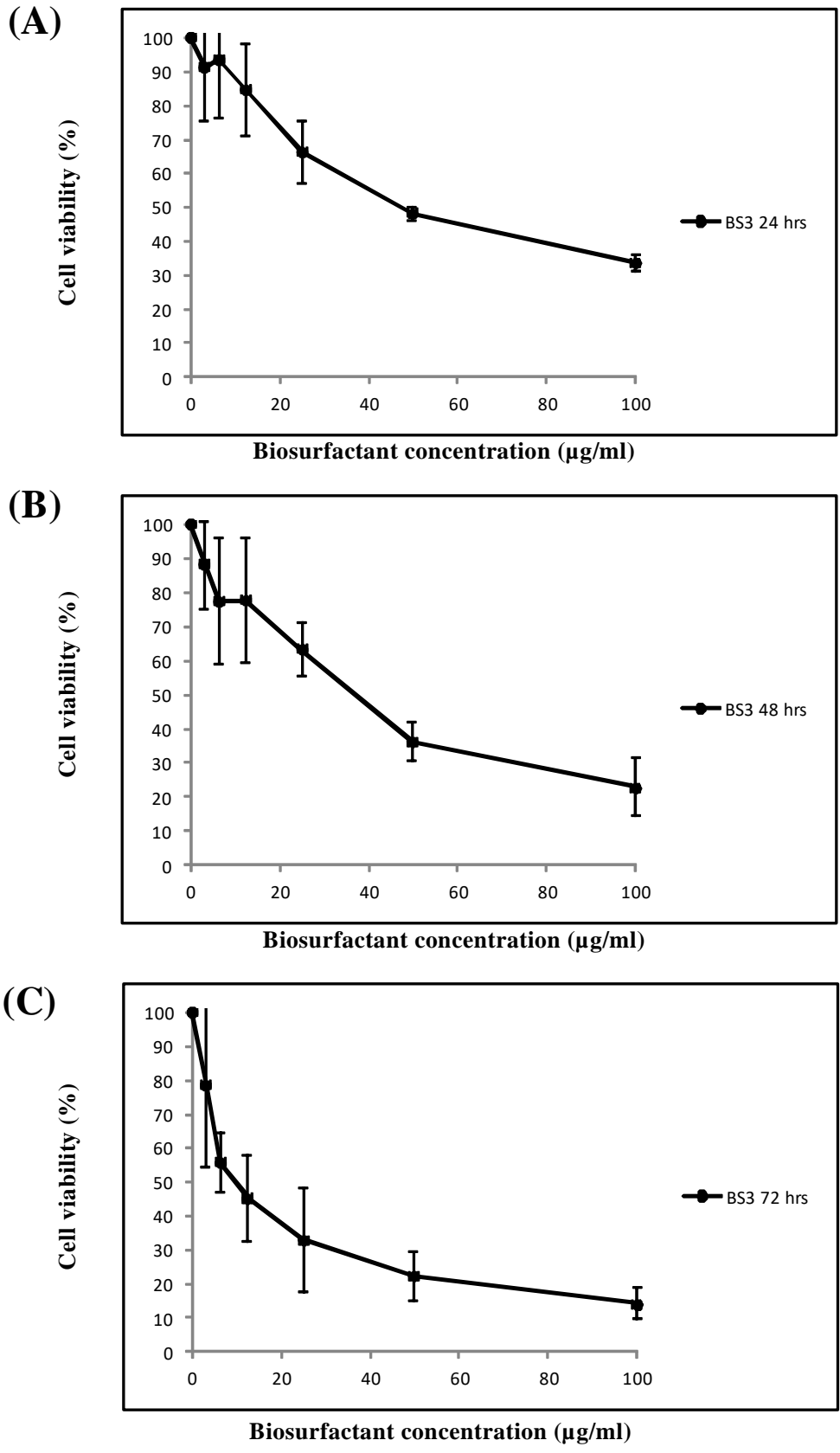


Figure 3.6. Plots showing the cytotoxicity of BS3 on MCF-7 cells after (A). 24 h (B). 48 h (C). 72 h ($n = 4, \pm SD$).

3.7.2.3 Sophorolipids (BS3)

THP-1 cells showed greater sensitivity to BS3 with IC₅₀ of 10.5, 25.58 and 6.78 (µg/ml) after 24, 48 and 72 h respectively, (Table 3.2). However, dose-response curves showed that BS3 had an IC₅₀ of 33.49 and 10.75 (µg/ml) on MCF-7 cells after 48 and 72 h (Table 3.2). However, (Rashad *et al.*, 2014) reported no activity which may be due to the fact that the sophorolipids tested were mixtures of acidic and lactonic congeners in comparison to the pure lactonic standard used in this research. Ribiero *et al.*, (2015) on the other hand reported IC₅₀ values of 30 µg/ml, 15 µg/ml, and 15 µg/ml of diacetylated sophorolipids on oncogene positive breast cancer cell line, MDA-MB-231 at 24, 48 and 72 h respectively which was not much different from that observed against MCF-7 in the current study. Further, BS3 was cytotoxic on HEK 293 cell lines with IC₅₀ of 21.53, 40.57 and 27.53 µg/ml after 24, 48 and 72 h respectively. Lactonic sophorolipids (BS3) contain a diacetylated disaccharide sophorose sugar moiety esterified to a long unsaturated fatty acid tail. The high potency of sophorolipid may be due to the lactonic form in contrast to previous reports using mixed isomers.

3.7.2.4 Doxorubicin (DOX)

THP-1 showed greater sensitivity to DOX compared to the four BSs with IC₅₀ values of 15.68, 6.48 and 2.95 (µg/ml) after 24, 48 and 72 h respectively. Cytotoxicity tests showed that DOX had an IC₅₀ of 11.12, 8.35 and 4.598 (µg/ml) on MCF-7 cells after 24-72 h. Structure-activity relationships have shown an important role for the structure and stereochemistry of the aminosugar (daunosamine) on the pharmacological activity of anthracyclines related to DOX based on the evidence that blocking the amino function resulted in a substantial loss of cytotoxic activity and reduced DNA-binding affinity, (Arcamone *et al.*, 1981; Zunino *et al.*, 2001).

3.7.2.5 Selectivity index

Another important parameter to determine in cytotoxicity studies against cancer cell lines is the selectivity index (SI) which is the toxicity against cancerous cells of the compound of interest relative to normal cells (Assanga *et al.*, 2013), in this case BSs and DOX against THP-1 relative to HEK 293 and against MCF-7 relative to HEK 293. With the exception of BS1b at 72 h, all BSs showed highest selectivity for THP-1 at 48 h in the order of BS3 > BS1b > BS2 > BS1a > DOX. Furthermore, after 24 and 48 h, BS3 was the best as it had low IC₅₀ (10.52, 5.58 µg/ml) and a high SI value (2.05, 7.27) respectively. However although BS3 had the best IC₅₀ (6.78 µg/ml) followed closely by BS1b (8.10 µg/ml), after 72 h, the SI of the latter was better than BS3 with values of 7.04 and 4.06 respectively. After 72 h, the best SI observed on MCF-7 line followed the order of BS1a > BS3 > BS2 > BS1b > DOX. Interestingly, although BS3 had lower IC₅₀ (10.75 µg/ml) after 72 h, its SI of 2.38 was lower than that of BS1a (2.54) even though the latter had an IC₅₀ of 33.08 µg/ml. In addition, although the positive control DOX, showed the highest anti-proliferative activity (with the exception of BS3), SI of

DOX in the two cancerous cell lines was less than that of all the BSs evaluated, which indicates that they are more specific and effective for slowing the growth of the tested cancer cell lines and hence may be potential candidates for use in human cancer therapy. However, further investigations will be required in this regard to validate this hypothesis.

Table 3.3. SI of BSs and DOX on THP-1 and MCF-7 cell lines relative to that of the normal cells HEK 293 at different time points

Compounds	THP-1			MCF-7		
	24 h	48 h	72 h	24 h	48 h	72 h
BS1a	0.32	3.52	1.72	0.40	2.13	2.54
BS1b	0.50	4.40	7.04	0.18	1.48	1.90
BS2	1.21	4.31	4.12	0.26	0.64	2.20
BS3	2.05	7.27	4.06	0.42	1.21	2.38
DOX	1.07	0.94	0.18	1.50	0.73	0.12

The table above compares selectivity index (SI) of BSs and DOX on THP-1/HEK 293 and MCF-7/HEK 293 cells at different time points. Order of THP-1 SI was BS3 > BS1b > BS2 > BS1a > DOX at (48 h) with the exception of BS1b at 72 h. Order of MCF-7 SI was BS1a > BS3 > BS2 > BS1b > DOX at (72 h).

3.8 Conclusions

In this chapter, the functional physico-chemical properties and biological activity of four microbial derived BSs, 95% rhamnolipids (BS1a), 90% rhamnolipids (BS1b), surfactin (BS2) and lactonic sophorolipid (BS3) were investigated. The hypothesis for their biocidal activity was that the BSs form mixed micelles which exert a detergent-like effect that disrupts the plasma membrane. There are few studies that systematically compare the anti-proliferative activity for structurally different BSs, determining DT and highest growth rate. The susceptibility to growth inhibition with BSs was greater in THP-1 than in MCF-7, likely because the THP-1 line has lower DT values and is a cell line with accelerated metabolism. The cancerous cell line MCF-7 was more susceptible than the non-cancerous line HEK 293, in accordance with the lower DT of MCF-7. Similar patterns with phytochemical plant extracts were reported by (Assanga *et al.*, 2013); who showed that short DT values implied increased sensitivity while longer DT values implied decreased sensitivity in cancerous and non-cancerous cell lines respectively. The BSs tested in this study were toxic to normal cells at higher concentrations than cancerous cells, however, lactonic sophorolipid (BS3) showed the closest cytotoxicity to DOX and therefore has high potential application as an anticancer agent. The physico-chemical characteristics of the selected BSs suggests that their mechanism of action may be due to biocidal activity on the cell membrane. The structural differences of the BSs and biological activities will be beneficial for the formulation of synergistic drug delivery.

CHAPTER 4 FORMULATION AND FUNCTIONAL CHARACTERISATION OF BIOSURFACTANT AND SPAN 60 BASED NIOSOMES

4.1 Introduction

The self-assembly of non-ionic amphiphiles in aqueous media results in closed bilayer structures which leads to the formation of niosomal vesicles. Niosomes are drug delivery vesicles (nano – micro metre sized) composed mainly of hydrated non-ionic surfactants with or without cholesterol (CHL) or its derivatives (Uchegbu *et al.*, 1998). Niosomes are also artificial liposomes designed to mimic biological membranes which potentially enables them to evade immune response detection and consequent expulsion from the body. Niosomes were formulated into the treatment cream Niosôme by Lancôme in 1986 to deliver retinol and vitamin E. Brewer and Alexander, (1992) examined the ability of synthetic, non-ionic surfactant vesicles (NISV) to enhance antibody responses to bovine serum albumin (BSA) and reported that NISV with entrapped antigen act as potent immunological adjuvants, promoting antibody titres equivalent to existing adjuvant systems.

Lactonic sophorolipids are microbial glycolipid biosurfactants, broad spectrum anti-inflammatory/anti-cancer agents and safe vectors in drug delivery formulations. Sophorolipids have also been identified as possible pharmaco-dermatological agents by the French company Soliance (<http://www.groupe-soliance.com>) (Delbeke *et al.*, 2016). Sophorolipids have been formulated into microemulsions, micelles and nanoparticles (Delbeke *et al.*, 2016), however, their combination with span 60 (S60) to form niosomes is a novel concept.

Other BSs that have been used for drug-delivery include cationic surfactin in liposomes for siRNA delivery, mannosyl erythriol lipids (MEL) for cellular transfection of DNA delivery (Inoh *et al.*, 2001 and sophorolipid gellan gold-plated nanoparticles conjugates, (Dhar *et al.*, 2011). Chen *et al.*, (2010), reported the use of surface tension, neutron reflectivity and dynamic light scattering measurements to study the adsorption behaviour of mono-rhamnose and di-rhamnose rhamnolipids (R1, R2) and their mixtures and their mixtures at the air-water interface.

This chapter briefly discusses experimental techniques employed to develop mixed biosurfactant-surfactant niosomes of intermediate hydrophobicity and compares the effectiveness of lactonic sophorolipids (BS3), rhamnolipids (BS1c), mixture of acidic and lactonic sophorolipids (BS4a and BS4b), surfactin (BS2) and synthetic surfactants in enhancing niosome formation based on particle size and structural morphology. The chapter further investigates the effect of various process variables such as sonication time, excipient ratio, temperature, concentration of cholesterol and dicetyl phosphate (DCP) which are expected to impart critical characteristics such as stability and enhanced microscopic architecture with the ultimate aim of producing biologically active niosome formulations for potential targeting of the BSs to target diseases such as cancer.

4.2 Materials and methods

4.2.1 Materials

The biosurfactants, R-90™ rhamnolipid (BS1c), surfactin (BS2), 1', 4''-sophorolactone 6', 6''-diacetate (BS3) from yeast (MW 688.80, 70% purity), Span 60 (S60), Cholesterol (CHL), dicetyl phosphate (DCP), were purchased from Sigma Aldrich (Gillingham, UK). REWOFERM SL ONE (BS4a) and SL 446 (BS4b) were kindly donated by Evonik Nutrition & Care GmbH Golschmidstr, Germany.

4.3 Formulation development

Preliminary investigations were undertaken to optimise the niosomes. Sophorolipid loaded niosomes were formulated using thin film hydration technique. The protocol was partially modified from (Balakrishnan *et al.*, 2009) in which span 60, CHL and DCP were used for the transdermal delivery of minoxidil niosomes. Due to the fact that the active ingredients in this research are also amphiphiles, initial optimisation involved the combination of biological and synthetic surfactants. To achieve this, 0, 10 and 20 mM cholesterol (CHL), 1', 4''-sophorolactone 6', 6''-diacetate (BS) from yeast and span 60 (S60), in different molar ratios (5:5, 7.8:2.5, 10:0 and 0:10 mM (Tables 4.1 and 4.2) respectively were dissolved in 8 ml of chloroform: methanol mixture (2:1, v/v) to dissolve the insoluble excipients in a round-bottom flask. Afterwards, 15 µM DCP was dissolved in 5 ml of chloroform: methanol mixture (2:1, v/v) and added to the lipids. The organic solvents were removed under vacuum in a rotary evaporator at 40°C for 10 min to form a thin film on the wall of the flask, and kept in a vacuumed desiccator for 2 h to remove the last traces of the organic solvent used. The surfactant film was then hydrated in 10 ml of deionised water and heated above the gel-liquid transition temperature (T_c) of sorbitan monoesters (53-55°C). The transition temperature (T_c) is the melting point of the acyl chains. All lipids have a characteristic T_c , which is contingent upon the nature of the polar head group and on the length and degree of unsaturation of the acyl chains. Above the T_c , lipids form a liquid-crystalline phase that constitutes increased mobility of the acyl chains. A reduction in temperature below the T_c creates a transition to a more rigid state. The active ingredients in this investigation are amphiphiles, therefore the gel-liquid transition of the niosomal dispersions were investigated at 60, 70 and 80°C. The resulting niosomal suspensions were shaken for 1 h in a horizontal mechanical shaking water bath at different temperatures (60, 70 and 80°C). The effect of temperature based on selected physico-chemical techniques were not statistically significant $p > 0.05$. Optimisation of the vesicle suspensions included sonication for 0, 3 and 40 min in an unheated ultrasonic water-bath (Clifton MU-8 series) with operating frequency of 30 – 40 kHz). Observations from the results obtained led to the selection of an intermittent process in three cycles of 1 min “on” and 1 min “off”, leading to the formation of multi-lamellar niosomes, which were left to mature overnight in a refrigerator (4°C). The resulting niosomes were characterised using dynamic-light scattering (DLS), pH meter, conductivity meter, ATR-FTIR, XRD and scanning electron microscopy in transmission mode (STEM).

Based on the results of the preliminary investigation niosomes were formulated with (BS1c, BS4a & BS4b and BS2 which were prepared by means of two different methods; the thin film hydration method (TFH) (Table 4.3) as described above (but by hydrating with phosphate buffer pH 7.4). BS1c vesicles were also formulated by direct dissolution (DD) (Table 4.4) – where specific amounts of BSs were dissolved in phosphate-buffered saline (pH 7.4) without any additives or sonication. On the basis of these results, optimised concentrations of BS3, BS4a and BS4b were also formulated with DCP (Table 4.5.) as well as from BS2 using the thin film hydration (Table 4.6). A different set of niosomes were formulated without DCP at selected concentrations of BSs (Table 4.7). The resulting niosomes were characterised using dynamic-light scattering (DLS), ATR-FTIR, XRD and scanning electron microscopy in transmission mode (STEM),

Table 4.1. Optimisation of amount of cholesterol (CHL) on blank span 60 (S60) and lactonic sphorolipids (BS3) only niosomes using thin film hydration method (TFH)

Starting Material	BS:S60:CHL (BLK) (mg)	BS:S60:CHL (BLK) (mg)	BS:S60:CHL (BLK) (mg)	BS:S60:CHL (BS3) (mg)	BS:S60:CHL (BS3) (mg)	BS:S60:CHL (BS3) (mg)
BS3	-	-	-	68.9	68.9	68.9
S60	43.6	43.6	43.6	-	43.6	43.6
CHL	-	38.6	77.2	-	38.6	77.2
DCP	8.2	8.2	8.2	8.2	8.2	8.2

Table 4.2. Optimisation of amount of cholesterol (CHL) on different concentrations of lactonic sphorolipids (BS3) loaded niosomes

Starting Material	BS:S60:CHL (BLK) (mg)	BS:S60:CHL (BLK) (mg)	BS:S60:CHL (BLK) (mg)	BS:S60:CHL (BS3) (mg)	BS:S60:CHL (BS3) (mg)	BS:S60:CHL (BS3) (mg)
BS3	34.5	34.4	34.5	53.3	53.3	53.3
S60	21.8	21.8	21.8	10.9	10.9	10.9
CHL	-	38.6	77.2	-	38.6	77.2
DCP	8.2	8.2	8.2	8.2	8.2	8.2

Table 4.3. Optimisation of different concentrations of R-90 rhamnolipids (BS1c) on four component niosomes using thin film hydration method (TFH)

Starting Material	BS:S60:CHL (BLK) (mg)	BS:S60:CHL (BS1c) (mg)					
BS1c	-	8.0×10^{-2}	1.0×10^{-1}	2.0×10^{-1}	3.0×10^{-1}	4.0×10^{-1}	6.0×10^{-1}
S60	43.6	43.6	43.6	43.6	43.6	43.6	43.6
CHL	38.6	38.6	38.6	38.6	38.6	38.6	38.6
DCP	8.2	8.2	8.2	8.2	8.2	8.2	8.2

Table 4.4. Optimisation of different concentrations of R-90 rhamnolipids (BS1c) on one component vesicles using direct dissolution (DD)

Starting Material	BS:S60:CHL (BS1c) (mg)					
BS1c	8.0×10^{-2}	1.0×10^{-1}	2.0×10^{-1}	3.0×10^{-1}	4.0×10^{-1}	6.0×10^{-1}
S60	-	-	-	-	-	-
CHL	-	-	-	-	-	-
DCP	-	-	-	-	-	-

Table 4.5. Optimisation of different concentrations of lactonic sophorolipids (BS3), Rewoform SL ONE (BS4a) & SL 446 (BS4b) sophorolipids on four component niosomes using thin film hydration method (TFH)

Starting Material	BS:S60:CHL (BS4a/b) (mg)	BS:S60:CHL (BS3/BS4a/b) (mg)	BS:S60:CHL (BS4a/b) (mg)	BS:S60:CHL (BS4a/b) (mg)	BS:S60:CHL (BS3/BS4a/b) (mg)	BS:S60:CHL (BS3/BS4a/b) (mg)
BS4a/b	8.0×10^{-2}	1.0×10^{-1}	2.0×10^{-1}	3.0×10^{-1}	4.0×10^{-1}	6.0×10^{-1}
S60	43.6	43.6	43.6	43.6	43.6	43.6
CHL	-	38.6	38.6	38.6	38.6	38.6
DCP	8.2	8.2	8.2	8.2	8.2	8.2

Table 4.6. Optimisation of different concentrations of surfactin (BS2) on four component niosomes using thin film hydration method (TFH)

Starting Material	BS:S60:CHL (BS2) (mg)					
BS2	8.0×10^{-2}	1.0×10^{-1}	1.65×10^{-1}	2.0×10^{-1}	3.0×10^{-1}	6.0×10^{-1}
S60	43.6	43.6	43.6	43.6	43.6	43.6
CHL	38.6	38.6	38.6	38.6	38.6	38.6
DCP	8.2	8.2	8.2	8.2	8.2	8.2

Table 4.7. Optimisation of different concentrations of R-90 rhamnolipids (BS1c), Rewoferm SL ONE (BS4a) & SL 446 (BS4b) sophorolipids and surfactin (BS2) on three component niosomes using thin film hydration method (TFH)

Starting Material	BS:S60:CHL (BLK) (mg)	BS:S60:CHL (BS1c) (mg)	BS:S60:CHL (BS1c) (mg)	BS:S60:CHL (BS1c) (mg)	BS:S60:CHL (BS4a/b) (mg)	BS:S60:CHL (BS2) (mg)
BS1c	-	1.0×10^{-1}	4.0×10^{-1}	6.0×10^{-1}	-	-
BS4a/b	-	-	-	-	1.0×10^{-1}	-
BS2	-	-	-	-	-	6.0×10^{-1}
S60	43.6	43.6	43.6	43.6	43.6	43.6
CHL	38.6	38.6	38.6	38.6	38.6	38.6
DCP	-	-	-	-	-	-

4.4 Lyophilisation of niosomes

The niosome dispersions were pre-frozen in a freezer at -80°C , after which they were removed and loaded without the addition of cryo-protectants onto the shelves of a benchtop manifold freeze-dryer ScanVac coolsafe freeze dryer (Vacuubrand chemistry hybrid pump, Germany) at a target temperature of -55°C . The samples were dried under this condition for 48 h.

4.5 Analytical characterisation

4.5.1 pH

The pH of the preliminary niosomal formulations was measured using a digital pH meter by placing the pH meter in a glass beaker containing formulated preparations. The pH meter directly reads out the pH of the formulation. A two pH standard solution was chosen (4.00 and 7.00) for calibration of the pH meter. The charge around colloids is reflected in the measurement of zeta potential. According to Sigma Aldrich, the pH of commercial 1mg/ml BS3 in water is 4.0-6.0, the pH of niosome encapsulated BS3 formulated at different gel-liquid transition temperatures were therefore measured to identify compositional changes.

4.5.2 Conductivity

Conductivity of preliminary niosomal formulations were carried out using a digital conductivity meter (Mettler Toledo (Switzerland)). The instrument was calibrated using a conductivity standard 1413 $\mu\text{S}/\text{cm}$ and adjusted to room temperature. The conductivity meter directly reads out the conductivity of the formulations. A change in the electrical conductivity of a surfactant containing solution relates to the aggregation of the surfactant molecules. Further analysis were obtained alongside zeta-potential measurements as described below.

4.5.3 Dynamic laser scattering (DLS)

Vesicle properties of the BSs loaded niosome dispersion such as particle size intensities, polydispersity index and zeta potential were determined by dynamic light scattering (DLS) using a Malvern Zetasizer Nano-ZS (Malvern, UK). Light scattering was monitored at a 173° scattering angle at 25°C. For the particle size and polydispersity index each sample was put in a plastic disposable cuvette until a third of the cuvette was filled and they were put in the Zetasizer, while for the zeta-potential and conductivity each sample was put in a Zetasizer cuvette to overflow, sealed and then put in the Zetasizer.

4.5.4 Attenuated total reflectance Fourier transform infrared spectroscopy (ATR-FTIR)

Interaction and entrapment of biosurfactants into the niosomal vesicles was studied using IR spectroscopy. Before ATR-FTIR analysis, the diamond crystal surface was cleaned and background spectra were collected. Samples were individually placed with just enough material to cover the crystal area. The pressure arm was positioned over the sample area and the arm of a Spectrum 100 series universal ATR accessory was locked into a precise position above the diamond crystal. This allowed force to be applied to the sample to ensure proper contact with the diamond crystal. IR spectra were collected between 400 and 4000 wave numbers (cm^{-1}) at a scan rate of 0.2 using a Perkin Elmer UATR Two infrared spectrometer.

4.5.5 X-ray diffraction (XRD)

X-ray diffraction patterns were obtained at room temperature to determine the crystalline or amorphous phases in all samples. Samples of starting materials and freeze-dried BSs loaded niosomes, as well as the freeze-dried blank formulations were evaluated on a D8 Advance X-ray Diffractometer (Bruker, Germany) in 2-theta geometry in reflection mode. Freeze dried samples were compressed using a clean pair of compression glasses and flattened in the sample holder. The operating conditions during the experiment were Cu K α radiation at 40 kV and 40 mA equipped with a primary Göbel mirror for parallel beam X-rays and removal of CuK β radiation; a primary 4° Soller slit; a 0.6 mm exit slit; knife edge; sample rotation at 15 rpm; a LynxEye silicon strip position sensitive detector set with an opening of 3°, the LynxIris set at 6.5 mm; and a secondary 2.5° Soller slit. The diffractograms were acquired using DIFFRAC plus XRD Commander version 2.6.1 software (Bruker-AXS), qualitative assessment with the aid of EVA version 16.0 (Bruker-AXS) and the PDF-2 database (ICDD, 2008) over a start to end diffraction angle of 2-40° 2 θ , step size of 0.02° and a counting time of 0.3 sec per step; with 176 active channels in the detector this is equivalent to a total counting time of 52.8 sec per step.

4.5.6 Scanning electron microscopy in transmission mode (STEM)

Morphological examination of BLK and BSs loaded niosomes were visualised by STEM. A 1 in 5 dilution of BSs loaded niosomes were dispersed in phosphate saline buffer (PBS) pH (7.4), in Roswell Park Memorial Institute medium (RPMI 1640) and Dulbecco's modified eagles medium (DMEM). Both cell culture media were supplemented with 10% heat inactivated foetal bovine serum and 1% penicillin/streptomycin. A drop of niosome dispersion diluted in PBS was applied to a carbon coated copper grid and left for 1 min to allow some of the particles to adhere to the carbon substrate. Excess dispersion was blotted off with a piece of filter paper and the sample was then air-dried. Additionally, the effect of osmotic shock on niosomal formulations was investigated by monitoring the change in vesicle diameter after incubation of niosome suspensions in cell culture media (DMEM and RPMI 1640 media) and visualised as previously described. The final samples were placed in the chamber of a Hitachi SU8030 field emission gun scanning electron microscope (Hitachi, Japan) and images acquired with a transmission detector at an accelerating voltage of 30 kV.

4.5.7 Statistical analysis of data

Data analysis was carried out with the software package Microsoft Excel version 2007. Results were expressed as a mean \pm standard deviation (S.D). ($n = 3$). Statistically significant difference was determined using one-way analysis of variance (ANOVA,) for the significant interrelation between the various groups with $p < 0.05$ considered as a minimal level of significance. The parameters compared were the effect of temperature on BS3 niosomes dispersed in deionised water and the effect on different BSs dispersed in PBS buffer.

4.6. Results and discussion

4.6.1 Preliminary investigations

The formation of niosomes involves the combination of an organic and an aqueous phase. The organic phase in this study were BSs, S60, CHL, with/without DCP and a mixture of two solvents (chloroform and methanol) to dissolve the insoluble excipients. However the solvents from the pre-niosomal phase are completely evaporated resulting in a formation of a thin lipid film on the wall of the round bottomed flask. Niosomes are obtained during the hydration of the lipid film with the aqueous phase (PBS) which forms a turbid milky dispersion and is then shaken in a heated water bath. Span 60 (S60) has a transition temperature of 53°C, while BS3 melts at 123°C and undergoes glass transition at 61°C (Delbeke *et al.*, 2016). Due to the fact that the active ingredients in this investigation are amphiphiles, the effect of gel-liquid transition of the niosomal dispersions were investigated at 60, 70 and 80°C. Hydration time was kept constant at 60 min, while the effect of temperature was investigated at 60, 70 and 80°C. The effect of temperature compared with selected physico-chemical techniques were not statistically significant $p > 0.05$.

The development of niosomes was initially undertaken by preparing various blank formulations at different CHL concentrations. The amount of the lipids and the surfactant was kept at (S60) 43.6 mg, (CHL) 38.6 mg and, (DCP) 8.2 mg respectively, while the solvent volume remained at 13 ml. In this research, the self-assembly in aqueous solution of BS3 and its mixture with S60 has been studied using mainly dynamic light scattering (DLS) at relatively low surfactant concentrations of ≤ 10 mM. Based on similar observations from (Penfold *et al*, 2011), the more hydrophobic BS3 in this study was observed to form a disordered dilute phase of tubules at a higher concentration of 10 mM with sparing proportion of large unilamellar vesicle structure in coexistence. In marked contrast, S60 forms larger multilamellar vesicles with small unilamellar vesicles as present. However, mixtures of BS3 and S60, exhibit a rich evolution in phase behaviour with solution composition and concentration. At 2.5 and 5 mM S60 concentrations, the multilamellar and disordered lamellar structures of both individual S60 and BS3 only niosomes evolves into large unilamellar structures, as the solution becomes richer in S60. Additionally, S60 surfactant exhibits self-assembly properties similar to those of other weak non-ionic surfactants that have relatively large head groups. However, the more hydrophobic nature of BS3 results in a more complex and unusual evolution in phase behaviour with concentration and composition when mixed with S60.

Penfold and co-workers reported that small unilamellar vesicles were formed in their investigation of individual lactonic sphorolipids optimally within a concentration range of 0.2 - 3 mM using small angle scattering (SANS) as the analytical technique (Penfold *et al*, 2011). Beyond this range (about 7 mM), there was transformation via a large unilamellar vesicular structure to a disordered dilute phase of tubules at higher concentrations from 10 to 30 mM. Additionally the mixture of the anionic surfactant, sodium dodecyl benzene sulfonate at both low and high concentrations transformed both the small unilamellar vesicles (obtained for low concentrations) and the more concentrated solutions resulting in disordered lamellar structures present for BS3 only, into globular micelles. Then through a series of evolutions, the globules were ultimately converted to a pure micellar phase as the solution became increasingly concentrated with sodium dodecyl benzene sulfonate (Penfold *et al*, 2011). The SANS measurements were made at relatively low surfactant concentration (< 30 mM) as a result of the low solubility of BS3 (differences in result may result from the use of D₂O at 30°C and using hydrogenous sphorolipids).

A number of theoretical assumptions are made based on existing literature, that S60 niosomes formed were multilamellar in nature based on strictly following the procedure of (BalaKrishan *et al* 2009) and general niosomes formed through thin film hydration method. Secondly the observation of small unilamellar vesicles made from roughly the same concentrations recorded from SANS measurements for lactonic sphorolipids is supported by quantitative analysis reported by (Penfold *et al* 2011) which showed that the niosomes showed somewhat larger symmetrical assemblies, than that allowed by the packing constraints associated with simple micellar structure but are consistent with small unilamellar vesicles.

However, the concentrations used in preliminary studies were higher than the optimum reported by (Penfold *et al* 2011), this is because the primary objective was the formation of sufficient amount of niosomes. There was an insufficient distribution of preliminary loaded BS3 niosomes observed by SEM, as a result of high crystallisation. In order to increase the formation of more niosomes the lipid concentrations were doubled and later dispersed in 5 and 10 ml volume of PBS. However, this resulted in precipitation which was visible on the round bottom flasks. Penfold *et al* (2011) reported that vesicle formation for BS3/BS4a/b were not observed beyond 7 mM. In this study, although insufficiently distributed as a result of high crystal formation, BS3 niosomal vesicles were observed at 10 mM. Differences in observations may arise from the combination of synthesised isomeric mixtures. However, the concentration of BS3 loaded niosomes exceeded by far the amount observed to be toxic to non-cancerous HEK 293 cells which as previously reported in chapter 3, section 3.7.2, has an IC₅₀ of 21.53 - 40.57 µg/ml after 24 - 72 h. Therefore new batches of niosomes were formulated with concentration ranging from 8.0×10^{-1} – 6.0×10^{-1} mg/ml at 60°C to allow for controlled release of the BSs.

4.6.2 Dynamic laser scattering (DLS)

Dynamic laser scattering (DLS), also known as photon correlation spectroscopy (PCS), determines the size of particles by measuring the Brownian motion of the particles in a liquid and works by illuminating a laser onto the particle and then analysing the intensity fluctuations in the scattered light. It can measure submicron particles in the range of 0.6 nm to 6 µm. In this study DLS was used to obtain information regarding particle size, polydispersity index (PDI), zeta potential and electrical conductivity. DLS calculates particle size distributions in terms of number, volume, or scattering intensity which often produces vastly differing results in terms of their mean values and the appearance of the distributions; however, exactly the same physical characteristics of a sample are represented, (Malvern, 2017).

4.6.2.1 Particle size, intensity and polydispersity index (PDI)

In this study, the intensity distributions were reported, while the number distribution was used to report the results obtained from the reference paper from which the water based niosomes were adapted. For corresponding blank niosomes (Balakrishnan *et al.*, 2009) reported z-diameter (cumulant mean) of 1240 (±47) nm and PDI of 1 (±0). In this study, the corresponding z-diameter obtained was 1170 (±71) nm (data not shown) and a lower PDI of 0.213 (± 0.27) (Table 4.9) which may be due to differences in hydration temperature used in the reference investigation 55°C while 60°C was used in this study. There were discrepancies in the particle sizes of niosomes as a result of the effect of CHL concentration. Interestingly, BS3 based niosomes prepared from suspensions with 20 mM of CHL had slightly lower sizes than those formulated with 10 mM. However, SEM morphological observations

(data not shown) clearly showed an increased size of niosomes as a result of CHL concentration. This discrepancy may be due to the fact that DLS makes no distinction between niosomes, aggregates and crystallisation of precipitated polymers. Thus the size of BS3 niosomes at both 60 and 80°C appear to be equally favourable to the formation of smaller vesicles than at 70°C (Table 4.8).

Additionally, BS3 loaded niosomes formulated with 10 mM CHL exhibited a lower PDI than their higher counterpart at both 60 and 80°C indicating that niosomes formulated at 70°C have a more narrow size distribution (Table 4.9). An equal amount of 10 and 20 mM CHL ratio have interchangeable stability on BS3 loaded niosomes. In addition to increases in size of niosomes due to CHL, there were also observed differences in the ratio of BS3 - S60 composition. A concentration of 5:5 mM BS3:S60 yielded smaller sized vesicles than 7.8:2.5 mM BS3:S60 particularly at 60 and 70°C, although the sizes of niosomes formed at both ratios and both temperatures are below 500 nm. Niosomes formed at 80°C appear to have larger sizes > 500 nm.

Table 4.8. Effect of temperature on size of 1', 4''-sophorolactone 6', 6''-diacetate loaded niosomes $n = 3$

BS3:S60:CHL (mM)	Particle size for peak 1 (nm)			
	60°C	70°C	80°C	Temperature trend (°C)
0:10:0	760 (±96)	281 (±7)	259 (±15)	80<70<60
0:10:10	369 (±13)	655 (±23)	370 (±39)	60<80<70
0:10:20	547 (±31)	750 (±217)	898 (±184)	60<70<80
5:5:0	498 (±20)	472 (±22)	419 (±88)	80<70<60
5:5:10	339 (±22)	392 (±18)	576 (±85)	60<70<80
5:5:20	338 (±99)	367 (±49)	277 (±54)	80<60<70
7.8:2.5:0	515 (±53)	381 (±25)	556 (±64)	70<60<80
7.8:2.5:10	373 (±9)	371 (±113)	784 (±63)	70<60<80
7.8:2.5:20	329 (±19)	391 (±37)	386 (±108)	60<80<70
10:0:0	373 (±16)	669 (±544)	418 (±63)	60<80<70
10:0:10	558 (±372)	646 (±173)	244 (±52)	80<60<70
10:0:20	1504 (±353)	495 (±174)	333 (±126)	80<70<60

BS3 – biosurfactant (1', 4''-sophorolactone 6', 6''-diacetate), S60 – span 60, CHL – cholesterol
 The table above compares the particle size obtained from the intensity of light scattered by blank and BS3 loaded niosomes (prepared by thin film hydration method) and hydrated in deionised (DI) water at different temperatures. The mean intensity and standard deviation of three ($n = 3$, \pm SD) measurements on different samples is reported and presented in parentheses. The particle size distributions were a combination of unimodal, bimodal and trimodal peaks, (see Appendix Table A4.1), but only the first peak is presented.

With the exception of 1.0×10^{-1} mg/l loaded niosome which had a monomodal distribution, all other concentrations of BS1c niosomes had bi and trimodal peaks (Table 4.10). The particle sizes of the niosomes followed an ascending order of $1.0 \times 10^{-1} < 4.0 \times 10^{-1} < 6.0 \times 10^{-1}$ mg/l corresponding to 546 (± 103) nm, 925 (± 287) nm and 943 (± 1213) nm respectively -these are the first formulations with nanometric sized mixed niosome. Additionally, 1.0×10^{-1} mg/l is also the first BSs formulation with monomodal distribution. All other formulations in this batch had large particle sizes ranging from 1277-2442 nm with corresponding trimodal distributions.

Table 4.9. Effect of temperature on PDI of 1', 4''-sophorolactone 6', 6''-diacetate loaded niosomes $n = 3$

BS3:S60:CHL (mM)	PDI			Temperature trend ($^{\circ}$ C)
	60 $^{\circ}$ C	70 $^{\circ}$ C	80 $^{\circ}$ C	
0:10:0	0.738 (± 0.21)	0.220 (± 0.01)	0.354 (± 0.08)	70<80<60
0:10:10	0.213 (± 0.27)	0.294 (± 0.12)	0.898 (± 0.10)	60<70<80
0:10:20	0.352 (± 0.16)	0.891 (± 0.11)	0.476 (± 0.11)	60<80<70
5:5:0	0.447 (± 0.07)	0.951 (± 0.06)	0.926 (± 0.11)	60<80<70
5:5:10	0.617 (± 0.09)	0.847 (± 0.13)	0.693 (± 0.02)	60<80<70
5:5:20	0.807 (± 0.05)	0.669 (± 0.06)	0.837 (± 0.05)	70<60<80
7.8:2.5:0	0.871 (± 0.22)	0.558 (± 0.02)	0.756 (± 0.07)	70<80<60
7.8:2.5:10	0.722 (± 0.11)	1.000 (± 0.00)	0.516 (± 0.10)	80<60<70
7.8:2.5:20	0.846 (± 0.14)	0.519 (± 0.02)	0.875 (± 0.11)	70<60<80
10:0:0	0.994 (± 0.01)	0.766 (± 0.22)	0.557 (± 0.07)	80<70<60
10:0:10	0.855 (± 0.25)	0.847 (± 0.06)	0.855 (± 0.13)	70 \leq 80=60
10:0:20	0.565 (± 0.46)	0.686 (± 0.05)	0.757 (± 0.08)	60<70<80
Mean (\pm SD)	0.669 (± 0.24)	0.687 (± 0.25)	0.708 (± 0.19)	60<70<80

BS3 – biosurfactant (1', 4''-sophorolactone 6', 6''-diacetate), S60 – span 60, CHL – cholesterol
The table above compares the PDI obtained from the intensity of light scattered by blank and BS3 loaded niosomes (prepared by thin film hydration method) and hydrated in deionised (DI) water at different temperatures. The mean intensity and standard deviation of three ($n = 3$, (\pm SD) measurements on different samples is reported and presented in parentheses.

A selection of partially corresponding concentrations of BS1c were dispersed in PBS (Table 4.11) and showed that the particle sizes followed an ascending order of $3.0 \times 10^{-1} < 4.0 \times 10^{-1} < 2.0 \times 10^{-1}$ mg/l. However, the particle size of BS1c vesicles at concentration of 1.0×10^{-1} mg/l was 280 nm which was higher than the other concentrations, and was limited by its bimodal distribution whose second peak was one-eighth the intensity of its major peak. The other concentrations had broad sized

trimodal peaks (Table 4.11). The formulation of BS4a niosomes resulted in similar particle size distributions with bimodal and trimodal peaks. Furthermore, although 1.0×10^{-1} mg/l had the lowest particle size of 1001 nm (Table 4.12), it also had the highest standard deviation attributed to its 3rd peak number. In this batch of BS4b loaded niosome formulations (Table 4.13), 1.0×10^{-1} mg/l BS once again had a distinct feature, being the formulation with the lowest particle size at 957 nm followed by $3.0 \times 10^{-1} < 2.0 \times 10^{-1}$ mg/l. The peak distribution in this batch of formulations similarly had an even number of bimodal and trimodal peaks. The particle size of BS2 loaded niosomes followed an ascending order of $1.65 \times 10^{-1} < 6.0 \times 10^{-1} < 4.0 \times 10^{-1}$ mg/l all of which had trimodal distributions (Table 4.14).

Based on the trends observed from the concentrations of BSs loaded niosomes (Table 4.15), three concentrations were selected for the final formulation of BS3. The particle size of the selected three followed an ascending order of $4.0 \times 10^{-1} < 6.0 \times 10^{-1} < 1.0 \times 10^{-1}$ mg/l with sizes 690 (± 892) nm < 1133 (± 713) nm < 2710 (± 1795) nm respectively. Overall, the mean PDI followed the order of BS3 < BS2 < BS4a < BS1cN/BS1cV. Interestingly, there was very little difference (0.002) between the PDI of BS1c niosomes and vesicles in spite of their size distributions. For the other formulations there is an acceptable agreement of the experimental size distribution with the observed PDI (Table 4.15).

Table 4.10. Particle size and intensities of niosomes loaded with different concentrations of rhamnolipids $n = 3$

BS1c loading (mg/l)	Peak 1 (nm)	Peak 2 (nm)	Peak 3 (nm)	Peak 1 (%)	Peak 2 (%)	Peak 3 (%)
8.0×10^{-2}	2442 (± 1585)	1853 (± 3210)	26 (± 45)	93 (± 13)	5 (± 9)	2 (± 4)
1.0×10^{-1}	546 (± 103)	-	-	100 (± 0)	-	-
2.0×10^{-1}	1872 (± 1645)	1935 (± 3000)	54 (± 93)	81 (± 21)	13 (± 12)	6 (± 10)
3.0×10^{-1}	1276 (± 525)	107 (± 106)	-	91 (± 9)	9 (± 9)	-
4.0×10^{-1}	925 (± 287)	103 (± 92)	1853 (± 3210)	84 (± 14)	14 (± 13)	3 (± 4)
6.0×10^{-1}	943 (± 1213)	1853 (± 3210)	-	92 (± 14)	8 (± 14)	-

The table above compares the particle size obtained from the intensity of light scattered by BS1c loaded niosomes (prepared by thin film hydration method) and hydrated in PBS buffer pH 7.4 at 60°C. The mean intensity and standard deviation of three ($n = 3$, (\pm SD) measurements on different samples is reported and presented in parentheses.

Table 4.11. Particle size and intensities of different concentrations of rhamnolipid loaded vesicles $n = 3$

BS1c loading (mg/l)	Peak 1 (nm)	Peak 2 (nm)	Peak 3 (nm)	Peak 1 (%)	Peak 2 (%)	Peak 3 (%)
1.0×10^{-1}	280 (± 19)	35 (± 5)	0	87 (± 5)	10 (± 0)	3 (± 5)
2.0×10^{-1}	237 (± 18)	71 (± 60)	3641 (± 3154)	72 (± 2)	20 (± 3)	6 (± 3)
3.0×10^{-1}	196 (± 94)	40 (± 13)	1814 (± 3143)	65 (± 13)	36 (± 14)	1 (± 2)
4.0×10^{-1}	214 (± 161)	138 (± 140)	1804 (± 3125)	55 (± 7)	44 (± 6)	2 (± 3)

The table above compares the particle size obtained from the intensity of light scattered by BS1c loaded vesicles (prepared by direct dissolution) and hydrated in PBS buffer pH 7.4 at room temperature. The mean intensity and standard deviation of three ($n = 3$, (\pm SD) measurements on different samples is reported and presented in parentheses.

Table 4.12. Particle size and intensities of different concentrations of Rewoferm SL ONE loaded niosomes $n = 3$

BS4a loading (mg/l)	Peak 1 (nm)	Peak 2 (nm)	Peak 3 (nm)	Peak 1 (%)	Peak 2 (%)	Peak 3 (%)
8.0×10^{-2}	2299 (± 2509)	339 (± 587)	0	84 (± 17)	14 (± 17)	2
1.0×10^{-1}	1001 (± 152)	128 (± 111)	1853 (± 3210)	67 (± 8)	33 (± 7)	0
2.0×10^{-1}	1176 (± 400)	1750 (± 3031)	49 (± 85)	99 (± 18)	1 (± 15)	0
3.0×10^{-1}	3350 (± 2771)	1919 (± 3154)	0	94 (± 13)	3 (± 13)	3
4.0×10^{-1}	2141 (± 2103)	399 (± 513)	1908 (± 3164)	83 (± 23)	12 (± 19)	4 (± 5)
6.0×10^{-1}	2389 (± 1716)	1850 (± 3109)	0	96 (± 12)	4 (± 12)	0

The table above compares the particle size obtained from the intensity of light scattered by BS4a loaded niosomes (prepared by thin film hydration method) and hydrated in PBS buffer pH 7.4 at 60°C. The mean intensity and standard deviation of three ($n = 3$, (\pm SD) measurements on different samples is reported and presented in parentheses.

Table 4.13. Particle size and intensities of different concentrations of Rewoferm SL 446 loaded niosomes $n = 3$

BS4b loading (mg/l)	Peak 1 (nm)	Peak 2 (nm)	Peak 3 (nm)	Peak 1 (%)	Peak 2 (%)	Peak 3 (%)
8.0×10^{-2}	2996 (± 1774)	843 (± 1375)	52 (± 90)	84 (± 21)	14 (± 17)	2 (± 3)
1.0×10^{-1}	957 (± 161)	185 (± 321)	0	67 (± 57)	33 (± 57)	0
2.0×10^{-1}	1263 (± 82)	1853 (± 3210)	0	99 (± 2)	1 (± 2)	0
3.0×10^{-1}	1216 (± 120)	1853 (± 3210)	44 (± 76)	94 (± 10)	3 (± 5)	3 (± 5)
4.0×10^{-1}	1384 (± 524)	3572 (± 3097)	53 (± 92)	83 (± 18)	12 (± 11)	4 (± 8)
6.0×10^{-1}	1744 (± 1233)	68 (± 59)	0	96 (± 3.5)	4 (± 3)	0

The table above compares the particle size obtained from the intensity of light scattered by BS4b loaded niosomes (prepared by thin film hydration method) and hydrated in PBS buffer pH 7.4 at 60°C. The mean intensity and standard deviation of three ($n = 3$, \pm SD) measurements on different samples is reported and presented in parentheses.

Table 4.14. Particle size and intensities of different concentrations of surfactin loaded niosomes $n = 3$

BS2 loading (mg/l)	Peak 1 (nm)	Peak 2 (nm)	Peak 3 (nm)	Peak 1 (%)	Peak 2 (%)	Peak 3 (%)
8.0×10^{-2}	2758 (± 2781)	47 (± 82)	0	97 (± 5)	3 (± 5)	0
1.0×10^{-1}	3542 (± 1470)	57 (± 99)	0	97 (± 6)	4 (± 6)	0
1.65×10^{-1}	3087 (± 2066)	141 (± 245)	48 (± 83)	84 (± 27)	11 (± 19)	5 (± 8)
2.0×10^{-1}	2461 (± 2434)	1912 (± 3161)	0	82 (± 19)	18 (± 19)	0
3.0×10^{-1}	1656 (± 392)	1571 (± 2721)	48 (± 84)	82 (± 32)	14 (± 25)	4 (± 7)
6.0×10^{-1}	1556 (± 712)	35 (± 61)	1853 (± 3210)	96 (± 7)	2 (± 4)	2 (± 3)

The table above compares the particle size obtained from the intensity of light scattered by BS2 loaded niosomes (prepared by thin film hydration method) and hydrated in PBS buffer pH 7.4 at 60°C. The mean intensity and standard deviation of three ($n = 3$, \pm SD) measurements on different samples is reported and presented in parentheses.

Porsunthorntawee *et al.*, (2009) observed micelles of about 10 nm in size at concentrations around the critical micelle concentration (CMC) and to spontaneously form bimodal vesicles of 50-250 nm size range above the CMC. With the formation of aggregates in the size range 350-550 nm, bimodal distributions were observed that decayed with increasing concentrations and only very large aggregates greater than 1500 nm remained at high concentrations.

Table 4.15. Comparison of the polydispersity index (PDI) of biosurfactant loaded niosomes and vesicles $n = 3$

BSs (mg/l)	BS1c niosomes	BS1c vesicles	BS2 niosomes	BS3 niosomes	BS4a niosomes	BS4b niosomes
8.0×10^{-2}	0.318 (± 0.135)	-	0.360 (± 0.17)	-	0.667 (± 0.23)	0.383 (± 0.23)
1.0×10^{-1}	0.979 (± 0.04)	0.544 (± 0.14)	0.286 (± 0.07)	0.35 (± 0.16)	0.597 (± 0.22)	0.537 (± 0.21)
1.65×10^{-1}	-	-	0.557 (± 0.28)	-	-	-
2.0×10^{-1}	0.401 (± 0.40)	0.643 (± 0.15)	0.656 (± 0.37)	-	0.622 (± 0.35)	0.310 (± 0.28)
3.0×10^{-1}	0.749 (± 0.23)	0.494 (± 0.20)	0.421 (± 0.122)	-	0.177 (± 0.06)	0.407 (± 0.20)
4.0×10^{-1}	0.812 (± 0.23)	0.567 (± 0.01)	-	0.245 (± 0.21)	0.671 (± 0.33)	0.757 (± 0.37)
6.0×10^{-1}	0.101 (± 0.18)	-	0.468 (± 0.36)	0.650 (± 0.30)	0.292 (± 0.25)	0.537 (± 0.36)

The table above compares the PDI obtained from the intensity of light scattered by different BSs loaded niosomes and vesicles (prepared by thin film hydration and direct dissolution methods) and hydrated in PBS buffer pH 7.4 at 60°C. The mean intensity and standard deviation of three ($n = 3$, (\pm SD) measurements on different samples is reported and presented in parentheses.

However, in the current study the size distribution was a combination of unimodal, bimodal and trimodal intensity peaks (Table 4.10-4.15) due to vesicle formation. The percentage intensities at each concentration of BSs formulated are presented beside their corresponding z-average particle size. Each percentage intensity peak corresponds to the overall distribution of particle size measured within the distribution. The range of concentrations investigated in this study (80-600 μ g/ml) were guided by the observations reported by Porsunthorntawee *et al.*, (2009) in which the electrical conductivity of a BS solution was used to investigate the structure of surfactant aggregates. It was found that the solution conductivity abruptly increased with increasing BS concentration. However, the maximum

solution conductivity was found at a BS concentration of 80 mg/l, which started decreasing at a BS concentration higher than 80 mg/l, and finally remained constant when the concentration was greater than 600 mg/l. In this research, although different physico-chemical techniques were used for evaluation, the final selection of the optimised concentrations of BSs was based on the observation of spherical morphologies visualised through STEM and observed at 100 µg/ml BS1c. Consequently, the other BSs were formulated at the same concentrations to enable the comparison of their self-assembling properties.

The discrepancies in the sizes and trends in the observed aggregates could have arisen from the differences in the composition of the rhamnolipids, the electrolytes used in the buffers, pH and temperatures. Additionally (Porsunthorntawee *et al.*, 2009) studied a wider range of concentrations, whereas this investigation was guided by the concentration of BSs cytotoxic activity on cancerous and non-cancerous cells previously reported (chapter 3). The controlled delivery of selected BSs in niosomes was hypothesised to reduce BSs cytotoxicity on non-cancerous cells, though this could not be undertaken because of time restraints.

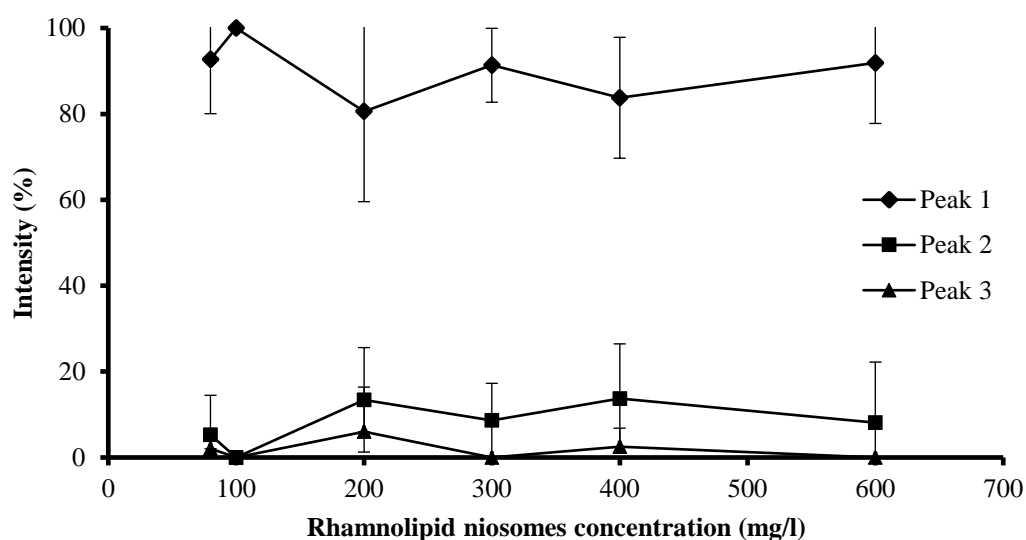


Figure 4.1. Representative graph of percentage intensity of (A) rhamnolipid niosomes (TLH) peaks 1, 2 and 3 represent unimodal, bimodal and trimodal distributions respectively.

Monodisperse samples have a lower PDI value, whereas higher value of PDI indicates a wider particle size distribution and the polydisperse nature of the sample. The PDI appears to increase with increased BS3 concentration at both 60 and 80°C. However, the values obtained for PDI did not correlate with the particle size distribution. This may be due to fact that DLS cannot discern between crystallised aggregates and niosomal structures, the combination of both structures with varied particle size consequently leads to higher PDI. Although there is evidence of aggregates coupled with

micron sized niosomes at 60°C which is the transition temperature of S60, further crystallisation may exist at 80°C. Additionally, the higher molecular weight of BS3 may distort niosome formation.

The niosomal size lies in the nanometric scale, and can be small unilamellar vesicles (SUVs), multilamellar vesicles (MLVs) or large unilamellar vesicles (LUVs). The usual range of PDI values is; 0-0.05 (monodisperse standard), 0.05-0.08 (nearly monodisperse), 0.08-0.7 (mid-range polydispersity), > 0.7 (very polydisperse). However, the acceptable value for PDI range is between 0.05 and 0.7, with values >0.7 indicating that the sample has a very broad size distribution and is probably not suitable for the DLS technique (Hasan, 2014). The presence of an unsaturated carbon-carbon double bond in the tail of BS3 (in which the head group is a disaccharide sophorose sugar) probably results in looser vesicle walls due to geometrical constraints, so gives elongated shapes and precludes the formation of conventional spherical vesicles. The obtained results are in accordance with that reported by (Baille *et al.*, 1985) and (Darwish, 1998) who reported the formation of non-spherical vesicles for niosomes prepared from a mixture of a single or double alkyl chain non-ionic surfactant with cholesterol. Changes in temperature are important considerations in drug delivery, however (Nguyen *et al.*, 2010) hypothesised that due to the dimeric sophorose sugar head, BS3 will be relatively insensitive to temperature even though it is a non-ionic surfactant. Overall, Based on Table 4.8, the size of BS3 loaded niosomes followed an ascending order of 80°C < 60°C and 70°C. However, the PDI (Table 4.15) followed a different trend with temperatures in ascending order of 70°C < 60°C < 80°C. The sizes of the BSs loaded niosomes and vesicles dispersed in PBS buffer were statistically significant $p < 0.05$, while, the PDI were not statistically significant $p > 0.05$.

4.6.2.2 Zeta potential

The continuous aqueous phase surrounding dispersed particles consists of two parts; an inner region, called the Stern layer, where the ions are strongly bound and an outer, diffuse region where they are less firmly attached. Within the diffuse layer there is a notional boundary inside which the ions and particles form a stable entity. When a particle moves (*e.g.* due to gravity), ions within the boundary move with it, but any ions beyond the boundary do not travel with the particle. This boundary is called the surface of hydrodynamic shear or slipping plane. The potential that exists at this boundary is known as the zeta potential. The zeta potential is the measure of the amount of charge on the particle and represents an index of particle stability. One of the major uses of zeta potential is to study colloid-electrolyte interactions. The major area of application of colloid-electrolyte phenomena is to understand stability and flocculation effects. The simplest model used to describe this phenomena is known as the DLVO (Deryaguin- Landau-Verwey-Overbeek) theory. This simply states that the stability of the colloid is a balance between the attractive Van der Waals' forces and the electrical repulsion due to the surface charge. The zeta potential is electrical potential that is used as an indicator of repulsive force.

There are three ways by which a solid particle (colloid) dispersed in a liquid media can acquire a surface charge (Nagarwal *et al.*, 2009). Firstly, by the adsorption of ions present in the solution. Secondly, by the ionisation of functional groups on the particle's surface. Thirdly, due to the difference in dielectric constant between the particle and the medium.

A zeta potential from 0 to ± 5 mV indicates rapid coagulation or flocculation; $\geq \pm 10$ to ± 30 mV suggests incipient instability; ± 30 to ± 40 mV is indicative of moderate stability; ± 40 to ± 60 mV alludes to good stability and $> \pm 61$ excellent stability (Vandamme and Brobeck, 2005). However, according to Malvern and (Müller *et al.*, 2001), a physically stable niosomal dispersion stabilised by electrostatic repulsion should have a minimum zeta potential value of ± 30 mV. A negative zeta potential (-) indicates an acidic formulation while a positive charge (+) signifies an alkaline formulation. The zeta potential also indicates whether the charged active material is encapsulated within the centre or adsorbed onto the surface of the nanoparticles. Thus consideration of the zeta potential is important in preventing aggregation of the particles. Zeta potential was used to characterise the thermo-responsive properties of BS3 loaded niosomes. Table 4.16 shows typical mean potentials at different temperatures for BS3 loaded niosomes with varying CHL content. However, 60°C was observed to be the most favourable temperature for zeta potentials although the values at other temperatures are above -30 mV indicating colloidal stability of an acidic formulation. In the results summarised in Table 4.16, the measured zeta potential values are consistent over a wide range of sample concentrations. The results obtained at 60, 70 and 80°C have a mean value of -52.85 (± 4.0), -48.27 (± 3.4), -47.17 (± 4.90) mV respectively. However, as the temperature increased above 60°C, the zeta potential numerically decreased in order of 60>70>80 with a standard deviation of (± 3.0). However this decrease was not statistically significant ($p > 0.05$).

The effect of 0, 10 and 20 mM CHL on the zeta potential of blank S60 niosomes changed as a function of temperature. At 60°C, BS3(0):S60(10):CHL(10) mM, the overall maximum zeta potential presented in (Table 4.16) was -57.17(± 1.2), at 70°C BS3(0):S60(10):CHL(0) mM CHL, -53.10 (± 0.3) was observed, while at 80°C BS3(0):S60(10):CHL(20) mM, -55.63 (± 2.9) was observed. A combination of one uniform and two intermittent patterns were observed at equal ratios of BS3(5):S60(5) mM mixed niosomes as follows; (i) a decrease from 70-60-80°C at 0 mM CHL (ii) a linear decrease from 60-70-80°C at 10 mM CHL (iii) another intermittent decrease at 20 mM CHL from 60-80-70°C. On the other hand, a uniform decreasing trend was observed in the effect of 0, 10 and 20 mM CHL on BS3(7.8):S60(2.5) from 60-70-80°C. With the exception of 0 mM CHL, in which a decrease of -0.37 mV was observed from 60-70°C, there was a uniform decrease in the effect of 10 and 20 mM CHL at BS3(10):S60(0) niosomes. Overall, the zeta potential of single S60 and BS3 formulated without CHL increased linearly across the hydration temperatures investigated. Additionally, the effect of temperature on the zeta potential of water based niosomes was highest at 60°C for BS3:S60:CHL BS3(7.8):S60(2.5):CHL(20), BS3(0):S60(10):CHL(10) and BS3(10):S60(0):CHL(10) with mean values of -58.20 (± 2.3) > -57.17 (± 1.2) > -56.70 (± 13.4)

respectively - all of which based on the definitions discussed earlier have good stabilities. Once again these results differed from the reference study where corresponding zeta potential < -30 mV were reported by (Balakrishnan *et al.*, 2009).

The zeta potential of different concentrations and BSs type, of PBS buffer based niosomes at optimised temperature and CHL incorporation are presented in Table A4.3 of the appendix. Specifically, the zeta potential of all concentrations of mixed BS1c niosomes investigated were above -30 mV, while corresponding single BS1c vesicles were below the stability range. The differences between both formulations may be due to the incorporation of S60 and CHL. However, Porsunthorntawee *et al.*, (2011) reported that the absolute value of the zeta potential of 2.6 mM rhamnolipid vesicles prepared in phosphate-buffer saline (PBS) solution (pH 7.4) with various amounts of CHL, first reduced with increasing CHL concentration before turning flat at a CHL concentration greater than $200 \mu\text{M}$ which implies the limitation of CHL in the vesicle formation. The effect of CHL was not investigated on buffer based niosomes, therefore an unbiased observation may not be possible, however, taking this into consideration, a comparison will be made on the assumption that the effect of CHL on buffer based niosomes are similar to the results obtained from DI water based niosomes, CHL was not observed to reduce the zeta potential of niosomes. However, with the exception of 6.0×10^{-1} BS2 which had a zeta potential of $-12.33 (\pm 11.69)$ the zeta potential measurements of optimised buffer based formulations were higher than -30 mV. The highest overall zeta potential in this group was observed at $-39.40 (\pm 4.5)$ mV for 6.0×10^{-1} BS4b which is lower than results obtained from DI water based niosomes. This may be due to the effects of ionic strength on the electric double layer (EDL). The inevitable presence of positively charged ions in the EDL of particles suspended in PBS better favours the interaction with multicomponent BSs than the highly negatively charged particle surface in DI water. The decrease in the zeta potential of single component BS1c suggests that the interaction between BSs and S60 is beneficial for the stability of the system. However, more sensitive methods (*e.g.* spectroscopic analysis) are required to discern differences in the adsorption patterns in these media.

As discussed previously, generally, a high zeta potential (negative or positive) is an indication that the system is electrically stabilised. A zero zeta potential, or isoelectric point (IEP), is where particles tend to agglomerate. Majority of dispersions contain ions which are divided into two types depending on their atomic charge. A positive charge is anionic while a negative charge is cationic. The ions attract oppositely charged particles, where positive ions are attracted to the negative surface of a particle and vice versa. As the zeta potential increases, the charged particles repel one another and this stabilises the system against aggregation. The cause of aggregation in vesicular systems is mainly due to van der Waals attraction. Many properties of colloids are determined by surface groups and the charge resulting from their ionisation. For example, the stability against coagulation of most colloids result from the delicate interplay of electrostatics and surface chemistry such as specific ion adsorption and the dissociation of ionisable surface groups. Although pH,

conductivity and concentration are important factors that govern zeta potential measurements, these factors do not adequately explain the differences observed in the preliminary water based and latter set of buffer based formulations. According to Malvern application notes, there is a direct relationship between pH of the surrounding medium and particle dispersant. The pH of all BS3 loaded niosomes fell within the acidic range from 3.4 – 5.1 (Table 4.17). Dissociation of acidic groups on the surface of a particle gives rise to a negatively charged surface whilst, a basic surface will take on a positive charge. In both cases, the magnitude of the surface charge depends on the acidic or basic strengths of the surface groups and on the pH of the solution.

Table 4.16. Effect of temperature on zeta potential of 1', 4''-sophorolactone 6', 6''-diacetate loaded niosomes $n = 3$

BS3:S60:CHL (mM)	Zeta potential (mV)			
	60°C	70°C	80°C	Trend
0:10:0	-52.83 (± 0.8)	-53.10 (± 0.3)	-54.83 (± 2.0)	60<70<80
0:10:10	-57.17 (± 1.2)	-50.70 (± 2.7)	-45.13 (± 3.6)	80<70<60
0:10:20	-49.30 (± 2.9)	-50.83 (± 3.0)	-55.63 (± 2.9)	60<70<80
5:5:0	-50.13 (± 3.1)	-50.50 (± 0.7)	-47.73 (± 0.5)	80<60 \leq 70
5:5:10	-55.57 (± 6.6)	-50.03 (± 2.2)	-46.77 (± 4.3)	80<70<60
5:5:20	-50.43 (± 2.7)	-42.0 (± 3.6)	-48.57 (± 3.2)	70<80<60
7.8:2.5:0	-51.87 (± 3.7)	-45.93 (± 6.3)	-42.50 (± 1.7)	80<70<60
7.8:2.5:10	-55.40 (± 6.7)	-47.23 (± 5.5)	-41.17 (± 2.8)	80<70<60
7.8:2.5:20	-58.20 (± 2.3)	-48.67 (± 3.9)	-46.83 (± 1.4)	80<70<60
10:0:0	-44.17 (± 10.5)	-44.50 (± 10.4)	-	60 \leq 70
10:0:10	-56.70 (± 13.4)	-44.63 (± 1.9)	-42.57 (± 5.5)	80<70<60
10:0:20	-52.47 (± 4.0)	-51.07 (± 9.4)	-	70<60
Mean (\pm SD)	52.85 (± 4.0)	48.27 (± 3.4)	47.17 (± 4.9)	80<70<60

BS3 – biosurfactant (1', 4''-sophorolactone 6', 6''-diacetate), S60 – span 60, CHL – cholesterol
 The table above compares the zeta potential of blank and BS3 loaded niosomes (prepared by thin film hydration method) and hydrated in deionised (DI) water at different temperatures. The zeta potential and standard deviation of three ($n = 3$, (\pm SD) measurements on different samples is reported and presented in parentheses.

Table 4.17. Effect of temperature on pH of 1', 4''-sophorolactone 6', 6''-diacetate loaded niosomes

BS3:S60:CHL (mM)	pH			
	60°C	70°C	80°C	Trend
0:10:10	5.1	4.9	4	80<70<60
5.0:5.0:10	4.3	4.2	3.4	80<60<70
7.8:2.5:10	4.3	4.1	3.4	80<70<60
10:0:0	4.1	4.3	3.8	80<60<70

According to sigma Aldrich BS3 has a pH of 4.0-6.0 (1 mg/mL in H₂O). Although the selected niosomal dispersions were formulated at different transition temperatures, their pHs were measured at room temperature. Differences in pH formulated at different transition temperatures were statistically significant $p < 0.05$.

Surfactant ions may be specifically adsorbed on the surface of a particle, leading, in the case of cationic surfactants, to a positively charged surface and, in the case of anionic surfactants, a negatively charged surface. With the exception of DCP (which is an anionic surfactant), all other components of BS3 loaded niosomes were non-ionic in nature. However, a negative zeta potential of -51.2 (± 3.55) mV was still observed in niosomes formulated without DCP. This could be due to residual electrolytes from ethoxylation catalyst (Akbari *et al.*, 2016). The zeta potential of the BSs loaded niosomes and vesicles dispersed in PBS buffer were statistically significant $p < 0.05$.

Conductivity can be defined as water's ability to conduct electrical current. This characteristic is affected by the total amount of ions dissolved in the water. Inorganic ions can interact with charged surfaces in one of two distinct ways (i) non-specific ion adsorption where they have no effect on the isoelectric point. (ii) specific ion adsorption, which will lead to a change in the value of the isoelectric point. The specific adsorption of ions onto a particle surface, even at low concentrations, can have a dramatic effect on the zeta potential of the particle dispersion. In some cases, specific ion adsorption can lead to charge reversal of the surface (Malvern technical notes, available online at:

<https://www.malvern.com/en/support/resource-center/technical-notes/TN101104ZetaPotentialIntroduction.html> - date accessed 15-8-17).

The zeta potential of low concentrations of BS loaded niosomes was shown to be sensitive to the ionising conditions of the surrounding aqueous buffer. Based on Malvern technical notes, conductivity range of 0.005 mS/cm –5mS/cm for measuring zeta potential is recommended <https://www.malvern.com/en/support/resource-center/technical-notes/TN140827-Zeta-Potential-Analysis-Using-Z-NTA.html> (date accessed 4-9-17). The distribution of preliminary BS3 mixed niosomes optimised at 60°C was predominantly bimodal, which did not affect the quality of the zeta potential obtained. Trimodal distributions at 80°C were equally unaffected (supplementary Table A4.1). Consequently the combination of bimodal and trimodal peaks observed for buffered niosomes does not sufficiently describe previous observations. Additionally, the highest conductivity observed for undiluted blank BS(0):S60(10):CHL(10), mixed BS3(7.8):S60(2.5):CHL(10) and BS3 only (10):S60(10) water based niosomes using a conductivity meter was $26.83 (\pm 2.55) \times 10^{-3}$, $89.03 (\pm 1.70) \times 10^{-3}$, and $40.00 (\pm 1.31) \times 10^{-3}$ $\mu\text{S}/\text{cm}$ at 80, 80 and 60°C respectively (Table A4.4). The conductivities of these same niosomes diluted and recorded from DLS ranged from $(8.43 (\pm 1.30) \times 10^{-3} - 17.50 (\pm 7.88) \times 10^{-3})$ mS/cm for 60°C and $(7.73 (\pm 0.23) \times 10^{-3} - 10.38 (\pm 9.56) \times 10^{-3})$ mS/cm for 80°C (Table A4.5). The reversal in the hydration temperature effect may be due to the fact that the DLS samples were diluted. Sonication was another process parameter observed to increase the conductivity of corresponding formulations (Table A4.5). Conductivities of blank unsonicated and blank sonicated niosomes hydrated at 60°C showed differences in conductivities at $2.05 (\pm 0.25) \times 10^{-3}$ and $8.43 (\pm 1.30) \times 10^{-3}$ mS/cm. Similarly, unsonicated and 3 min sonicated BS3 (5.0):S60 (5.0):CHL (10) mM mixed niosomes had conductivities of $4.67 (\pm 6.96) \times 10^{-3}$ and $7.49 (\pm 8.75) \times 10^{-3}$ mS/cm. This effect was further established between 3 and 40 min sonicated BS3 (7.8):S60 (2.5):CHL (10)

mM which had conductivities of $5.98 (\pm 1.18) \times 10^{-3}$ and $9.147 (\pm 4.68) \times 10^{-3}$ mS/cm. However a consistent pattern was not observed on the effect of sonication across temperature ranges, so no correlation between conductivity and the effect of sonication was established (Table A4.5).

Conversely, the conductivities of optimised concentrations (1.0 , 2.0 and 6.0×10^{-1}) of BS3 (as well as other BS) loaded into niosomes were considerably higher at $21.93 (\pm 2.76)$, $21.43 (\pm 2.04)$ and $22 (\pm 1.66)$ mS/cm and (>19 mS/cm) respectively which are very high (Table A4.6). The lowest concentration of water based BS3 loaded niosomes was > 3000 times (5 mM) more than buffer based BSs loaded niosomes. As discussed above, the specific adsorption of ions onto a particle surface, at low concentrations, can have a dramatic effect on the zeta potential of the particle dispersion. The other difference between preliminary water based and buffer based formulations was that the first set of colloids were dispersed in deionised water while the latter set were dispersed in PBS pH 7.4. The zeta potential of blank niosomes originally formulated in PBS pH 7.4 was diluted with deionised water and measured. The result obtained $61.97 (\pm 2.55)$ mV closely corresponded with that obtained in preliminary investigations. However, it is necessary to obtain readings in a continuous dispersant phase. However (Pornsunthorntawee *et al.*, 2011) reported the formation of rhamolipid vesicles dispersed in PBS pH 7.4 with zeta potentials ranging from -15 to -30 mV. Malvern recommends using the diffusion barrier technique for high conductivity samples to minimise the impact of the measurement process, by loading about $20 \mu\text{l}$ sample and diluting with solvent. Although buffered niosomal samples were diluted, the resultant mixture was thoroughly aspirated before measurements. Corbett and co-workers investigated the electrophoretic mobility of protein samples through the diffusion barrier using a laser Doppler electrophoresis (LDE) where measurements were recorded before the sample diffused into the electrodes (Corbett *et al.*, 2011) and this will therefore be considered for future work.

4.6.3 Analytical characterisation

4.6.3.1 Attenuated total reflectance Fourier transform infrared spectroscopy (ATR-FTIR)

Attenuated Fourier transform infrared spectroscopy (ATR-FTIR) was used to analyse the bonding between BS and niosome components. All BSs used in this study are characterised by a hydrophilic head (sugars, amino acids) and hydrophobic hydrocarbon tails of different chain length. S60 is a monoester formed from the dehydration of sorbitol (a sugar alcohol) with stearic acid as its R group. CHL contains steroid rings with a hydroxyl group, two methyl groups and a hydrocarbon tail. The steroid core structure is composed of seventeen carbon atoms, bonded in four fused rings (three six-member cyclohexane rings and one five-member cyclopentane ring). The ability of S60 to form vesicles depends on its structure, critical packing parameter (CPP), hydrophilic–lipophilic balance, and presence of CHL. The relatively large hydrophobic moieties in S60 may lead to intercalation of BSs into the bilayers leading to an increased affinity among the non-polar portions of the

membrane (Manconi *et al.*, 2002). Interactions between CHL and S60 in the bilayer of niosomes involve hydrogen bonding (Kumar *et al.*, 2011). Dicapryl palmitate (DCP) may be incorporated as a stabiliser in a vesicular system. It has a net negative charge and a long fatty chain (C16) which provides electrostatic and steric stabilisation to the niosomal dispersion. DCP is a complex mixture of diesters of cetyl alcohol and phosphoric acid (Table 4.18). All three standards have similar functional groups which is why they have similar wavenumbers. Initially, spectrophotometric studies were performed in order to prove complex formation by measuring the differences in transmittance due to complexation. However, the characteristic ATR-FTIR peaks of the individual components were completely masked by water hydrated in the niosomal suspensions (data not shown), although some peaks were visible after freeze drying (supplementary data A4.1). However, there were little differences in the wavenumbers of loaded niosomes (Tables A4.6 – A4.11), therefore comparison between effect of CHL and temperature on preliminary niosomes as well as effect of DCP in the final formulations are presented in Tables (4.19 – 4.24).

Table 4.18. Assignment of wavenumbers (cm⁻¹) present in pure span 60, cholesterol and dicetyl phosphate standards based on possible intermolecular/intramolecular interactions analysed by ATR-FTIR analysis

ATR-FTIR cm ⁻¹)		
S60	CHL	DCP
3389	3391	3380
2917	2917	2917
2850	2850	2849
1735	1736	1736
1467	1467	1468
1380	1379	1379
1218	-	-
1173	1174	1175
1060	1055	1079
-	-	1049
885	-	889
721	721	814
-	-	720
-	-	562
-	-	535
		494
		461

S60 - span 60, CHL – cholesterol, DCP – dicetyl phosphate

Table 4.19. Effect of temperature on wavenumbers (cm⁻¹) present in BS3(0):S60(10.0):CHL(10.0/20) blank niosomes at 10 and 20 mM CHL analysed by ATR-FTIR analysis

ATR-FTIR (cm ⁻¹)			
BS3(0):S60(10):CHL (10) mM niosome 60°C	BS3(0):S60(10):CHL (10) mM niosome 70°C	BS3(0):S60(10):CHL (10) mM niosome 80°C	BS3(0):S60(10):CHL (20) mM niosome 80°C
3402	3398	3375	3430
2955	2955	2956	2918
2917	2918	2917	2918
2857	2849	-	2857
2849	1736	2849	2849
1737	1467	1735	1736
-	1378	1705	-
1467	1365	1468	1466
1378	1220	1379	1377
1365	1176	-	1365
1220	1082	1220	1220
-	1054	1197	-
1176	1022	1175	1177
	953	1080	
1054	926	1052	1054
1022	890	-	1022
953	840	-	953
-	800	-	926
890	721	890	890
840	504	815	840
800	-	-	800
721	-	721	721
-	-	560	593
-	-	536	-
503	-	506	502
-	-	495	-
-	-	462	-

Table 4.20. Effect of temperature on wavenumbers present in two different concentrations of 1', 6''-diacetate 6', 6''- sophorolactone loaded in BS3(5):S60(5):CHL(10) and BS3(7.8):S60(2.5):CHL(10) mM loaded niosomes analysed by ATR-FTIR analysis

ATR-FTIR (cm ⁻¹)					
BS3(5):S60(5):CHL (10) mM niosome 60°C	BS3(7.8):S60(2.5):CHL (10) mM niosome 60°C	BS3(5):S60(5):CHL (10) mM niosome 70°C	BS3(7.8):S60(2.5):CHL (10) mM niosome at 70°C	BS3(5):S60(5):CHL (10) mM niosome at 80°C	BS3(7.8):S60(2.5):CHL (10)mM niosome 80°C
3403	3427	3387	3404	3402	3403
2918	2919	2918	2919	2919	2919
2849	2849	2849	2849	-	2849
1739	1742	1736	1742	1743	1742
1467	1468	1466	1467	1467	1467
1377	1377	1365	1377	1366	1377
-	1366	-	-	-	-
1236	1230	1235	1266	1235	1236
1171	1171	1175	1169	1169	1170
-	1110	-	-	-	-
-	1081	-	1080	-	1080
1054	1052	1054	1053	1052	1053
-	1022	-	-	-	-
953	953	-	953	-	953
-	926	-	-	-	-
891	891	-	891	-	891
840	840	-	840	-	840
800	800	-	800	799	800
721	721	721	721	721	721
-	593	-	603	-	603
-	564	-	563	564	563
-	536	-	-	-	535
-	520	-	-	-	-
-	505	-	-	-	-
-	495	-	495	-	495

Table 4.21. Effect of temperature on wavenumbers present in BS3(10):S60(0):CHL(0) mM loaded niosomes analysed by ATR-FTIR analysis

ATR-FTIR (cm ⁻¹)		
BS3(10):S60(0):CHL(0) mM niosome at 60°C	BS3(10):S60(0):CHL(0) mM niosome at 70°C	BS3(10):S60(0):CHL(0) mM niosome at 80°C
3426	3393	3405
-	2955	-
2918	2917	2919
2849	2849	2849
1736	1734	1743
1467	1467	1467
1377	1378	1377
1265	-	1236
1220		1236
1176	1178	1169
1071	1083	1080
1053	1054	1053
1022	1022	-
953	959	953
891	890	891
840	-	840
800	-	-
721	-	-
503	-	-

Table 4.22. Comparison of components (BS, S60, CHL DCP) effect on 1.0×10^{-1} mg/l rhamnolipid standards loaded in niosomes formulated with and without DCP (using thin film hydration method) as well as rhamnolipid vesicles formulated (using direct dissolution) and blank niosomes analysed by ATR-FTIR

Peak number	ATR-FTIR(cm^{-1})				
	BS1c STD	1.0×10^{-1} mg/l NIO-DCP-BS1c	1.0×10^{-1} mg/l NIO-BS1c	1.0×10^{-1} mg/l VES-BS1c	0 mg/l NIO-BSs
1	3257	3370	3363	3366	3360
2	2924	2918	2918	2918	2918
3	2855	2850	2850	2851	2851
4	1726	1736	1736	1736	1736
5	1655	1467	1467	1466	1466
6	1575	-	-	-	-
7	1397	1378	-	-	-
8	1317	-	-	-	-
9	1123	1163	-	1172	1171
10	1046	1057	1059	1059	1057
11	981	954	984	-	-
12	916	-	-	-	-
13	881	-	-	-	-
14	-	860	867	-	-
15	831	-	-	-	-
16	808	-	-	-	-
17	-	721	721	-	-
18	704	-	-	-	-
19	663	-	-	-	-
20	543	-	-	-	-
21	-	517	523	-	-
22	483	-	-	-	-

Table 4.23. Comparison of components (BS, S60, CHL DCP) effect on 1.0×10^{-1} mg/l Rewoferm SL ONE standards loaded in four component (4CN) (BS:S60:CHL:DCP) and three component (BS:S60:CHL) niosomes (3CN) analysed by ATR-FTIR

ATR-FTIR (cm^{-1})			
Peak number	BS4a STD	1.0×10^{-1} mg/l BS4a 4CN	1.0×10^{-1} mg/l BS4a 3CN
1	3368	3398	3365
2	2928	2917	2918
3	2855	2850	2850
4	-	1736	1737
5	1641	-	-
6	1553	-	-
7	-	1467	1467
8	1415	-	-
9	-	1378	1378
10	1369	-	-
11	1247	-	-
12	1170	1168	-
13	1077	-	-
14	-	1057	1057
15	1034	-	-
16	-	953	985
17	-	860	863
18	-	721	721
19	-	522	524

Table 4.24. Comparison of components (BS, S60, CHL, DCP) effect on 6.0×10^{-1} mg/l surfactin standards loaded in four component (4CN) (BS:S60:CHL:DCP) and three component (BS:S60:CHL) niosomes (3CN) analysed by ATR-FTIR

ATR-FTIR (cm^{-1})			
Peak number	BS2 STD	6.0×10^{-1} mg/l BS2 4CN	6.0×10^{-1} mg/l BS2 3CN
1	3300	-	3355
2	2957	-	-
3	2927	2920	2918
4	-	2851	2850
5	1719	1736	1734
6	1643	-	-
7	1467	1465	1467
8	1387	-	1378
9	1232	-	-
10	1034	1055	1058
11	-	-	983
12	-	-	863
13	-	-	721
14	-	-	523

4.6.3.2 X-ray diffraction (XRD)

Diffraction or scattering are a distinct category of analytical techniques where electromagnetic radiation in the form of Fourier transform of the pair wise correlation function is used as an interference pattern to observe structural features. A technical rule of thumb employed in our laboratories describes crystal phase of $> 70\%$ as fully crystalline while phases below 30% are considered amorphous. With the exception of BS1c and BS2, all standards used in formulating niosomes are crystalline (appendix Table A4.13). The percentage crystallinities of all (but BS2 which has an amorphous profile) standards listed are in agreement with corresponding diffractograms in Figs (4.2 - 4.9). The XRD patterns of BS4a and BS4b were not analysed due to their liquid amorphous states. Amorphous solids can exist as either super-cooled liquids (a viscous equilibrium liquid form) or as a glassy solid non-equilibrium form of the same material. The temperature at which one form converts into the other is known as the glass transition temperature. However amorphous materials

can age or relax over time due to stress and temperature. Aged materials show decreased physical and chemical reactivity compared to unaged materials. However water hydration can reverse the aging and reactivity of amorphous materials.

The mean effect of temperature on BS3 loaded niosomes (Table A4.14) is observed to follow the order of $80 < 60 < 70^{\circ}\text{C}$, however at all temperatures, the percentages crystallinities were above 70% which may indicate that the combined effects of niosome components are more important variables in the final state of formulations in this research. The crystalline and amorphous phases of 8.0×10^{-2} - 6.0×10^{-1} mg/l BSs loaded niosomes are presented in Table A4.15 of the appendix. Although the crystal phases at all concentrations are above 70%, 1.0×10^{-1} mg/l BS1c, BS4a/BS4b and 6.0×10^{-1} mg/l BS2 had the highest crystallinities of 88.35, 84.77, 88.15 and 84.48 % respectively. This does not necessarily indicate a relationship between optimisation, because 2.0×10^{-1} BS2 has a crystal phase of 84.83% however when observed with SEM, the customary spherical morphology associated with niosomal formulations were not observed (see next section).

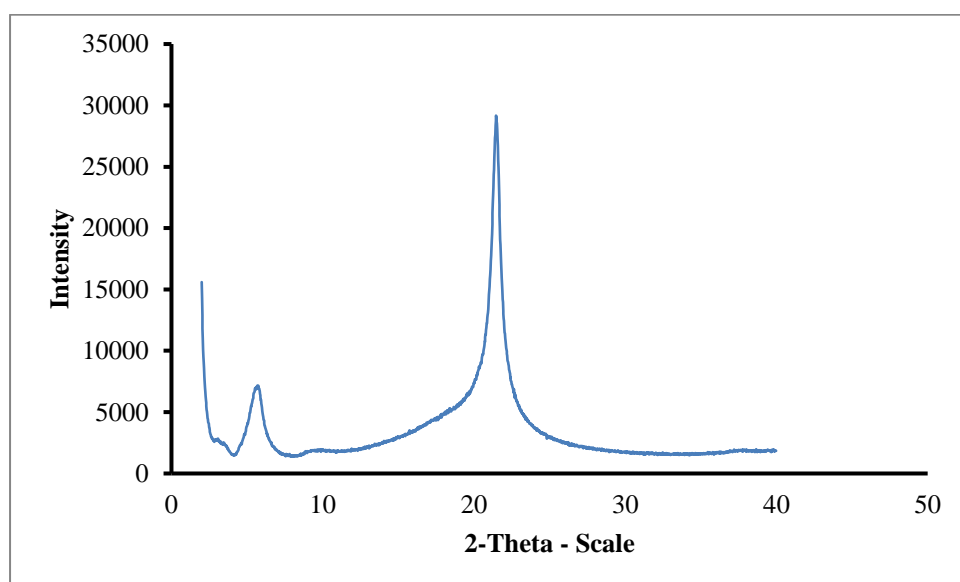


Figure 4.2. XRD diffractogram of pure span 60 (S60) standard.

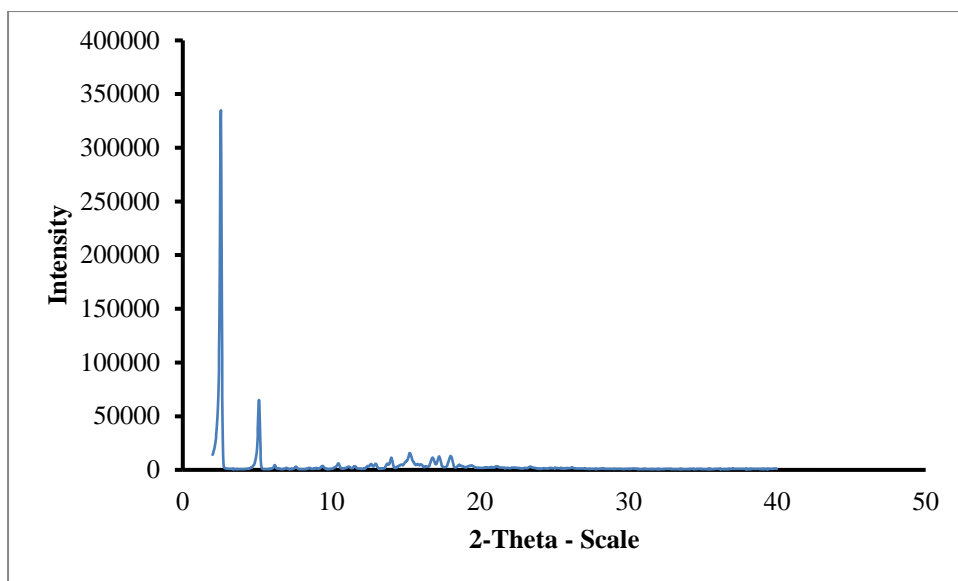


Figure 4.3. XRD diffractogram of pure cholesterol (CHL) standard.

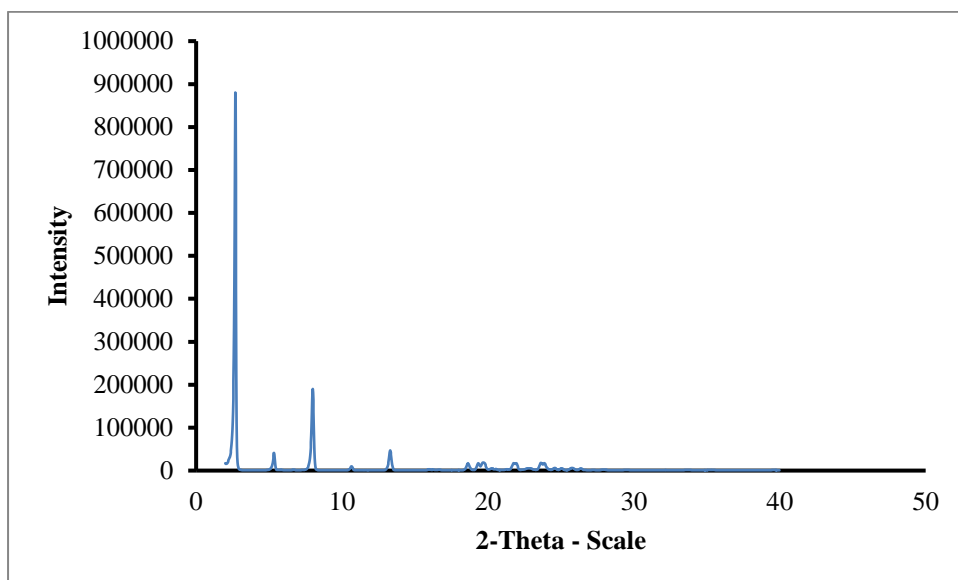


Figure 4.4. XRD diffractogram of pure dicetyl phosphate (DCP) standard.

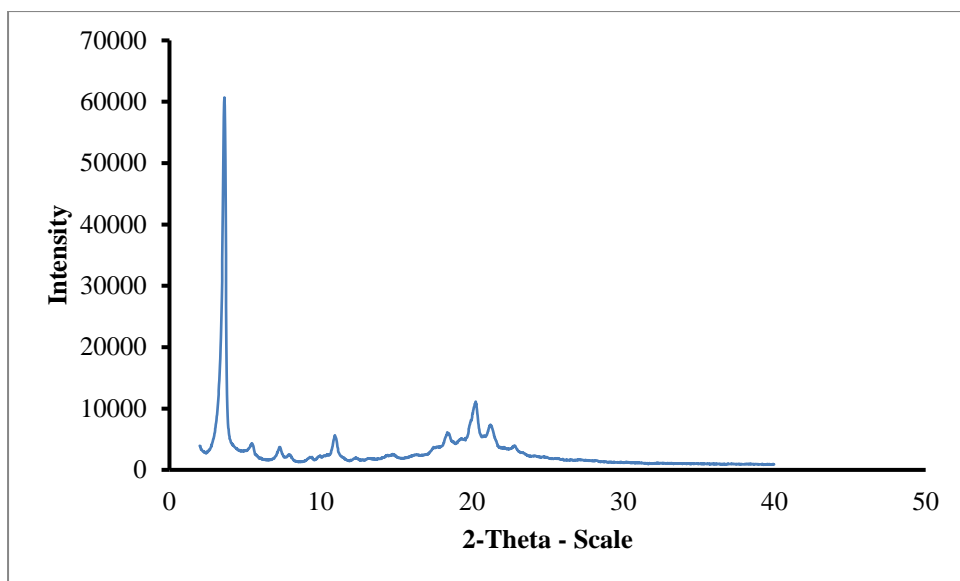


Figure 4.5. XRD diffractogram of pure 1', 4''-sophorolactone 6', 6''-diacetate (BS3) standard.

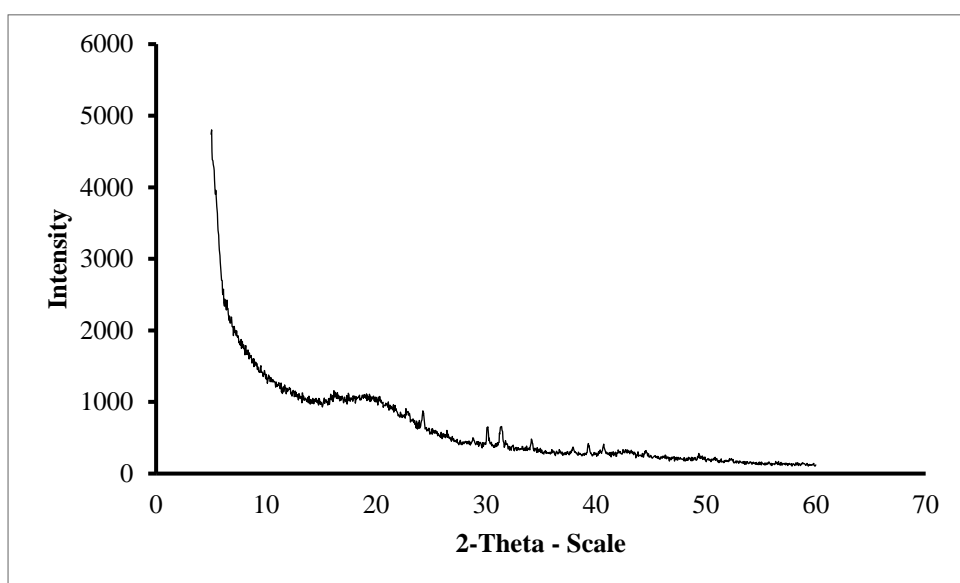


Figure 4.6. XRD diffractogram of pure rhamnolipid standard.

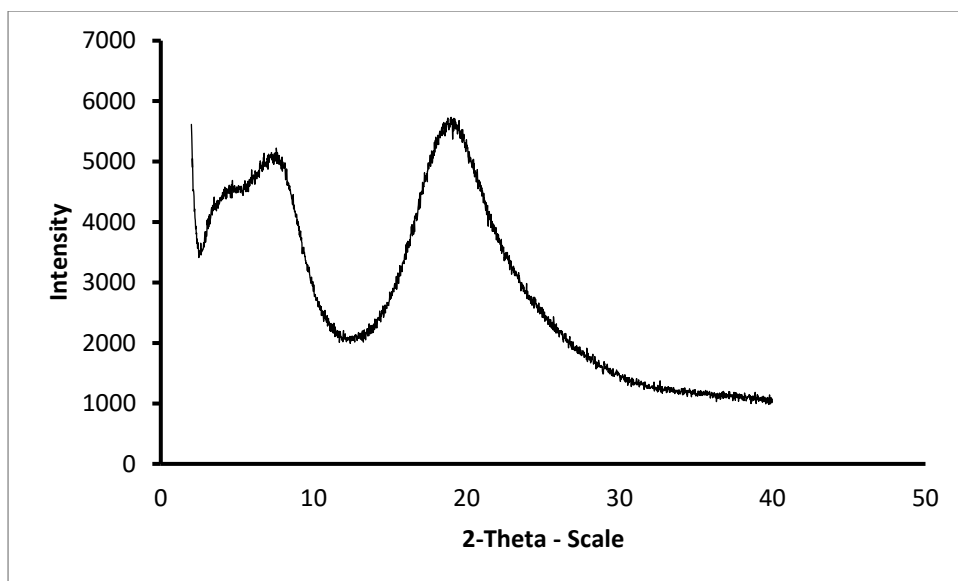


Figure 4.7. XRD diffractogram of pure surfactin standard.

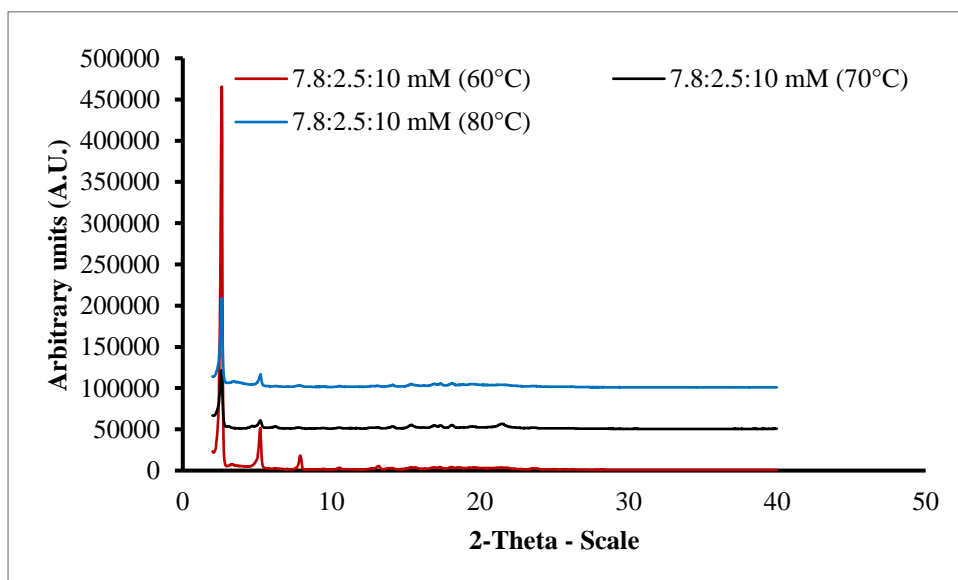


Figure 4.8. Representative XRD diffractograms showing effect of temperature on BS3:S60:CHL in 7.8:2.5:10 mM loaded niosomes.

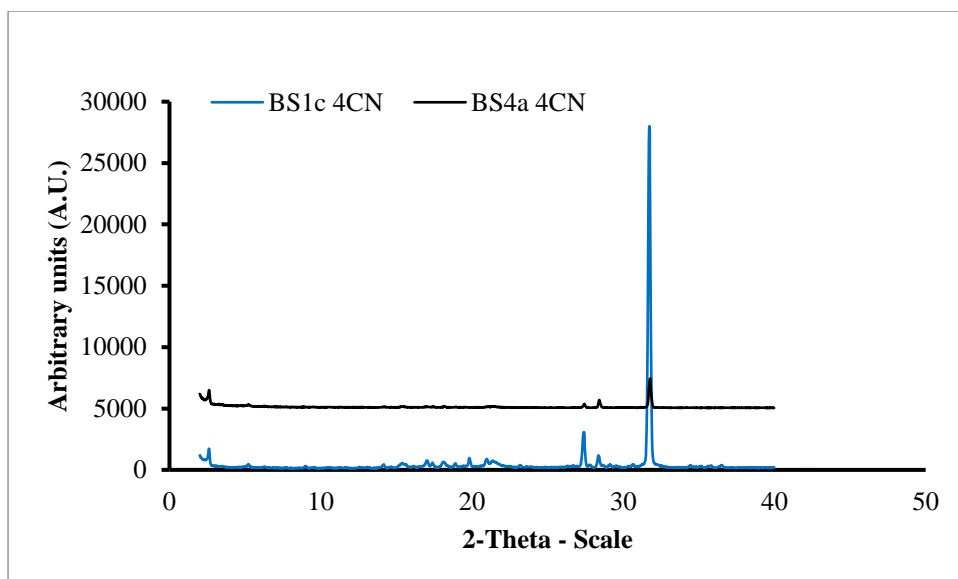


Figure 4.9. Representative XRD diffractograms showing effect of temperature on 1.0×10^{-1} mg/l BS1c and BS4a loaded niosomes.

4.6.3.3 Scanning electron microscopy in transmission mode (STEM)

SEM was used to investigate the surface morphologies of the niosomes and estimate changes in size with various formulation and processing variables. The sizes of pure S60, CHL and DCP standards measured by SEM (Fig 4.10) ranged from 679 μm – 1.19 mm, 7.67 – 34.9 μm and 178 – 347 μm . All three components are insoluble in water and were therefore dissolved in organic solvents for formulation development.

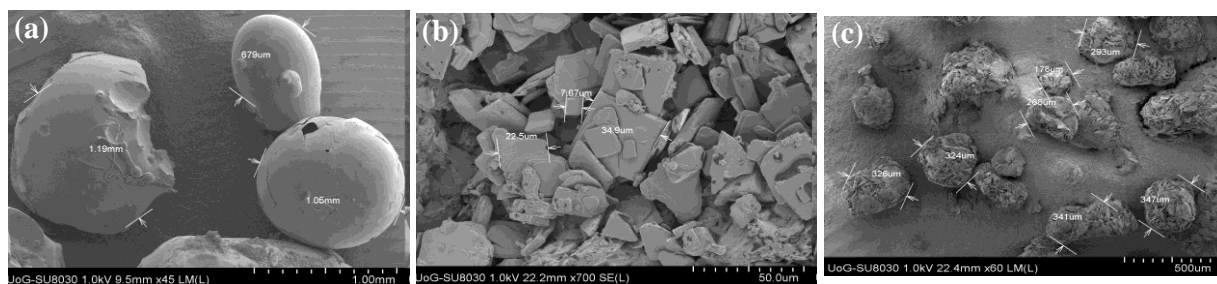


Figure 4.10. SEM of pure: (a) Span 60 (b) Cholesterol (c) Dicetyl phosphate standards.

S60 has a transition temperature of 53°C, while BS3 melts at 123°C and undergoes glass transition at 61°C. It is therefore possible that preparation temperature affects the PDI and particle size in general. For example, it has been reported that particle size of BS3 used as capping agents for cobalt nanoparticles decreased with increasing temperature (Kasture *et al.*, 2007). Therefore the effect of temperature was investigated at 60, 70 and 80°C (Fig 4.11).

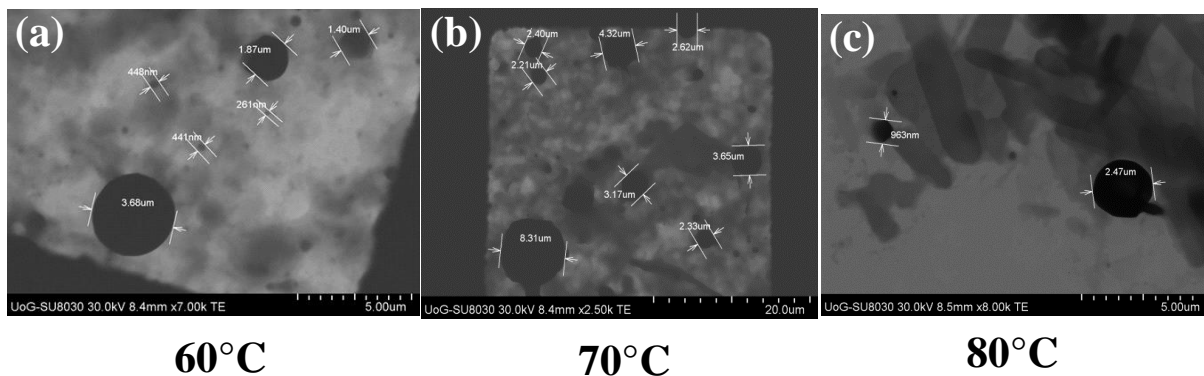


Figure 4.11. Representative STEM images of BS:S60:CHL 0:10:10 mM (blank) niosomes at different temperatures.

It has been reported that niosomes prepared without CHL formed a gel and only on the addition of CHL was a homogenous niosome dispersion obtained (Yoshioka *et al.*, 1994), originally cited in (Uchegbu, and Vyas, 1998). However in this study, unsonicated blank niosomes prepared without CHL were formed. The sizes of these blank unsonicated S60 niosomes (Fig 4.12) formulated at 70°C ranged from 218 – 1700 nm while the sizes of the same blank niosomes sonicated for 40 min (Fig 4.13) ranged from 13.1 – 2010 nm. In addition, the customary spherical morphology of niosomes were observed.

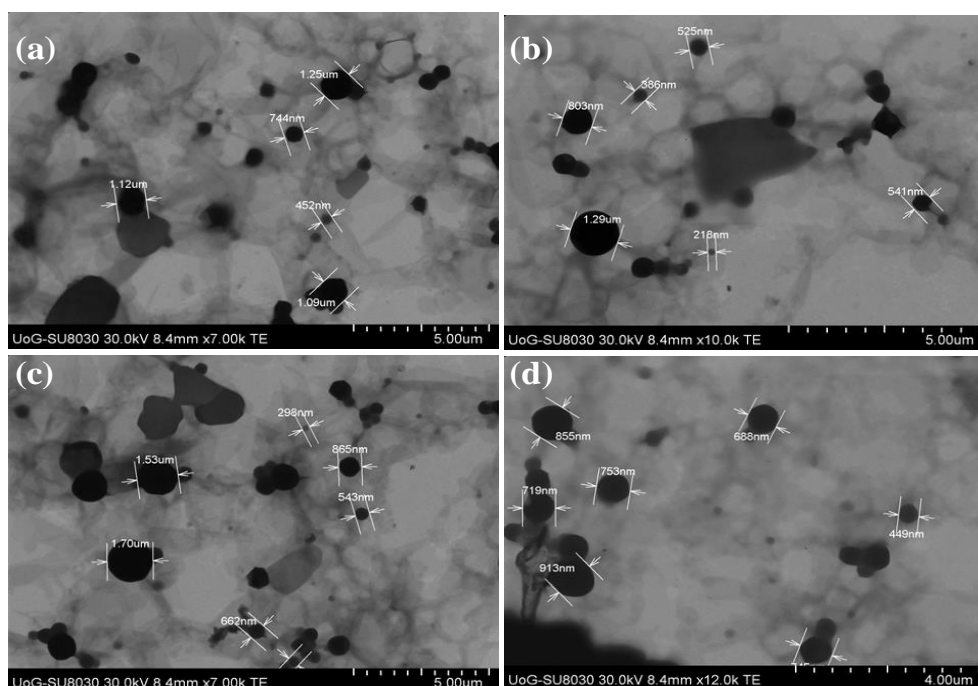


Figure 4.12. STEM images of unsonicated BS3(0):S60(10):CHL(0) mM blank niosomes formulated at 70°C visualised and at different angles.

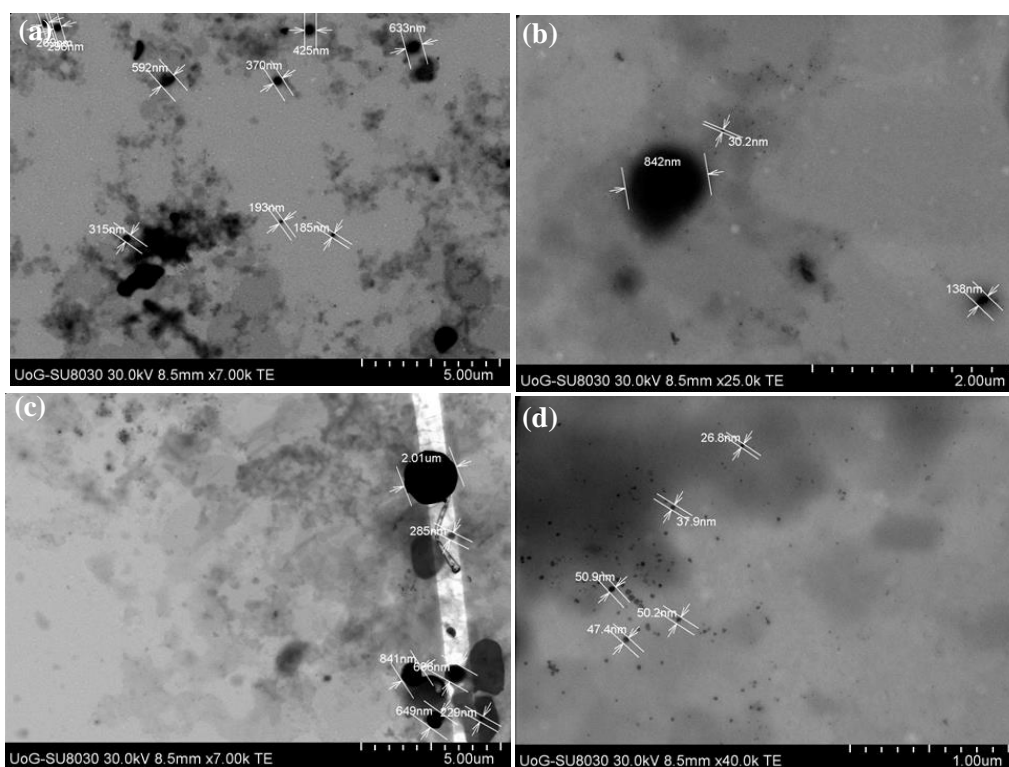


Figure 4.13. STEM images of sonicated (40 min) BS3(0):S60(10):CHL(0) mM blank niosomes formulated at 70°C and visualised at different angles.

Sonication was observed to create many more nanometre sized niosomes, however, a few micrometre sized niosomes were resistant to the effect of sonication. The presence or absence of CHL did not appear to have any discernible effect on the morphology of the blank S60 niosomes formed supplementary (Fig A4.2) with sizes of blank niosomes containing CHL ranging from 29.2 – 1290 nm. However when blank niosomes containing CHL were sonicated, nanometre sizes of 12.1 - 561 nm with aggregation and undefined morphologies were observed. There was formation of square shaped spheres, which may be due to the absence of CHL (Fig A4.3) and crystallisation (Fig A4. 4) which may be due to prolonged sonication time. The addition of CHL did not discernibly improve the morphology of BS3(7.8):S60(2.5):CHL(10) mM niosomes obtained with no sonication (Fig 4.5), and there were a few imperfect spheres formed, however the niosomes formed were predominantly in the nanometre size range and grouped in aggregated clusters with an overall size range of 39.2 – 2160 nm. The same formulations when sonicated for 40 min appeared to be more defined but still lacked a perfect spherical morphology and had sizes ranging from 15.1 – 1010 nm (data not shown). Niosomes obtained from BS3(5):S60(5):CHL(0) mM mixtures had dense spherical diameters which appeared to be breaking down, with sizes ranging from 24.8 - 1470 nm (Fig A4.6). While the morphology of BS3(5):S60(5):CHL(0) niosomes were well-defined (data not shown). With the exception of two spherical niosomes, the morphologies of BS3(5):S60(5):CHL(10) mM niosomes were irregular, however when sonicated for 40 min there appeared to be better defined geometrical shapes. However

a double amount of CHL appeared to have a more favourable effect on BS3(5):S60(5):CHL(20) mM (data not shown) with sizes ranging from 62.8 – 1540 nm, with a combination of square and large spherical niosomes. The interaction between the bulky nature of both BS3 and S60 dispersed in equal proportion may have adapted to higher CHL content under this conditions.

Although low yield was achieved with BS3(10):S60(0):CHL(10) at 60°C (Fig 4.14ci), when the same formulation was hydrated at 70°C, large vesicles were observed to have formed (Fig 4.14ciii). Overall, temperature was observed to have a more favourable effect on pure BS3 with CHL than combination of BS3 and S60 which may be due to reduced steric hindrance. On the other hand the combination of BS3:S60:CHL (7.8:2.5:10) at 60°C (Fig 4.14bi) showed a better morphology than the same formulation at 70°C as observed earlier. As a result all subsequent niosomes with BSs (BS1c, BS4a and BS4b) loading were formulated at 60°C.

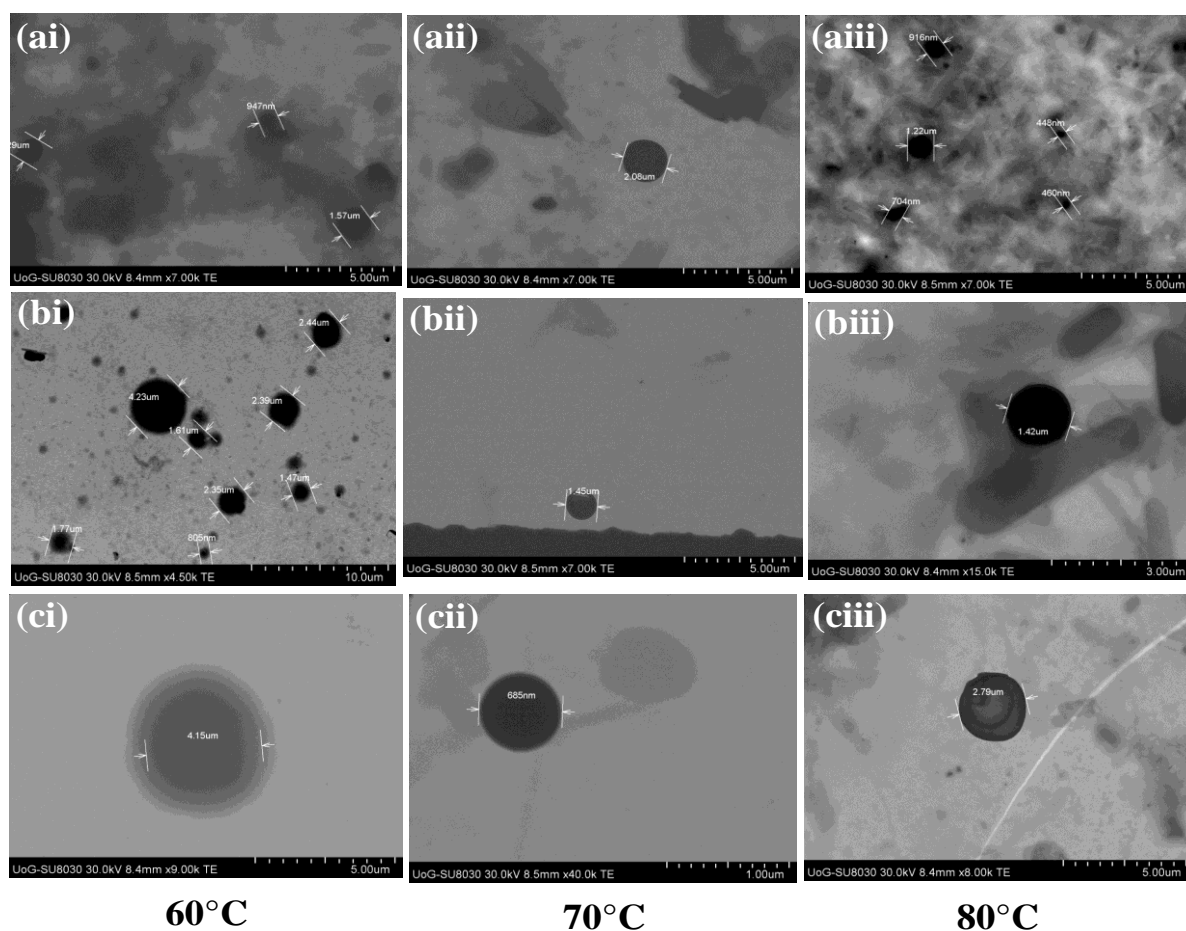


Figure 4.14. Representative STEM image of BS:S60:CHL in (a), 5:5:10 (b), 7.8:2.5:10 (c) 10:0:10 mM formulations at different temperatures.

Pornsunthorntawee *et al.*, (2009; 2011) investigated the formation of rhamnolipid vesicles with and without CHL by means of two different methods; (i) direct sonication of an aqueous dispersion of the various components (bulk) and (ii) by solubilisation of the components through

evaporation of the organic solvent to form a film inside the vessel and reported a reduction in size of the formed vesicles. However in the research reported in this thesis, there was a marked increase in size (Fig 4.16 (a) and (c) which may be due to the addition of other additives such as S60 and DCP. The presence of an anionic surfactant such as DCP with a high degree of hydrophilicity always resulted in vesicles that were larger than the uncharged ones (niosomes formulated without DCP). This can be related to an optimised ion-dipole interaction between the hydroxyl group of CHL and the ionised phosphate group of DCP (Shah and Shulman, 1967). However this was contrary to blank niosomes formulated with S60, CHL and DCP which had an average size of 2.56 μm (Fig 4.17a) while those formulated with S60, CHL in the absence of DCP had an average size of 151 nm (Fig 4.17b). However although their distribution was considerable they were very closely packed together which may have had a reductive effect on their sizes. This was further confirmed when 1.0 mg/l BS4a was formulated individually with CHL and S60 only (Fig 4.18). Although the absolute spherical shape typical of niosomes was not achieved, clear definition and less aggregation was observed when CHL was used as an additive. Israelachvili and co-workers observed that a cone shaped amphiphile plus a wedge shaped one (*e.g.* CHL) cooperate to form bilayer membranes *in vivo* (Israelachvili *et al.*, 1980) and the STEM images (Fig 4.16a and b) supported this observation. Although rhamnolipids have the ability to self-assemble without any additives, the vesicles formed appeared to be less defined than the niosomes formed with CHL. The direct dissolution was only used to formulate BS1c vesicles in this research, therefore, all comparisons of vesicle properties below refer to niosomes that were prepared by means of the thin layer hydration method. Single tailed surfactants (*e.g.* sodium dodecyl sulphate) tend to form micelles while double-tailed surfactants (BS1c) generally leads to the formation of bilayer structures in aqueous solution (Segota, 2006; Antonietti and Forster, 2003; Kodama *et al.*, 2006).

Comparison between niosomes prepared from 2.0×10^{-2} mg/l BS1c and BS4a showed the initiation of the bilayer formation is more evident in BS4a adding further evidence that BS1c standard possess greater self-assembling properties (Fig 4.19). The niosomes prepared have the same concentration of BSs although an exception was made for BS2 where 1.65×10^{-1} mg/l (Fig 4.21) was investigated while 4.0×10^{-1} mg/l was omitted. This concentration was the CMC observed in a previous investigation, however there was very poor and nearly indistinguishable formation of spherical aggregates identifiable as either micelles or vesicles below this concentration (8.0×10^{-2} – 1.0×10^{-1} mg/l) as well as between (2.0 - 3.0×10^{-1} mg/l). This was obvious among the other BSs where formation of spherical aggregates were observed at concentration ranges of (1.0×10^{-1} and 6.0×10^{-1} mg/l), particularly for BS1c and BS2 (Fig 4.20a and b) 130 (30) where spherical aggregates were observed. Although, the average size of 6.0×10^{-1} mg/l BS2 (Fig 4.20b) measured using STEM was 130 (± 30) nm, which is an excellent size for nanoparticulate drug delivery, the electrostatic repulsion between the niosomes is very low as previously observed in the zeta potential measurements.

Fig 4.22 shows a representative image of optimised 1', 4''-sophorolactone 6', 6''-diacetate (BS3) with a size of 474 nm which is an ideal size suitable for anticancer niosomal drug delivery of BSs. Although the optimum niosome concentration of 4.0×10^{-1} mg/l is higher than the IC_{50} of free BS3 (2.5×10^{-2} mg/l) obtained in chapter 3, the rate of BSs release will ultimately determine the level of efficiency. However, microscopic visualisation of optimised niosomal dispersions using STEM revealed severe distortion of vesicles dispersed in cell culture medium (Fig 4.15), which essentially negates the investigation. However BSs are multifunctional compounds with broad spectrum of biological activities including anti-inflammatory dressings for wound healing which are not hindered by size.

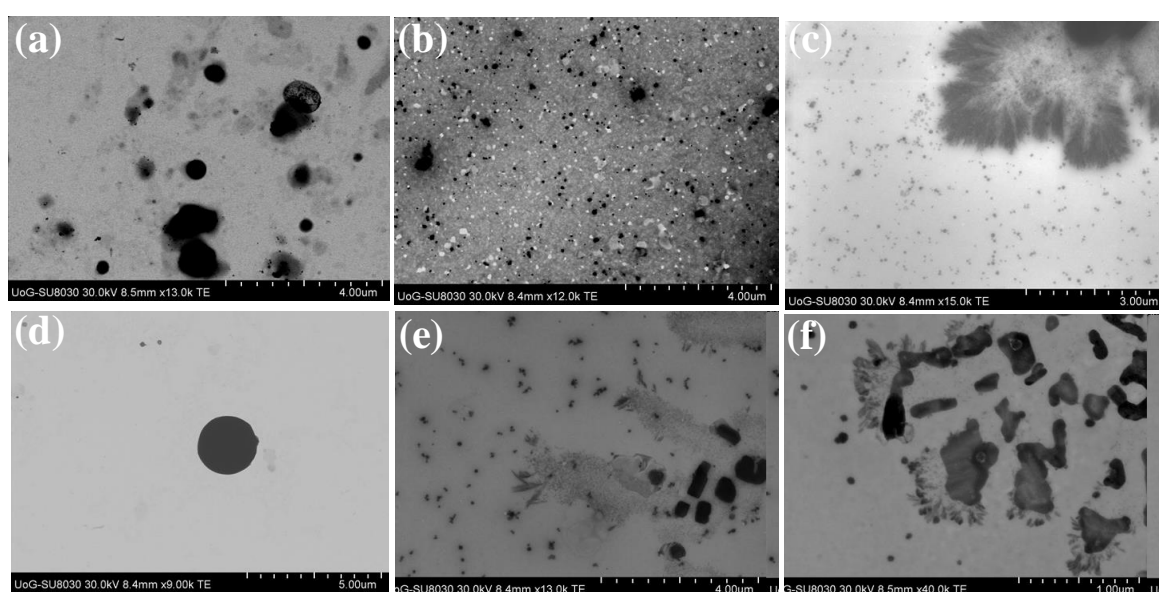


Figure 4.15. Effect of osmotic shock: (a) Rhamnolipids (BS1c) in PBS (b) Rhamnolipids (BS1c) in RPMI (c) Rhamnolipids (BS1c) in DMEM (d) Rewoferm SL ONE (BS4a) in PBS (e) Rewoferm SL ONE (BS4a) in RPMI (f) Rewoferm SL ONE (BS4a) in DMEM.

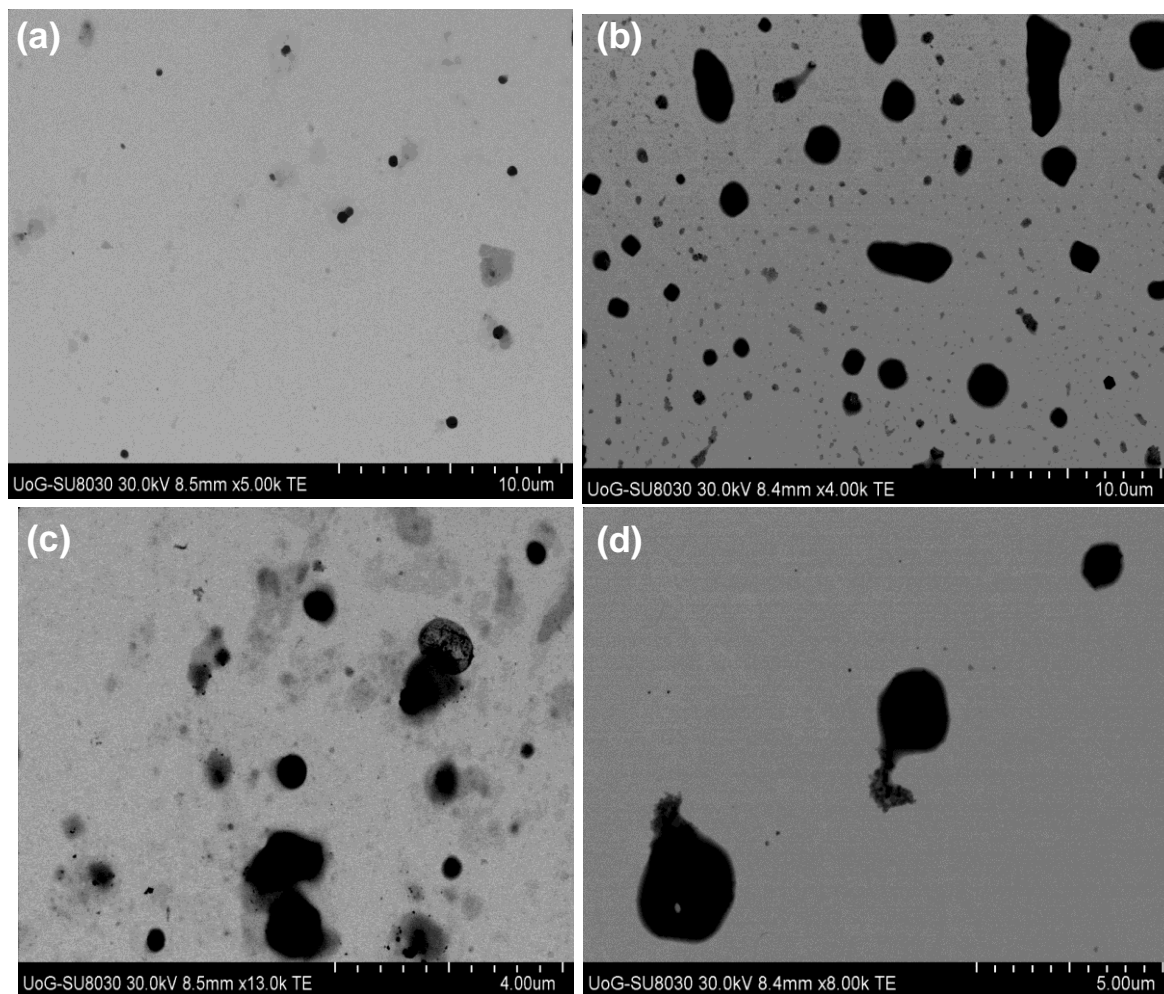


Figure 4.16. STEM images of 1.0×10^{-1} mg/l rhamnolipid niosomes and vesicles prepared by TLH and DD at different magnifications (a) Rhamnolipid niosomes, (b) rhamnolipid vesicles (c) rhamnolipid niosomes, (d) rhamnolipid vesicles.

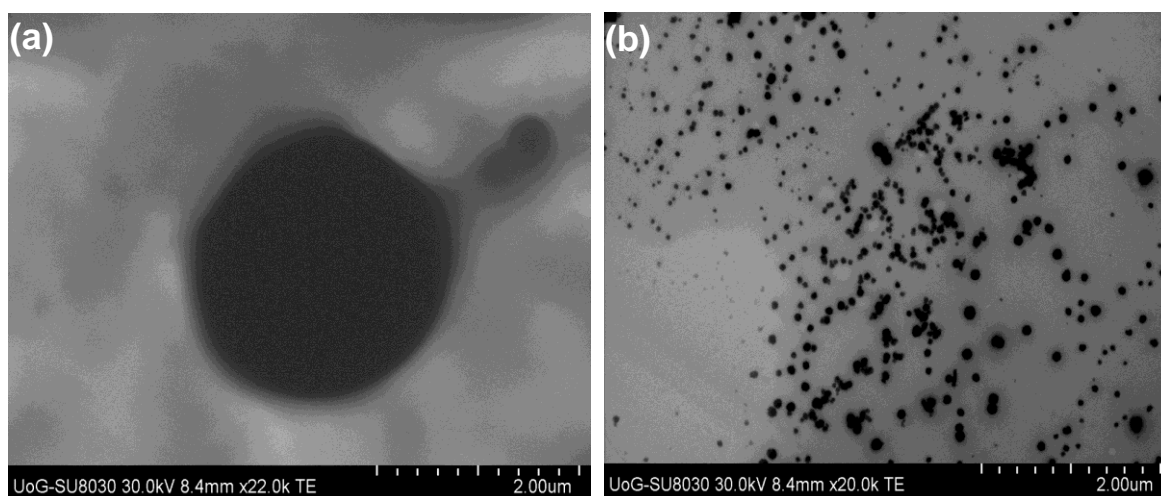


Figure 4.17. The effect of DCP on blank niosomes composed of (a) span 60, CHL and DCP, (b) S60 and CHL only.

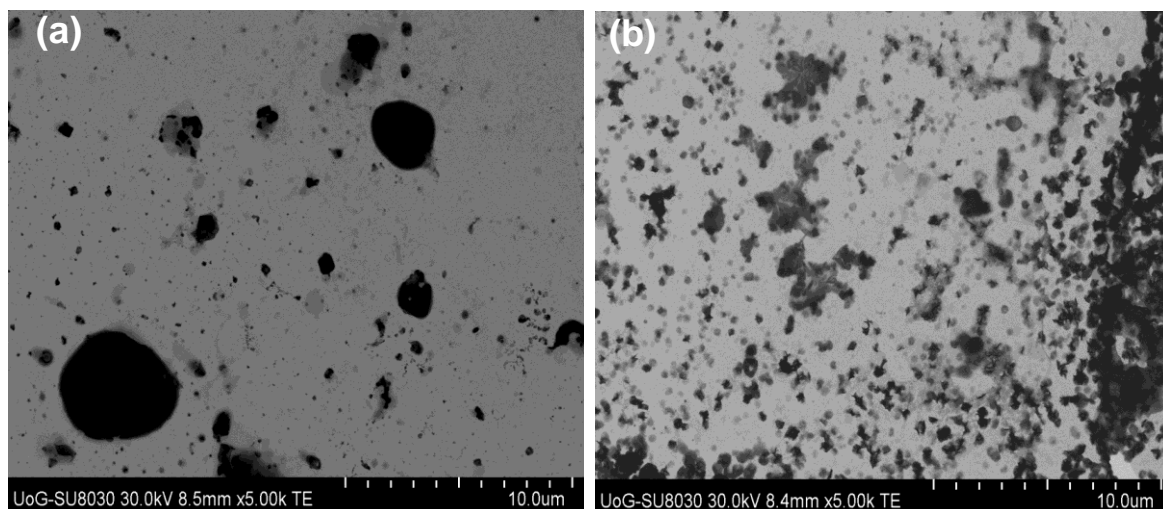


Figure 4.18. Effect of CHL on 1.0 mg/l SL ONE (a) niosome vehicle formulated with S60 and CHL only, (b) Niosome vehicle formulated with S60 and DCP only.

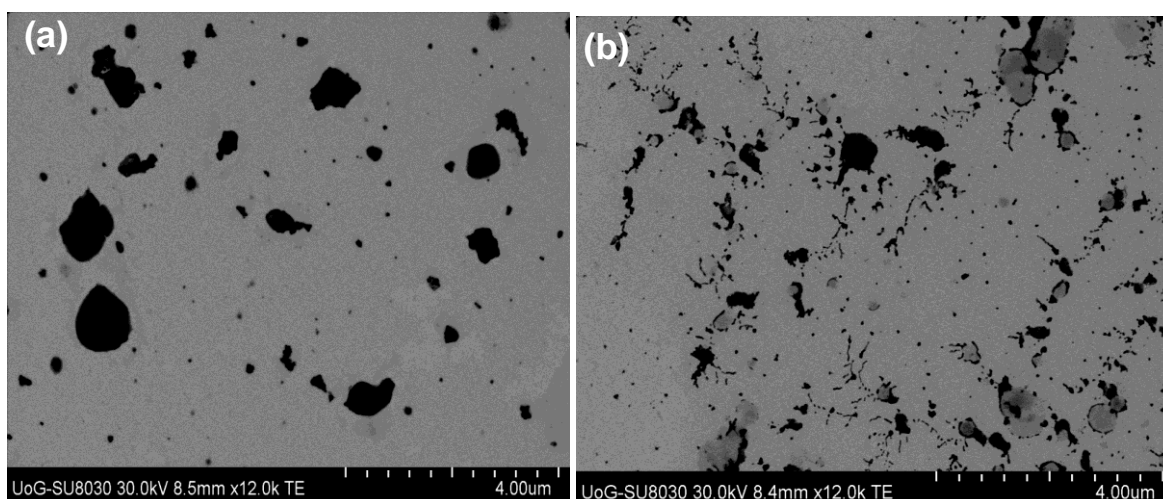


Figure 4.19. Comparison of the initiation of mono and bilayer self-assembly in 2.0×10^{-2} mg/l (a) rhamnolipids and (b) SL ONE.

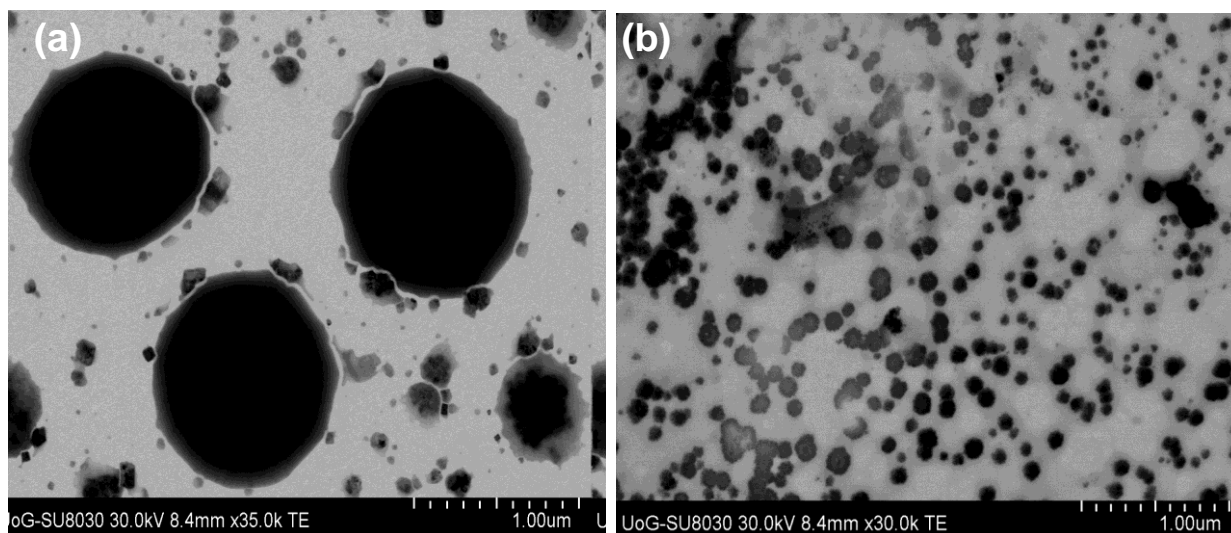


Figure 4.20. Comparison of rhamnolipid and surfactin loaded niosomes.

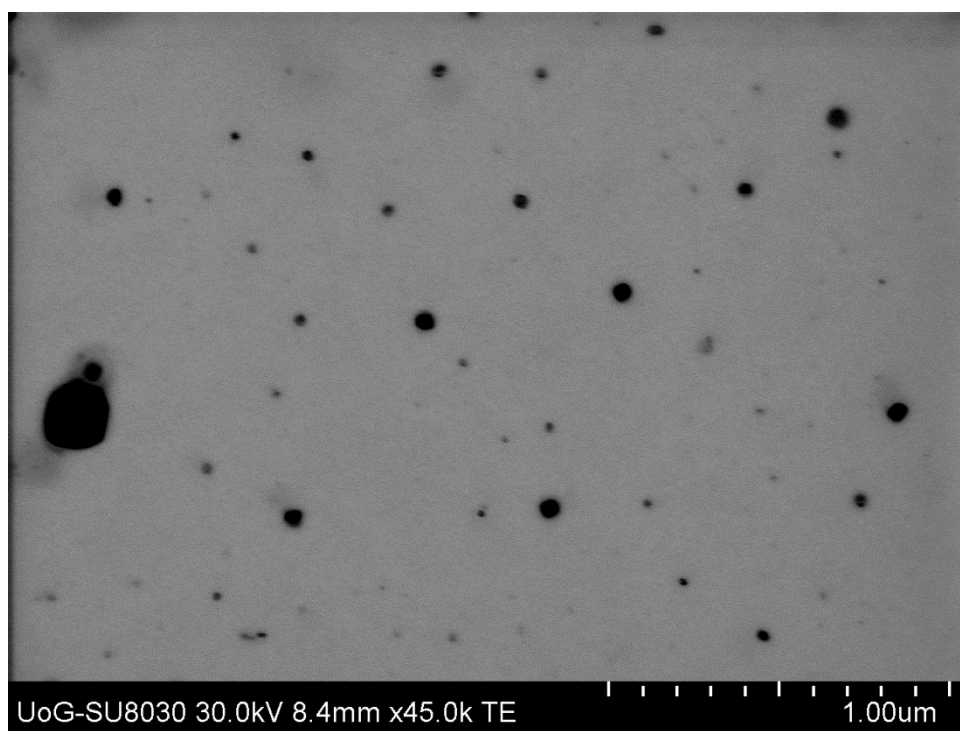


Figure 4.21. Surfactin loaded niosome at 1.65×10^{-1} mg/l.

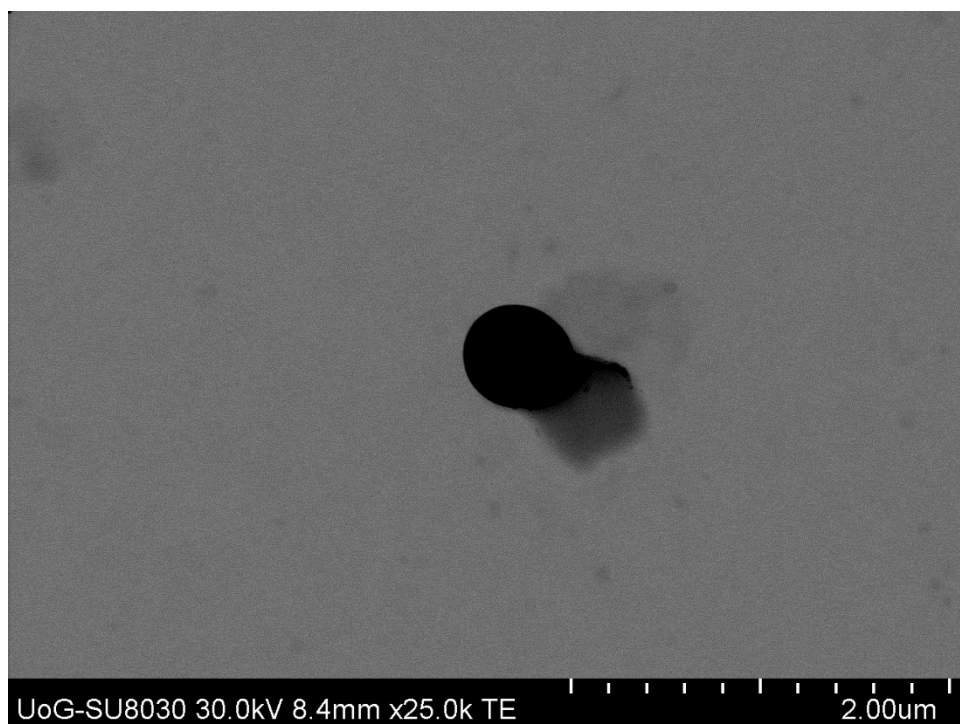


Figure 4.22. 4.0×10^{-1} mg/l, 1', 4''-sophorolactone 6', 6''-diacetate (BS3) loaded niosomes.

4.7 Conclusion

In this study, niosomes and mixed niosomes incorporating a poorly water-soluble biosurfactant (BS3) 5 – 10 mM and soluble biosurfactants (BS1c, BS2, BS4a and BS4b) 8.0×10^{-2} – 6.0×10^{-1} mg/l were formulated and characterised for potential biomedical applications. The effect of temperature was observed to produce a combination of monomodal and bimodal (60°C); bimodal (70°C); bimodal and trimodal (80°C) distributions on preliminary formulated niosomal dispersions. Therefore, the optimum hydration temperature selected for further analysis was 60°C. The mean PDI followed the order of BS3<BS2<BS4a<BS1cN/BS1cV. All optimised preliminary loaded single and mixed niosomes (BS3:S60:CHL (0:10:10, 5:5:10, 7.8:2.5:10 and 10:0:0 mM dispersed in deionised water had negative zeta potentials above -30 mV with and without DCP. Low conductivities < 5 mS/cm were observed for niosomes dispersed in deionised water whereas the conductivities of buffer dispersed concentrations were above 5 mS/cm. However when diluted in water for DLS measurement blank buffer formulated niosome showed a zeta potential > -30 mV which was comparative to its corresponding deionised water formulations.

The FTIR spectra of formulated niosomes showed similar wavenumbers with parallel groups while percentage crystallinities > 70% were observed in both sets of formulations but higher in optimised BS1c, BS2, BS4a and BS4b loaded formulations. Although well-defined morphologies were observed in blank niosomes formulated at 70°C, mixed loaded niosomes were less defined. Unsonicated niosomes had ideal spherical morphologies but large particle sizes which gradually reduced with sonication. Increase in the amount of CHL content (20 mM) was observed to stabilise

mixed niosomes formulated at equal concentrations BS3(5):S60(5) mM. Microscopic examination of BS3 (7.8):S60(2.5):CHL(10) mM revealed a range of polydisperse but well defined niosomes particularly at 60°C. Single BS3(10):S60(0):CHL(0) mM loaded niosomes had less defined morphologies in comparison to blank and lower concentrations of mixed niosomes which may be due to the ratio dispersed >7 mM. However the inclusion of an equal molar ratio of CHL was observed to enhance the definition of sparsely distributed niosomes. The biosurfactants investigated showed compatible self-assembling properties with the niosome carrier formulated, including BS1c and BS2 which showed good morphologies at optimised concentrations. However, 4×10^{-1} mg/l BS3 had an ideal size of 474 nm visualised using STEM. However, morphological examination of BSs loaded niosomes in cell culture media showed severe distortion of loaded vesicles.

CHAPTER 5 COMPOSITE BIOSURFACTANT LOADED LYOPHILISED WAFER DRESSINGS FOR POTENTIAL CHRONIC WOUND HEALING

5.1 Introduction

A composite material is a multi-phase combination of two or more components with different properties and forms that not only maintain the main characteristics of the original components, but also show new characteristics which are not possessed by any of the individual components. K-carrageenan (CARR) and sodium alginate (SA) are naturally derived linear anionic polysaccharide polymers selected for the formulation of composite wafers due to their biocompatibility, biodegradability, immunogenicity, and non-toxicity (Paşcalău *et al.*, 2013). Various authors have reported on the composite formulation of these two polymers. Roh and Shin (2005), reported that the pore size of the composite film formulation of CARR and SA decreased with an increasing CARR content which was further reduced by a crosslinking reaction with CaCl₂. Popa *et al.*, (2011) observed that the pore size of non-crosslinked composite CARR and SA hydrogels were homogeneously distributed but increased with increasing CARR content > 60%. Additionally, Pascalau *et al.*, (2011) reported that composite films showed better mechanical properties and improved swelling behaviour than CARR and SA alone. Pawar *et al.*, (2014) reported that a composite blend of blank (BLK) polyox-CARR (75/25) and polyox-SA (50/50) showed relatively higher swelling and adhesion than drug loaded (DL) blends in lyophilised wafers for delivery of commercial anti-microbials to target infected chronic wounds.

Wafers are obtained from polymer solutions or gels which are freeze-dried to yield solid porous structures that can easily be applied to exuding wound surfaces, (Matthews *et al.* 2005). Additionally, wafers have higher drug-loading capacity than films (Boateng *et al.*, 2009). The physical stability of a lyophilised polymer matrix may preserve the size, shape and physical form of contained compounds unlike a conventional gel suspension, where crystal ripening, agglomeration and polymorphic changes may occur (Ayensu *et al.*, 2012). Additionally, the porous nature of lyophilised wafers increases their capacity to absorb large amounts of exudate and consequently maintains a moist environment without damaging newly formed tissue (Boateng *et al.*, 2010).

Biosurfactants (BSs) are broad-spectrum compounds reported to have therapeutic effects which include anti-microbial and anti-inflammatory activities, and therefore potential wound healing effect (Seydlova and Svobova, 2008). BSs are sub-divided into low and high molecular weight compounds with glycolipids and lipopeptides being the most studied classes among the low molecular weight compounds. Rhamnolipids and sophorolipids are glycolipid BSs produced by microorganisms, while surfactin, a secondary metabolite from bacteria is classed under lipopeptides. Rhamnolipids exist as a family of congeners which comprises of various substitutions of mono and di-rhamnose sugars attached to one or two hydrocarbon chains respectively. Rhamnolipids have anti-microbial

activity against various bacteria species including *Listeria monocytogenes* (Magalhães and Nitschke, 2013), *Pseudomonas aeruginosa* and *Bacillus subtilis* (Sotirova *et al.*, 2008). Accordingly, Rhamnolipids can be incorporated into the wafers as solutions of dissolved (small) RL ions or as dry soluble solid. Sophorolipids are good skin moisturisers, mildly anti-microbial, and enhance healthy skin cell growth (stimulated fibroblast metabolism and collagen neosynthesis (Concaix *et al.*, 2003). They exist as two types: lactonic and acidic sophorolipids, and can also be incorporated in wafers either as solutions of dissolved (small) molecules, ions or as dry soluble (acidic), insoluble (lactonic) or as a soluble intermediate mixture of both forms. Surfactins have seven repeating units of amino acid, are zwitterionic in nature and partially soluble in water.

In this chapter the incorporation of BSs in lyophilised wafers wound dressings made from a composite mixture of k-CARR/ SA for the study of possible synergistic effects on the mechanical properties and fluid handling properties of the obtained wafers is proposed. Pawar *et al.*, (2014) formulated a composite blend of polyox with either CARR or SA in lyophilised wafers for delivery of commercial anti-microbials to target infected chronic wounds. Although (Lu-Kwang *et al.*, 2013) patented the mixture of rhamnolipids and sophorolipids in gelatin-alginate hydrogel wound dressings, to the best of our knowledge this is the first comprehensive characterisation of rhamnolipids, sophorolipids and surfactin loaded in bioactive freeze-dried CARR:SA wafers. The effects of total polymer weight and / or ratio of CARR:SA has been studied by physico-chemical characterisation which provides a means to select optimised formulations that will be used to describe differences in distribution of CARR:SA. Physico-chemical and bio-analytical techniques used include scanning electron microscopy, texture analysis (mechanical strength and mucoadhesion), ATR-FTIR, XRD and exudate handling properties

5.2 Materials

Rhamnolipid (R-90™) was purchased from Sigma Aldrich (Gillingham, UK) while sophorolipid (REWOFERM SL ONE) was kindly donated by Evonik Nutrition & Care GmbH Golschmidstr. 100. D-45127. Carrageenan (Gelcarin GP 812 NF) was obtained from IMCD Ltd. (Sutton, UK); sodium phosphate tribasic, dodecahydrate (>98%), bovine serum albumin (BSA) were all purchased from Sigma–Aldrich (Gillingham, UK). SA, sodium chloride, tris(hydroxy)aminomethane, calcium chloride dehydrate and ethanol (laboratory grade) were all purchased from Fisher Scientific (Leicestershire, UK). Gelatin was obtained from Fluka Analytical, (Steinheim, Germany) and calcium chloride from Sigma Aldrich, (Steinheim, Germany).

5.3 Methods

5.3.1 Formulation development

Blank (BLK) CARR and SA gels at concentrations of 1.0, 1.5, 2.0, 2.5 and 3.0% w/w (Tables 5.1) were initially formulated. This was followed by further formulation development and optimisation of

BLK composite CARR and SA) gels at concentrations of (1.0, 1.5, and 2.0% w/w total polymer) with the following CARR:SA ratios; 0:1, 0:1.5, 0:2, 1:1, 1:2, 1:3, 2:1 and 3:1). The formulations were stirred on a magnetic stirrer at 70-90°C to form a uniform gel. The drug loaded (DL) gels were prepared by the addition of BSs to the composite polymeric gel (as described above), for (1.5 and 2.0% w/w) gels to obtain final BSs concentration of 0.1% rhamnolipids (BS1c), surfactin (BS2) and REWOFERM SL ONE (BS4a) and 0.2% of BS1c respectively for CARR:SA 1:3 (1.5%) containing 5% BS4a (w/w) for the optimised gels as summarised in Tables 5.2 and 5.3.

The homogeneous gels (1 g) were poured into each mould of twenty four-well plates (diameter 35 mm) (CorningR_ CellBINDR; Sigma–Aldrich) and then freeze-dried in a Virtis Advantage XL 70 freeze dryer (Biopharma Process Systems, Winchester, UK). This involved initially cooling and freezing the samples from room temperature to -5°C and then -50°C and then heated in a series of thermal ramps to room temperature (at 200 mTorr). The bulk of the frozen water was removed by sublimation (primary drying) and the residual unfrozen water contained within the freeze concentrate was removed by desorption to the gas phase (secondary drying). Lyophilised wafers were then removed from the freeze-dryer and stored in glass desiccators containing silica gel until required for characterisation.

Table 5.1. Composition of single polymers used in preliminary optimisation of freeze-dried wafers from 1 -3% w/w total polymer gels

Starting Material (w/w)	1.0%	1.5%	2.0%	2.5%	3.0%
CARR (mg)	1000.0	1500.0	2000.0	2500.0	3000.0
Total solids	1000.0	1500.0	2000.0	2500.0	3000.0
SA (mg)	1000.0	1500.0	2000.0	-	-
Total solids	1000.0	1500.0	2000.0	-	-

Table 5.2. Composition of polymers and BSs used in selected optimised freeze-dried wafers obtained from 1.5% w/w total polymer gels

Starting Material	CARR:SA (BLK) (mg)	CARR:SA (0.1% BS1c/BS4a) (mg)	CARR:SA (0.2% BS1c) (mg)	CARR:SA (5% BS4a) (mg)
CARR	375.0	375.0	375.0	375.0
SA	1125.0	1125.0	1125.0	1125.0
BS1c/BS4a	-	1.5	-	-
BS1c	-	-	3.0	-
BS4a	-	-	-	75.0
Total solids	1500.0	1501.5	1503.0	1575.0

Table 5.3. Composition of polymers and BSs used in selected optimised freeze-dried wafers obtained from 2.0% w/w total polymer gels

Starting Material	CARR:SA (BLK) (mg)	CARR:SA (0.1% BS1c/BS2/BS4a) (mg)	CARR:SA (0.2% BS1c) (mg)	CARR:SA (5% BS4a) (mg)
CARR	666.7	666.7	666.7	666.7
SA	1333.3	1333.3	1333.3	1333.3
BS1c/BS2/BS4a	-	2.0	-	-
BS1c	-	-	4.0	-
BS4a	-	-	-	100.0
Total solids	2000.0	2002.0	2004.0	2100.0

5.3.2 Scanning electron microscopy

Surface morphology of the lyophilised wafers was analysed by a Hitachi SU 8030 (Hitachi High-Technologies, Krefeld, Germany) scanning electron microscope at an accelerating voltage of 1 kV. Wafers were cut into thin slices and mounted on aluminium stubs (15 mm diameter) with ‘Agar Scientific G3347N’ double-sided-adhesive carbon tabs and sputter coated with chromium at 125 mA for 80 s. Images of the wafers were acquired at a working distance of approximately 15.0 mm at magnifications of 500X–1500X. The formulations analysed by SEM are summarised in Table 5.4.

Table 5.4. Lyophilised wafers prepared from different gels containing different ratio combinations of CARR and SA, used to analyse surface morphology

CARR:SA (BLK)					CARR:SA (DL)	
1%	1.5%	2%	2.5%	3%	1.5%	2%
(1:0)	(1:0)	(1:0)	%(1:0)	(1:0)	(1:3)0.1% BS1c	(1:2)0.1% BS1c
(0:1)	(0:1)	(0:1)	-	-	-	-
(1:1)	(1:1)	(1:1)	-	-	(1:3)0.2% BS1c	(1:2)0.2% BS1c
(1:2)	(1:2)	(1:2)	-	-	(1:3)0.1% BS4a	(1:2)0.1% BS4a
(1:3)	(1:3)	(1:3)	-	-	(1:3)5% BS4a	(1:2)5% BS4a
(2:1)	(2:1)	(2:1)	-	-	-	(1:2)0.1% BS2

5.3.3 X-Ray diffraction

X-ray diffraction analyses of the prepared wafers were performed using a D8 Advance X-Ray diffractometer (Bruker AXS GmbH, Karlsruhe, Germany). The lyophilised wafers were compressed to a width size of 0.5 mm using a clean pair of compression glasses and mounted on the sample holder. The transmission diffractograms were acquired from 5° to 45° 2θ, step size of 0.02°

and a scan speed of 0.4 s per step. Diffraction patterns of the wafers and starting materials were obtained with DIFFRAC plus XRD commander software (Bruker AXS GmbH, Karlsruhe, Germany). The copper X-ray tube was set to 40 kV and 40 mA. A Göbel mirror was used which produced a parallel beam of CuK α radiation ($\lambda = 1.54184 \text{ \AA}$) using a divergent slit of 0.6 mm. A Lynx Eye position sensitive detector was used with an opening of 3°.

5.3.4 Attenuated total reflectance Fourier transform infrared spectroscopy (ATR-FTIR)

ATR-FTIR spectrophotometer was used in combination with (Thermo Nicolet; Thermo Scientific, Loughborough, UK), ZnSe attenuated total reflectance (ATR) accessory to characterise the wafers. The FTIR was equipped with potassium bromide (KBr) beam splitter and MCT detector. The wafers were placed on ZnSe ATR crystal and maximum pressure was applied by using a pressure clamp accessory to allow for intimate contact of the wafers with the ATR crystal. Similarly, the pure starting materials (CARR, SA, BS1c and BS4a) were analysed as controls. Spectra were recorded at 4 cm⁻¹ resolution within a range of 400–4000 cm⁻¹ using OMNICR_ software. True absorbance of each sample was obtained by background subtracting spectral information for the ATR crystal.

5.3.5 Mechanical strength ('hardness')

The mechanical properties (resistance to compressive deformation and ease of recovery) of the freeze-dried wafers were investigated by compressing on a Texture Analyser (Stable Microsystems Ltd., Surrey, UK) equipped with a 5 kg load cell and *Texture Exponent-32R* _ software program. All BLK and final optimised DL wafers were compressed using a 6 mm (P/6) cylindrical stainless steel probe (StableMicrosystems Ltd. Surrey, UK) in compression mode. The effects of total polymer content in gel and different ratios in wafers and combinations of CARR:SA wafers were evaluated. The 'hardness' (resistance to deformation) of the wafers were evaluated by compressing the samples at five different locations ($n = 4$) to a depth of 1 mm at a speed of 0.20 mm/s using a trigger force of 0.00100 N and withdrawn till it lost complete contact with the wafer. The same settings were used to determine the effects of BS1c and BS4a (0.1 - 5%, w/w) on optimised polymers 1.5% (CARR: SA 1:3) and 2% (CARR: SA 1:2) formulations.

5.3.6 Swelling studies

With the exception of wafers prepared from 1.0 and 1.5% SA gel, the formulations listed in Table 5.3 were used for the swelling studies. The swelling studies were carried out as described by (Pawar *et al.*, 2014). In brief, the wafers were immersed in simulated wound fluid (SWF) containing (2% BSA, 0.02 M calcium chloride, 0.4 M sodium chloride, 0.08 M tris(hydroxyl)aminomethane in deionised water, pH 7.5 adjusted using dilute HCL) at room temperature. The change in weight of the hydrated wafers began after the first 5 min, followed by a 10 min reading. Subsequent measurements were then determined every 15 min up to 240 min. The hydrated wafers and measuring cups were carefully

blotted with tissue paper to remove excess SWF on the surface and then weighed immediately on an electronic balance (European Instruments, Oxford, UK). The effect of polymer and drugs on swelling performance was evaluated for the five formulations. Percentage swelling index I_s (%) was calculated using Eq. (5.1) (Boateng *et al.*, 2008).

$$I_s (\%) = \frac{W_s - W_d}{W_d} \times 100 \quad (5.1)$$

Where W_d is the dry weight of samples before hydration and W_s is the swollen weight of samples at different time of hydration.

5.3.7 Porosity measurements

The porosity of wafers was determined by the solvent displacement method. The geometrical dimensions (thickness and diameter) of samples were measured by a digital Vernier calliper electronic micrometre gauge and total pore volume (V_0) was calculated. After that, samples were weighed (W_0) before immersing in 10 ml of absolute ethanol for 3 h to reach saturation. Ethanol displaced the void space of wafers. Finally, the lyophilised wafer samples were carefully removed from the solvent, blotted with tissue paper to remove excess solvent and immediately weighed (W_1) to avoid loss of ethanol because of its volatile nature. The porosity of the dressings was calculated from equation 5.2.

$$\text{Porosity (\%)} = (W_1 - W_0) / (\rho_{eth} V_0) \times 100 \quad (\text{Chavda } et al., 2012)$$

(5.2)

ρ_{eth} : density of ethanol = 0.789 g/cm³

5.3.8 Water absorption (Aw), equilibrium water content, water reabsorption (ReAw) and reversibility of equilibrium water content (ReEWC)

Water absorption (Aw) and equilibrium water content (EWC) tests were performed to investigate the maximum water uptake and water holding capacities respectively of BLK and BSs loaded wafers. Wafers were incubated in 5 ml of SWF at 37°C continuously for 24 h. Before weighing, the samples were blotted carefully with tissue paper to remove excess fluid on the surface. The process was repeated and each re-hydrated wafer sample was weighed. The weight of absorbed water was calculated and then divided by the weight of SWF present in the original wafer before drying. The calculated value was considered as an indicator of the reversibility of water absorption of the wafer through dehydration-rehydration cycle.

The effect of drug (BSs) concentration in these studies was determined and the experiments were performed in triplicate ($n = 3$) for each sample. Percentage of Aw and, EWC, were calculated by equations 5.3 and 5.4.

$$Aw(\%) = \frac{W_s - W_i}{W_i} \times 100 \text{ (Kim et al., 2007)}$$

(5.3)

$$EWC(\%) = \frac{W_s - W_i}{W_s} \times 100 \text{ (Kim et al., 2007)}$$

(5.4)

Where W_s and W_i are the swollen and initial weights before immersion into SWF respectively.

5.3.9 Evaporative water loss

The SWF were drained from the same lyophilised wafer samples that had been incubated for Aw and EWC after 24 h, measured and dried in the oven at 37°C for another 24 h. The weight of the samples were recorded hourly for 6 h and a final reading after 24 h. Evaporative water loss was calculated according to equation 5.5:

$$\text{Water loss (\%)} = W_t / W_0 \times 100 \text{ (Kim et al., 2007)} \quad (5.5)$$

Where W_t and W_0 are the weight after time 't' and initial weight after 24 h immersion time respectively.

5.3.10 Water vapour transmission rate

The wafers were mounted on the opening of a 5 ml Eppendorf tube containing 4 ml water with 8 mm air gap between the samples and water surface. The whole set up was placed in an air-circulated oven at 37°C for 24 h. The WVTR was calculated using equation 5.6:

$$WVTR = \frac{W_i - W_t}{A} \times 10^6 \text{ g/m}^2 \text{ day}^{-1} \text{ (Kim et al., 2007)}$$

(5.6)

Where A is the area of the opening of the eppendorf tube (πr^2), W_i and W_t are the weight of the whole set up before and after being placed into the oven respectively.

5.3.11 Thermogravimetric analysis (TGA)

The residual moisture content of the wafers was determined by thermogravimetric analysis (TGA) using a Q5000-IR TGA instrument (TA Instruments, Crawley, UK). About 1.0 - 1.5 mg of sample was loaded and analysed with dynamic heating from room temperature (~25°C) to 300°C at a heating rate of 10°C/min under inert nitrogen (N_2) gas at a flow rate of 50 mL/min. The percentage water content was calculated at 175°C using *TA Instruments Universal Analysis 2000* software program.

5.3.12 *In vitro* adhesion studies

Adhesive measurements were performed on the wafers using a TA.HD *plus* Texture Analyser (Stable Microsystems Ltd.) fitted with a 5 kg load cell in tensile mode. The wafer ($n = 4$) was attached to an adhesive probe (75 mm diameter) using double-sided adhesive tape. The surface of a 6.67% (w/v) gelatine solution, allowed to set as a solid gel in a Petri dish (86 mm diameter), was equilibrated with 0.5 mL 2% (w/w) BSA containing SWF to mimic a wound surface with thin exudate. The probe, lined with wafer, was set to approach the model wound surface with the following pre-set conditions: pre-test speed 0.50 mm/s; test speed 0.50mm/s; post-test speed 1.00 mm/s; applied force 0.05 N; contact time 60.00 s; trigger type auto; trigger force 0.05 N and return distance of 10.00 mm. The adhesive characteristics were determined by the maximum force (stickiness) required to detach the wafer from the model wound surface, total work of adhesion (WOA) was represented by the area under the force versus distance curve, whereas cohesiveness was defined as the distance travelled by wafer till detached and calculated using the *Texture Exponent 32R* software.

5.3.13 Statistical analysis of data

Data analysis was carried out with the software package Microsoft Excel version 2007. Results were expressed as a mean \pm standard deviation (S.D). ($n = 3$). Statistically significant difference was determined using one-way analysis of variance (ANOVA,) for the significant interrelation between the various groups with $p < 0.05$ considered as a minimal level of significance. The groups compared were the selected optimised BLK/BSs 1.5(1:3) vs %(1:2)CARR:SA, the BLK vs BSs of both 1.5(1:3) and 2%(1:2)CARR:SA and the BSs vs BSs of 1.5(1:3) and 2%(1:2)CARR:SA loaded wafers.

5.4 Results and discussion

5.4.1 Preliminary formulation development and optimisation

The ideal wound dressing should minimise infection and pain, prevent excessive fluid loss, maintain a moist healing environment, promote epithelial restoration, and be biocompatible. In addition, dressings should have adequate adherence to the wound area and must be easy to apply and remove to ensure patient compliance and comfort. In addition to the application of dressings, wound treatment includes irrigation of the affected area with an anaesthetic solution followed by application of prophylactic antibiotics to prevent wound infection. Re-application of the antibiotic formulation and repeated changing of dressings by either the healthcare provider or the patient continues until the wound heals. This is often an inconvenient process and needs some basic improvement (Thakur *et al.*, 2008). Coverage in the form of advanced wound dressings evolved to satisfy these factors. Unlike traditional dressings such as gauze and cotton wool that take no active part in the wound healing process, advanced dressings are designed to have biological activity either on its own or the release of bioactive constituents (drugs) incorporated within the dressing (Boateng *et al.*, 2008). Bioadhesive,

polymeric (synthetic, semi-synthetic or naturally derived) dressings are potentially useful in the treatment of local infections where it may be beneficial to achieve increased local concentrations of antibiotics while avoiding high systemic doses thus reducing patient exposure to an excess of drug beyond that required at the wound site (Langer, 1980).

Hydrophilic gels called hydrogels are polymeric materials that exhibits the ability to swell and retain a significant fraction of water within its structure without dissolving, (Ahmed, 2015). In recent years, hydrogels have found a wide range of biomedical applications including controlled drug delivery systems as well as transdermal systems, replacement blood vessels, dental materials, ophthalmic applications, contact lenses, wound dressing and a variety of other related and potential uses. Polysaccharides, are natural biomolecules, which include hyaluronic acid/ hyaluronate, cellulose, dextran, chitin and chitosan, heparin, CARR and SA have been used in wound management as dressing materials. In this study, CARR and SA were selected because they are biodegradable, biocompatible, non-toxic, cheap and readily available.

Formulation of wafers containing only CARR was discontinued due to rapid disintegration during swelling which led to the decision to use a composite mixture of CARR and SA that can be combined without major compromise of physical properties. Additionally, the mixture of these two gelled hydrocolloids, act synergistically as a result of the similarity in the type of polysaccharide gelling mechanism. CARR forms a gel with potassium and calcium ions but also shows gelation under salt-free conditions helped by physical bonds, being a thermosensitive hydrogel. Thermoreversible gels, such as CARR, melt at elevated temperature and the gelation of the biopolymer is obtained by lowering the temperature. The temperature-induced gelation allows for an easy formation of gels with different shapes, due to the versatility of CARR. In comparison to CARR (and various other biopolymers), SA has been more extensively studied and characterised. Further, SA has a similar gelation mechanism to CARR, consequently in this study, the development of gels composed of mixtures of different ratios of CARR:SA was optimised. Furthermore, salts were not added during the mixing of gels, while thermal energy was first applied on the composite gels during their physical mixing on a magnetic stirrer after which gels were lyophilised under vacuum conditions. Overall, the purpose of this work was to prepare optimised CARR:SA composite wafers loaded with BSs that could be used as wound dressings. The influence of the CARR:SA ratio on the composite wafer properties were studied in order to establish the optimal composition of the polymers. Several characterisation methods such as: ATR-FTIR, XRD, TGA, SEM were used, and the mechanical properties and the fluid handling properties of the obtained composite wafers were studied to determine the best conditions required to achieve the most adequate response in terms of the mechanical stability, exudate uptake and functionality of the developed systems. Two formulations 1.5%(1:3) and 2%(1:2) CARR:SA total polymer content in gel (w/w) from the preliminary studies showed desired characteristics required in wafers on the basis of an ideal balance between toughness (4 - 6N), porosity above 65% which corresponded to maximum water uptake and

water holding capacities. These were therefore loaded with BSs and further characterised to compare with their corresponding BLK (*i.e.* no BSs present) formulations. In all mechanical and bioanalytical techniques investigated p value was greater than 0.05 for 1.5%(1:3) and not significantly different to 2%(1:2)CARR:SA. With the exception of EWC in 2%(1:2) where $p = 0.05$, the effects of the different BSs loaded into both 1.5%(1:3) and 2%(1:2)CARR:SA wafers were not statistically significant ($p > 0.05$) in all mechanical and bioanalytical techniques investigated. However, the incorporation of BSs loaded into BLK 1.5%(1:3)CARR:SA wafers was statistically significant in eight out of the thirteen wafer techniques analysed ($p < 0.05$). However, only three of the same characteristics were significant when BSs was incorporated into 2%(1:2) wafers.

5.4.2 Scanning electron microscopy (SEM)

SEM analysis is key to understanding the morphological architecture and evolution of polymers adapting to heterogeneous compositions. The morphologies of wafers obtained from 1.0, 1.5, 2.0 (Fig 5.1ai-5.1aiii), 2.5 and 3.0 % w/w CARR gels (Fig 5.1ci-5.1cii) are described as follows;

Wafers from 1% CARR gels (Fig 5.1(ai) showed a network of thin sheets and the largest estimated pore sizes were observed in this category $173.77 (\pm 75.99) \mu\text{m}$ (Table 5.5), while 1.5% CARR gels yielded wafers with denser sheets. At 2% the benefits of closer interaction appears to have reached its optimum and once again thin sheets complemented by the smallest pore size of $79.06 (\pm 23.22) \mu\text{m}$ in this range were observed. Wafers obtained from 2.5% CARR gels (Fig 5.1ci) were characterised by a broad leaf-like matrix with large pores, whereas those obtained from 3% CARR gels had a more distinctive topography interspersed with uniform pores. In comparison to pure CARR wafers, SA only wafers (Fig 5.1bi-5.1biii) have a more uniform microstructure with very neat broad planar network assembly and a distribution of interconnected large jagged and small spherical pores. The wafers obtained from 1% SA gels (Fig 5.1bi) are characterised by a very neat arrangement of broad glassy leafy walls with a variable distribution of jagged pores. Larger and regular interconnected leaves were observed for wafers obtained from 1.5% SA gels, although the number of pores observed were less evenly distributed in comparison with wafers obtained from 1% SA gels. However a point of similarity is that the pores observed were a combination of medium - large jagged sizes. A spongy matrix of uniform, interconnected pores was observed in wafers obtained from 2% SA gels. The pore sizes observed in the matrix of 1-2% CARR gels (Fig 5.1ai-5.1aiii) were larger than corresponding wafers obtained from 1-2% SA gels (Fig 5.1bi-5.1biii).

The influence of different ratios of CARR and SA on the pore sizes of BLK composite wafers are shown in Table 5.5. The morphologies of 1%(1:1) CARR:SA composite wafers (Fig 5.2ai) have non-uniform appearance suggesting the dominance of CARR polymers in this composite mixture. However in 1.5%(1:1) CARR:SA (Fig 5.2aii) composite wafers, a uniform cluster of broad leafy layers (an associated characteristic of SA) interspersed with large pores was observed. In 2%(1:1) CARR:SA wafers (Fig 5.2aiii), a selection of large petal-like interconnected layers arranged in a

uniform network was observed. Interestingly, the largest mean pore size across all formulations 180.25 (± 53.44) μm (Table 5.5) was observed in this composition, which suggests an equal effect of CARR and SA. Additionally, the topography was interspersed with an even distribution of broad uniform pores. The morphology of 1%(1:2)CARR:SA wafers (Fig 5.2bi) was a combination of seemingly translucent leafy layers with thin walls and more defined flat sheets. Large jagged gaps were observed between the leafy layers while just a few smaller pores appeared between the stalk-like networks. The morphology of 1.5%(1:2) wafers (Fig 5.2bii) resembled a pile of dry leaves with a large central nest-like indentation. The morphology of 2%(1:2) CARR:SA wafers (Fig 5.2biii) was a porous assembly which looks like the pocket of an egg carton. This is a very interesting development, because, the gelation of alginates have been reported to take place when divalent (Ca^{++} , Sr^{++} , and Ba^{++}) or trivalent cations (Fe^{+++} and Al^{+++}), interact ionically with blocks of guluronic acid residues, resulting in the formation of a three-dimensional network usually described as an “egg-box” model (Grant *et al.*, 1973; Mohamadnia *et al.* , 2008; Sachan *et al.*, 2009). However, in the absence of any of these physical cross-linking agents the result suggests that, CARR and SA have interacted to form this “egg-box” interconnecting network matrix.

Table 5.5. Comparison of the mean pore sizes (\pm SD) (μm) of single, composite and optimised selected BSs loaded wafers $n = 3$

(%, w/w)	1:0	0:1	(μm)		
1	173.77 (± 75.99)	126.10 (± 45.04)	-	-	-
1.5	146.56 (± 53.65)	85.63 (± 25.64)	-	-	-
2	79.06 (± 23.22)	65.78 (± 13.90)	-	-	-
2.5	90.66 (± 28.08)	-	-	-	-
3	97.88 (± 22.35)	-	-	-	-
	1:1	1:2	1:3	3:1	
1.5	87.07 (± 30.26)	169.00 (± 38.66)	78.80 (± 15.92)	-	
2	180.25 (± 53.44)	87.10 (± 19.37)	89.07 (± 22.22)	153.80 (± 34.30)	
	0.1% BS1c	0.2% BS1c	0.1% BS4a	5% BS4a	0.1% BS2
1.5	136.60 (± 50.95)	122.26 (± 46.30)	98.21 (± 42.52)	141.13 (± 47.15)	-
2	93.35 (± 57.14)	194.00 (± 56.94)	132.21 (± 67.77)	72.41 (± 34.31)	207.83 (± 90.37)

There was no specific pattern in the overall morphology of 1%(1:3) CARR:SA wafers (Fig 5.2ci), however the wafers were characterised by dry leaf-like layers with a combination of circular and hexagonal shaped pores. 1.5%(1:3) CARR:SA wafers (Fig 5.2cii) have a slanted interconnected network characterised by long leaves curled slightly at their tips with a combination of small round, keyhole shaped and large pores. The layers of 2%(1:3) CARR:SA wafers (Fig 5.2ciii) showed a solid matrix interspersed with large jagged pores. The pore size was distributed in a range of 78.80 (± 15.92)

- 180.25 (± 53.44) μm . With the exception of 1.5%(1:2) CARR:SA which had a mean pore size of 169.00 (± 38.66) μm , (Table 5.5) all other composites are structurally closer to CARR or SA depending on the ratio (Fig 5.3ai-biii). Meanwhile the pore sizes of BSs loaded wafers ranged from 72 (± 34.31) - 207.83 (± 90.37) μm . With the exception of 0.1% BS1c and 5% BS4a, the pore sizes of all other wafers formulated with 2% w/w total polymer content in gel were larger than corresponding wafers formulated with 1.5% total polymer content in gel. Overall, the largest pore size was observed in 0.1% BS2 loaded wafers.

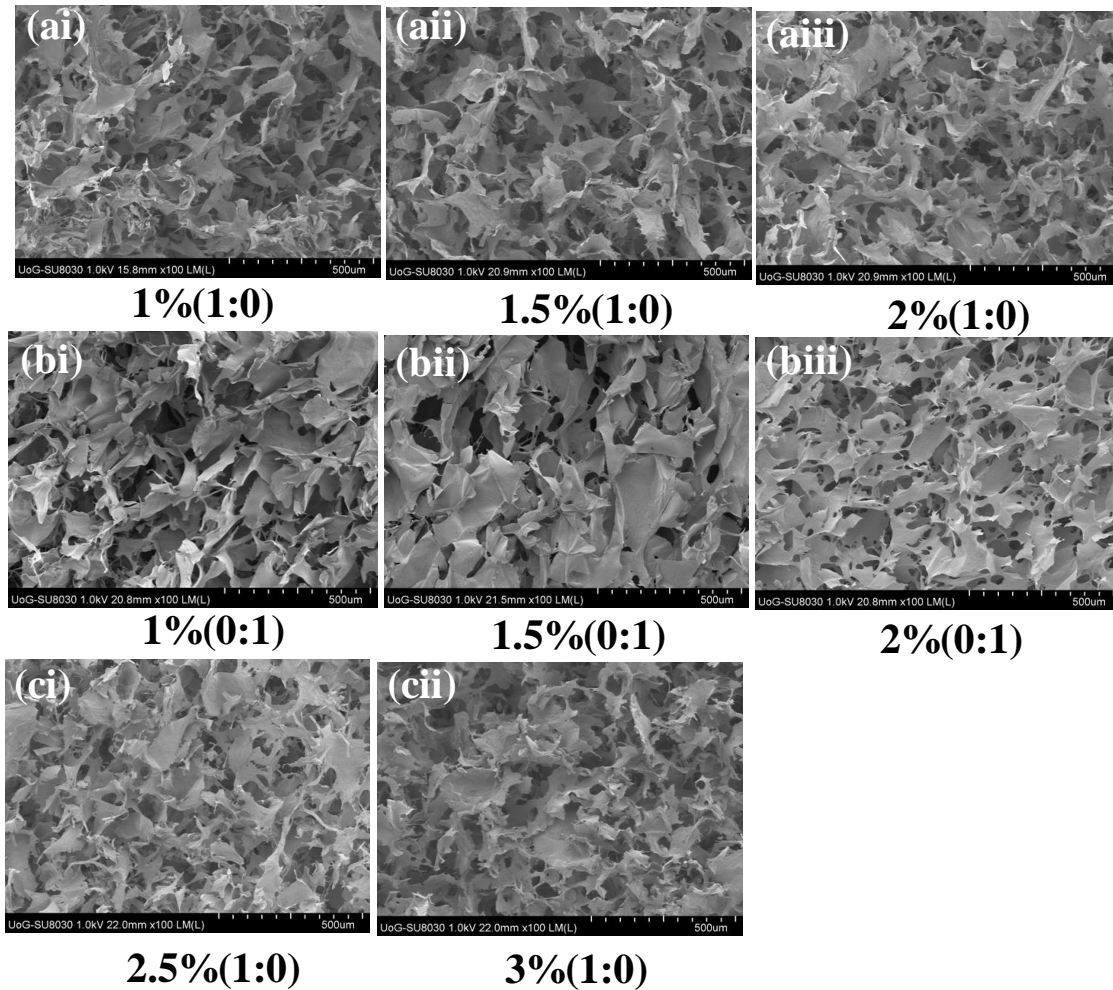


Figure 5.1. SEM comparison of selected single polymer wafers prepared from pure CARR (ai) 1%(1:0) (aii) 1.5%(1:0) (aiii) 2%(1:0) pure SA (bi) 1%(0:1) (bii) 1.5%(0:1) (biii) 2%(0:1) and higher total polymer weight pure CARR gels (ci) 2.5%(1:0) (cii) 3%(1:0).

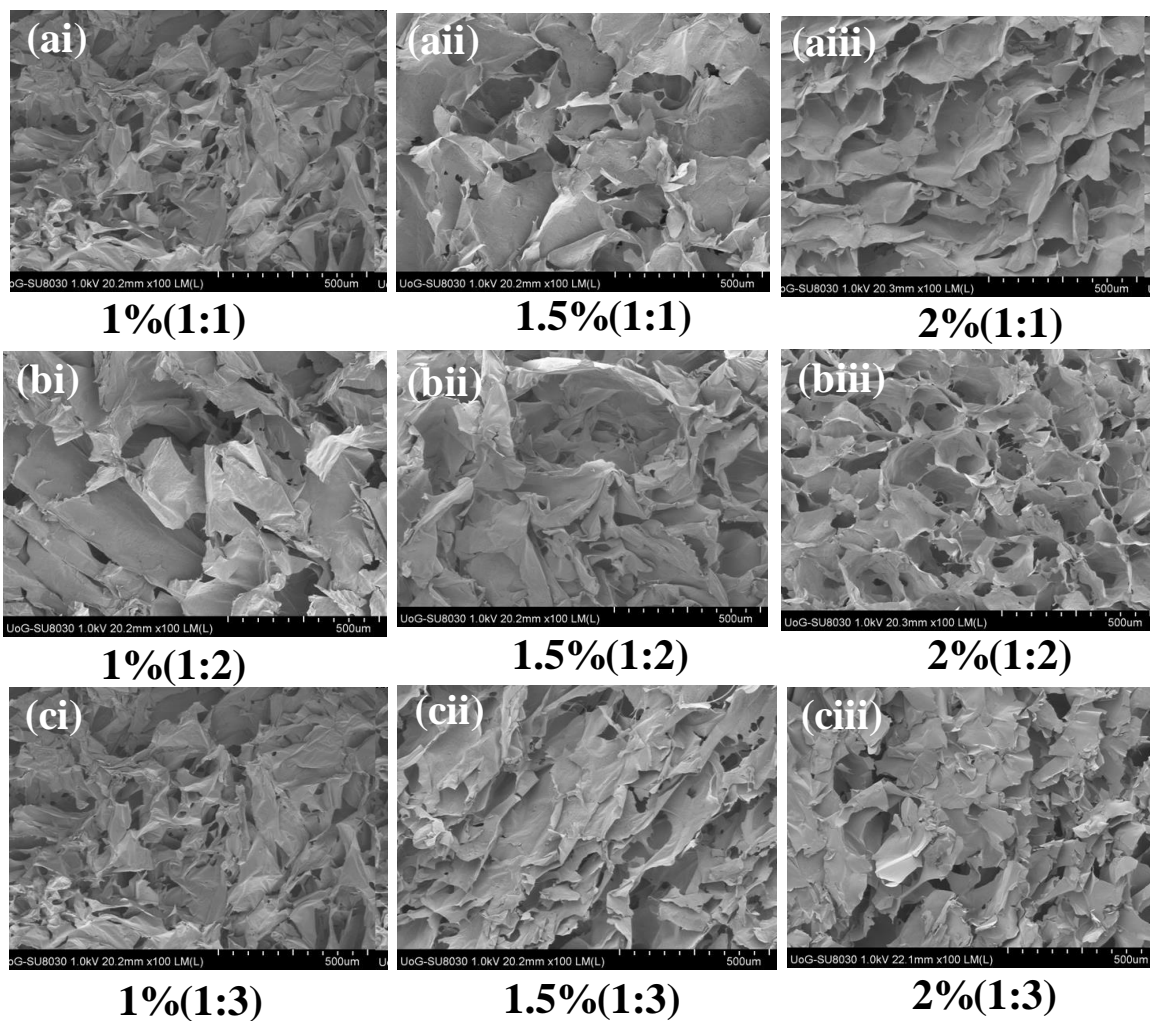


Figure 5.2. SEM images of composite wafers obtained from 1.0, 1.5 and 2.0 % (total polymer weight) CARR:SA gels at ratios of 1:0, 0:1, 1:1, 1:2 and 1:3 respectively.

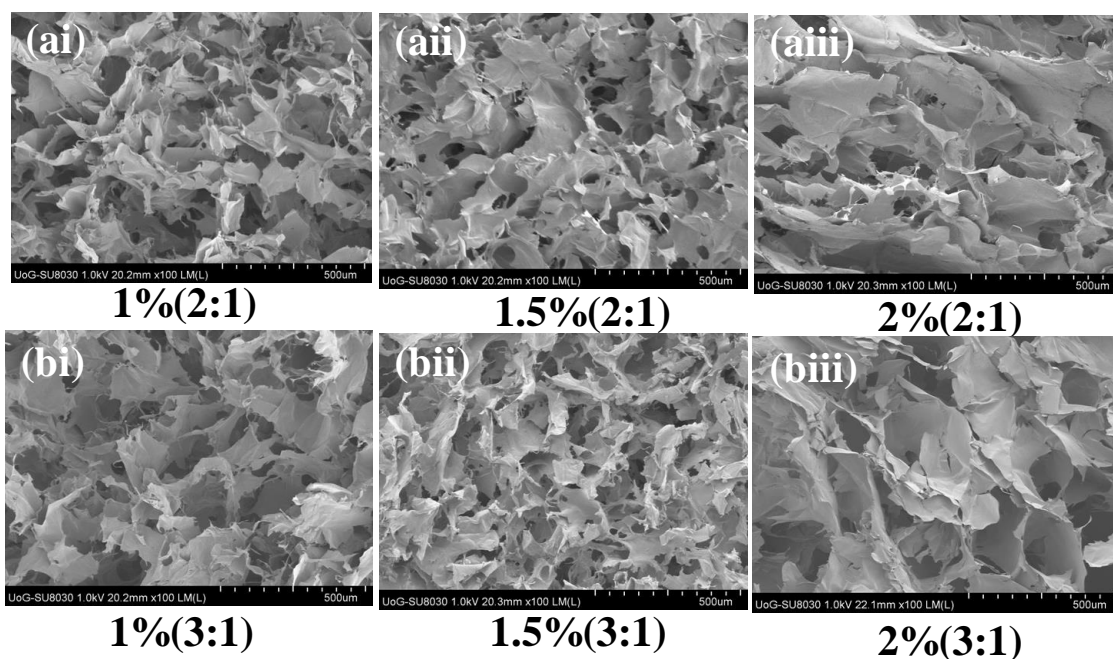


Figure 5.3. Comparison of (ai) 1%(2:1) (aii) 1.5%(2:1) (aiii) 2%(2:1) (bi) 1%(3:1) (bii) 1.5%(3:1) (biii) 2%(3:1) CARR:SA wafers.

The morphology of 1.5%(1:3)BLK wafers as previously described have a slanted interconnected network characterised by long leaves curled slightly at their tips with a combination of small round, keyhole shaped and large pores. The addition of 0.1% BS1c (Fig 5.4a) was observed to have transformed the slanted network of 1.5%(1:3) CARR:SA BLK wafers into large looser sheets dotted with a variety of small - medium pores with undefined shapes. An increase in the amount of drug to 0.2% BS1c (Fig 5.4c), however, was observed to have tightened and created a denser network interspersed with an even distribution of small oval and large sized pores. Addition of 0.1% BS4a (Fig 5.4b) transformed the slanted network of its corresponding blank matrix into a vertical network of interconnected leafy-sheets embedded with small and large pores. The loading of 5% BS4a (Fig 5.4g) transformed the matrix into a uniform network of floral, glassy leaves interspersed with equally large floral pores.

The loading of 0.1% BS1c (Fig 5.4d) into 2%(1:2)CARR:SA enlarged its egg pockets into broad smooth sheets interspersed with a few large pores. The loading of 0.2% BS1c (Fig 5.4f) broadened and expanded the sheets even further reducing the size of the pores dotted around the surface topography. The loading of 0.1% BS4a (5.4e) transformed the egg pocket matrix into broad flower-like sheets interspersed with prominent gap-sized pores and retained slight traces of the egg box matrix. The loading of 5% BS4a (Fig 5.4h) was observed to have deformed the egg-like matrix into broad thin-walled planar sheets with small dots on the surface and large gaps. With the exception of 5% BS4a, all other loaded BSs were not visible on the wafer surface or pore walls, suggesting there

were fully incorporated within the interior wafer matrix. The difference in the pore sizes of the selected optimised BLK and BSs loaded wafers were not statistically significant ($p > 0.05$).

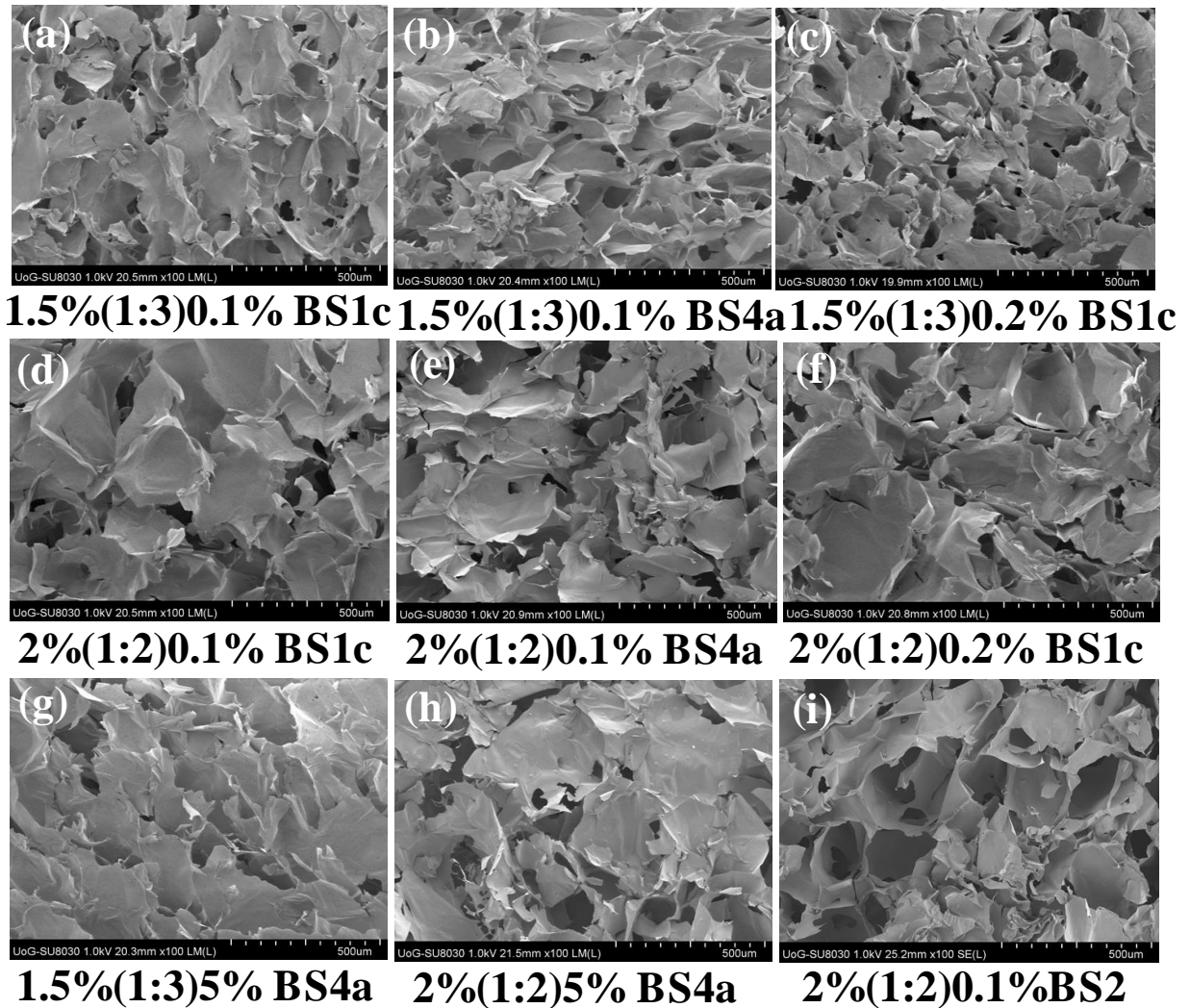


Figure 5.4. Comparison of 1.5%(1:3) and 2%(1:2) BSs loaded wafers.

5.4.3 Mechanical strength ('hardness')

Ideal mechanical properties of wound dressings include flexibility, durability, pliability, elasticity and resistance to stresses exerted by different parts of the body particularly around the elbows and knees (Khan *et al.*, 2000). Wound dressings should withstand some frictional stresses during day-to-day activities when applied on the wound so that if there are any accidental frictional stresses, the dressing will absorb the energy without breaking and will thus provide a protective effect over the wound.

Table 5.6. Reproducibility in ‘hardness’ of (a) four BLK freeze-dried wafers from 1 – 3% (1:0) CARR:SA, 1 - 2%(0:1), 1 – 2%(1:1, 1:2, 1:3) CARR:SA and (b) BSs loaded wafers from optimised selected 1.5%(1: 3) and 2%(1:2) CARR:SA compressed at five different locations to a depth of 1 mm at a speed of 0.20 mm/s, using 6 mm diameter stainless steel probe (standard deviations given in parenthesis). The ‘hardness’ is peak resistance force of the wafers to deformation and corresponds to the maximum force attained in the Texture Analyser plot

Single wafers	(BLK) (N)		Composite wafers (N)				
			(BLK)				
1 (% w/w)	1:0	0:1	1:1	1:2	1:3	2:1	3:1
1	1.55 (±0.2)	0.61 (±0.1)	0.24 (±0.1)	0.87 (±0.1)	0.23 (±0.0)	0.40 (±0.0)	0.13 (±0.0)
2	1.53 (±0.2)	0.63 (±0.2)	0.32 (±0.1)	0.70 (±0.2)	0.18 (±0.0)	0.39 (±0.0)	0.11 (±0.0)
3	1.48 (±0.2)	0.57 (±0.1)	0.28 (±0.0)	0.71 (±0.2)	0.29 (±0.0)	0.47 (±0.1)	0.11 (±0.0)
4	1.29 (±0.2)	0.61 (±0.1)	0.48 (±0.1)	0.87 (±0.2)	0.28 (±0.0)	0.43 (±0.1)	0.13 (±0.0)
1.5 (% w/w)	1:0	0:1					
1	0.40 (±0.1)	2.16 (±0.2)	4.02 (±0.6)	4.33 (±0.4)	4.50 (±0.6)	0.80 (±0.1)	0.44 (±0.1)
2	0.35 (±0.1)	2.08 (±0.3)	4.33 (±0.5)	4.11 (±0.4)	3.89 (±0.6)	0.73 (±0.1)	0.39 (±0.1)
3	0.46 (±0.1)	1.94 (±0.3)	4.68 (±0.1)	3.78 (±0.5)	3.90 (±0.6)	0.74 (±0.1)	0.44 (±0.1)
4	0.33 (±0.1)	1.83 (±0.4)	4.12 (±0.6)	3.59 (±0.4)	4.03 (±0.8)	0.65 (±0.1)	0.44 (±0.1)
2 (% w/w)	1:0	0:1					
1	0.60 (±0.1)	4.40 (±1.0)	8.34 (±1.5)	4.77 (±0.3)	7.72 (±1.3)	0.74 (±0.2)	3.75 (±0.2)
2	0.67 (±0.2)	6.22 (±1.1)	8.52 (±0.5)	4.26 (±0.5)	7.65 (±0.8)	0.47 (±0.1)	3.02 (±0.3)
3	0.42 (±0.1)	5.04 (±1.0)	8.30 (±0.5)	4.82 (±0.5)	8.29 (±1.3)	0.62 (±0.3)	3.66 (±0.4)
4	0.60 (±0.1)	4.44 (±1.0)	9.81 (±0.4)	4.79 (±0.5)	8.39 (±1.0)	0.52 (±0.1)	2.99 (±0.3)
2.5 (% w/w)	1:0	0:1					
1	0.83 (±0.2)	-	-	-	-	-	-
2	0.86 (±0.0)	-	-	-	-	-	-
3	0.97 (±0.1)	-	-	-	-	-	-
4	0.90 (±0.1)	-	-	-	-	-	-
3 (% w/w)	1:0	0:1					
1	1.76 (±0.3)	-	-	-	-	-	-
2	1.12 (±0.2)	-	-	-	-	-	-
3	1.51 (±0.2)	-	-	-	-	-	-
4	1.39 (±0.3)	-	-	-	-	-	-

(b)

1.5%(1:3) DL wafers	0.1% BS1c	0.2% BS1c	0.1% BS4a	5% BS4a	0.1% BS2 (N)
1	2.77 (±0.5)	2.78 (±0.3)	2.86 (±0.3)	3.43 (±0.3)	-
2	2.63 (±0.4)	2.81 (±0.3)	2.94 (±0.4)	3.14 (±0.3)	-
3	2.60 (±0.5)	3.09 (±0.2)	3.18 (±0.5)	3.40 (±0.2)	-
4	2.81 (±0.4)	3.09 (±0.4)	2.97 (±0.4)	3.93 (±0.6)	-
2%(1:2) DL wafers					(N)
1	5.01 (±0.6)	4.40 (±0.6)	5.46 (±0.5)	5.95 (±0.7)	4.53 (±1.0)
2	5.38 (±0.7)	4.48 (±0.6)	5.72 (±0.8)	5.57 (±0.7)	4.31 (±0.8)
3	5.56 (±0.7)	4.50 (±0.5)	5.60 (±0.7)	5.65 (±0.5)	4.66 (±0.8)
4	5.71 (±0.7)	4.77 (±0.5)	5.29 (±0.3)	5.70 (±0.6)	4.04 (±0.8)

Hardness is a measure of the peak force required to compress wafers to a required depth. With the exception of 1%(1:0) CARR:SA which showed similar hardness to 3%(1:0), the resistance to compression of pure CARR wafers increased in commensurate proportions to total polymer concentration. The events occurring involved increase in resistance to compression from initial contact until the peak force when the maximum (given) depth of compression was attained. The resistance to compression of pure SA on the other hand increased in accordance with total polymer weight $1\% < 1.5\% < 2\%$. Interestingly changes in resistance to compression were not commensurate to the 0.5% increase in polymer content. Rather there was an exponential increase which did not follow any general trend, however, based on the SEM images in which a hierarchical network order was observed, interconnectivity of polymer matrix may contribute to mechanical stiffness. Boateng *et al.*, (2010) reported a peak force of $17.1 (\pm 2.1)$ N for 2% w/w SA which is considerably higher than the value $5.02 (\pm 1.2)$ N obtained in this research. A possible explanation may be due to differences in mannuronic/guluronic ratios (M/G) of SA which in this investigation is (1.56) and affects mechanical properties as well as the sources of the alginates (Sachan *et al.*, 2009).

Generally guluronic acid side chains make gels and formulation harder while mannuronic acid chains makes gels and subsequent formulations more flexible. This difference was observed in the SEM micrographs where SA wafers of same magnification showed elongated pores unlike those reported in Fig 5.2 (Boateng *et al.*, 2010).

The resistance to compression of 1 – 2%(1:1) increased in accordance with total polymer weight, which was similar to the SA only wafer. This similarity to pure SA matrix may indicate that SA has a stronger influence on resistance to compression compared to CARR. The difference in the effect of the total polymer weight is observed in the increased resistance to compression from 1 - 1.5%(1:2). However the increased resistance to compression was less obvious in 1.5 - 2%(1:2) total polymer weight. CARR:SA 1%(1:3) wafers had the lowest resistance to compression of all compositions containing high SA content which contradicts previous observations. However it has already been observed that the behaviour of 1% formulations have individual concentration dependencies. An increase in mechanical strength beginning from 1-1.5%(1:3) CARR:SA formulations followed by doubled resistance from 1.5 – 2% (1:3) with values of 4.08 (± 0.7)N for 1.5%(1:3) and 8.01 (± 1.1)N for 2%(1:3) was observed. The resistance to compression of 1-2%(2:1) and 1-2%(3:1) were lower than other compositions particularly 1%(3:1) CARR:SA which showed a hardness of 0.12 (± 0.0)N. However the hardness of 1.5 and 2% of 2:1 and 3:1 CARR:SA were numerically comparable to those observed in pure CARR wafers obtained from 1.5 and 2% gels.

Generally three main behaviours were observed, (i) influence of different ratios of CARR and SA in 1% compositions, (ii) influence of different ratios of CARR and SA in 1.5 - 2% total polymer weight (iii) an initial high resistance to compression followed by a doubled resistance 1:1 and 1:2 ratios. These observations predominantly coincided with increasing order in polymer network. Six composite formulations were observed to have potential mechanical strength with resistance to compression ranging from 3.95 – 8.75 N. These formulations were 1.5%(1:1), 1.5%(1:2), 1.5%(1:3) and 2% (1:1), 2%(1:2) and 2%(1:3), however, comparison with their corresponding SEM micrographs revealed similar wafer matrix. These formulations were therefore selected for bioanalytical evaluation of their fluid handling properties after which 1.5%(1:3) and 2%(1:2) BLK wafers were selected for BSs (0.1% BS1c, 0.1% BS4a, 0.2% BS1c, and 5% BS4a) loading. The mechanical strength of BLK 1.5%(1:3) BLK wafers was higher than that of all formulated BSs loaded wafers, while with the exception of 0.2% BS1c the reverse was the case for 2% (1:2) BLK and the remaining concentrations of BSs loaded wafers. The difference between the mechanical strength of BLK and BSs loaded wafers was statistically significant ($p < 0.05$) in only one of the optimised 1.5%(1:3)CARR:SA wafers. However, no statistical difference ($p > 0.05$) was observed between the different types and concentrations of BSs; 0.1% BS1c, 0.2% BS1c, 0.1% BS4a and 5% BS4a loaded into both optimised wafers i.e. 1.5%(1:3) and 2%(1:2)CARR:SA wafers.

5.4.4 X-ray diffraction (XRD)

X-Ray diffraction is used to investigate the structure of matter at the molecular level. This technique is more commonly used to determine the chemical compositions of microcrystals in powders. However material scientists, also use it to investigate the orientation of polymeric molecules in fibres and films. In this research, XRD was used to determine the crystalline or amorphous properties of selected formulated wafers 1% (1:0, 0:1,1:1, 1:2, 1:3:2:1 and 3:1).

Five peaks were observed between 2-theta of 20 - 60° for pure CARR wafers (Fig 5.5). CARR showed an amorphous nature with the presence of additional peaks at 28.39 and 40.58 which may be attributed to inorganic salt impurities from KCl (Prasad *et al.*, 2009) whereas with the exception of one peak observed in pure SA wafers around 2- theta of 20° no sharp peaks were observed which confirms the amorphous nature of SA (Fig 5.6). These results agree with observations reported by Pawar *et al.*, (2014) in which two peaks were reported for pure CARR of the same grade.

A very intense crystalline peak was observed in the matrix of 1.5%(1:2)CARR:SA, while two sharp peaks were observed in 2%(2:1); both of which are between 20 and 30° 2-theta scale (appendix Figs A5.4 and A5.8). However, in all cases the most dominant peak was sharpest in 1:2 ratios and especially at 1.5%(1:2) CARR:SA. The crystalline impurity at 2-theta =20° was most intense in one of the two optimised selected BLK 2%(1:2) as shown in (Fig 5.8).

As previously reported in chapter 4, section 4.6.3.2 4.7, although BS2 standard had an amorphous profile compared to its calculated state, the percentage crystallinity of pure BS1c standard was in agreement with its corresponding diffractogram. BS4a and BS4b were not analysed by XRD due to their liquid amorphous states. The BSs loaded wafers (Fig 5.9 – 5.13) showed homogenous amorphous patterns although wafers loaded in 2%(1:2)CARR:SA had higher calculated percentages of 82.34% for 2%(1:2)5% BS4a while 1.5%(1:3)0.2% BS1c had the lowest content of 66.17% (appendix Table A5.1).

The molecular dispersity of BSs in CARR:SA wafers will have high surface energy due to less ordered amorphous structures than the semi-crystalline form. Additionally, the decreased crystallinity of BSs may help to improve characteristics such as exudate absorption and its prolonged retention at wound sites which can increase the bioavailability and ultimately reduce the frequency of dressing application. Amorphous matrixes allow greater molecular interaction between solutes and solvents hence BSs are more soluble and dressings are expected to release BSs to stimulate pro-inflammatory cytokines and neutrophils which prevents maceration around the wound bed and subsequently promote wound healing.

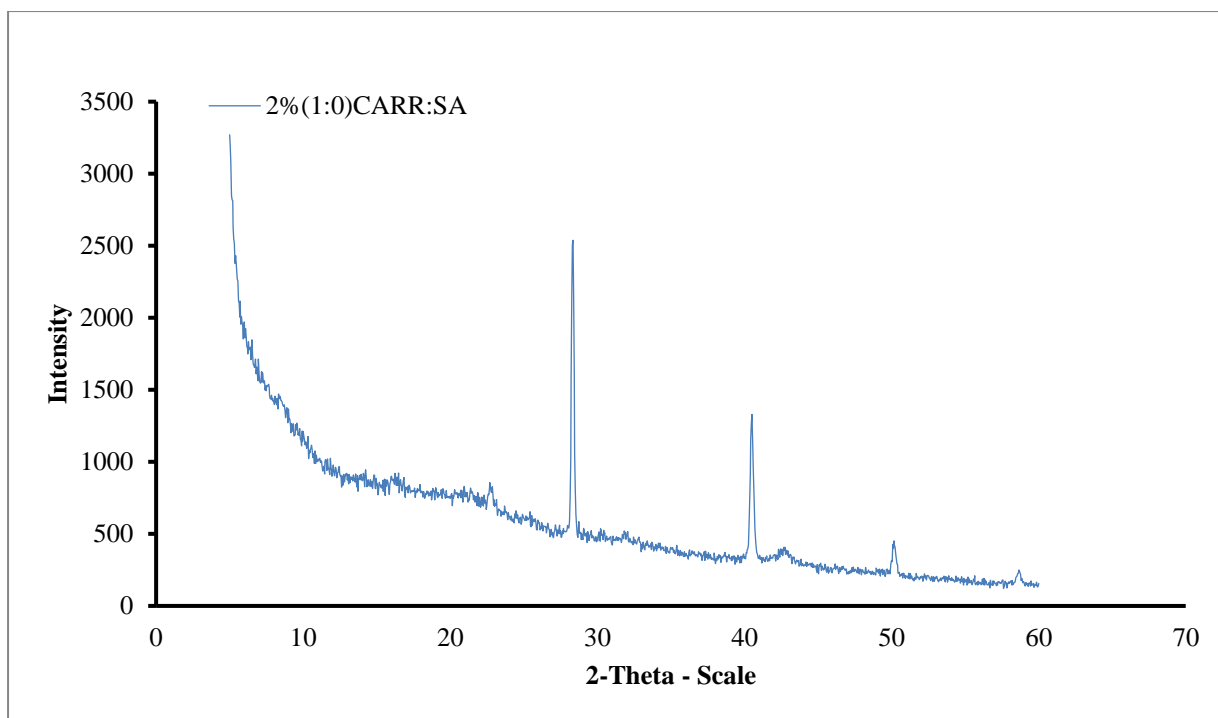


Figure 5.5. XRD diffractogram of 2%(1:0)CARR:SA wafers.

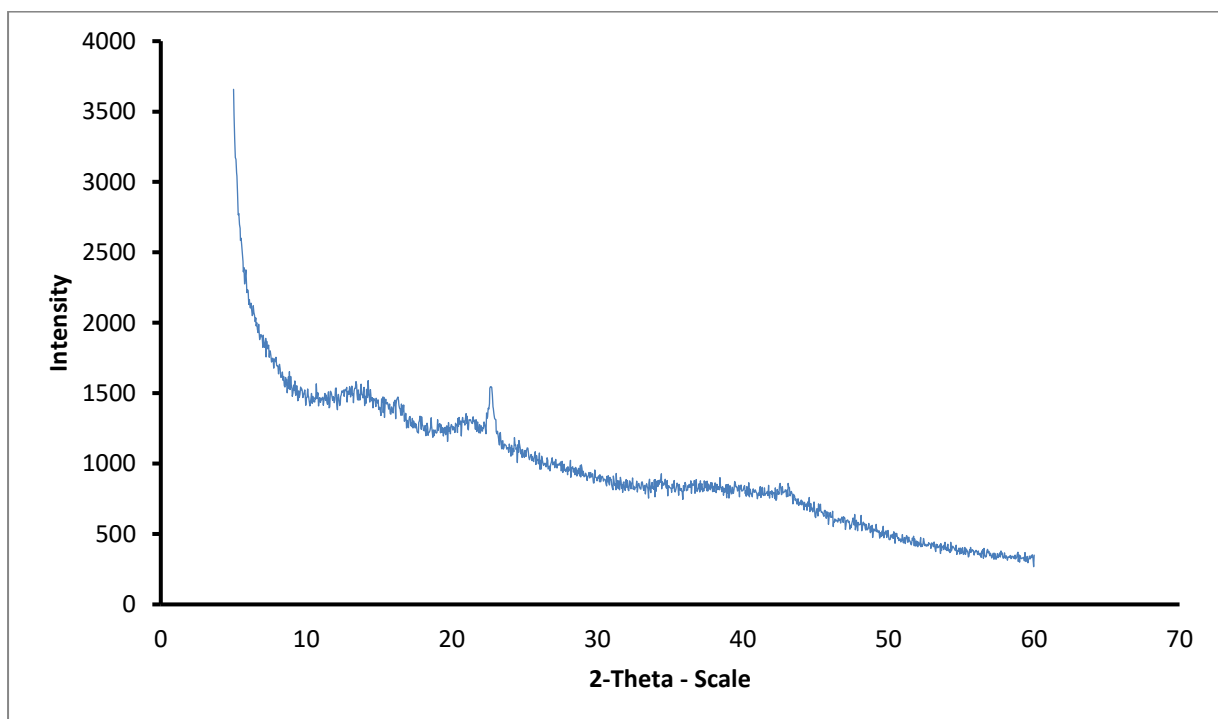


Figure 5.6. XRD diffractogram of 1.5%(0:1)CARR:SA wafers.

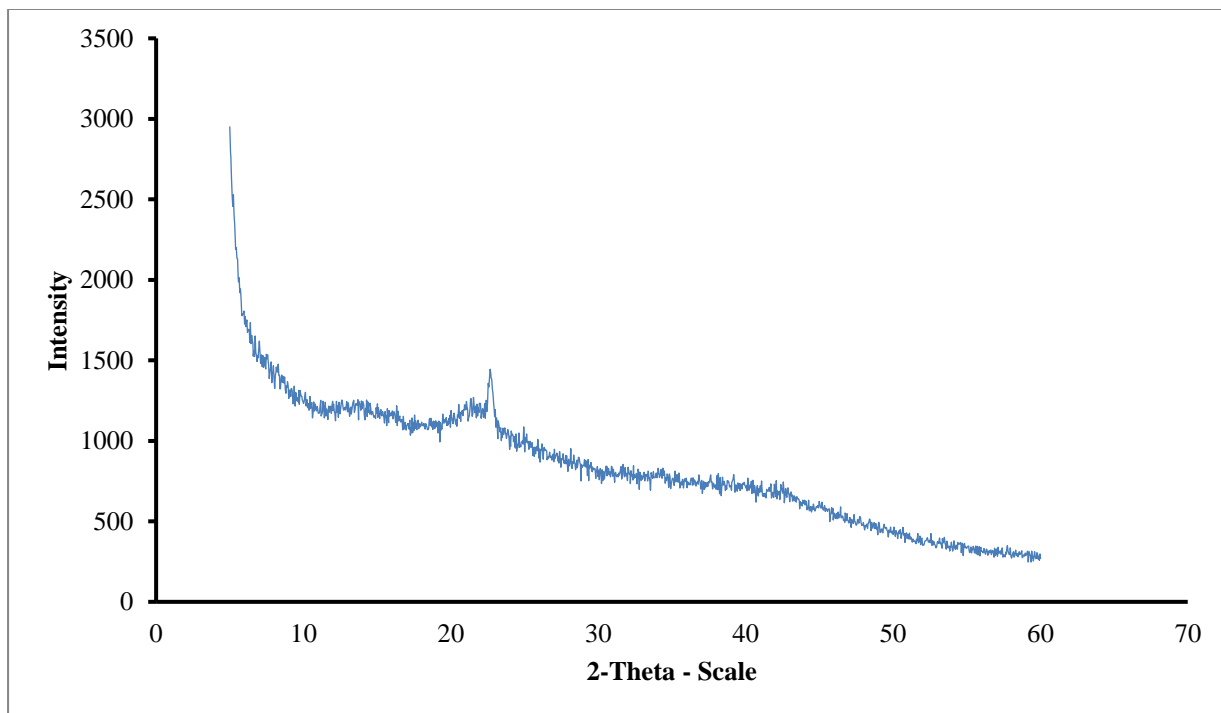


Figure 5.7. XRD diffractogram of optimised selected 1.5%(1:3)CARR:SA wafers.

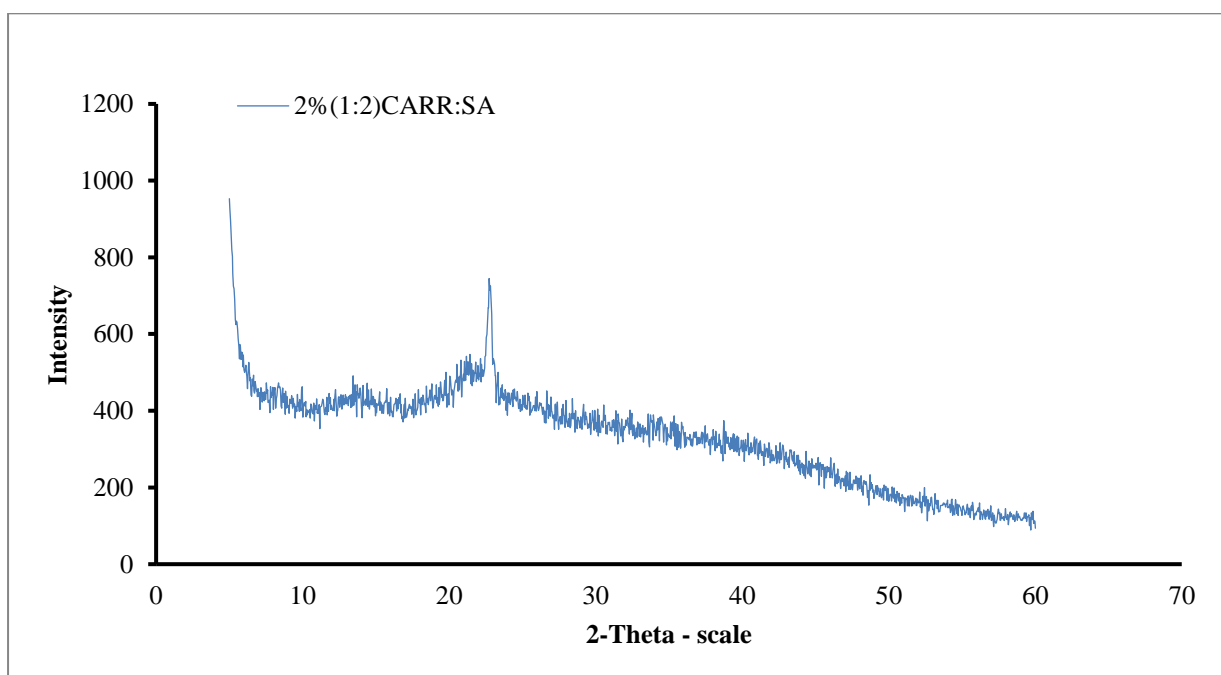


Figure 5.8. XRD diffractogram of optimised selected 2%(1:2)CARR:SA wafers.

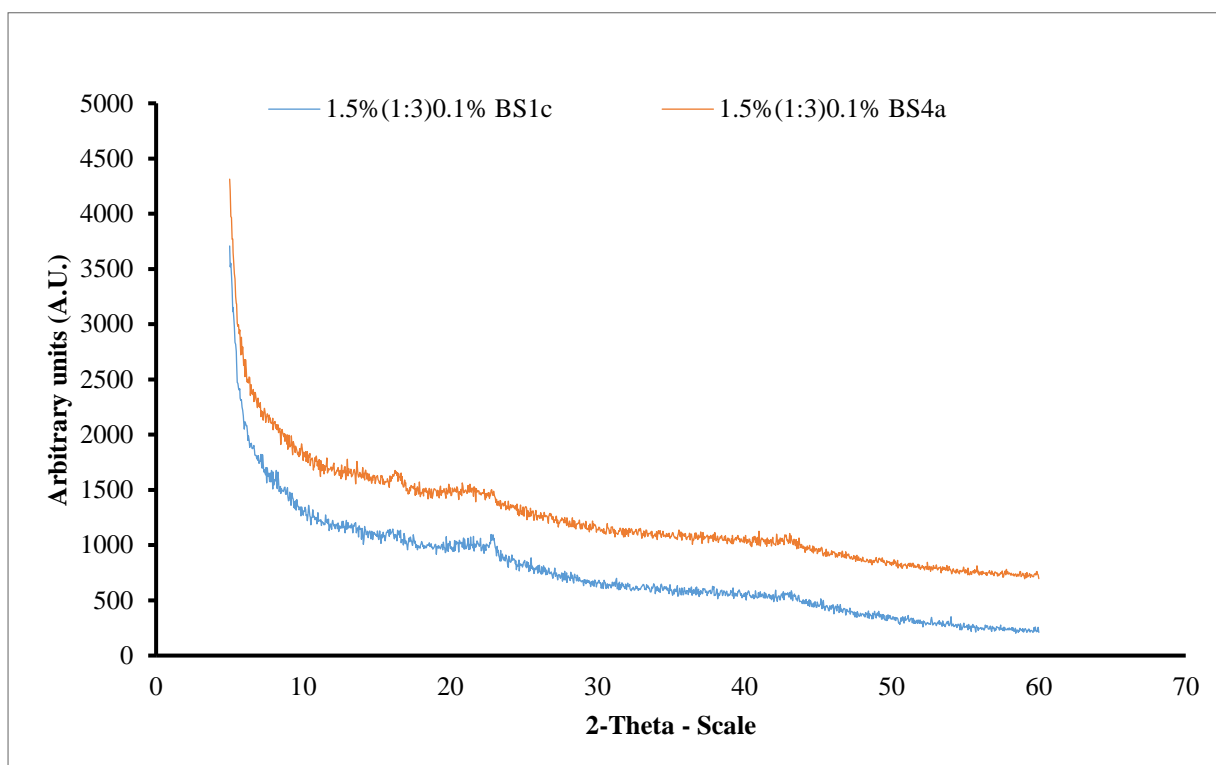


Figure 5.9. XRD diffractograms of 1.5%(1:3)CARR:SA wafers loaded with 0.1% BS1c and 1.5%(1:3)CARR:SA wafers loaded with 0.1% BS4a.

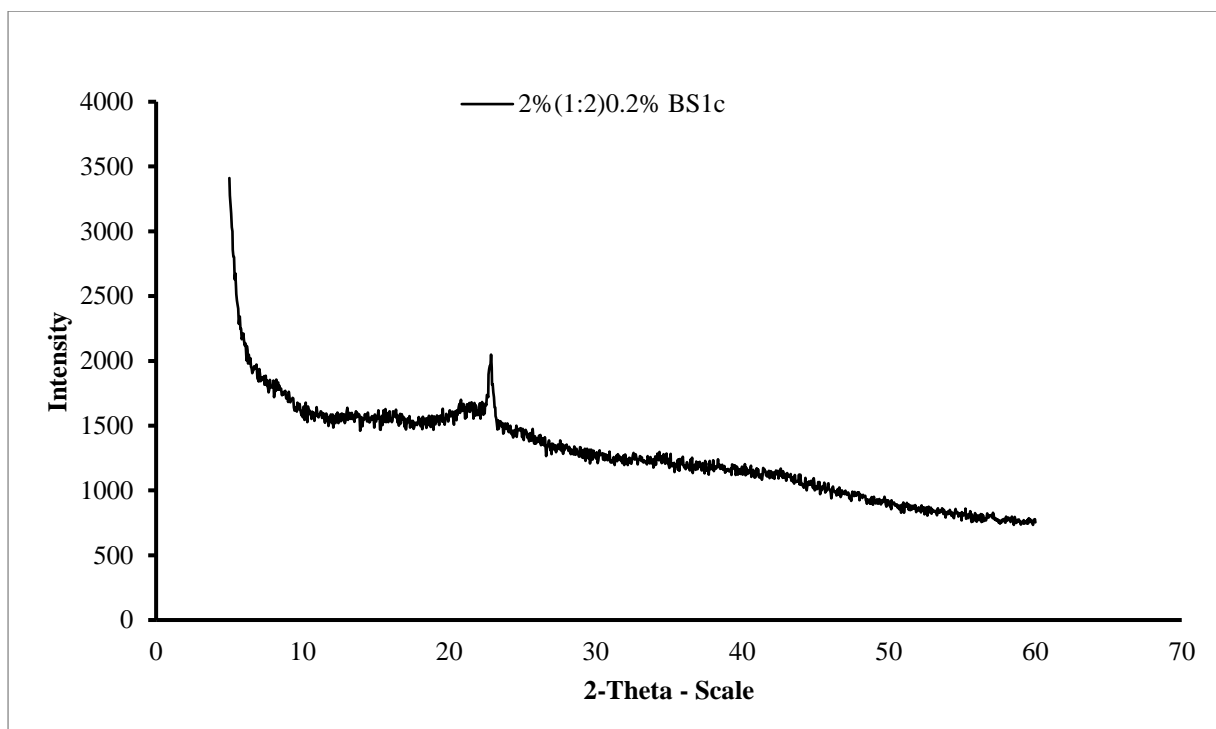


Figure 5.10. XRD diffractograms of 2%(1:2)CARR:SA wafers loaded with 0.2% BS1c.

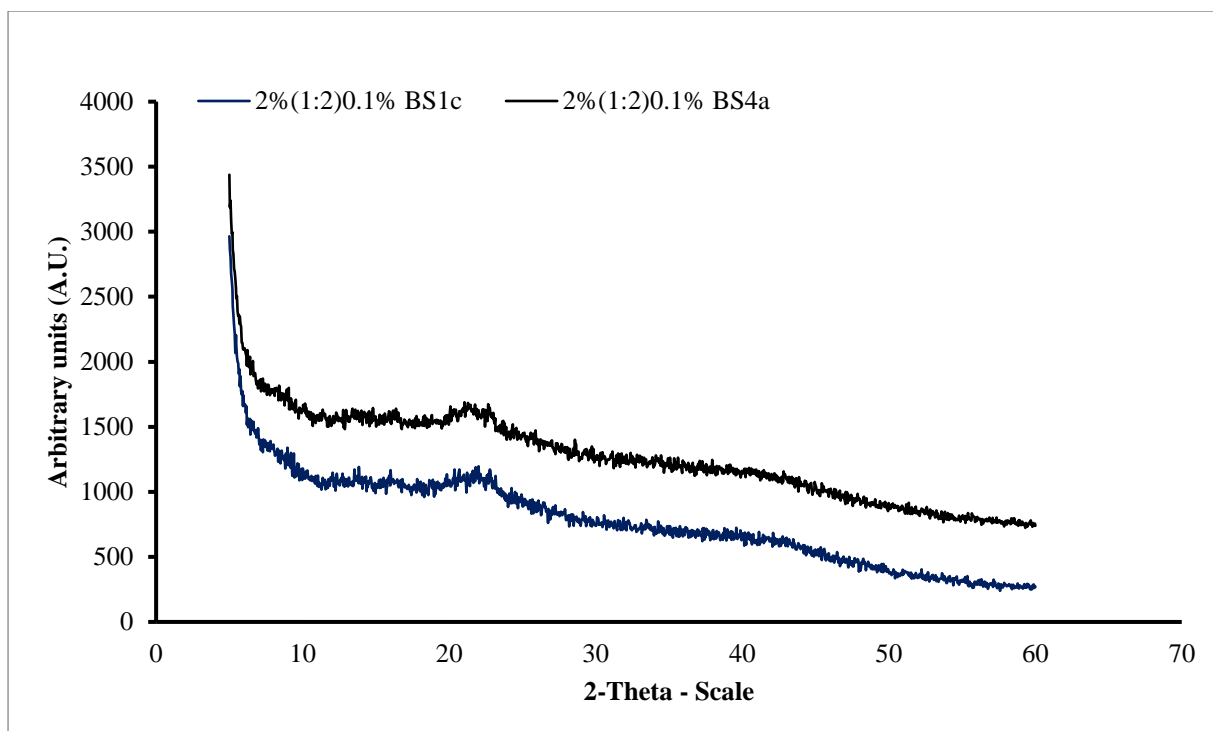


Figure 5.11. XRD diffractograms of 2%(1:2)CARR:SA loaded with 0.1% BS1c and 2%(1:2)CARR:SA wafers loaded with 0.1% BS4a.

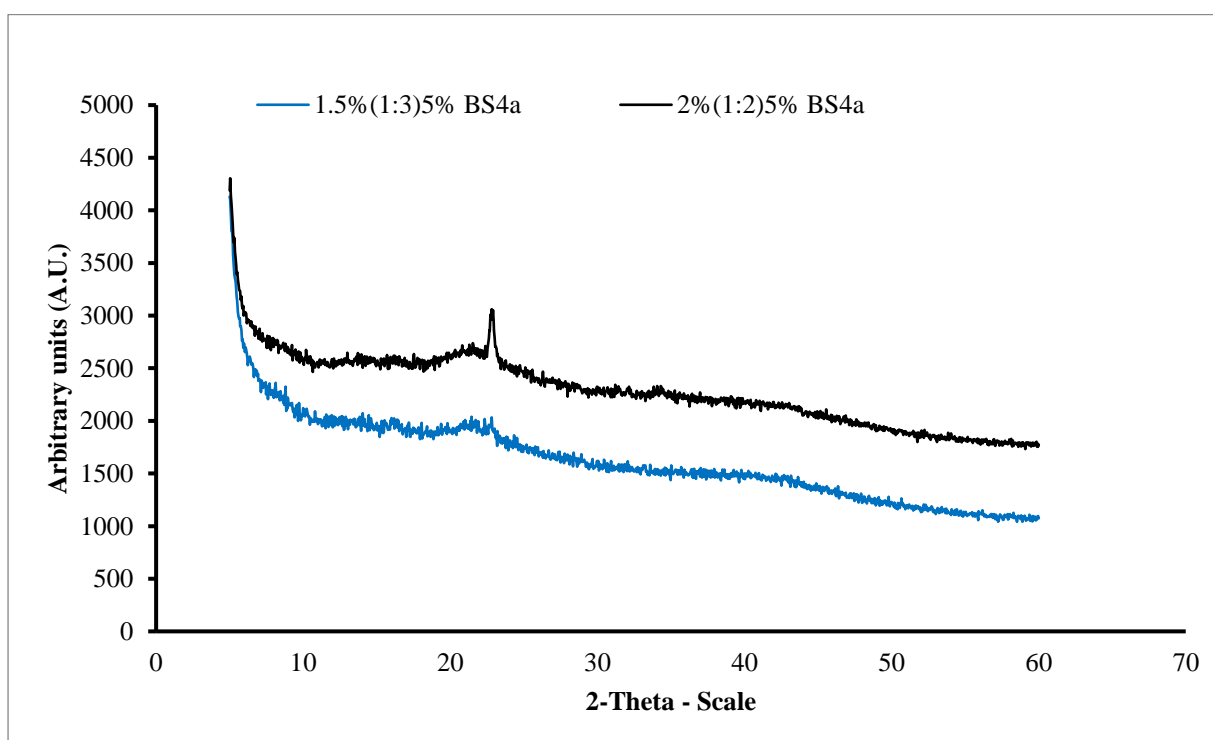


Figure 5.12. XRD diffractograms of 1.5%(1:3)CARR:SA loaded with 5% BS4a and 2%(1:2)CARR:SA wafers loaded with 5% BS4a.

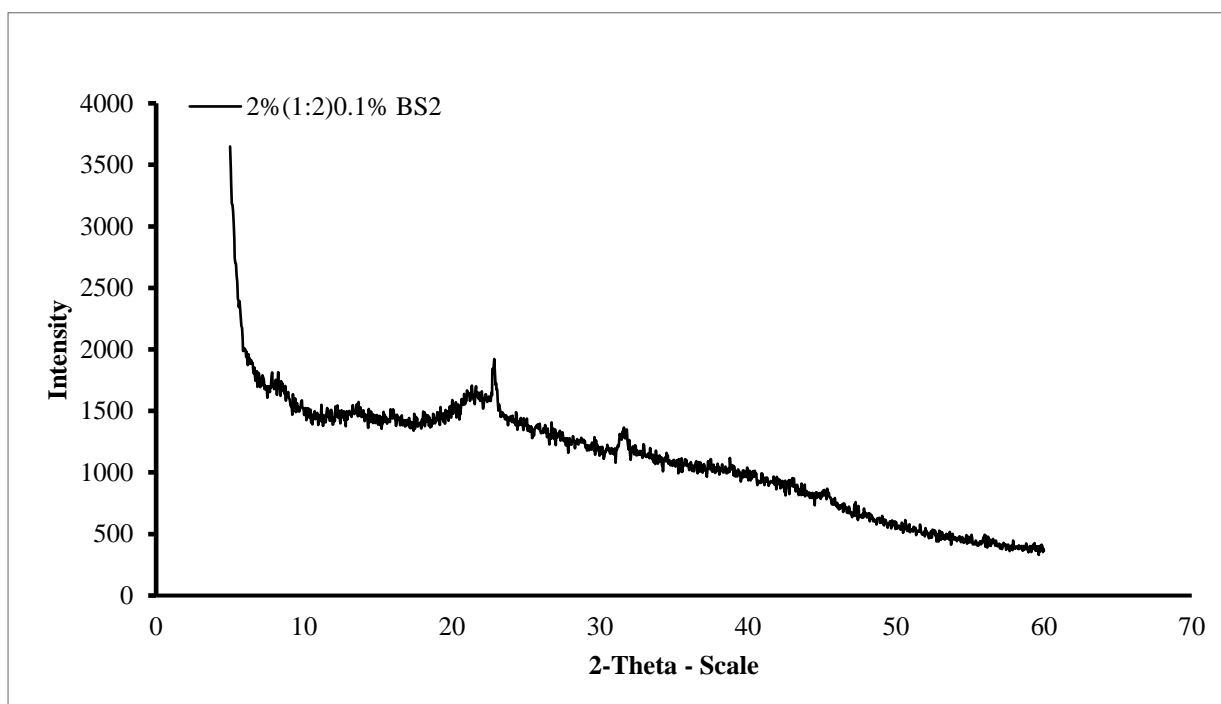


Figure 5.13. XRD diffractogram of 2%(1:2)CARR:SA wafers loaded with 0.1% BS2.

5.4.5 Attenuated total reflectance Fourier transform infrared spectroscopy (ATR-FTIR)

FTIR spectral analysis of BLK and BSs loaded wafers is a direct method used to evaluate molecular interactions such as hydrogen bonding or complexation by monitoring the band shift of a given functional group (Liu *et al.*, 2013). Hydrogen bonds are formed between the proton-donor and proton-acceptor molecules which shifts the bands to lower wavenumbers. As a result of hydrogen bonding, the covalent bonds in the donor and acceptor groups are weaker, while the energy barrier for angle deformation becomes higher (Caykara *et al.*, 2005). Infra-red spectroscopy was employed to characterise the structure and the possible interactions in CARR and SA networks in comparison with their pure standards. Both CARR and SA are polyelectrolytes tending to form physical hydrogels with uni/polyvalent metallic cations (Krol *et al* 2016).

Table 5.7 shows the FTIR spectra of CARR, SA, BSs standards and their representative single wafer formulated in different ratios and total polymer content in gel. The peaks observed at 3373, 1221, 1037/1157, 924 and 844, cm^{-1} can be attributed to O-H stretching, sulphate ester, C-O stretching of pyranose ring, 3,6-anhydro-D-galactose and, galactose 4-sulphate of pure CARR standard respectively. All five peaks detected in the standard were present in 1 - 3%(1:0) CARR:SA wafers (supplementary data). However there was an additional peak at 1356 - 1374 cm^{-1} attributed to sulphate (SO_3) groups stretching in 1.5 - 3% CARR:SA(1:0) wafers. A peak suspected to be C-O stretching of pyranose ring was observed in pure CARR powder and 1%(1:0)CARR:SA. In the FTIR spectrum of pure SA powder, O-H stretching, asymmetric -COO-stretching, (C-OH deformation

vibration) symmetric and (C-C stretching) were detected at vibrational frequencies of 3244, 1595, 1407 and 1025 cm^{-1} respectively. All four functional groups including C-O stretching at 1084 cm^{-1} were detected in 1 - 2% (0:1) CARR:SA wafers (appendix Table A5.3). The influence of different ratios of CARR and SA on the shifting of FTIR characteristic bands is shown for representative formulations (Table 5.8). Each formulation is structurally closer to CARR or to SA depending on the ratio. Additionally, there appears to be very little difference in the wavenumbers of different BSs loaded in composite wafers as shown in representative formulations Table 5.8.

Table 5.7. Wavenumbers of various polymer and BSs starting materials and representative single CARR and SA wafers based on possible intermolecular/intramolecular interactions analysed by ATR-FTIR analysis

Peak number	CARR STD	SA STD	BS1c STD	BS2 STD	BS4a STD	1.5%(1:0)	1.5%(0:1)
1	3373	3244	3257	3300	3368	3368	3252
2	-	1595	2924-2855	2957-2927	2928-2855	1373	1598
3	1221	1407	1726	1719	-	1224	1408
4	-	-	1655	1643	1641	1156	1083
5	925	1025	1575	-	1553	925	1028
6	844	-	-	1467	1415	844	-
7	-	-	1397	1387 (shoulder)	1369	-	-
8	-	-	1317	1232	1247	-	-
9	-	-	1123	-	1170	-	-
10	-	-	-	-	1077	-	-
11	-	-	1046	1034 (shoulder)	1034	-	-
12	-	-	981	-	-	-	-
13	-	-	916	-	-	-	-
14	-	-	881	-	-	-	-
15	-	-	831	-	-	-	-
16	-	-	808	-	-	-	-
17	-	-	704	-	-	-	-
18	-	-	663	-	-	-	-

Table 5.8. Comparison of wavenumbers present in selected optimised CARR:SA:BLKs and representative CARR:SA:BSs loaded wafers based on ATR-FTIR analysis

Peak number	1.5%(1:3)	2%(1:2)	1.5%(1:3)0.2% BS1c	1.5%(1:3)0.1% BS4a	2%(1:2)0.1% BS2	2%(1:2)5% BS4a
1	3337	3340	3283	3284	3288	3286
2	1599	1600	1598	1599	1599	1599
3	1410	1412	1411	1411	1411	1411
4	1255	1254	1255	1255	1252	1251
5	1029	1029	1028	1029	1027	1027
6	931	930	931	932	930	929
7	-	846	846	-	846	846

5.4.6 Fluid handling properties

The ability of wound dressings to absorb exudates and provide a moist wound environment is necessary for the healing process. This biological function can be analysed by water uptake as well as water loss characteristics as analysed below.

5.4.6.1 Swelling

The driving force for swelling is the entropy increase when water diffuses into the polymer network. A gel made of hydrophobic polymers has a non-favoured interaction with water and does not swell much while gels made from hydrophilic polymers absorb large amounts of water and consequently swells to a great extent. Swelling brings tension into the gel network by stretching it and hence, lowers the entropy. A complex interaction between diffusion, dissolution and erosion mechanisms has been used to explain drug release from hydrophilic matrices. Fluid uptake (swelling) of the preliminary set of 1-3% pure CARR wafers, though solid and tactile eroded in less than one hour which led to the decision to formulate composite wafers comprising CARR and SA polymers. During the preliminary swelling studies, the swelling capacity was observed to increase with increasing concentration of SA. However, the water uptake of the samples reached the maximum value within 30 min of incubation in the swelling medium (Fig 5.14) after which the matrix begins to disintegrate. Among the different ratios of CARR:SA analysed, maximum swelling capacity was observed in 1.5%(1:1). The 1.5%(1:3)CARR:SA:BLK wafers showed maximum swelling capacity 5825 (\pm 169)% which decreased in 2%(1:2)CARR:SA:BLK wafers 2975 (\pm 94)% which may be due to the repulsive forces between the negatives charges of sulphate and carboxylate groups. These anionic groups are protonated at acidic pH, while at highly basic conditions the groups are in ionised form.

Consequently, results obtained from swelling and porosity in conjunction with other characterisation techniques led to the selection of 1.5%(1:3) and 2%(1:2) CARR:SA for BSs loading. Figs 5.15 -5.16 shows the change in swelling capacity (%) of the BSs loaded wafers with time. The swelling pattern observed in BLK formulations was also observed between all the 1.5%(1:3)CARR:SA:BSs (Fig 5.15) which had higher maximum swelling capacities than 2%(1:2)CARR:SA:BSs (Fig 5.16). This suggests that the swelling mechanism depends mainly on the hydration of the polymer chains. However, the maximum swelling capacities of 1.5%(1:3)CARR:SA 0.1 and 0.2% BS1c coincided with the wetting phase which occurs within the first 5 min. There was a significant time gap between the maximum swelling capacities of 0.1% and 5% BS4a (15 and 165 min) respectively. Additionally, 1.5%(1:3) 0.1% BS4 wafers had the overall maximum swelling capacity 3934 (± 305)% for BSs loaded wafers in this study. The previous pattern was continued partly in 2%(1:2)0.1% BS4b in which the maximum swelling 3292 (± 229)% was observed but showed the second longest duration of its series at 90 min. The longest duration for swelling observed in 2%(1:2) loaded wafers was 120 min which occurred in both 2%(1:2)0.1% BS1c and BS2. However, the lowest maximum swelling capacity 1706 (± 112)% was observed in 2%(1:2)0.1% BS2. It may be surmised from the results of the investigation that 1.5%(1:3)CARR:SA wafers loaded with 0.1% BSs may be suitable for fast release while corresponding 2%(1:2)CARR:SA may be more suitable for sustained release. The difference in the wetting, maximum hydration and degradation (after 4 hr) between BLK and BSs loaded wafers was statistically significant ($p < 0.05$) in only 1.5%(1:3)CARR:SA wafers. However, no statistical difference ($p > 0.05$) was observed between the different types and concentrations of BSs; 0.1% BS1c, 0.2% BS1c, 0.1% BS4a and 5% BS4a loaded into both optimised selected wafers 1.5%(1:3) and 2%(1:2)CARR:SA wafers.

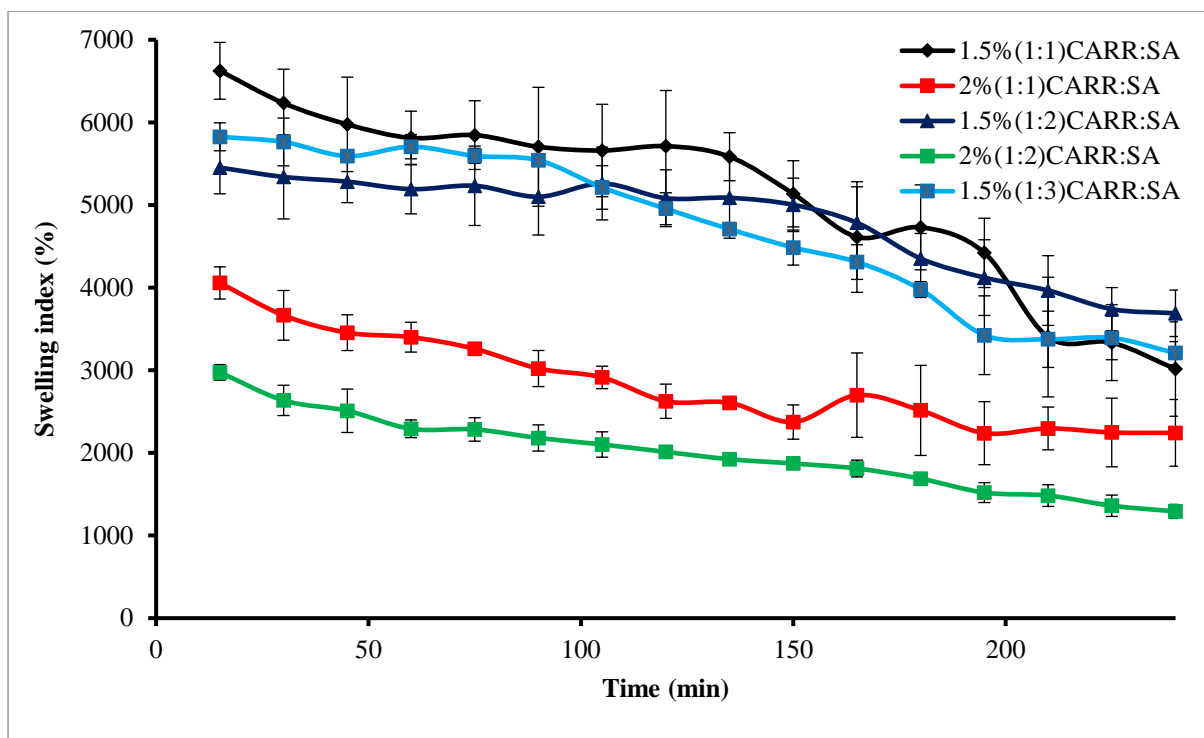


Figure 5.14. Swelling profiles (% swelling index against time of BLK CARR:SA wafers (1:1 and 1:2 ratios) of 1.5 and 2% total polymer weight, and 1:3 ratio of 1.5% total polymer weight in the presence of normal SWF.

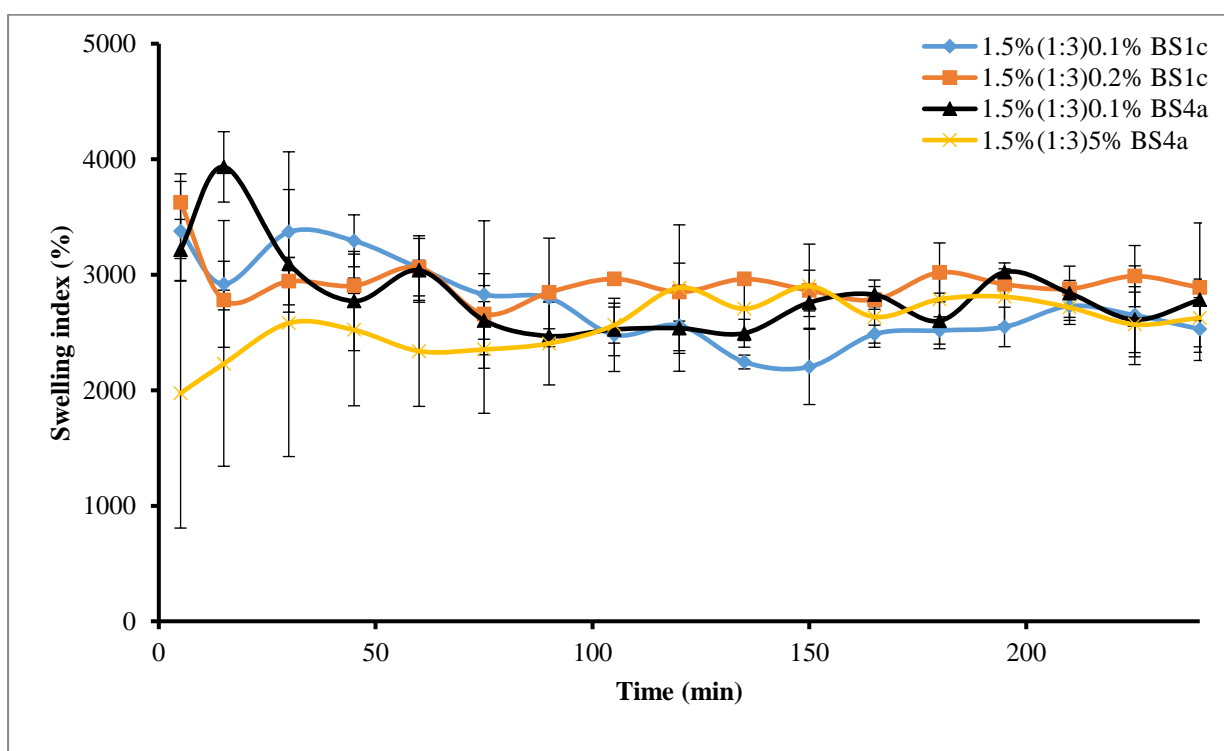


Figure 5.15. Swelling profiles (% swelling index against time of CARR:SA 1.5% (1:3) wafers loaded with 0.1% BS1c, 0.2% BS1c, 0.1% BS4a and 5% BS4a in normal SWF.

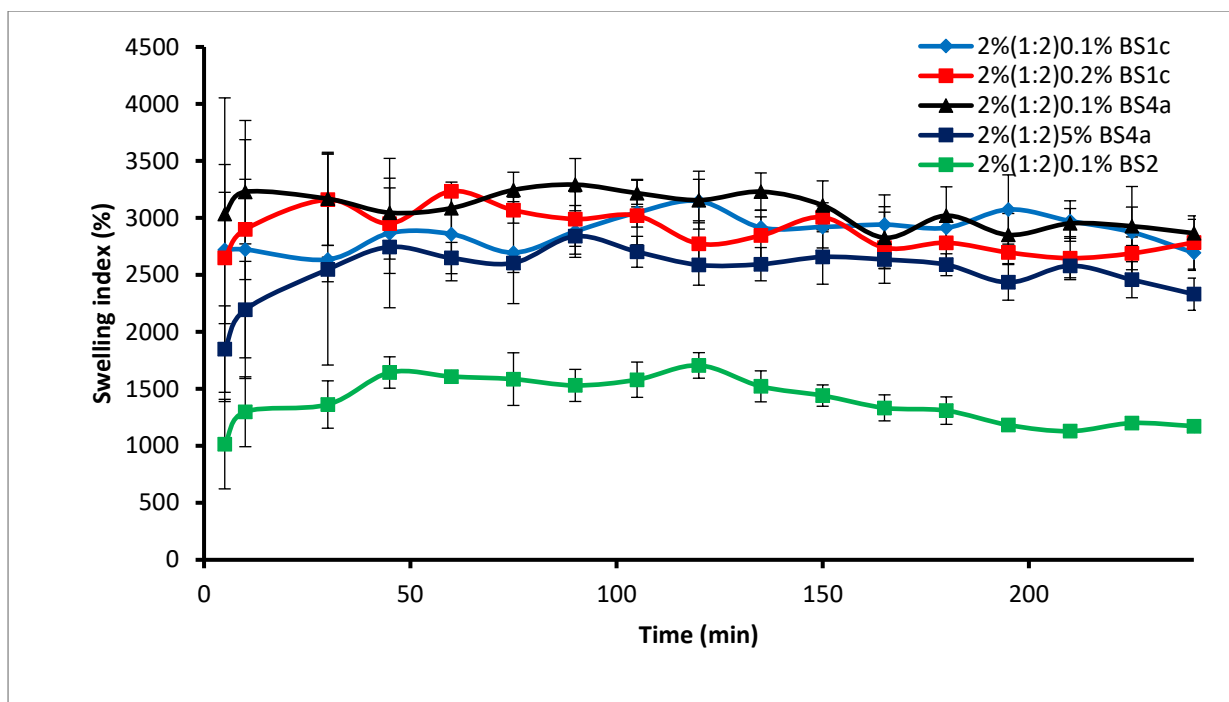


Figure 5.16. Swelling profiles (% swelling index against time of CARR:SA 2%(1:2) wafers loaded with 0.1% BS1c, 0.2% BS1c, 0.1% BS4a and 5% BS4a in normal SWF.

5.4.6.2 Pore analysis

The porosities of single 2%(0:1), composite CARR:SA with different ratios/total polymer content in gel and BSs loaded wafers in optimised selected compositions are reported in Table 5.9. Overall, the maximum porosity of BLK formulations was observed in single 2% SA gel at 100%. This was followed by 1.5%(1:3) and 2%(1:2) CARR:SA wafers with porosities of 90.48% and 67.79% respectively. On the other hand, the lowest porosity occurred for 2%(1:1)CARR:SA wafers. The effect of a higher CARR ratio investigated at 2%(3:1) resulted in an observed percentage of 53.98%. It may therefore be stated that higher SA content enhances the porosity of composite wafers. The pattern observed in BLK composites was replicated in the porosities of all BSs loaded in selected optimised 1.5%(1:3) >98% which were higher than 2%(1:2) <90%. However BSs clearly enhances the porosity of the composite wafers as all investigated formulations were above 70%. Porous wound dressings have the advantage of high exudate uptake, however excess porosity may lead to maceration at the wound site and microbial infection. The difference in the pore analysis of BLK and BSs loaded wafers was statistically significant ($p < 0.05$) in only 1.5%(1:3)CARR:SA wafers. However, no statistical difference ($p > 0.05$) was observed between the different types and concentrations of BSs; 0.1% BS1c, 0.2% BS1c, 0.1% BS4a and 5% BS4a loaded into both optimised selected wafers 1.5%(1:3) and 2%(1:2)CARR:SA wafers.

Table 5.9. Comparison of the porosities of single, composite and BSs loaded wafers

(%, w/w)	CARR :SA 0:1	Pore analysis (%)		
1.5	-			
2.0	100.00 (± 7.20)			
	1:1	1:2	1:3	3:1
1.5	49.92 (± 11.10)	50.83 (± 1.40)	90.48 (± 17.20)	-
2.0	43.26 (± 10.21)	67.79 (± 15.10)	49.25 (± 5.04)	53.98 (± 7.25)
	0.1% BS1c	0.2% BS1c	0.1% BS4a	5% BS4a
1.5	100.00 (± 6.62)	100.00 (± 3.97)	97.34 (± 3.37)	98.94 (± 2.04)
2.0	76.91 (± 5.92)	81.36 (± 1.89)	72.48 (± 3.55)	86.41 (± 9.08)

5.4.6.3 Water absorption (A_w), equilibrium water content (EWC), water reabsorption (ReA_w) and reversibility of equilibrium content (ReEWC)

The A_w , EWC, ReA_w and ReEWC of wound dressings are important characteristics required for quick absorption of exudates as well as good indicators of the reversibility of water absorption of the wafer through dehydration-rehydration cycle. The effect of CARR:SA ratios as well as BSs loading on these properties was analysed and reported for 1.5%(1:3) and 2%(1:2) formulations in Table 5.10. The A_w of all BLK 1.5% CARR:SA ratios wafers were higher than corresponding 2% formulations with maximum 3074 (± 241)% and minimum 1943 (± 412) values observed for 1.5%(1:2) and 2%(1:3) respectively. The EWC of both sets of BLK formulations ranged from 94.95 - 96.84%. Furthermore, the A_w of optimised selected 1.5%(1:3) BSs loaded wafers were all higher than corresponding 2%:(1:2) formulations with values ranging from 2699 (± 157) - 3569 (± 262)% and 1915 (± 592) - 2459 (± 275)% respectively. Interestingly 5% BS4a simultaneously had the highest and lowest A_w respectively for 1.5% and 2% optimised selected wafers. This pattern was consistent in the ReA_w of 1.5% BSs wafers, however there was a slight deviation between 0.2% BS1c and 0.1 % BS4a of 2%(1:2) loaded wafers which interchanged positions between A_w and ReA_w values.

Additionally, the EWC of 1.5% BSs loaded wafers was $\geq 97\%$ while corresponding 2% BSs wafers ranged from 95.02 - 97.05% which indicates optimum stability of wafers after fluid uptake at body temperature (37°C). Similarly the ReEWC of DL wafers remained above 90% indicating just $\pm 2\%$ loss after 48 h. These results suggest that the optimised selected BSs loaded wafers prepared in this study may have high potential as new wound dressing materials, which provide and maintain the adequate moist environment required to prevent scab formation and dehydration of the wound bed. The difference in the A_w and EWC of the selected optimised BLK and BSs loaded wafers were not statistically significant ($p > 0.05$).

Table 5.10. Comparison of the water absorption (Aw), equilibrium water content (EWC), water reabsorption (ReAw) and reversibility of equilibrium content (ReEWC)

1.5	0:1	1:1	1:2	1:3	3:1
Aw	-	2521 (\pm 468)	3074 (\pm 241)	2826 (\pm 135)	-
EWC	-	96.12 (\pm 0.63)	96.84 (\pm 0.23)	96.58 (\pm 0.16)	-
ReAw	-	-	-	-	-
ReEWC	-	-	-	-	-
2	0:1	1:1	1:2	1:3	3:1
Aw	2369 (\pm 75)	1974 (\pm 180)	2574 (\pm 590)	1943 (\pm 412)	2854 (\pm 407)
EWC	95.95 (\pm 0.12)	95.15 (\pm 0.43)	96.14 (\pm 0.84)	94.95 (\pm 1.15)	96.57 (\pm 0.44)
ReAw	-	-	-	-	-
ReEWC	-	-	-	-	-
1.5	0.1% BS1c	0.2% BS1c	0.1% BS4a	5% BS4a	0.1 BS2
Aw	2699 (\pm 157)	3560 (\pm 122)	3458 (\pm 458)	3569 (\pm 262)	-
EWC	97.46 (\pm 0.24)	97.53 (\pm 0.05)	97.61 (\pm 0.57)	97.00 (\pm 0.57)	-
ReAw	1517 (\pm 123)	1665 (\pm 135)	1770 (\pm 125)	1916 (\pm 262)	-
ReEWC	93.79 (\pm 0.47)	94.31 (\pm 0.42)	94.63 (\pm 0.37)	94.98 (\pm 0.68)	-
	0.1% BS1c	0.2% BS1c	0.1% BS4a	5% BS4a	0.1% BS2
Aw	2358 (\pm 102)	2302 (\pm 205)	2459 (\pm 275)	1915 (\pm 592)	2024 (\pm 342)
EWC	96.60 (\pm 0.26)	97.05 (\pm 0.27)	96.64 (\pm 0.37)	96.00 (\pm 0.21)	95.20 (\pm 0.83)
ReAw	1452 (\pm 158)	1483 (\pm 31)	1448 (\pm 219)	1353 (\pm 81)	1434 (\pm 186)
ReEWC	93.51 (\pm 0.67)	93.68 (\pm 0.13)	93.45 (\pm 0.93)	93.11 (\pm 0.37)	93.41 (\pm 0.83)

5.4.6.4 Evaporative water loss (EWL)

The water loss from the 1.5%(1:3) BSs and 2%(1:2)BSs loaded wafers at 37°C were compared to examine their behaviour when used as a dressing over a chronic wound. As shown in Table 5.11, the loss of water from 1.5%(1:3) and 2%(1:2) BSs wafers ranged from about 9 - 10% and 8 – 10% respectively after 1 h and increased up to 43-52% and 36 – 44% within 6 h. After 24 h, the loss of water was about 85 - 86% and 85- 86% respectively.

Table 5.11. Comparison of the Evaporative water loss (EWL) of 1.5%(1:3) CARR:SA:BSs and 2%(1:2) CARR:SA:BSs wafers

1.5%(1:3) CARR:SA	1	2	3	4	5	6	24 h (%)
BLK	-	-	-	-	-	-	-
0.1% BS1c	90.54 (±1.41)	81.05 (±2.48)	72.11 (±3.69)	64.56 (±4.38)	57.83 (±4.99)	51.86 (±5.43)	14.36 (±1.20)
0.1% BS4a	91.70 (±0.13)	83.44 (±0.32)	75.32 (±0.50)	68.53 (±0.76)	62.49 (±1.24)	57.24 (±1.29)	14.40 (±0.84)
0.1% BS2	-	-	-	-	-	-	-
0.2% BS1c	89.99 (±2.13)	79.87 (±4.08)	70.17 (±5.77)	62.15 (±6.91)	55.10 (±7.89)	48.87 (±8.78)	14.48 (±1.21)
5% BS4a	90.63 (±0.90)	81.50 (±1.59)	72.90 (±2.13)	65.66 (±2.47)	59.44 (±2.74)	53.62 (±3.07)	15.22 (±0.03)
<hr/>							
2%(1:2) CARR:SA							
BLK	93.40 (±0.37)	87.45 (±0.69)	77.80 (±1.41)	74.46 (±1.61)	69.54 (±1.88)	64.79 (±1.91)	14.41 (±0.67)
0.1% BS1c	90.56 (±0.11)	80.90 (±0.55)	71.63 (±0.84)	63.67 (±1.23)	56.75 (±1.41)	50.50 (±1.38)	15.65 (±0.62)
0.1% BS4a	91.58 (±0.63)	83.07 (±0.79)	75.10 (±0.78)	68.16 (±1.02)	61.88 (±1.26)	56.12 (±1.42)	14.19 (±0.28)
0.1% BS2	92.82 (±1.61)	85.12 (±3.33)	73.22 (±6.05)	68.53 (±7.07)	62.08 (±8.22)	56.40 (±8.95)	16.16 (±1.40)
0.2% BS1c	90.61 (±0.46)	81.18 (±2.03)	73.16 (±2.02)	65.74 (±2.72)	59.34 (±3.23)	53.44 (±3.65)	15.62 (±0.76)
5% BS4a	90.07 (±1.13)	80.06 (±2.22)	70.89 (±2.90)	62.85 (±3.32)	55.77 (±3.79)	49.32 (±4.02)	15.28 (±0.38)

Although, there was a 1% difference between the first and final water loss measurements for the two readings which is the closest parallel observed between bioanalytical characterisation so far, the difference in the EWL of the selected optimised BLK and BSs loaded wafers were not statistically significant ($p > 0.05$). However both dressings will lose water content when exposed to air under dry conditions during short periods as a result of quick exudate uptake from the wound into the dressing by an active upward-directed process when used in early-stage exuding wounds (Kim *et al.*, 2007).

These dressings may therefore be more beneficial to wounds with more exudates in early-stages of wound healing.

5.4.6.5 Water vapour transmission rate

A moist environment enhances the healing process more effectively rather than a dry one, (Dyson *et al.*,1988), therefore, a good dressing must be able to keep the wound environment moist to a certain level. Additionally, it must possess an appropriate WVTR. If the WVTR is fairly high then there are chances of dehydration of wound as well as adherence of the dressing to wound bed. Contrary to this, if the WVTR is fairly low then there may be excessive accumulation of exudate under the dressing which can cause maceration of health tissue or leakage of exudate from the edges of the dressing, which may promote microbial infection.

Table 5.12. Comparison of the water vapour transmission rate (WVTR) of BLK 1.5 and 2%(0:1, 1:1, 1:2, 1:3, 3:1) CARR:SA wafers

1.5%	1	2	3	4	24 h (g/m ² day ⁻¹)
0:1	-	-	-	-	-
1:1	87.53 (±4.28)	199.76 (±4.27)	317.66 (±6.61)	595.70 (±50.41)	3082 (±285)
1:2	89.03 (±1.31)	201.27 (±3.46)	318.79 (±4.61)	644.94 (±24.17)	2777 (±105)
1:3	105.07 (±6.21)	250.13 (±57.90)	376.89 (±69.67)	735.29 (±76.06)	3054 (±184)
3:1	-	-	-	-	-
<hr/>					
2%					
0:1	124.12 (±19.57)	225.42 (±24.83)	346.33 (±30.39)	660.59 (±49.66)	2920 (±132)
1:1	84.32 (±3.71)	189.58 (±7.09)	300.68 (±9.63)	585.14 (±13.90)	2661 (±114)
1:2	89.41 (±2.59)	198.63 (±2.04)	311.24 (±2.04)	577.78 (±4.63)	2657 (±69)
1:3	130.72 (±63.72)	318.04 (±103.78)	491.77 (±167.47)	886.95 (±219.86)	3285 (±690)
3:1	130.72 (±41.68)	260.88 (±44.32)	386.70 (±45.70)	731.14 (±112.37)	3330 (±439)

The effect of CARR:SA ratios on the WVTR of BLK 1.5% and 2% total polymer content wafers are presented in Table 5.12. The WVTR observed after 1 h ranged from (87.53 - 105.07; 84.32 - 130.72) g/m²h⁻¹, and after 24 h from (2777 – 3082; 2657 - 3285) g/m²day⁻¹ for 1.5 and 2% respectively. Specifically for the optimised selected wafers, the WVTR was observed to be higher for 1.5%(1:3) 105.07 g/m²h⁻¹ after 1 h in comparison to 2%(1:2) 89.41 g/m²h⁻¹. This observation remained

consistent after 24 h, 3054 g/m²day⁻¹ and 2657 g/m²day⁻¹. A statistical difference was observed in the WVTR of BLK and BSs of only 2%(1:2)CARR:SA wafers. However, no statistical difference ($p > 0.05$) was observed between the different types and concentrations of BSs; 0.1% BS1c, 0.2% BS1c, 0.1% BS4a and 5% BS4a loaded into both optimised selected wafers 1.5%(1:3) and 2%(1:2)CARR:SA wafers.

It has been recommended that a rate of 2000–2500 g/m²day⁻¹ would provide adequate level of moisture without risk in wound dehydration (Queen *et al.*, 1987). Based on the above discussion, it may be claimed that WVTR of all the samples fall above the prescribed range of WVTR, therefore the BSs loaded wafers in this study may be useful in the case of wounds with abnormally high exudates.

Table 5.13. Comparison of the water vapour transmission rate (WVTR) of BSs loaded 1.5%(1:3) and 2%(1:2)CARR:SA wafers

1.5%(1:3) CARR:SA	1	2	3	4	5	6	24 h (g/m ² day ⁻¹)
0.1% BS1c	126 (±5)	278 (±5)	615 (±20)	832 (±45)	990 (±56)	1148 (±66)	3080 (±143)
0.2% BS1c	127 (±3)	277 (±9)	590 (±27)	806 (±37)	958 (±51)	1106 (±61)	2982 (±145)
0.1% BS4a	129 (±5)	275 (±9)	498 (±36)	672 (±53)	818 (±56)	965 (±67)	2828 (±157)
5% BS4a	133 (±2)	273 (±5)	433 (±38)	586 (±38)	725 (±37)	864 (±38)	2702 (±49)
0.1% BS2	-	-	-	-	-	-	-
2%(1:2) CARR:SA							
0.1% BS1c	133 (±4)	289 (±2)	593 (±16)	855 (±45)	1037 (±89)	1189 (±113)	2968 (±99)
0.2% BS1c	128 (±3)	284 (±4)	597 (±47)	888 (±96)	1092 (±140)	1243 (±154)	2988 (±87)
0.1% BS4a	129 (±1)	283 (±16)	549 (±125)	794 (±215)	974 (±257)	1115 (±260)	2862 (±255)
5% BS4a	128 (±5)	310 (±75)	509 (±107)	659 (±112)	796 (±115)	934 (±118)	2724 (±163)
0.1% BS2	78 (±1)	192 (±4)	310 (±7)	431 (±9)	558 (±11)	721 (±87)	3062 (±188)

5.4.6.6 Thermogravimetric analysis (TGA)

TGA was used to estimate the amount of water present in single SA and composite CARR:SA wafers prepared and lyophilised under similar conditions. The moisture content of single BLK and composite CARR:SA wafers at 1.5 and 2% total polymer content ranged from 13.75 and 15.16% Table 5.14, which is an acceptable volume for lyophilised wafers. Momoh *et al.*, (2015) reported a moisture content of 18.24% for pure SA powder which had the same mannuronic – guluronic (M/G) ratio of 1.56 as that used in this study M/G. However, loss of moisture content was analysed around 175 °C in this study. Additionally, the moisture content of optimised selected 1.5%(1:3) and 2%(1:2) CARR:SA wafers which had been subjected to EWL were 14.36 (± 1.20)% and 14.41 (± 0.67)% Table 5.14 respectively after 24 h in a 37°C oven. These results correspond to those obtained from TGA analysis. The moisture content affects the exudate handling properties and improves the adhesion of the formulations.

Table 5.14. Residual moisture of optimised formulations analysed by TGA

Moisture content (%)	0:1	1:1	1:2	1:3	3:1
1.5%	-	14.18 (± 0.64)	14.46 (± 0.10)	14.86 (± 0.53)	-
2.0%	14.36 (± 0.06)	13.75 (± 0.33)	14.23 (± 0.10)	15.16 (± 0.18)	13.77 (± 1.33)

5.4.6.6 Mucoadhesion

The stickiness, work of adhesion (WOA) and cohesiveness of single, composite and DL (BSs) loaded wafers are presented in Table 5.15. The maximum stickiness observed for single CARR and SA wafers were 0.34 and 0.31 N at 1% w/w total polymer content in gel. The stickiness of optimised selected 1.5%(1:3) was higher than 2%(1:2) at 0.60 and 0.55 N. Interestingly, the highest stickiness was observed in single 1.5% CARR total polymer content in gel 0.81 N. The effect of BSs reduced and increased the stickiness of 1.5%(1:3) and 2%(1:2). The trends observed for the stickiness of single, composite and BSs loaded wafers were observed in the values recorded for WOA Table 5.16. The trends observed for single CARR and SA as well as optimised composites were also observed in the cohesiveness of formulated wafers presented in Table 5.17. Pawar *et al.*, (2014) associated the decreased stickiness of DL wafers in 2% BSA SWF to decreased porosity due to added drugs and subsequent sodium sulphate formation which inhibited the rapid hydration of the wafers. However in this study, results obtained from pore analysis showed that the incorporation of drugs enhanced the porosities of the matrixes they were loaded into. Tobyn *et al.*, (1997), reported that increased ionic strength of the media and the presence of sodium and potassium ions results in decreased WOA.

Table 5.15. Comparison of the mucoadhesive stickiness of single, composite BLK and drug loaded wafers

Stickiness (N)					
Single wafers	1:0	0:1			
1 (% , w/w)	0.34 (± 0.12)	0.31 (± 0.02)	-	-	-
1.5 (% , w/w)	0.14 (± 0.02)	0.28 (± 0.06)	-	-	-
2 (% , w/w)	0.16 (± 0.01)	0.29 (± 0.02)	-	-	-
2.5 (% , w/w)	0.18 (± 0.03)	-	-	-	-
3 (% , w/w)	0.20 (± 0.00)	-	-	-	-
Composite wafers	1:1	1:2	1:3	2:1	3:1
1 (% , w/w)	0.29 (± 0.11)	0.36 (± 0.14)	0.24 (± 0.02)	0.26 (± 0.09)	0.18 (± 0.04)
1.5 (% , w/w)	0.81 (± 0.06)	0.47 (± 0.14)	0.60 (± 0.19)	-	-
2 (% , w/w)	0.42 (± 0.09)	0.35 (± 0.11)	0.61 (± 0.22)	-	0.47 (± 0.17)
DL loaded wafers	0.1% BS1c	0.2% BS1c	0.1% BS4a	5% BS4a	-
1:3(1.5%)	0.55 (± 0.02)	0.56 (± 0.10)	0.58 (± 0.13)	0.48 (± 0.05)	-
1:2(2%)	0.59 (± 0.08)	0.57 (± 0.10)	0.51 (± 0.19)	0.48 (± 0.17)	-

Table 5.16. Comparison of the mucosal work of adhesion of single, composite and drug loaded wafers

Work of adhesion (WOA) (N.mm)					
Single wafers	1:0	0:1			
1 (% , w/w)	0.61 (± 0.20)	0.37 (± 0.03)	-	-	-
1.5 (% , w/w)	0.23 (± 0.00)	0.35 (± 0.10)	-	-	-
2 (% , w/w)	0.30 (± 0.02)	0.22 (± 0.04)	-	-	-
2.5 (% , w/w)	0.41 (± 0.19)	-	-	-	-
3 (% , w/w)	0.23 (± 0.01)	-	-	-	-
Composite wafers	1:1	1:2	1:3	2:1	3:1
1 (% , w/w)	0.38 (± 0.17)	0.72 (± 0.37)	0.45 (± 0.02)	0.23 (± 0.11)	0.30 (± 0.03)
1.5 (% , w/w)	1.19 (± 0.12)	0.68 (± 0.31)	1.09 (0.48)	-	-
2 (% , w/w)	0.47 (± 0.20)	0.54 (± 0.21)	1.91 (± 1.99)	-	0.67 (± 0.24)
DL loaded wafers	0.1% BS1c	0.2% BS1c	0.1% BS4a	5% BS4a	-
1:3(1.5%)	0.59 (± 0.19)	0.78 (± 0.15)	0.59 (± 0.17)	0.54 (± 0.04)	
1:2(2%)	0.63 (± 0.05)	0.76 (± 0.16)	0.60 (± 0.18)	0.50 (± 0.15)	

Table 5.17. Comparison of the mucoadhesive cohesiveness of single, composite and drug loaded wafers

Cohesiveness (mm)					
Single wafers	1:0	0:1	-	-	-
1 (% , w/w)	3.61 (±0.51)	2.92 (±1.21)	-	-	-
1.5 (% , w/w)	3.01 (±0.33)	2.40 (±0.54)	-	-	-
2 (% , w/w)	4.03 (±1.36)	1.61 (±0.49)	-	-	-
2.5 (% , w/w)	4.90 (±2.38)	-	-	-	-
3 (% , w/w)	2.29 (±0.09)	-	-	-	-
Composite wafers	1:1	1:2	1:3	2:1	3:1
1 (% , w/w)	2.05 (±0.28)	3.14 (±0.67)	3.62 (±0.45)	1.50 (±0.39)	3.50 (±0.57)
1.5 (% , w/w)	3.61 (±0.43)	2.84 (±0.86)	5.49 (±3.31)	-	-
2 (% , w/w)	2.16 (±0.38)	2.98 (±0.80)	4.91 (±2.87)	-	3.30 (±0.88)
DL loaded wafers	0.1% BS1c	0.2% BS1c	0.1% BS4a	5% BS4a	-
1.5%(1:3)	2.15 (±0.44)	3.30 (±1.73)	3.14 (±2.15)	2.12 (±0.29)	-
2%(1:2)	1.94 (±0.23)	2.24 (±0.36)	2.07 (±0.21)	1.97 (±0.33)	-

Although a decrease in the OH of DL composite wafers were observed in comparison to BLKs, it is possible that sodium sulphate which is present in the optimised selected wafers increased the ionic strength of the SWF resulting in decreased adhesion due to decreased rate of initial hydration which is essential for effective chain interpenetration with the mucosal substrate and subsequent adhesive interaction. However, the cohesiveness of 2%(1:2) was higher (2.98 mm) than its BSs loaded formulations (1.94 – 2.24) mm which was a departure from the corresponding stickiness and WOA. The difference in the stickiness of BLK and BSs loaded wafers was statistically significant ($p < 0.05$) in only 2%(1:2)CARR:SA wafers. While the difference in the WOA of BLK and BSs loaded wafers was statistically significant ($p < 0.05$) in only 1.5%(1:3)CARR:SA wafers. In addition the difference between the cohesiveness of BLK and BSs loaded wafers was statistically significant ($p < 0.05$) in both optimised 1.5%(1:3) and 2%(1:2)CARR:SA wafers. Further, no statistical difference ($p > 0.05$) was observed between the different types and concentrations of BSs; 0.1% BS1c, 0.2% BS1c, 0.1% BS4a and 5% BS4a loaded into both optimised selected wafers 1.5%(1:3) and 2%(1:2)CARR:SA wafers.

Cohesiveness is the intermolecular attraction which holds the wafer and the model wound substrate together. From the results obtained, it can be concluded that the wafers generally possessed good adhesive strength with the wound substrate, furthermore, decreased stickiness and WOA is an advantage because it maintains a balance between prolonged retention at the wound site and the need

to avoid damaging sensitive newly formed tissue during the healing process in the course of dressing change.

5.5 Conclusions

The main objective for this chapter was the formulation design, development and optimisation of stable composite BSs loaded wafers as potential dressings to treat chronic wounds. Initially five gels with total polymer content (1.0, 1.5, 2.0, 2.5 and 3.0% w/w) with different ratios of CARR:SA were used to formulate wafers. Different characterisation techniques (TA, SEM, XRD and ATR-FT-IR) were utilised to observe the physico-chemical properties of BLK and BSs loaded wafers. The results suggested that out of the five formulations, only composite wafers prepared from 1.5% and 2% w/w total polymer content in gel with CARR:SA ratios of 1:3 and 1:2 respectively showed desired characteristics required in wafers on the basis of an ideal balance between toughness (4 – 6N), porosity above 65% that fell within range of optimum moisture handling properties which are essential functional characteristics. Molecular dispersity of all BSs with the exception of 5% sophorolipids loaded in 2%(1:2) CARR:SA was observed across all formulations. The incorporation of BSs was observed to affect mechanical strength, exudate handling properties and mucoadhesion of optimised selected BLK and DL (BSs) loaded wafers. The results obtained from XRD diffractograms showed that all formulations (single, composite and BSs loaded) were amorphous. Similar vibrations identified in the seven functional groups of composite wafers were observed in ATR-FTIR wavenumbers. BSs loaded in 1.5%(1:3) predominantly showed higher fluid handling properties than BSs loaded in 2%(1:2) and therefore has potential for application onto highly exuding chronic wounds.

CHAPTER 6 LYOPHILISED WAFER DRESSINGS LOADED WITH BIOSURFACTANT BASED NIOSOMES FOR POTENTIAL CHRONIC WOUND HEALING

6.1 Introduction

The chronic nature and associated complications of non-healing wounds have led to the emergence of nanotechnology based therapies aimed at facilitating the healing process and ultimately repairing the injured tissue. A number of engineered nanotechnologies have been proposed demonstrating unique properties and multiple functions that address specific problems associated with wound repair mechanisms (Hamdan *et al.*, 2017). A high surface area to volume ratio endows nanostructures with unique features (Korrapati *et al.*, 2016) such as a high probability of interaction with the biological target and an enhanced penetration into the wound bed (Mordoski *et al.*, 2015). This results in nanoparticles having the ability to deliver a sustained and controlled release of therapeutics that result in an accelerated healing process (Parani *et al.*, 2016). Molecular dispersity of resulting nano-structures gives rise to high surface energy due to less ordered amorphous structures. The increase in surface energy allows greater molecular interaction between the solute and solvent hence they are more soluble and are expected to release drugs quickly when applied to the wound site which can help to rapidly reduce bacterial infection for example (Pawar *et al* 2014).

There are two main categories of nanomaterials used in wound healing: (i) nanomaterials that exhibit intrinsic properties beneficial for wound treatment and (ii) nanomaterials employed as delivery vehicles for therapeutic agents (Kalashnikova *et al.*, 2015, Tocco *et al.*, 2012). Mohamadnia *et al.*, (2008) and Paşcalău *et al.*, (2012) applied the first category of nanomaterials by formulating composite mixture of two bioactive polymers into beads and oxidised hydrogels respectively. Degim and co applied the second category of nanomaterials by developing chitosan gels containing liposome-loaded epidermal growth factor (EGF) (Degim *et al* 2011).

There are very few existing reports of the BSs used in this study (rhamnolipids, sophorolipids and surfactin) in literature where the physico-chemical and bioanalytical characteristics of their corresponding niosomes loaded into dressings have been extensively investigated. (Ju and colleagues patented both previously listed categories of nanomaterials combining rhamnolipids, sophorolipids and gas vesicles within gelatin-alginate hydrogels (Ju *et al.*, 2013). Recently Zouari and co-workers reported that a crude *Bacillus subtilis* SPB1 lipopeptide BS based gel which produced five clusters of isoforms including surfactin – accelerated the healing process of excision wounds induced on experimental rats (Zouari *et al.*, 2016). However, to the best of our knowledge, the application of these BSs has not been investigated in lyophilised wafer dressings for potential chronic wound healing. In this chapter, further novelty was achieved through combination of both previously described categories of nanomaterials by lyophilising niosomes loaded into composite CARR:SA

gels. In addition to being the first reported study of lyophilised wafer loaded niosome dressings, this is also the first systematic comparison of two sets of multicomponent loaded wafers which differ by the inclusion and exclusion of a negative charge inducer (DCP) in the niosomes.

Formulated BSs based multi-lamellar niosomes were incorporated into selected optimised bioactive composite CARR:SA gels and lyophilised to obtain the wafers. Physico-chemical and bioanalytical techniques used include SEM, texture analysis (mechanical), ATR-FTIR, XRD, exudate handling properties (swelling index, water vapour transmission rate, equilibrium water content, porosity, water absorption, evaporative water loss, water reabsorption and reversibility of equilibrium water content). The synergistic effects of these novel-dressings such as swelling, optimum water vapour transmission rate (WVTR), mechanical strength and morphological appearance, makes them suitable candidates for wound healing applications.

6.2 Materials and methods

This section discusses the methods used for the formulation and characterisation of BSs loaded niosomal gels (Refer to section 4.2 and 5.2)

6.3 Methods

6.3.1 Formulation of BSs loaded niosomes

BSs loaded niosomes were formulated as described in chapter 4, section 4.3

6.3.2 Formulation of composite gels

CARR and SA based composite gels were formulated as described in chapter 5, section 5.3.1

6.3.3 Formulation of wafers loaded with BSs based niosomes

Optimised 2% CARR:SA (1:2) formulated from the previous chapter was selected as the total polymer content in composite gel to load niosomes into as a result of better morphology and optimum moisture handling properties. After niosomes were prepared from chapter 4, 2 ml of the BSs loaded niosomes were dispersed into optimised 2% CARR:SA (1:2) composite gels. Lyophilisation of the combined niosomal gel composition resulted in composite wafers with BSs based niosomes including DCP (CARR:SA:BSs-NIO-DCP) (Table 6.1) and composite wafers with BSs based niosomes without DCP (CARR:SA:BSs-NIO) (Table 6.2).

Table 6.1. Composition of composite wafers comprising BSs and DCP based niosomes including (CARR:SA:BSs-NIO-DCP) loaded into selected optimised freeze-dried wafers obtained from 2% w/w total polymer gels

Starting Material	CARR:SA (BLK) (mg)	CARR:SA (BS1c) (mg)	CARR:SA (BS4a/b) (mg)	CARR:SA (BS1c ^{***}) (mg)	CARR:SA (BS2 ^{***}) (mg)
CARR	666.7	666.7	666.7	666.7	666.7
SA	1333.3	1333.3	1333.3	1333.3	1333.3
S60	43.6	43.6	43.6	43.6	43.6
CHL	38.6	38.6	38.6	38.6	38.6
DCP	8.2	8.2	8.2	8.2	8.2
BS1c	-	1.0 x 10 ⁻³	-	-	-
BS4a	-	-	1.0 x 10 ⁻³	-	-
BS4b	-	-	-	6.0 x 10 ⁻³	-
BS2	-	-	-	-	6.0 x 10 ⁻³

BSs^{***} equals a six-fold BSs concentration of unmarked. 100, 0.001

Table 6.2. Composition of composite wafers comprising BSs based niosomes without DCP (CARR:SA:BSs-NIO) loaded into selected optimised freeze-dried wafers obtained from 2% w/w composite gels

Starting Material	CARR:SA (BLK) (mg)	CARR:SA (BS1c) (mg)	CARR:SA (BS4ab/) (mg)	CARR:SA (BS1c ^{***}) (mg)	CARR:SA (BS2 ^{***}) (mg)
CARR	666.7	666.7	666.7	666.7	666.7
SA	1333.3	1333.3	1333.3	1333.3	1333.3
S60	43.6	43.6	43.6	43.6	43.6
CHL	38.6	38.6	38.6	38.6	38.6
DCP	-	-	-	-	-
BS1c	-	1.0 x 10 ⁻³	-	-	-
BS4a	-	-	1.0 x 10 ⁻³	-	-
BS4b	-	-	-	6.0 x 10 ⁻³	-
BS2	-	-	-	-	6.0 x 10 ⁻³

BSs^{***} equals a six-fold BSs concentration of unmarked.

6.3.4 Scanning electron microscopy (SEM)

Surface morphology of the composite lyophilised wafers with BSs based niosomes including DCP was analysed as described in chapter 5, section 5.3.2. The formulations analysed are summarised in Table 6.3.

Table 6.3. Lyophilised composite wafers with BSs based niosomes wafers prepared from 2% w/w total polymer gels, used to analyse surface morphology

CARR:SA:BSs-NIO-DCP					CARR:SA:BSs-NIO				
BLK	BS1c	-	BS4a	BS4b	BLK	BS1c	-	BS4a	BS4b
-	BS1c***	BS2***	-	-	-	BS1c***	BS2***	-	-

BSs*** equals a six-fold BSs concentration of unmarked.

6.3.5 X-Ray diffraction

X-ray diffraction characterisation of the prepared wafers were performed as described in chapter 5, section 5.3.3

6.3.6 Attenuated total reflectance Fourier transform infrared spectroscopy (ATR-FTIR)

ATR-FTIR characterisation of the prepared wafers were performed as described in chapter 5, section 5.3.4

6.3.7 Mechanical strength ('hardness')

The mechanical properties (resistance to deformation and ease of recovery) of the prepared wafers were performed as described in chapter 5, section 5.3.5

6.3.8 Swelling studies

Swelling studies of the prepared wafers were performed as described in chapter 5, section 5.3.6

6.3.9 Porosity measurements

Porosity of the prepared wafers were performed as described in chapter 5, section 5.3.7

6.3.10 Water absorption (A_w), equilibrium water content (EWC), water reabsorption (ReA_w), reversibility of equilibrium water content (ReEWC) and stability of water absorption

Water absorption, equilibrium water content, water reabsorption and reversibility of equilibrium water content of the prepared wafers were performed as described in chapter 5, section 5.3.8. Additionally, the stability of selected wafers were investigated by repeating the water absorption experiments at 0 and 1 month after formulation time.

6.3.11 Evaporative water loss

Evaporative water loss of the prepared wafers were performed as described in chapter 5, section 5.3.9

6.3.12 Water vapour transmission rate

Water vapour transmission rate of the prepared wafers were performed as described in chapter 5, section 5.3.10.

6.3.13 Statistical analysis of data

Data analysis was carried out with the software package Microsoft Excel version 2007. Results were expressed as a mean \pm standard deviation (S.D). ($n = 3$). Statistically significant difference was determined using one-way analysis of variance (ANOVA,) for the significant interrelation between the various groups with $p < 0.05$ considered as a minimal level of significance. The groups compared were the selected optimised 2%(1:2)CARR:SA composite wafers with BSs based niosomes including DCP (CARR:SA:BLK/BSs-NIO-DCP), 2%(1:2)CARR:SA composite wafers with BSs based niosomes without DCP (CARR:SA:BLK/BSs-NIO) and the reference 2%(1:2)CARR:SA composite wafers with free BSs, CARR:SA:BLK/BSs.

6.4 Results & discussion

6.4.1 Formulation of composite wafers dressings loaded with BSs based niosomes

In this investigation both CARR and SA were individually but consecutively dissolved in the same solvent. Lyophilised wafers were produced by freeze-drying polymer gels to yield solid porous structures whose physical architecture resembles those of foam dressings which are made from porous polyurethane (Pawar *et al.*, 2014). The objective of this chapter was to develop a composite dressing formulation containing BSs based niosomes with and without DCP and to evaluate their physico-chemical properties. Six niosomal dispersions with biosurfactant (BS1c, BS2, BS4a and BS4b) concentrations ranging from 80 – 600 $\mu\text{g/ml}$ were formulated. The selection of which niosomes to load into composite polymer gels was based on morphological examination by SEM. The optimum niosome concentration observed when visualised by SEM for BS1c, BS4a and BS4b was 100 $\mu\text{g/ml}$. Although spherical vesicles were observed at BS2's critical micelle concentration (CMC), the distribution at the highest loading of 600 $\mu\text{g/ml}$ was more pronounced. However, 600 $\mu\text{g/ml}$ of BS1c*** loaded niosomes was formulated into CARR:SA:BSs-NIO-DCP wafers, in order to match and compare with the optimised BS2**** loaded wafers. Differences observed between the CARR:SA:BSs-NIO-DCP formulations are due to BSs type, concentrations and variation in process parameters. The similarities or lack thereof between CARR:SA:BSs-NIO-DCP, CARR:SA:BSs-NIO and reference composite CARR:SA wafers will be briefly reported. The physico-chemical and bioanalytical characteristics of the various composite wafers were investigated. These included (i) wafers with blank niosomes (no BSs) incorporating DCP (CARR:SA:BLK-DCP), (ii) composite wafers with blank (no BSs) niosomes only (CARR:SA:BLK) as controls (no DCP), (iii) composite

wafers with BSs based niosomes including DCP (CARR:SA:BSs-NIO-DCP) and (iv) composite wafers loaded with BSs based niosomes only (CARR:SA:BSs-NIO) with no DCP.

6.4.2 Scanning electron microscopy (SEM)

Among, the twelve wafers selected for morphological examination, traces of the optimised “egg pocket box” configuration from the composition of 2% CARR:SA (1:2) were observable in only four (Fig’s 6.1 and 6.2). These are BS1c and BS2 CARR:SA:BSs-NIO-DCP, BS4a and BS4b and CARR:SA:BSs-NIO and CARR:SA:BS2. The incorporation of BSs based niosomes was observed to have transformed the other group of composite wafers into a new morphology with less evenly distributed but wider pores. Two extreme patterns were observable in both groups; these were pronounced definitions of the egg pores in CARR:SA:BS1c-NIO-DCP and the rigid matrix of CARR:SA:BS2-NIO wafers. The egg pocket pores were observed to have flattened out into dimensionless sheets in other compositions. Additionally, the niosomes were not visible on the wafer surface or pore walls which suggests that they were fully incorporated within the interior of the wafer matrix.

This visual evidence was compared with size of the pores Table 6.4. There were five pairs of wafers loaded with an even division of CARR:SA:BSs-NIO-DCP and CARR:SA:BSs-NIO wafers. However, due to the distribution of pores within the matrix, an average of a minimum number of four pores was evaluated while the maximum was eleven. For some wafers, there were different parallel sets, for this reason selecting a set would not have given a true representation of the variations of individual networks. It is possible that the incorporation of drugs (BSs) and niosomes reduced the distribution of pores in the “egg pocket box” matrix, which resulted in a higher distribution of pores in CARR:SA:BSs-NIO-DCP than in CARR:SA:BSs-NIO’s.

With the exception of BS1c, the estimated pore sizes of all other CARR:SA:BSs-NIO-DCP loaded wafers were larger than CARR:SA:BSs-NIO loaded wafers. The mean size of pores (including BLK and BSs) (Table 6.4) for the following groups analysed: CARR:SA:BLK/BSs-NIO-DCP, BSs CARR:SA:BLK/BSs-NIO, CARR:SA:BLK/BSs were 158.00 (± 49.58) - 212.83 (± 50.64) μm , 146.26 (± 62.74) - 192.25 (± 62.89) μm and 93.35 (± 57.14) - 207.83 (± 90.37) μm respectively. The lowest mean size followed an order of CARR:SA: BLK/BSs < CARR:SA:BLK/BSs-NIO < CARR:SA:BLK/BSs-NIO-DCP. However, the difference in the pore sizes of CARR:SA:BLK/BSs-NIO-DCP, CARR:SA:BLK/BSs-NIO and CARR:SA:BLK/BSs wafers was not statistically significant ($p > 0.05$). The differences observed in the pore size morphologies of the CARR:SA:BSs-NIO-DCP and CARR:SA:BSs-NIO wafers can affect functional properties such as rate of hydration, swelling, adhesion and consequent drug release characteristics in the presence of wound exudate. Wafers with high porosity can absorb high exudate because of higher rate of water ingress which leads to higher swelling and subsequent diffusion of drug from the swollen matrix (Boateng *et al.*, 2008). Highly exuding chronic wounds such as diabetic foot and venous ulcers limit the application of

less porous dressings such as those observed in CARR:SA:BSs-NIO and CARR:SA:BS2 wafers due to the high amount of exudate which causes maceration of surrounding healthy skin resulting from the collection of excess exudate beneath the dressing. Furthermore, BS1c-CARR:SA:BS1c-NIO-DCP wafers (Fig 6.1) may offer a better drug delivery dressing because of their more porous nature compared with BS1c-CARR:SA:BSs-NIO wafer (Fig 6.2), and can therefore absorb high exudate volumes as well as keep the wound environment moist for rapid healing. However, excessive hydration may cause wafer wetting and formation of slippery mucilage which can decrease the adhesion properties at the wound site (Matthews *et al.*, 2005; Matthews *et al.*, 2006), therefore require more frequent dressing changes.

Table 6.4. Comparison of the mean pore sizes (\pm SD) of wafers CARR:SA:BSs-NIO-DCP, CARR:SA:BSs-NIO and CARR:SA:BSs

Formulations	BLK	BS1c	BS4a	BS4b	BS1c***	BS2	BS2***
	(μm)						
CARR:SA:BSs-NIO-DCP	158.00 (± 49.58)	212.83 (± 50.64)	196.83 (± 50.35)	178.20 (± 28.31)	174.43 (± 47.63)	-	165.53 (± 67.45)
CARR:SA:BSs-NIO	192.25 (± 62.89)	147.58 (± 42.77)	179.71 (± 45.19)	146.26 (± 62.74)	-	-	154.26 (± 91.38)
CARR:SA:BSs	93.35 (± 57.14)	194.00 (± 56.94)	132.21 (± 67.77)	-	-	207.83 (± 90.37)	-

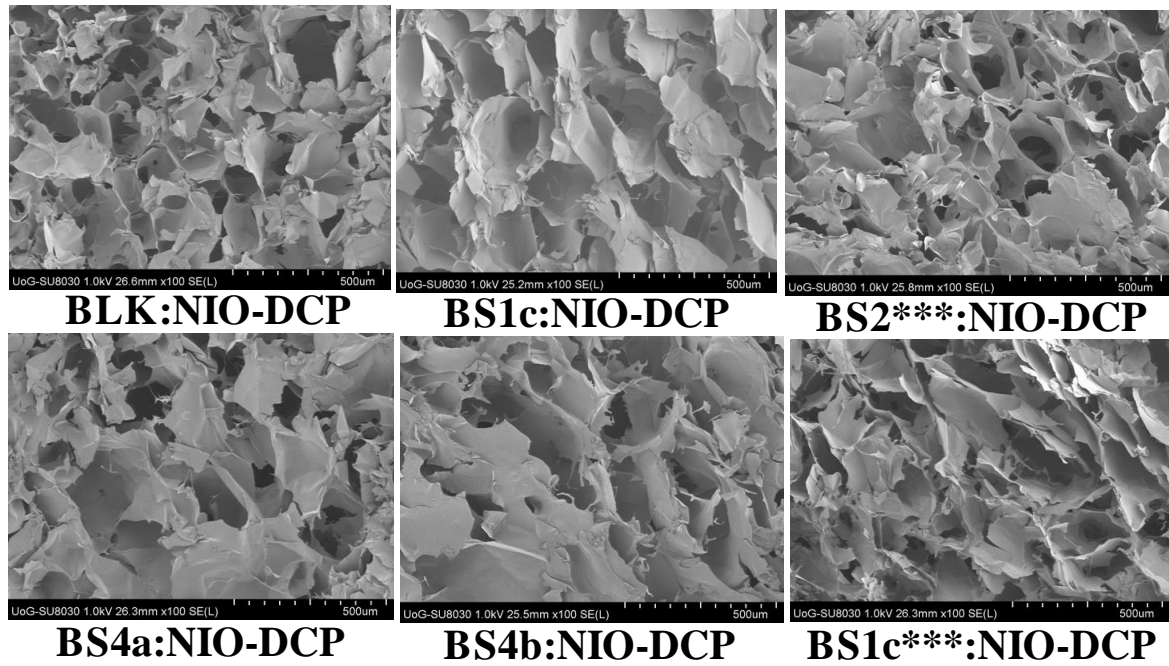


Figure 6.1. Comparison of BLK and CARR:SA:BSs-NIO-DCP wafers. Unmarked and BS*** equals 100 and 600 $\mu\text{g/ml}$ BSs loaded in niosomes.

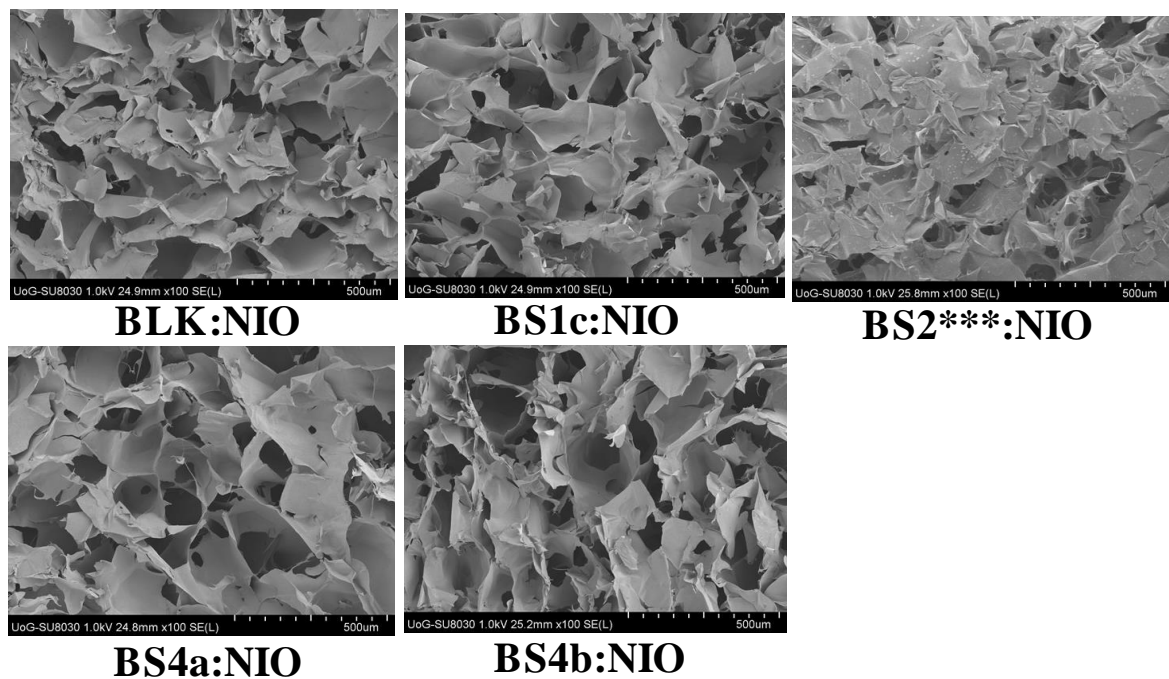


Figure 6.2. Comparison of BLK and CARR:SA:BSs-NIO. Unmarked and BS*** equals 100 and 600 $\mu\text{g/ml}$ BSs loaded in niosomes. Several SEM images were taken of each sample, and all discernible pores on each image were measured and averaged.

6.5.3 Mechanical strength ('hardness')

The human skin which is the largest organ in the body is a barrier that protects the body from environmental factors. The dermis layer in particular, protects the body from external physical force and as it has to be stretched to adapt to the movement of body parts, viscoelasticity is a critical property of the dermis (Nemoto *et al.*, 2012). The mechanical properties of polymers can be used to mimic the viscoelasticity of the skin as well as being formulated into solid supports for wound dressings, however in these investigations, the functionalities of primary importance are the latter characteristics. Ideal mechanical properties of wound dressings include flexibility, durability, pliability, elasticity and resistance to stresses exerted by different parts of the body, particularly around the elbows and knees. Wound dressings should withstand some frictional stresses during day-to-day activities when applied on the wound so that if there are any accidental frictional stresses, the dressing will absorb the energy without breaking and will thus provide its protective effect over the wound.

In this investigation, two general trends were observed; firstly, the mechanical hardness of CARR:SA:BSs-NIO-DCP wafers were higher than both CARR:SA:BSs-NIO and reference CARR:SA:BSs wafers (Table 6.5), following the order of CARR:SA:BSs-NIO-DCP > CARR:SA:BSs > CARR:SA:BSs-NIO > CARR:SA:BSs. Secondly, the mean mechanical strength of measured points on a single CARR:SA:BS2***-NIO-DCP was measured as 10.06 (± 1.7)N (which is too high). Overall, however, the mean hardness of four CARR:SA:BS1c:NIO-DCP wafers was 9.55 (± 0.40)N which is higher than the mean hardness of four CARR:SA:BS2***:NIO-DCP measured as 8.80 (± 1.09)N. A wound dressing that is too hard can cause contact irritation and consequently reduce patient compliance; on the other hand a wound dressing that is too soft will not hold up to the rigours of an active lifestyle. Furthermore, the mechanical strength of BS1c was observed to be consistently higher than BS2 in all groups of 1460 isome loaded formulations. However, local group trends between BSs were also observed; firstly there was a negligible difference of 0.03N between the mechanical strength of CARR:SA:BS4a and CARR:SA:BS4b, both of which are higher than CARR:SA:BS1c:NIO-DCP which was also > CARR:SA:BLK:NIO-DCP. However an entirely different trend was observed in parallel concentrations of CARR:SA:BSs:NIO; CARR:SA:BS4b > CARR:SA:BLK:NIO > CARR:SA:BS1c > CARR:SA:BS4a. Lastly, CARR:SA:BS4a:NIO showed the lowest mechanical strength 3.52 (± 0.27)N. The difference in the mechanical strength of CARR:SA:BLK/BSs-NIO-DCP, CARR:SA:BLK/BSs-NIO and CARR:SA:BLK/BSs wafers was statistically significant ($p < 0.05$).

Table 6.5. Reproducibility in ‘hardness’ of selected optimised niosome loaded freeze dried wafers compressed at five different locations to a depth of 1 mm at a speed of 0.20 mm/s, using 6 mm diameter stainless steel probe (standard deviations given in parenthesis). The ‘hardness’ is peak resistance force of the wafers to deformation and corresponds to the maximum force attained in the Texture Analyser plot

CARR:SA:BSs-NIO- DCP (N)	BLK	BS1c	BS4a	BS4b	BS1c** *	BS2	BS2***
1	4.67 (±0.7)	7.31 (±1.1)	8.12 (±1.2)	7.21 (±0.3)	9.48 (±1.0)	-	10.06 (±1.7)
2	4.80 (±0.4)	6.80 (±1.8)	-	-	9.89 (±0.7)	-	7.46 (±2.8)
3	4.34 (±0.8)	5.62 (±0.7)	-	-	9.82 (±0.7)	-	9.15 (±1.0)
4	4.77 (±1.1)	5.95 (±2.1)	6.35 (±1.1)	-	9.01 (±1.7)	-	8.51 (±2.8)
CARR:SA:BSs-NIO (N)							
1	4.61 (±0.7)	4.28 (±1.3)	3.19 (±0.6)	4.75 (±0.7)	5.18 (±0.8)	-	4.68 (±0.8)
2	4.88 (±0.7)	4.62 (±0.5)	3.5 (±0.4)	4.72 (±1.3)	6.79 (±1.4)	-	4.53 (±1.9)
3	4.88 (±0.3)	3.57 (±0.9)	3.52 (±1.0)	4.9 (±1.0)	6.28 (±0.7)	-	4.88 (±0.8)
4	4.52 (±0.3)	4.97 (±0.8)	3.85 (±0.4)	4.73 (±0.9)	5.57 (±1.2)	-	4.47 (±1.1)
CARR:SA:BSs (N)							
1	4.77 (±0.3)	5.01 (±0.6)	5.46 (±0.5)	-	-	4.53 (±1.0)	-
2	4.26 (±0.5)	5.38 (±0.7)	5.72 (±0.8)	-	-	4.31 (±0.8)	-
3	4.82 (±0.5)	5.56 (±0.7)	5.60 (±0.7)	-	-	4.66 (±0.8)	-
4	4.79 (±0.5)	5.71 (±0.7)	5.29 (±0.3)	-	-	4.04 (±0.8)	-

With the exception of BS4 and BS4b CARR:SA:BSs-NIO-DCP wafers, reproducibility in ‘hardness’ was $n = 4$

The resistance to compression of CARR:SA:BSs-NIO-DCP wafers may also be due to the electrostatic interaction of the charge inducer with the excipients. This is the first distinct observation attributable to the effect of DCP on the component systems. The textures of CARR:SA:BSs-NIO-DCP wafers were also observed to be stiffer than CARR:SA:BSs-NIO and CARR:SA:BSs. The charge inducer DCP is a crystalline anionic surfactant and although the relative amount incorporated into niosomes is the lowest fraction of the entire composition Table 6.2, it appears to have contributed to the stiffness of the wafer network. Consequently, there may be less entropic mobility of its internal chains.

6.4.4 X-ray diffraction (XRD)

XRD is a primary technique for determining the degree of crystallinity in pharmaceutical materials such as drugs, polymers and formulations combining the two. Polymer molecules are often partially crystalline (semi-crystalline) with crystalline regions dispersed within amorphous material. Crystalline polymers are denser than amorphous polymers so the degree of crystallinity can be obtained from the measurement of density. In this chapter XRD was used to determine the crystalline or amorphous properties of all BLK and CARR:SA:BSs-NIO-DCP/CARR:SA:BSs-NIO wafers.

The XRD diffractograms of pure CARR, SA and formulated BLK and BSs CARR-SA has already been discussed in chapter 5, section 5.4.3 as predominantly amorphous but with the observation that the composition of both CARR and SA into wafers shifted the crystalline impurity from 2-theta of 28.5° to 22.7 and selectively appeared in three out of eight CARR:SA:BSs wafers. This same pattern differed only in CARR:SA:BSs-NIO-DCP and CARR:SA:BSs-NIO wafers where the crystalline impurity although absent in BLK was observed in both CARR:SA:BSs-NIO-DCP and CARR:SA:BSs-NIO wafers.

Table 6.6. Composition of crystalline and amorphous phases of CARR:SA:BSs-NIO-DCP, CARR:SA:BSs-NIO and CARR:SA:BSs lyophilised wafers

CARR:SA:BSs-NIO-DCP (%)	BLK	BS1c	BS4a	BS4b	BS1c***	BS2	BS2***
Crystal phase	17.98	21.25	17.51	31.62	16	-	20.09
Amorphous phase	82.02	78.75	82.49	68.38	84	-	79.91
<hr/>							
CARR:SA:BSs-NIO (%)							
Crystal phase	16.19	18.57	24.35	51.08	-	-	24.21
Amorphous phase	83.81	81.43	75.65	48.92	-	-	75.79
<hr/>							
CARR:SA:BSs (%)							
Crystal phase	19.24	20.64	19.97	-	-	21.56	-
Amorphous phase	80.76	79.36	80.03	-	-	78.44	-

As already established in chapter 4, crystal phase of > 70% will be described as fully crystalline while phases below 30% will be considered amorphous based on a technical criteria employed in our laboratories. In the combination of fully crystalline niosomes and amorphous composite CARR:SA polymers, (and with the exception of BS4b-CARR:SA:BSs-NIO wafers which was semi-crystalline), all other CARR:SA:BSs-NIO-DCP/CARR:SA:BSs-NIO wafers were fully amorphous Table 6.6. The crystalline properties of polymeric formulations affect various characteristics such as water uptake, bioadhesion and biodegradability of the polymers. Amorphous structures may help to improve the performance of dressings such as exudate absorption, prolonged retention at wound site which can ultimately increase the bioavailability of the drug and reduce the need for frequent changes

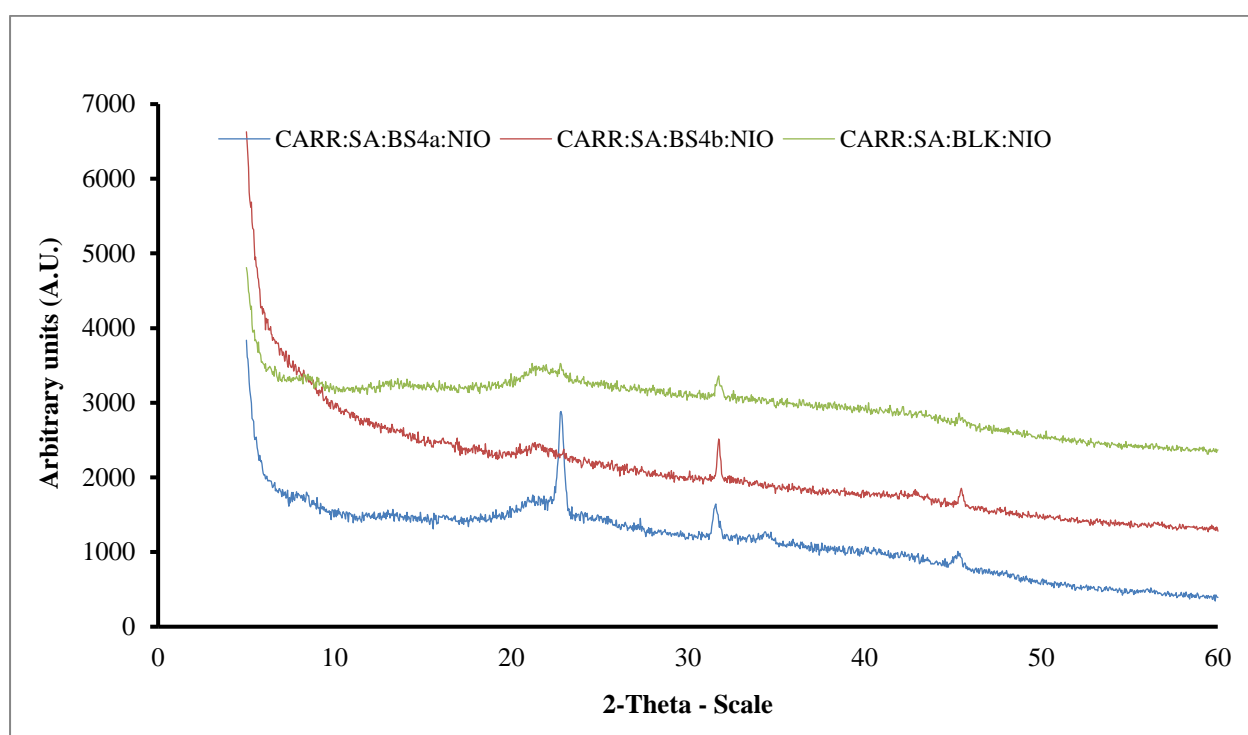


Figure 6.3. Representative XRD diffractograms of CARR:SA (1:2) wafers obtained from 2% w/w total polymer gels loaded with BLK niosomes (CARR:SA:BLK/BSs-NIO).

6.4.5 Attenuated total reflectance Fourier transform infrared spectroscopy (ATR-FTIR)

Attenuated Fourier transform infrared spectroscopy (ATR-FTIR) was used to analyse the bonding between the polymer matrix and niosomes. ATR-FTIR characterisation showed limited interaction between pre-formed niosomes and the polymer matrix. Consequently, the higher mechanical strength observed in both CARR:SA:BSs-NIO-DCP and CARR:SA:BSs-NIO wafers appears to be independent of the weak interaction between the niosome systems and polymer matrix. Although, BSs-NIO-DCP and BSs-NIO niosomes were dispersed into the polymer network, in this particular system, the electrostatic attractions and the secondary Van der Waals bonding between the

ionised anionic sulphate groups of CARR and the ionised carboxyl acid groups (COO^-) of SA are the predominant interactions leading to the formation of CARR:SA:BSs-NIO-DCP and CARR:SA:BSs-NIO wafer dressings.

The ATR-FTIR spectra of pure CARR and SA wafers possess both common and specific absorption bands. The common bands are: at $1035\text{--}1084\text{ cm}^{-1}$ of the C O C (cyclic ether) stretching vibration, the band at $2928\text{--}2932\text{ cm}^{-1}$ of C H stretching, and a broad band due to the hydrogen bound OH group appeared between 3200 and 3400 cm^{-1} attributed to the complex vibrational stretching, associated with free, inter and intra molecular bound hydroxyl groups. CARR spectrum is characterised by a band at 1225 cm^{-1} due to the S O of sulphate stretch. The SA spectrum on the other hand is characterised by two specific strong absorption bands at 1600 cm^{-1} and 1407 cm^{-1} attributed to asymmetric and symmetric stretching vibrations of COO^- groups on the polymeric backbone (Pascalau *et al.*, 2011).

In this research, 2%(1:2) CARR:SA wafer was formed due to the physical interaction of CARR:SA molecular chains which resulted in seven functional groups including OH stretch. The incorporation of niosomes in CARR:SA:BSs:NIO-DCP was observed to have masked galactose-4-sulphate of CARR resulting in the appearance of six functional groups. However the pattern of seven functional groups continued in CARR:SA:BSs:NIO wafers. The transmittances of all concentrations of BSs loaded niosomes without DCP (CARR:SA:BSs:NIO) had a $0\text{--}3\text{ cm}^{-1}$ range increment than corresponding concentrations of BSs loaded niosomes incorporated with DCP (CARR:SA:BSs:NIO-DCP) however there was a 52 cm^{-1} increase in the OH-stretch.

There were no differences in the wavenumbers of the six recurring functional groups Table 6.7, therefore detailed analysis was carried out on only the OH group. The appearance of the COO^- bands at 1600 cm^{-1} , 1412 cm^{-1} , and of S-O band at 1254 cm^{-1} in the FTIR spectra of CARR:SA composite wafers confirms the miscibility of the composite formulation (chapter 5, section 5.4.4).

The characteristic absorption bands in the spectra of CARR:SA:BLK-NIO-DCP / CARR:SA:BLK-NIO / CARR:SA:BLK composite wafers showed shifts at wavenumbers 1599 , 1602 and 1600 cm^{-1} . BS4b and BS2*** loaded niosomes were not formulated thus comparison exists only between CARR:SA:NIO-DCP and CARR:SA:NIO with peaks at 1599 , 1600 , 1411 , 411 cm^{-1} and 1252 , 1252 cm^{-1} for carboxylate and sulphate groups respectively. However the wavenumber shift observed across the three specific functional group of interest described above was only 1 cm^{-1} which is negligible.

Table 6.7. Assignment of various functional groups present in CARR:SA:BSs-NIO-DCP, CARR:SA:BSs-NIO and CARR:SA:BSs lyophilised wafers based on possible intermolecular interactions as analysed by ATR-FTIR analysis

Functional groups	BLK	BS1c	BS4a	BS4b	BS1c***	BS2	BS2***
CARR:SA:BSs-NIO-DCP							
(cm ⁻¹)							
O-H stretching	3284	3288	3288	3279	3302	-	3268
Asymmetric -COO-stretching	1599	1602	1599	1599	1599	-	1598
C-OH deformation vibration	1411	1412	1411	1411	1411	-	1410
symmetric							
Sulphate ester	1252	1252	1252	1252	1252	-	1251
C-C stretching	1027	1029	1027	1027	1027	-	1027
3, 6 anhydrogalactose residue	930	931	930	930	930	-	929
Galactose-4-sulphate	-	-	846	846	846	-	
CARR:SA:BSs-NIO (cm⁻¹)							
O-H stretching	3336	3341	3287	3278	-	-	3294
Asymmetric -COO-stretching	1602	1601	1599	1600	-	-	1599
C-OH deformation vibration	1411	1411	1410	1411	-	-	1411
symmetric							
Sulphate ester	1252	1252	1252	1252	-	-	1252
C-C stretching	1028	1027	1027	1027	-	-	1027
3, 6 anhydrogalactose residue	931	931	930	931	-	-	930
Galactose-4-sulphate	846	846	-	-	-	-	-
CARR:SA:BSs (cm⁻¹)							
O-H stretching	3340	3279	3286	-	-	3288	
Asymmetric -COO-stretching	1600	1598	1598	-	-	1599	
C-OH deformation vibration	1412	1411	1411	-	-	1411	
symmetric							
Sulphate ester	1254	1251	1251	-	-	1252	
C-C stretching	1029	1027	1027	-	-	1027	
3, 6 anhydrogalactose residue	930	929	929	-	-	930	
Galactose-4-sulphate	846	846	846	-	-	846	

Additionally, with the exception of OH stretch in CARR:SA:BS1c-NIO, which was one wavenumber higher than the reference BLK composite wafers, all other CARR:SA:BSs-NIO-DCP and CARR:SA:BSs-NIO wafers had lower transmittances. Additionally, the interaction of BSs with their respective composite polymer matrix as observed from their wavenumbers are weak. This may be due to the fact that while free BSs were added during the thermal mixing of composite gels in chapter 5, niosomes were added in solid lyophilised clusters and niosomal dispersions for CARR:SA:BSs-NIO-DCP and CARR:SA:BSs-NIO wafers respectively. The surfaces of these preformed particles are far less reactive and provide less energetic drive for bonding with composite polymer gels.

6.4.6 Fluid handling properties

6.4.6.1 Swelling

The degree of swelling of the dressing material determined through this investigation was calculated using percentage swelling index I_s (%) Eq. (5.1) (Boateng *et al.*, 2008). There are several parameters affecting the swelling ratio including hydrophilicity, stiffness and pore structure of a matrix (Archana *et al.*, 2013). The driving force for the absorption of fluid or swelling process is generally a balance of three forces; osmotic, electrostatic and entropy-favoured dissolution of polymer in water. The control of drug release often involves a series of interrelated events such as polymer surface wetting, hydration, hydrogel formation and erosion/dissolution/degradation. When a solid is immersed in a liquid the initial wetting process is referred to as immersional wetting. However, the type of wetting that occurs when a liquid spreads over a solid surface is referred to as spreading wetting. Wettability may be improved by the inclusion of surfactants (Florence and Atwood, 2011). In this investigation the wetting process was observed to occur within the first five min and this stage involves the introduction of the polymer into the simulated wound fluid.

Figs 6.4-6.6 shows the change in swelling capacity (%) of the wafers with time. CARR:SA:BLK wafers showed maximum swelling capacity 2975 (± 94)% which decreased in the CARR:SA:BLK-NIO-DCP wafers 1966 (± 45)% (Fig 6.4) and even more so in CARR:SA:BLK-NIO 1397 (± 75)% (Fig 6.5). This difference was also observed between the CARR:SA:BLK-NIO-DCP and CARR:SA:BLK-NIO wafers although the differences occurred during the first 5 and 75 min respectively. The CARR:SA:BSs wafer showed maximum swelling capacity for BS1c and BS4a of 3376 (± 431)% and 3934 (± 305)% respectively which were dramatically reduced in CARR:SA:BSs-NIO-DCP at swelling indexes of 1506 (± 94)% and 1792 (± 155)%. The differences observed may be due to the incorporation of niosomal vesicles. However, the pattern was partly reversed between CARR:SA:BSs-NIO-DCP and CARR:SA:BSs-NIO with the maximum swelling index for CARR:SA:BS1c-NIO observed to be higher than CARR:SA:BS1c-NIO-DCP. However the swelling index for CARR:SA:BS4a-NIO was lower than CARR:SA:BS4a-NIO-DCP. The difference in the

wetting and maximum hydration of CARR:SA:BLK/BSs-NIO-DCP, CARR:SA:BLK/BSs-NIO and CARR:SA:BLK/BSs wafers was statistically significant ($p < 0.05$), however their degradative difference after 4 hr was not statistically significant ($p > 0.05$).

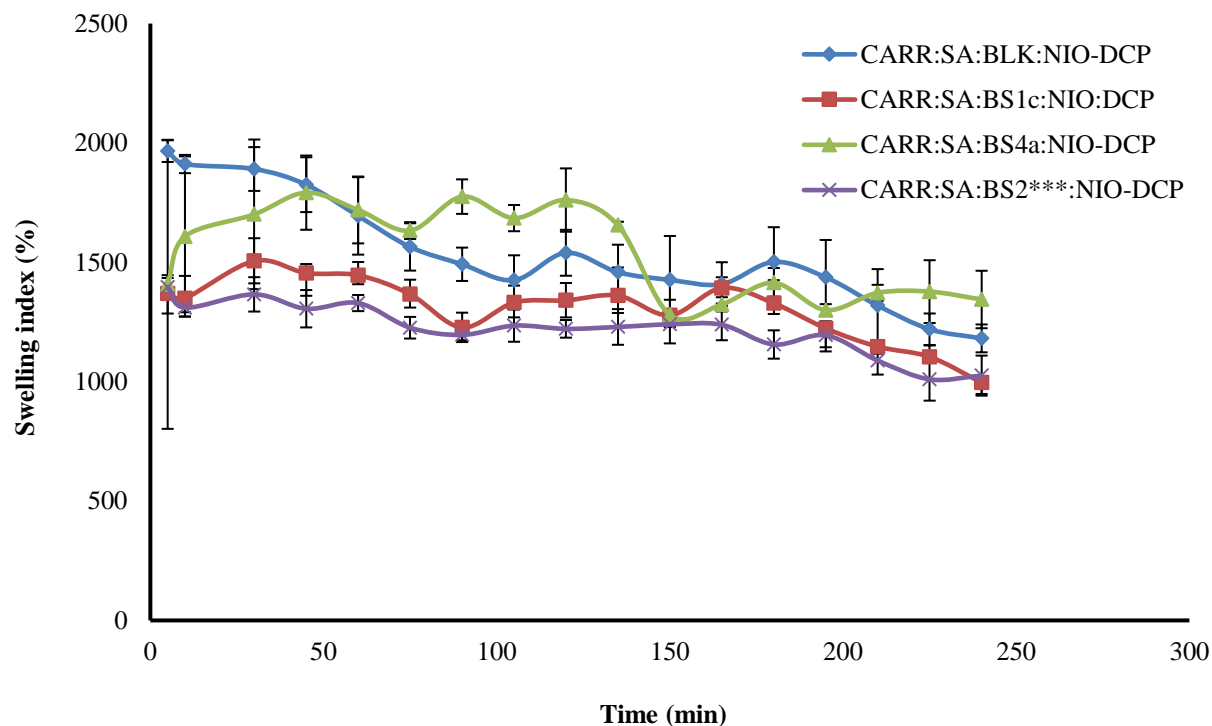


Figure 6.4. Swelling index of CARR:SA:BLK-NIO-DCP, CARR:SA:BS1c-NIO-DCP, CARR:SA:BS4a-NIO-DCP and CARR:SA:BS BS2*-NIO-DCP wafers. Unmarked and BS*** equals 100 and 600 $\mu\text{g/ml}$ BSs loaded in niosomes.**

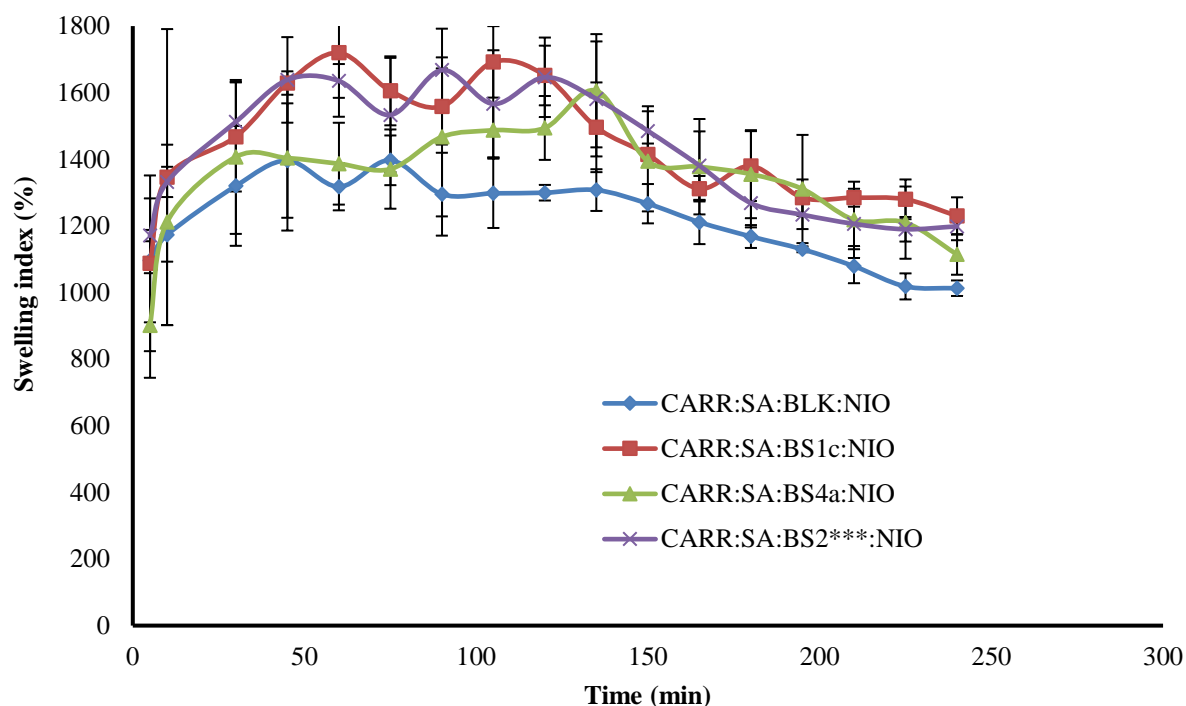


Figure 6.5 Swelling index of CARR:SA:BLK-NIO, CARR:SA:BS1c-NIO, CARR:SA:BS4a-NIO and CARR:SA: BS2*-NIO wafers. Unmarked and BS*** equals 100 and 600 μ g/ml BSs loaded in niosomes.**

Incidentally, a six-fold increase in CARR:SA:BS1c*** (Fig 6.6) concentration resulted in a pronounced reduction 1458 (118)% as well as longer duration of 165 min, which was 45 min more in comparison to CARR:SA:BS1c.

The swelling values of CARR:SA:BS4a-NIO-DCP at 100 and 200 μ g/ml were higher than CARR:SA:BS4b:NIO-DCP (data not shown). It was observed that higher concentration in both individual BSs resulted in faster attainment of maximum swelling capacity at 5 and 15 min respectively. Overall with the exception of BS2, the maximum swelling rate of CARR:SA:BSs (free BSs) wafers was observed to be higher than both CARR:SA:BSs:NIO-DCP and CARR:SA:BSs:NIO. An obvious departure from the maximum swelling capacity of the same series of BSs was observed in CARR:SA:BS2 with its highest capacity of 1706 (\pm 112)% (Fig 6.6). The swelling may be lower due to the presence of its characteristic amino acids. A higher concentration of BS2*** incorporated in niosome loaded wafers resulted in lower maximum swelling rates in comparison to CARR:SA:BSs. However the swelling index of CARR:SA:BSs:NIO 1669 (\pm 124)% was higher than CARR:SA:BSs:NIO-DCP 1396 (\pm 38)% at duration times of 90 and 5 min respectively.

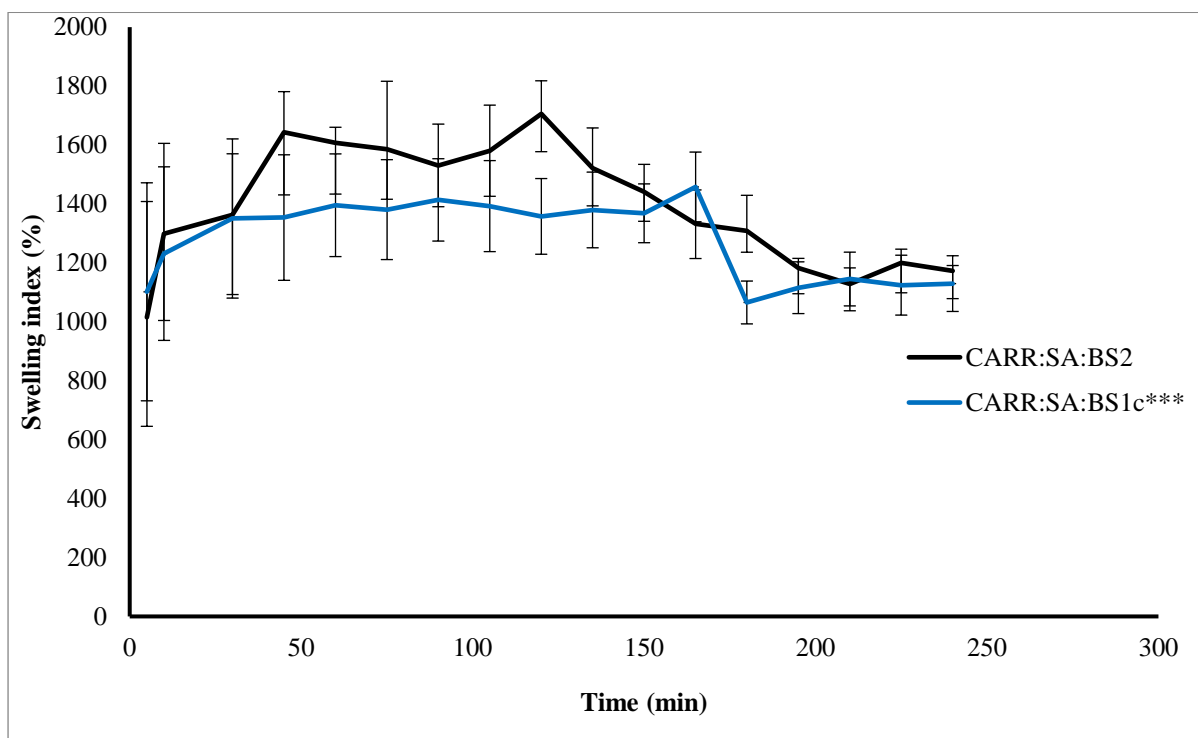


Figure 6.6. Swelling index of CARR:SA:BS2 and CARR:SA:BS1c* wafers. Unmarked and BS*** equals 100 and 600 µg/ml BSs loaded in niosomes.**

One critical difference between the current study and the referenced study in chapter 5, section 5.3.6 could account for the differences in the results. BSs have the ability to spontaneously self-assemble in water, a phenomenon that was observed with BS1c in chapter 4, section 4.6.3.3. Both BS1c and BS4a are soluble in water and belong to the same glycolipid family. They also have bulky sugar head groups. Although not investigated by SEM it is possible that the same vesicular self-assembly observed in BS1c may have occurred in BS4a. BS2 on the other hand is a cyclic lipopeptide with limited solubility in water, a characteristic which may hinder spontaneous self-assembly and which may have reduced swelling. However, the self-assembly of both BS4a and BS2 will require further study.

6.4.6.2 Pore analysis

The results of the pore analysis of niosome loaded wafers are summarised in Table 6.8. The changes in the surface structure and reduced porosity of CARR:SA:BSs-NIO wafers could be attributed to the lack of DCP in the niosomal composition. This effect was observed in all BLK and DL matrix. However, as previously observed, BS4a/b followed a reverse trend with an increased porosity > 50% for CARR:SA:BSs-NIO wafers while in CARR:SA:BSs-NIO-DCP wafers both BS4a/b niosomal formulated matrix showed a reduced porosity < 50%. CARR:SA:BS2-NIO which had a six fold concentration loading in comparison to the other formulations also showed low porosity

< 50%. However even lower porosity < 40% was observed in a one fold loading of CARR:SA:BS2 in the egg box matrix. Conversely, a six fold loading of CARR:SA:BS1c-NIO also showed a reduced porosity of < 40% which indicates that the two highest concentrations of BSs and BS2 in particular are incompatible with the “egg pocket box matrix.

The results differed from those observed with the concentrations of the referenced CARR:SA:BS1c and CARR:SA:BS4a wafers loaded with just the pure BSs described in chapter 5. Previously both two fold and 1000 fold increments resulted in increased porosity ranging from 76 – 100%. However, similar porosities of about 67% were observed in both BLK “egg pocket box” and CARR:SA:BLK-NIO-DCP wafers. However it is not possible to conclusively establish that the reduced porosities observed in Table 6.8 is the result of interference within the niosomal loading of BSs, because the porosities observed in both pure and niosomal formulated BS1c wafers are relatively comparable with porosities of 76.91 and 73.91% respectively. The difference between the pore analysis of CARR:SA:BLK/BSs-NIO-DCP, CARR:SA:BLK/BSs-NIO and CARR:SA:BLK/BSs wafers was not statistically significant ($p > 0.05$).

Table 6.8. Comparison of the porosities of CARR:SA:BSs-NIO-DCP, CARR:SA:BSs-NIO and reference CARR:SA:BSs wafers

(%)	BLK	BS1c	BS4a	BS4b (2 ^{hH})	BS1c*	BS	BS2***
					**	2	
CARR:SA:BSs-NIO-DCP	67.52 (± 6.73)	73.91 (±20.32)	46.05 (±4.29)	61.15 (±5.93)	31.51 (±15.21)	-	-
CARR:SA:BSs-NIO	56.79 (±15.04)	63.74 (±9.75)	56.31 (±26.41)		-	-	41.24 (±5.28)
CARR:SA:BSs	67.79 (±15.10)	76.91 (±5.92)	72.48 (±3.55)		-	31.78 (±10.45)	

There was only a 2% difference between porosities of 100 and 200 µg/ml loading of CARR:SA:BS4a-NIO-DCP wafers (data not shown).

6.4.6.3 Water absorption (A_w), equilibrium water content (EWC), water reabsorption ($Re A_w$) and reversibility of equilibrium content (ReEWC)

The equilibrium water content (EWC) and water absorption (A_w) of wound dressing are important for quick absorption of exudates. Two reference systems CARR:SA:BSs (A) and CARR:SA:BSs (B) were investigated in this section. The difference between CARR:SA:BSs(A) and CARR:SA:BSs(B) was a matter of aging. Three wafers which include a BLK and two DL from CARR:SA:BSs(B) were analysed immediately after being formulated. While five wafers from different set were more

extensively investigated. The stability of wafers were studied after 0 and 1 month formulation time, although, the difference in the A_w of CARR:SA:BLK/BSs-NIO and CARR:SA:BLK/BSs (A and B) wafers was statistically significant ($p < 0.05$), for EWC ($p = 0.05$).

Nevertheless, there was a 300-500% and 3% decrease in the A_w and EWC respectively of reference system CARR:SA:BSs (B) to reference system CARR:SA:BSs (A). However, irrespective of the times of their investigations, the A_w /EWC of both reference systems in areas where they overlap were higher than CARR:SA:BSs-NIO wafers (Table 6.9). The obtained values for % water re-absorption are shown in Table 6.8. The water reabsorption of CARR:SA:BLK-NIO 1405 (± 237) > CARR:SA:BLK 1154 (± 511). However, the Re A_w of CARR:SA:BS1c 1452 (± 158) and CARR:SA:BS4a 1448 (± 219) were > CARR:SA:BS1c:NIO 1360 (± 593) and CARR:SA:BS4a:NIO 1387 (± 205)%. The calculated value was considered as an indicator of the reversibility of water absorption of the wafer through dehydration-rehydration cycle which were in agreement with initial moisture content. These results suggest that the optimised selected BSs loaded wafers prepared in this study may have high potential as new wound dressing materials, which provide and maintain the adequate moist environment required to prevent scab formation and dehydration of the wound bed.

Table 6.9. Comparison of the water absorption (A_w), equilibrium water content (EWC) and water reabsorption (Re A_w) of CARR:SA:BSs-NIO-DCP, CARR:SA:BSs-NIO and CARR:SA:BSs wafers

CARR:SA:BSs-NIO (%)	BLK	BS1c	BS4a	BS4b	BS1c***	BS2***	BS2
A_w	1393 (± 167)	2047 (± 342)	2143 (± 33)	1026 (± 159)	-	1496 (± 601)	-
EWC	93.25 (± 0.72)	95.26 (± 0.80)	95.54 (± 0.07)	91.01 (± 1.20)	-	93.18 (± 2.21)	-
Re A_w	1405 (± 237)	1360 (± 593)	1387 (± 205)	1251 (± 556)	-	1762 (± 276)	-
Re-EWC	93.24 (± 1.12)	93.11 (± 0.67)	93.18 (± 1.01)	92.56 (± 0.65)	-	94.55 (± 0.83)	-
EWL	16.49 (± 0.37)	15.73 (± 2.04)	14.77 (± 0.72)	19.26 (± 1.33)	-	17.04 (± 2.49)	-
CARR:SA:BSs(A)							
A_w	1592 (± 77)	2358 (± 102)	2459 (± 275)	-	1756 (± 251)	-	2024 (± 342)
EWC	94.08 (± 0.26)	96.60 (± 0.26)	96.64 (± 0.37)	-	94.55 (± 0.72)	-	95.20 (± 0.83)
Re A_w	1154 (± 511)	1452 (± 158)	1448 (± 219)	-	-	-	1434 (± 186)
Re-EWC	92.02 (± 0.24)	93.51 (± 0.67)	93.45 (± 0.93)	-	-	-	93.41 (± 0.83)
EWL	16.89 (± 1.15)	15.65 (± 0.62)	14.19 (± 0.28)	-	-	-	14.98 (± 0.75)
CARR:SA:BSs(B)							
A_w	2574 (± 590)	2855 (± 228)	2899 (± 343)	-	-	-	-
EWC	96.14 (± 0.84)	96.60 (± 0.26)	96.64 (± 0.37)	-	-	-	-
Re A_w	-	-	-	-	-	-	-
Re-EWC	-	-	-	-	-	-	-
EWL	-	-	-	-	-	-	-

The A_w and EWC of BLK and all investigated reference wafers are higher than CARR:SA:BSs-NIO.

6.4.6.4 Evaporative water loss (EWL)

The water loss from the BLK and CARR:SA:BLK-NIO and CARR:SA:BSs wafers at 37°C was evaluated to examine its behaviour when used as a dressing over a chronic wound. The difference in the EWL of CARR:SA:BLK/BSs-NIO-DCP, CARR:SA:BLK/BSs-NIO and CARR:SA:BLK/BSs wafers was not statistically significant ($p > 0.05$). However, as shown in Table 6.10, the loss of water for CARR:SA:BSs-NIO wafers ranged from 6-16% after 1 h and increased up to 30-59% within 6 h. After 24 h, the loss of water was about 69-79%. It is interesting to note that BS2*** which had the highest rate of water loss after the first hour, retained the highest amount of moisture after 24 h, which may be due to the type of BSs or its six fold concentration. On the other hand, CARR:SA:BS1c-NIO which had the initial lowest water loss at 6% retained the least amount of moisture after 24 h (in this case BS1c had the same amount of BSs loaded as CARR:SA:BS4a/b-NIO). However, for the reference wafers (BSs only wafers), water loss after 1 h ranged from 7-10%; 35-50% after 6 h, and 79-86% after 24 h. There was just a 1% difference between the water loss of six-fold concentration of BS1c*** and a one-fold BS2, which makes a clear case for BS2 having better moisture holding capacities. However, more importantly, CARR:SA:BSs-NIO dressings have better evaporative water loss potential in comparison to pure composite CARR:SA:BSs wafers. This implies both dressings will lose water content when exposed to air under dry conditions during short periods as a result of quick exudate uptake from the wound into the dressing by an active upward-directed process when used in early-stage exuding wounds (Kim *et al.*, 2007). These dressings may therefore be more beneficial to wounds with more exudates in early-stages of wound healing.

Table 6.10. Comparison of the Evaporative water loss (EWL) of CARR:SA:BSs-NIO-DCP, CARR:SA:BSs-NIO and CARR:SA:BSs wafers

CARR:SA:BSs-	1	2	3	4	5	6	24 h (%)
NIO							
BLK	91.06 (± 1.10)	84.06 (± 2.02)	72.72 (± 3.19)	69.10 (± 3.44)	63.43 (± 3.98)	57.74 (± 3.98)	16.46 (± 1.25)
BS1c	93.38 (± 0.81)	87.29 (± 1.37)	77.07 (± 2.20)	73.40 (± 2.57)	68.02 (± 3.09)	62.59 (± 3.53)	14.41 (± 1.02)
BS4a	93.01 (± 1.39)	84.49 (± 3.01)	73.10 (± 4.68)	67.84 (± 5.65)	61.33 (± 6.54)	55.85 (± 7.15)	15.90 (± 1.29)
BS4b	95.32 (± 1.40)	84.42 (± 3.03)	72.90 (± 4.94)	67.12 (± 5.86)	60.68 (± 6.84)	55.72 (± 7.51)	16.83 (± 2.26)
BS2	88.79 (± 0.44)	72.69 (± 0.66)	57.96 (± 1.02)	46.04 (± 0.80)	36.77 (± 0.72)	30.11 (± 0.67)	19.49 (± 0.58)
CARR:SA:BSs							
BLK	93.40 (± 0.37)	87.45 (± 0.69)	77.80 (± 1.41)	74.46 (± 1.61)	69.54 (± 1.88)	64.79 (± 1.91)	14.41 (± 0.67)
BS1c	90.56 (± 0.11)	80.90 (± 0.55)	71.63 (± 0.84)	63.67 (± 1.23)	56.75 (± 1.41)	50.50 (± 1.38)	15.65 (± 0.62)
BS4a	91.58 (± 0.63)	83.07 (± 0.79)	75.10 (± 0.78)	68.16 (± 1.02)	61.88 (± 1.26)	56.12 (± 1.42)	14.19 (± 0.28)
BS2	92.82 (± 1.61)	85.12 (± 3.33)	73.22 (± 6.05)	68.53 (± 7.07)	62.08 (± 8.22)	56.40 (± 8.95)	16.16 (± 1.40)
BS1c***	92.28 (± 1.67)	85.72 (± 2.52)	79.70 (± 3.40)	73.96 (± 4.20)	66.69 (± 6.03)	60.75 (± 6.80)	15.27 (± 0.69)

6.4.6.5 Water vapour transmission rate

According to (Dyson *et al.*, 1988), a moist environment enhances the healing process more effectively than a dry one. The control of evaporative water loss, following injuries, is of major importance to the overall condition of the patient; whether this control is naturally sloughed off by eschar or through a dressing. It is therefore important to evaluate the water vapour transmission rate of potential wound dressings. In this study *in vitro* technique was used to make comparisons between CARR:SA:BSs-NIO-DCP, CARR:SA:BSs-NIO and CARR:SA:BSs wafers as potential prototype materials, under controlled conditions.

As previously noted BS4a and BS4b are sophorolipids with different ratios of their acid and lactonic isomers. Although, the ratio of lactonic to acid is higher in both BSs, visual examination of the viscous mixtures suggests that BS4a is a more concentrated form. Analysis by UPLC-MS further confirms this observation. The formulation conditions of CARR:SA:BS4a/b-NIO-DCP whose WVTR are reported in Table 6.12 vary in terms of concentration 100 and 200 $\mu\text{g/ml}$ for BS4a and BS4a*-CARR:SA:BSs-NIO-DCP respectively.

The combinations of these variations resulted in a WVTR that followed the order BLK > BS4a > BS4b > BS4*** all of which fall within the ideal ($2000\text{--}2500 \text{ gm}^{-2} \text{ day}^{-1}$) (Queen *et al.*, 1987) Consequently a doubled concentration and hydration time of BSs resulted in lower WVTR, all of which are lower than CARR:SA:BLK-NIO-DCP. This suggests a synergistic effect of BSs and CARR:SA:BSs-NIO-DCP loaded wafers. The differences that exist between CARR:SA:BSs-NIO wafers are a combination of BSs type and concentration, with the exception of BS2*** which had six-times the concentration of the other BSs loaded niosomes. The trends observed from the WVTR of CARR:SA:BLK/BSs-NIO followed a descending order of BS2*** > BS4a > BS1c > BLK. As reported in Table 6.12, BS2*** had the highest WVTR which may be due to the effect of the type of BSs as well as concentration. Interestingly, the difference observed between all CARR:SA:BSs-NIO wafers including BLK was less than $150 \text{ g/m}^2 \text{ day}^{-1}$ which suggests that the lack of charge inducer (DCP) which may have allowed the domination of CHL as the driving force for the WVTR of CARR:SA:BLK/BSs:NIO wafers. All reported WVTR of CARR:SA:BSs-NIO ranged between 2978 (± 105) to 3139 (± 133) which is above the ideal ($2000\text{--}2500 \text{ gm}^{-2} \text{ day}^{-1}$) recommended by (Queen *et al.*, 1987)

The WVTR of BSs loaded in the reference study followed the order of BS2 > BS1c > BS4a > BLK > BS1c > BS1c***. Once again a six fold increase in concentration of BSs resulted in lower WVTR which suggests saturation kinetics. Therefore it may be reasonably deduced based on BSs type that the WVTR of BLK; CARR:SA:BSs-NIO > CARR:SA:BSs > CARR:SA:BSs-NIO-DCP, for BS1c; CARR:SA:BSs > CARR:SA:BSs-NIO and for BS4a; CARR:SA:BSs-NIO > CARR:SA:BSs > CARR:SA:BSs-NIO-DCP. The difference between the WVTR of CARR:SA:BLK/BSs-NIO-DCP, CARR:SA:BLK/BSs-NIO and CARR:SA:BLK/BSs wafers was statistically significant ($p < 0.05$).

Table 6.11. Comparison of the water vapour transmission rate (WVTR) of CARR:SA:BSs-NIO-DCP, CARR:SA:BSs-NIO and CARR:SA:BSs wafers

CARR:SA:BSs-NIO-DCP	1	2	3	4	5	6	24 h (g/m ² h ⁻¹)
BLK	124 (±4)	299 (±8)	419 (±7)	535 (±7)	-	-	2493 (±32)
BS4a	127 (±6)	302 (±12)	424 (±15)	538 (±18)	-	-	2432 (±54)
BS4b (2 h)H	117 (±1)	288 (±4)	407 (±5)	519 (±6)	-	-	2360 (±23)
BS4a**	122 (±3)	279 (±8)	393 (±12)	500 (±13)	-	-	2294 (±25)
CARR:SA:BSs-NIO							
BLK	84 (±5)	207 (±40)	338 (±70)	456 (±77)	577 (±78)	718 (±119)	2950 (±191)
BS1c	86 (±4)	236 (±68)	390 (±138)	534 (±187)	673 (±215)	790 (±212)	2978 (±105)
BS4a	94 (±7)	205 (±9)	323 (±9)	443 (±11)	569 (±13)	690 (±15)	2989 (±57)
BS2***	93 (±7)	211 (±15)	333 (±20)	461 (±25)	590 (±29)	714 (±33)	3139 (±133)
CARR:SA:BSs							
BLK	89 (±3)	199 (±2)	311 (±2)	578 (±5)	-	-	2657 (±69)
BS1c	133 (±4)	289 (±2)	593 (±16)	855 (±45)	1037 (±89)	1189 (±113)	2968 (±99)
BS2	78 (±1)	192 (±4)	310 (±7)	431 (±9)	-	721 (±87)	3062 (±188)
BS4a	129 (±1)	283 (±3)	549 (±125)	794 (±215)	974 (±257)	1115 (±260)	2862 (±255)
BS1c***	128 (±3)	294 (±12)	417 (±14)	530 (±17)	-	-	2527 (±63)

Unmarked and BSs equals 100 and 200 µg/ml BSs loaded niosomes in wafers. The duration of the mechanical shaking of BS4b niosomes loaded into CARR:SA:BS4b-NIO-DCP used for these comparison were twice as long (2 h)H as the other loaded niosomes.**

6.7 Conclusions

The focus of this study was the formulation and characterisation of composite wafers loaded with BSs based niosomes as potential dressings to treat chronic wounds and comparing their functional properties with those loaded with the standard BSs. Characterisation of the two different systems (CARR:SA:BLK-NIO-DCP and CARR:SA:BSs-NIO-DCP) (CARR:SA:BLK-NIO and CARR:SA:BSs-NIO) showed a change in state which was observed in their microscopic structure and physical properties and is expected to impact on their wound healing performances. The results showed an increase in mechanical strength for these composite wafers loaded with BSs based niosomes. The incorporation of a charge inducer (DCP) during niosome formation helped to improve porous structures in the formulated wafers. This helped to improve mechanical strength which is expected to improve ease of hydration of composite wafers. XRD studies showed decreased crystallinity of DCP with molecular dispersion of the BSs within the wafer polymer matrix. ATR-FTIR analysis showed significant similarities between the interaction of six recurrent functional groups, while weak Van der Waals interactions were observed in the OH stretch of niosomes and free BSs within the optimised selected composite polymer of CARR:SA:BSs-NIO-DCP/CARR:SA:BSs-NIO and CARR:SA:BSs studies. Additionally, both CARR:SA:BSs-NIO-DCP/CARR:SA:BSs-NIO wafers showed lower swelling capacity compared to reference CARR:SA:BSs (described in chapter 5) due to the effect of free BSs in the reference wafers which allowed a higher rate of water ingress and hence the enhanced water absorption. However CARR:SA:BSs-NIO-DCP wafers had optimum WVTR followed by CARR:SA:BSs, while CARR:SA:BSs-NIO wafers were above the recommended average but CARR:SA:BSs-NIO had higher capacity to retain water after 24 h than non BSs loaded composite wafers.

Overall, the CARR:SA:BSs-NIO-DCP wafers in this study, showed improved mechanical and comparable bioanalytical properties in comparison to the reference composite polymer systems CARR:SA:BSs and can be potentially used for highly exuding wounds such as chronic ulcers.

CHAPTER 7 SUMMARY COMMENTS AND FUTURE WORK

7.1 Summary comments

The physico-chemical and biological analysis of microbial biosurfactants (BSs) for applications towards cancer therapies, wound healing dressings and drug delivery is an interdisciplinary investigation and novel design of BSs which spans four experimentally related chapters organised in order of study. The aim of this project was firstly to test the anticancer activity of several BSs on two cancerous and one non-cancerous cell lines (human leukaemia monocyte (THP-1), human Caucasian breast adenocarcinoma (MCF-7) and non-cancerous human embryo kidney (HEK 293) cell lines. The second aim involved, the formulation and testing of free and niosomal BSs based composite polymeric wafers.

Anticancer activity was successfully detected and compared in all BSs selected for investigation in cancerous cells (chapter 3), however, the selected BSs were toxic to non-cancerous cells although at higher concentrations than cancerous cells and at longer time intervals. Overall, lactic sophorolipid (BS3) showed the closest cytotoxicity to doxorubicin (DOX) and therefore has high potential application as an anticancer agent. After 48 and 72 h, the anticancer activities of BS1a and BS1b observed in their respective IC_{50} values were higher in both tested cancerous cells (THP-1 and MCF-7) in comparison to the non-cancerous cells (HEK 293). BS2 on the otherhand showed higher sensitivity on THP-1 cells from 24-72 h, however the IC_{50} of BS2 on MCF-7 was lower from 24-48 h, but higher after 72 h in comparison to HEK 293. The anticancer activity observed in the IC_{50} of BS3 was lower from 24-72 h on THP-1 and lower from 48-72 h in MCF-7 in comparison to HEK 293. These results indicate that a slow release of BSs may improve the selectivity in non-cancerous cells.

The objective of formulating single and BSs based niosomes were partially met based on the results from chapter 4. This is because with the exception of 1.0×10^{-1} ug/ml BS1c and 4.0×10^{-1} ug/ml BS3, the particle size of both water and buffer based niosomes were > 1000 nm with bi and trimodal distributions. However with the exception of 6.0×10^{-1} ug/ml BS2 the zeta potential of niosomes in water and buffer had acceptable stabilities > -30 mV. XRD showed crystalline patterns in all BLKs and BSs loaded niosomes which is beneficial for long term storage and distribution. ATR-FTIR showed similarities between all freeze-dried niosome formulations irrespective of the number of components incorporated during their formulations. There were more crystal aggregates observed within the morphologies of water based niosomes in comparison to spherical niosomes, however, the SEM micrographs of 1.65×10^{-1} and 6.0×10^{-1} ug/ml BS2 niosomes formulated with DCP and BLK niosomes without DCP showed the widest distribution among formulation groups. However, the application of BSs loaded niosomes in cancer therapy was not met due to deformation of niosomes dispersed in cell culture media and this will need to be resolved in future studies.

The lyophilised polymeric wafers formulated based on only CARR exhibited weak mechanical and exudate handling properties. Therefore formulation development and optimisation of composite formulations (comprising CARR and SA) was undertaken resulting in the selection of two novel optimised lyophilised BLK wafers. The incorporation of selected BSs in the optimised wafer dressings was successfully achieved with improved mechanical strength in comparison to BLK wafers. Additionally, there were observable differences between the mucoadhesive properties of BSs loaded wafers in comparison to their corresponding BLK formulations. Although BLK and DL wafers showed low peak force and WOA, which indicates that low strain in wafer removal which may encourage patient compliance, the cohesiveness of the optimised wafers showed distinguishable differences on addition of BSs. The compatibility of BSs within the wafer matrix was confirmed by seven characteristic functional groups including OH derived from the individual polymers which were consistently transmitted in the ATR-FTIR wavenumbers of BLK and DL wafers. With the exception of 5% BS4a, which was the highest concentration of BSs loaded, the other DL BSs were not visible on the surface or pore walls of the lyophilised composite wafers which indicates compatibility.

The formulation of BSs loaded niosomes in lyophilised composite polymeric wafers was successfully achieved. The incorporation of BLK and BSs loaded niosomes with and without DCP into the wafers affected the mechanical and bio-analytical properties in comparison to wafers loaded with the standard BSs. Additionally, the BLK and BSs loaded niosomes were not visible on the surface and pore walls of the lyophilised wafer matrix indicating there were well incorporated within the wafer matrix. Both BLK and BSs niosome loaded wafers showed the characteristic functional groups of their lyophilised wafer matrix. XRD diffractograms showed amorphous patterns in both BLK and BSs loaded niosomes incorporated into wafers.

However, the key functional characteristic of testing the release of BSs from both sets of wafers in chapters 5 and 6 respectively were not achieved due to the constraints of time. Furthermore, *in vitro* wound healing (cell migration assay) and cell viability (MTT assay) testing of the BSs and BSs based niosome loaded wafers on relevant cultured cells were also not achieved and both will be undertaken as part of future work. However, given the already established safety of CARR and SA based wafer dressings in previous studies, it is anticipated that the DL wafers will be safe for use as dressing material. Overall, the composite wafers containing BSs based niosomes loaded into wafers in this study, showed improved mechanical and comparable bioanalytical properties in comparison to the reference composite polymer systems and can be potentially used for highly exuding wounds such as chronic ulcers.

7.2 Future work

As summarised in section 7.1 above, although most of the formulation development and functional physico-chemical characteristics were achieved, some advanced characteristics and biological performance of the wafers were not completed. Future work will therefore involve the following

1. The BSs tested were toxic to the model non-cancerous cells used, although at higher concentrations than the cancerous cells. Future work will therefore investigate the optimised BSs based niosomes to target previously tested cell lines THP-1, MCF-7 and HEK 293, and keratinocyte cells. BSs encapsulated niosomes will be formulated, followed by *in vitro* cytotoxicity studies using microplate analysis to evaluate the potency of BSs encapsulated niosomes on previously tested cancerous and non-cancerous cell lines, THP-1, MCF-7 and HEK 293 (chapter 3).
2. Studies for the dissolution and release characteristics will be conducted for drug loaded wafers described in chapters 5 and 6. Stability studies of the DL wafers based on the International conference on harmonisation (ICH) guidelines will be conducted. These will cover drug and polymer stability with the help of HPLC/LC-MS and gel permeation chromatography (GPC) technique respectively.
3. In addition, BSs incorporated niosomes loaded into wafers as drug delivery dressing to wound sites will be investigated. This will involve *in vitro* studies using microplate analysis to evaluate the potency of BSs encapsulated niosomes as well as *in vitro* wound healing effect on human keratinocyte cells available in house, using cell migration studies and cells observed under light and confocal microscopy.
4. Further, optimised BSs and BSs based niosome loaded wafers will be investigated *in vivo*, using a rat model to fully confirm their safety and efficacy and therefore suitability for use in human subjects suffering from chronic wounds.

CHAPTER 8 REFERENCES

1. Abdelkader, H., Ismail, S., Kamal, A. and Alany, R., 2011. Design and evaluation of controlled-release niosomes and discomes for naltrexone hydrochloride ocular delivery. *Journal of Pharmaceutical Sciences*, 100(5), pp.1833-1846.
2. Abdel-Mawgoud, A., Aboulwafa, M. and Hassouna, N., 2008. Characterisation of surfactin produced by *Bacillus subtilis* isolate BS5. *Applied Biochemistry and Biotechnology*, 150(3), pp.289-303.
3. Abdel-Mawgoud, A., Hausmann, R., Lepine, F., Markus, M. and Deziel, E., 2011, 'Rhamnolipids: Detection, Analysis, Biosynthesis, Genetic Regulation, and Bioengineering of Production', In Soberón-Chávez G. (Ed) *Biosurfactants*, vol 20, pp 13 – 55, Springer, USA, (Available at: <http://link.springer.com/10.1007/978-3-642-14490-5>).
4. Abdel-Rahem, R., 2008. The influence of hydrophobic counterions on micellar growth of ionic surfactants. *Advances in Colloid and Interface Science*, 141(1), pp.24-36.
5. Ahmed, E., 2015. Hydrogel: Preparation, characterisation, and applications: A review. *Journal of Advanced Research*, 6(2), pp.105-121.
6. Akbari, J., Saeedi, M., Morteza-Semnani, K., Rostamkalaei, S., Asadi, M., Asare-Addo, K. and Nokhodchi, A., 2016. The design of naproxen solid lipid nanoparticles to target skin layers. *Colloids and Surfaces B: Biointerfaces*, 145, pp.626-633.
7. Alam, M., Zubair, S., Farazuddin, M., Ahmad, E., Khan, A., Zia, Q., Malik, A. and Mohammad, O., 2013. Development, characterisation and efficacy of niosomal diallyl disulfide in treatment of disseminated murine candidiasis. *Nanomedicine: Nanotechnology, Biology, and Medicine*, 9(2), pp.247-256.
8. Alenzi, F., 2004. Links between apoptosis, proliferation and the cell cycle. *British Journal of Biomedical Science*, 61(2), pp.99-102.
9. Almdal, K., Dyre, J., Hvidt, S. and Kramer, O., 1993, November. What is a 'gel'?. In *Makromolekulare Chemie. Macromolecular Symposia* (Vol. 76, No. 1, pp. 49-51). Hüthig & Wepf Verlag.
10. Almeida, C. and Barry, S., 2010. Cancer: basic science and clinical aspects. *John Wiley & Sons*.
11. Alves, F., Zaniquelli, M., Loh, W., Castanheira, E., Oliveira, M. and Feitosa, E., 2007. Vesicle–micelle transition in aqueous mixtures of the cationic dioctadecyldimethylammonium and octadecyltrimethylammonium bromide surfactants. *Journal of Colloid and Interface science*, 316(1), pp.132-139.

12. Antonietti, M. and Förster, S., 2003. Vesicles and liposomes: a self-assembly principle beyond lipids. *Advanced Materials*, 15(16), pp.1323-1333.
13. Arcamone, F., Animati, F., Bigioni, M., Capranico, G., Caserini, C., Cipollone, A., De Cesare, M., Ettore, A., Guano, F., Manzini, S., Monteagudo, E. and Pratesi, G. 1981. Doxorubicin: anticancer antibiotics, In *Medicinal Chemistry Series, vol 17, Academic Press*, New York.
14. Archana, D., Dutta, J. and Dutta, P., 2013. Evaluation of chitosan nano dressing for wound healing: Characterisation, *in vitro* and *in vivo* studies. *International Journal of Biological Macromolecules*, 57, pp.193-203.
15. Ardrey, R., 2003. Liquid chromatography - mass spectrometry: an introduction. *John Wiley & Sons*. Available at: <http://books.google.com/books?hl=en&lr=&id=f1QiHP3wsAcC&pgis=1>. Date accessed 6-5-2015.
16. Arunothayanun, P., Uchegbu, I. and Florence, A., 1999. Osmotic behaviour of polyhedral non-ionic surfactant vesicles (niosomes). *Journal of Pharmacy and Pharmacology*, 51(6), pp.651-657. Assanga, I., Gil-Salido, A., Lujan, L., Rosas-Durazo, A., Acosta-Silva, A., Rivera-Castañeda, E. and Rubio-Pino, J., 2013. Cell growth curves for different cell lines and their relationship with biological activities. *International Journal of Biotechnology and Molecular Biology Research*, 4(4), pp.60-70.
17. Ayensu, I., Mitchell, J. and Boateng, J., 2012. Development and physico-mechanical characterisation of lyophilised chitosan wafers as potential protein drug delivery systems via the buccal mucosa. *Colloids and Surfaces B: Biointerfaces*, 91, pp.258-265.
18. Baillie, A., Florence, A., Hume, L., Muirhead, G. and Rogerson, A., 1985. The preparation and properties of niosomes—non-ionic surfactant vesicles. *Journal of Pharmacy and Pharmacology*, 37(12), pp.863-868.
19. Baillie, A., Coombs, G., Dolan, T. and Laurie, J., 1986. Non-ionic surfactant vesicles, niosomes, as a delivery system for the anti-leishmanial drug, sodium stibogluconate. *Journal of Pharmacy and Pharmacology*, 38(7), pp.502-505.
20. Balakrishnan, P., Shanmugam, S., Lee, W., Lee, W., Kim, J., Oh, D., Kim, D., Kim, J., Yoo, K., Choi, G. and Woo, J., 2009. Formulation and *in vitro* assessment of minoxidil niosomes for enhanced skin delivery. *International Journal of Pharmaceutics*, 377(1-2), pp.1-8.
21. Barreleiro, P., Olofsson, G., Brown, W., Edwards, K., Bonassi, N. and Feitosa, E., 2002. Interaction of octaethylene glycol n-dodecyl monoether with dioctadecyldimethylammonium bromide and chloride vesicles. *Langmuir*, 18(4), pp.1024-1029.
22. Barth, A., 2000. The infrared absorption of amino acid side chains. *Progress in Biophysics and Molecular Biology*, 74(3), pp.141-173.

23. Bayindir, Z. and Yuksel, N., 2010. Characterisation of niosomes prepared with various non-ionic surfactants for paclitaxel oral delivery. *Journal of Pharmaceutical Sciences*, 99(4), pp.2049-2060.
24. Beanes, S., Dang, C., Soo, C. and Ting, K., 2003. Skin repair and scar formation: the central role of TGF-beta. *Expert Reviews in Molecular Medicine*, 5(8), pp.1-22.
25. Bellisola, G. and Sorio, C., 2012. Infrared spectroscopy and microscopy in cancer research and diagnosis. *American Journal of Cancer Research*, 2(1), pp.1-21.
26. Bergstrom, S., Theorell, H. and Davide, H., 1946. Pyolipic acid, a metabolic product of *Pseudomonas-pyocyanea*, active against *mycobacterium-tuberculosis*. *Archives of Biochemistry*, 10(1), pp.165-166.
27. Bhalodia, R., Basu, B., Garala, K., Joshi, B. and Mehta, K., 2010. Buccoadhesive drug delivery systems: A review. *International Journal of Pharma and Bio Sciences*, 6(2), pp.1-32.
28. Bhardwaj, S., Dwivedia, K. and Agarwala, D., 2015. A review: HPLC method development and validation. *International Journal of Analytical and Bioanalytical Chemistry*, 5(4), pp.76-81.
29. Biswal, S., Murthy, P., Sahu, J., Sahoo, P. and Amir, F., 2008. Vesicles of non-ionic surfactants (niosomes) and drug delivery potential. *International Journal of Pharmaceutical Sciences and Nanotechnology*, 1(1), pp.1-8.
30. Boateng, J., Matthews, K., Stevens, H. and Eccleston, G., 2008. Wound healing dressings and drug delivery systems: a review. *Journal of pharmaceutical sciences*, 97(8), pp.2892-2923.
31. Boateng, J., Auffret, A., Matthews, K., Humphrey, M., Stevens, H. and Eccleston, G., 2010. Characterisation of freeze-dried wafers and solvent evaporated films as potential drug delivery systems to mucosal surfaces. *International Journal of Pharmaceutics*, 389(1), pp.24-31.
32. Boateng, J., Pawar, H. and Tetteh, J., 2015. Evaluation of *in vitro* wound adhesion characteristics of composite film and wafer based dressings using texture analysis and FTIR spectroscopy: a chemometrics factor analysis approach. *RSC Advances*, 5(129), pp.107064-107075.
33. Boateng, J. and Catanzano, O., 2015. Advanced therapeutic dressings for effective wound healing - a review. *Journal of Pharmaceutical Sciences*, 104(11), pp.3653-3680.
34. Boddupalli, B., Mohammed, Z., Nath, R. and Banji, D., 2010. Mucoadhesive drug delivery system: An overview. *Journal of Advanced Pharmaceutical Technology & Research*, 1(4), p.381.

35. Brewer, J. and Alexander, J., 1992. The adjuvant activity of non-ionic surfactant vesicles (niosomes) on the BALB/c humoral response to bovine serum albumin. *Immunology*, 75(4), p.570.
36. Byeon, S., Lee, Y., Kim, B., Shen, T., Lee, S., Park, H., Park, S., Rhee, M. and Cho, J., 2008. Surfactin blocks NO production in lipopolysaccharide-activated macrophages by inhibiting NF-kappaB activation. *Journal of Microbiology and Biotechnology*, 18(12), pp.1984-1989.
37. Caló, E. and Khutoryanskiy, V., 2015. Biomedical applications of hydrogels: A review of patents and commercial products. *European Polymer Journal*, 65, pp.252-267.
38. Campos, A., Groth, A. and Branco, A., 2008. Assessment and nutritional aspects of wound healing. *Current Opinion in Clinical Nutrition and Metabolic Care*, 11(3), pp.281-288.
39. Cao, X., Liao, Z., Wang, C., Yang, W. and Lu, M., 2009. Evaluation of a lipopeptide biosurfactant from *Bacillus natto TK-1* as a potential source of anti-adhesive, antimicrobial and antitumour activities. *Brazilian Journal of Microbiology*, 40(2), pp.373-379.
40. Cao, X., Liao, Z., Wang, C., Cai, P., Yang, W., Lu, M. and Huang, G., 2009. Purification and antitumour activity of a lipopeptide biosurfactant produced by *Bacillus natto TK-1*. *Biotechnology and Applied Biochemistry*, 52(Pt 2), pp.97-106.
41. Cao, X., Zhao, S., Liu, D., Wang, Z., Niu, L., Hou, L. and Wang, C., 2011. ROS-Ca₂⁺ is associated with mitochondria permeability transition pore involved in surfactin-induced MCF-7 cells apoptosis. *Chemico-Biological Interactions*, 190(1), pp.16-27.
42. Capra, R., Baruzzi, A., Quinzani, L. and Strumia, M., 2007. Rheological, dielectric and diffusion analysis of mucin/carbopol matrices used in amperometric biosensors. *Sensors and Actuators B: Chemical*, 124(2), pp.466-476.
43. Carafa, M., Santucci, E., Alhaique, F., Coviello, T., Murtas, E., Riccieri, F., Lucania, G. and Torrisi, M., 1998. Preparation and properties of new unilamellar non-ionic/ionic surfactant vesicles. *International Journal of Pharmaceutics*, 160(1), pp.51-59.
44. Ceulemans, J. and Ludwig, A., 2002. Optimisation of carbomer viscous eye drops: an *in vitro* experimental design approach using rheological techniques. *European Journal of Pharmaceutics and Biopharmaceutics*, 54(1), pp.41-50.
45. Champion, J., Gilkey, J., Lamparski, H., Retterer, J. and Miller, R., 1995. Electron microscopy of rhamnolipid (biosurfactant) morphology: effects of pH, cadmium, and octadecane. *Journal of Colloid and Interface Science*, 170(2), pp.569-574.

46. Chavda, H., Patel, R., Modhia, I. and Patel, C., 2012. Preparation and characterisation of superporous hydrogel based on different polymers. *International Journal of Pharmaceutical Investigation*, 2(3), p.134.
47. Chen, J., Song, X., Zhang, H., Qu, Y. and Miao, J., 2006. Sophorolipid produced from the new yeast strain *Wickerhamiella domercqiae* induces apoptosis in H7402 human liver cancer cells. *Applied Microbiology and Biotechnology*, 72(1), pp.52-59.
48. Chen, M., Penfold, J., Thomas, R., Smyth, T., Perfumo, A., Marchant, R., Banat, I., Stevenson, P., Parry, A., Tucker, I. and Grillo, I., 2010. Solution self-assembly and adsorption at the air– water interface of the monorhamnose and dirhamnose rhamnolipids and their mixtures. *Langmuir*, 26(23), pp.18281-18292.
49. Christova, N., Tuleva, B., Kril, A., Georgieva, M., Konstantinov, S., Terziyski, I., Nikolova, B. and Stoineva, I., 2013. Chemical structure and *in vitro* antitumour activity of rhamnolipids from *Pseudomonas aeruginosa* BN10. *Applied Biochemistry and Biotechnology*, 170(3), pp.676-689.
50. Concaix, F., Institut Français du Pétrole and Sophor S, 2003. Use of sophorolipids comprising diacetyl lactones as agent for stimulating skin fibroblast metabolism. U.S. Patent 6,596,265.
51. Corbett, J., Connah, M. and Mattison, K., 2011. Advances in the measurement of protein mobility using laser Doppler electrophoresis–the diffusion barrier technique. *Electrophoresis*, 32(14), pp.1787-1794.
52. Creighton, T., 1993. Proteins: structures and molecular properties. Macmillan.
53. Dahrazma, B., Mulligan, C. and Nieh, M., 2008. Effects of additives on the structure of rhamnolipid (biosurfactant): a small-angle neutron scattering (SANS) study. *Journal of Colloid and Interface Science*, 319(2), pp.590-593.
54. Darwish, I., 1998. Preparation and Characterisation of Niosomes Formed from Mixed Non-ionic Surfactants and Cholesterol: I. Span 60/Tweens/Cholesterol Niosomes. *Alexandria Journal of Pharmaceutical Sciences*, 12, pp.33-38.
55. Delbeke, E., Movsisyan, M., Van Geem, K. and Stevens, C., 2016. Chemical and enzymatic modification of sophorolipids. *Green Chemistry*, 18(1), pp.76-104.
56. del Burgo, P., Aicart, E. and Junquera, E., 2007. Mixed vesicles and mixed micelles of the cationic–cationic surfactant system: didecyltrimethylammonium bromide/dodecylethyltrimethylammonium bromide/water. *Colloids and Surfaces A: Physicochemical and Engineering Aspects*, 292(2), pp.165-172.
57. Denard, B., Lee, C. and Ye, J., 2012. Doxorubicin blocks proliferation of cancer cells through proteolytic activation of CREB3L1. *eLife*, 2012(1), pp.1-14.

58. DeVita, V.T. and Chu, E., 2008. A history of cancer chemotherapy. *Cancer Research*, 68(21), pp.8643-8653.
59. Déziel, E., Lepine, F., Dennie, D., Boismenu, D., Mamer, O.A. and Villemur, R., 1999. Liquid chromatography/mass spectrometry analysis of mixtures of rhamnolipids produced by *Pseudomonas aeruginosa* strain 57RP grown on mannitol or naphthalene. *Biochimica et Biophysica Acta - Molecular and Cell Biology of Lipids*, 1440, pp.244-252.
60. Déziel, E., Lepine, F., Milot, S. and Villemur, R., 2000. Mass spectrometry monitoring of rhamnolipids from a growing culture of *Pseudomonas aeruginosa* strain 57RP. *Biochimica et Biophysica Acta - Molecular and Cell Biology of Lipids*, 1485(2-3), pp.145-152.
61. Dhar, S., Mali, V., Bodhankar, S., Shiras, A., Prasad, B. and Pokharkar, V., 2011. Biocompatible gellan gum-reduced gold nanoparticles: cellular uptake and subacute oral toxicity studies. *Journal of Applied Toxicology*, 31(5), pp.411-420.
62. Dhivya, S., Padma, V. and Santhini, E., 2015. Wound dressings - a review. *BioMedicine*, 5(4), p.22.
63. Dole, M., Patel, P., Sawant, S. and Shedpure, P., 2011. Advance applications of Fourier transform infrared spectroscopy. *International Journal of Pharmaceutical Sciences Review and Research*, 7, pp.159-166.
64. Duarte, C., Gudina, E.J., Lima, C.F. and Rodrigues, L.R., 2014. Effects of biosurfactants on the viability and proliferation of human breast cancer cells. *AMB Express*, 4(1), p.40.
65. Dušek, K. and Patterson, D., 1968. Transition in swollen polymer networks induced by intramolecular condensation. *Journal of Polymer Science Part A-2: Polymer Physics*, 6(7), pp.1209-1216.
66. Dutta, S., Parida, S., Maiti, C., Banerjee, R., Mandal, M. and Dhara, D., 2016. Polymer grafted magnetic nanoparticles for delivery of anticancer drug at lower pH and elevated temperature. *Journal of Colloid and Interface Science*, 467, pp.70-80.
67. Dyson, M., Young, S., Pendle, C., Webster, D. and Lang, S., 1988. Comparison of the effects of moist and dry conditions on dermal repair. *Journal of Investigative Dermatology*, 91(5), pp.434-439.
68. Elsayed, M. and Cevc, G., 2011. The vesicle-to-micelle transformation of phospholipid–cholate mixed aggregates: a state of the art analysis including membrane curvature effects. *Biochimica et Biophysica Acta (BBA)-Biomembranes*, 1808(1), pp.140-153.
69. Engberts, J and Kevelam, J., 1996. Formation and stability of micelles and vesicles. *Current Opinion in Colloid & Interface Science*, 1(6), pp.779-789.
70. Falabella, A., 2006. Debridement and wound bed preparation. *Dermatologic Therapy*, 19(6), pp.317-325.

71. Falanga, V., 2005. Wound healing and its impairment in the diabetic foot. *Lancet*, 366(9498), pp.1736-1743.
72. Fathalla, D., Abdel-Mageed, A., Abdel-Hamid, F. and Ahmed, M., 2014. *In vitro* and *in vivo* evaluation of niosomal gel containing aceclofenac for sustained drug delivery. *International Journal of Pharmaceutical Sciences Research*, 1: 105. doi: <http://dx.doi.org/10.15344/2394-1502/2014/105>.
73. Fernandez, P., Willenbacher, N., Frechen, T. and Kühnle, A., 2005. Vesicles as rheology modifier. *Colloids and Surfaces A: Physicochemical and Engineering Aspects*, 262(1), pp.204-210.
74. Fontana, A., De Maria, P., Siani, G. and Robinson, B., 2003. Kinetics of breakdown of vesicles from didodecyldimethylammonium bromide induced by single chain surfactants and by osmotic stress in aqueous solution. *Colloids and Surfaces B: Biointerfaces*, 32(4), pp.365-374.
75. Florence, A. and Attwood, D., 2011. *Physicochemical Principles of Pharmacy*. Pharmaceutical press.
76. Fuoss, R. and Strauss, U., 1948. Electrostatic interaction of polyelectrolytes and simple electrolytes. *Journal of Polymer Science*, 3(4), pp.602-603.
77. Ghobril, C. and Grinstaff, M., 2015. The chemistry and engineering of polymeric hydrogel adhesives for wound closure: a tutorial. *Chemical Society Reviews*, 44(7), pp.1820-1835.
78. Ghosh, S., Roy, A., Banik, D., Kundu, N., Kuchlyan, J., Dhir, A. and Sarkar, N., 2015. How does the surface charge of ionic surfactant and cholesterol forming vesicles control rotational and translational motion of rhodamine 6G perchlorate (R6G ClO₄)? *Langmuir*, 31(8), pp.2310-2320.
79. Gorin, P., Spencer, J. and Tulloch, A., 1961. Hydroxy fatty acid glycosides of sophorose from *Torulopsis magnoliae*. *Canadian Journal of Chemistry*, 39(4), pp.846-855.
80. Gosain, A. and DiPietro, L., 2004. Aging and wound healing. *World Journal of Surgery*, 28(3), pp.321-326.
81. Grant, G., Morris, E., Rees, D., Smith, P. and Thom, D., 1973. Biological interactions between polysaccharides and divalent cations: the egg-box model. *FEBS Letters*, 32(1), pp.195-198.
82. Grever, M., Chabner, B. and Shoemaker, D., 2001. Cancer drug discovery and development. *Cancer: Principles and Practice of Oncology*. Philadelphia, Lippincott Raven, pp.328-339.

83. Gu, J., Robinson, J. and Leung, S., 1987. Binding of acrylic polymers to mucin/epithelial surfaces: structure-property relationships. *Critical Reviews in Therapeutic Drug Carrier Systems*, 5(1), pp.21-67.
84. Gudiña, E., Rangarajan, V., Sen, R. and Rodrigues, L., 2013. Potential therapeutic applications of biosurfactants. *Trends in Pharmacological Sciences*, 34(12), pp.667-675.
85. Hamdan, S., Pastar, I., Drakulich, S., Dikici, E., Tomic-Canic, M., Deo, S. and Daunert, S., 2017. Nanotechnology-driven therapeutic Interventions in Wound Healing: Potential Uses and Applications. *ACS Central Science*, 3(3), pp.163-175.
86. Hanahan, D. and Weinberg, R., 2011. Hallmarks of cancer: the next generation. *Cell*, 144(5), pp.646-674.
87. Harding, S., 2006. Trends in muco-adhesive analysis. *Trends in Food Science & Technology*, 17(5), pp.255-262.
88. Hareendran, A., Bradbury, A., Budd, J., Geroulakos, G., Hobbs, R., Kenkre, J. and Symonds, T., 2005. Measuring the impact of venous leg ulcers on quality of life. *Journal of Wound Care*, 14(2), pp.53-57.
89. Harshada, K. 2014. Biosurfactant: a potent antimicrobial agent. *Journal of Microbiology and Experimentation*. 1(5), pp. 2-5.
90. Hasan, A, 2014. Design and *in vitro* characterisation of small unilamellar niosomes as ophthalmic carrier of dorzolamide hydrochloride. *Pharmaceutical development and technology*, 19(6), pp.748-754.
91. Henderson, B., Nair, S., Pallas, J. and Williams, M., 2011. Fibronectin: a multidomain host adhesin targeted by bacterial fibronectin-binding proteins. *FEMS Microbiology Reviews*, 35(1), pp.147-200.
92. Hermisson, J. and Pennings, P., 2005. Soft sweeps. *Genetics*, 169(4), pp.2335-2352.
93. Holmberg, K., Jönsson, B., Kronberg, B. and Lindman., 2003. *Polymers in Solution. Surfactants and Polymers in Aqueous Solution. Second Edition*, John Wiley & Sons, Ltd, Chichester, UK. pp.193-214. Available at: <http://dx.doi.org/10.1002/0470856424.ch9>.
94. Hu, J., Zhang, X. and Wang, Z., 2010. A review on progress in QSPR studies for surfactants. *International Journal of Molecular Sciences*, 11(3), pp.1020-1047.
95. Hue, N., Serani, L. and Laprvote, O., 2001. Structural investigation of cyclic peptidolipids from *Bacillus subtilis* by high-energy tandem mass spectrometry. *Rapid Communications in Mass Spectrometry*, 15(3), pp.203-209.
96. Ibrahim, M., Sammour, O., Hammad, M. and Megrab, N., 2008. *In vitro* evaluation of proniosomes as a drug carrier for flurbiprofen. *AAPS PharmSciTech*, 9(3), pp.78-790.

97. Inoh, Y., Kitamoto, D., Hirashima, N. and Nakanishi, M., 2001. Biosurfactants of MEL-A increase gene transfection mediated by cationic liposomes. *Biochemical and Biophysical Research Communications*, 289(1), pp.57-61.
98. Israelachvili, J., Marčelja, S. and Horn, R., 1980. Physical principles of membrane organisation. *Quarterly reviews of biophysics*, 13(2), pp.121-200.
99. Jameson, J. and Havran, W.L., 2007. Skin $\gamma\delta$ T-cell functions in homeostasis and wound healing. *Immunological Reviews*, 215(1), pp.114-122.
100. Jibry, N., Heenan, R. and Murdan, S., 2004. Amphiphilic gels for drug delivery: formulation and characterisation. *Pharmaceutical Research*, 21(10), pp.1852-1861.
101. Joshi-Navare, K., Khanvilkar, P. and Prabhune, A., 2013. Jatropha oil derived sophorolipids: Production and characterisation as laundry detergent additive. *Biochemistry Research International*. Article ID 169797, 11 pages. doi:10.1155/2013/169797
102. Ju, L., Dashtbozorg, S. and Vongpanish, N., The University Of Akron, 2016. Wound dressings with enhanced gas permeation and other beneficial properties. U.S. Patent 9,468,700.
103. Junquera, E., Arranz, R. and Aicart, E., 2004. Mixed vesicle formation on a ternary surfactant system: didodecyldimethylammonium bromide/dodecylethyldimethylammonium bromide/water. *Langmuir*, 20(16), pp.6619-6625.
104. Kabanov, A., Batrakova, E. and Alakhov, V., 2002. Pluronic® block copolymers as novel polymer therapeutics for drug and gene delivery. *Journal of Controlled Release*, 82(2), pp.189-212.
105. Kakinuma, A., Sunino, H., Isono, M., Tamura, G. and Arima, K., 1969. Determination of fatty acid in surfactin and elucidation of total structure of surfactin. *Agricultural and Biological Chemistry*. 33(6), pp.973-976.
106. Kasture, M., Singh, S., Patel, P., Joy, P., Prabhune, A., Ramana, C. and Prasad, B., 2007. Multiutility sophorolipids as nanoparticle capping agents: synthesis of stable and water dispersible Co nanoparticles. *Langmuir*, 23(23), pp.11409-11412.
107. Kazarian, S. and Chan, K., 2006. Applications of ATR-FTIR spectroscopic imaging to biomedical samples. *Biochimica et Biophysica Acta - Biomembranes*, 1758(7), pp.858-867.
108. Kazi, K., Mandal, A., Biswas, N., Guha, A., Chatterjee, S., Behera, M. and Kuotsu, K., 2010. Niosome: a future of targeted drug delivery systems. *Journal of Advanced Pharmaceutical Technology & Research*, 1(4), p.374.
109. Kim, I., Yoo, M., Seo, J., Park, S., Na, H., Lee, H., Kim, S. and Cho, C., 2007. Evaluation of semi-interpenetrating polymer networks composed of chitosan and poloxamer for wound dressing application. *International Journal of Pharmaceutics*, 341(1), pp.35-43.

110. Kirby, C. and Gregoriadis, G., 1984. Dehydration-Rehydration Vesicles: A Simple Method for High Yield Drug Entrapment in Liposomes. *Bio/Technology*, 2(11), pp.979-984.
111. Kodama, T., Ohta, A., Toda, K., Katada, T., Asakawa, T. and Miyagishi, S., 2006. Fluorescence-probe study of vesicle and micelle formations in a binary cationic surfactants system. *Colloids and Surfaces A: Physicochemical and Engineering Aspects*, 277(1), pp.20-26.
112. Koksall, C. and Bozkurt, A., 2003. Combination of hydrocolloid dressing and medical compression stocking versus Unna's boot for the treatment of venous leg ulcers. *Swiss Medical Weekly*, 133(25-26), pp.364-368.
113. Korrapati, P., Karthikeyan, K., Satish, A., Krishnaswamy, V., Venugopal, J. and Ramakrishna, S., 2016. Recent advancements in nanotechnological strategies in selection, design and delivery of biomolecules for skin regeneration. *Materials Science and Engineering: C*, 67, pp.747-765.
114. Kumar, G. and Rajeshwarrao, P., 2011. Non-ionic surfactant vesicular systems for effective drug delivery—an overview. *Acta Pharmaceutica Sinica B*, 1(4), pp.208-219.
115. Kumbhar, D., Wavikar, P. and Vavia, P., 2013. Niosomal gel of lornoxicam for topical delivery: *in vitro* assessment and pharmacodynamic activity. *AAPS PharmSciTech*, 14(3), pp.1072-1082.
116. Kupiec, T., 2004. Quality-control analytical methods: gas chromatography. *International Journal of Pharmaceutical Compounding*, 8(4), pp.305-309.
117. Kurtzman, C., Price, N., Ray, K. and Kuo, T., 2010. Production of sophorolipid biosurfactants by multiple species of the *Starmerella (Candida) bombicola* yeast clade. *FEMS Microbiology Letters*, 311(2), pp.140-146.
118. Lamke, L., Nilsson, G. and Reithner, H., 1977. The evaporative water loss from burns and the water-vapour permeability of grafts and artificial membranes used in the treatment of burns. *Burns*, 3(3), pp.159-165.
119. Langer, R., 1980. Invited review polymeric delivery systems for controlled drug release. *Chemical Engineering Communications*, 6(1-3), pp.1-48.
120. Lee, S., Posthauer, M., Dorner, B., Redovian, V. and Maloney, M., 2006. Pressure ulcer healing with a concentrated, fortified, collagen protein hydrolysate supplement: a randomised controlled trial. *Advances in Skin & Wound Care*, 19(2), pp.9296.
121. Lee, J., Nam, S., Seo, W., Yun, H., Hong, S., Kim, M. and Cho, K., 2012. The production of surfactin during the fermentation of *Cheonggukjang* by potential probiotic *Bacillus subtilis* CSY191 and the resultant growth suppression of MCF-7 human breast cancer cells. *Food Chemistry*, 131(4), pp.1347-1354.

122. Levitzki, A. and Klein, S., 2010. Signal transduction therapy of cancer. *Molecular Aspects of Medicine*, 31(4), pp.287-329.
123. Li, F., Zhao, D., Luo, Q., Liu, R. and Yin, R., 2008. Research on surface-modification of Nano-TiO₂ by span 60. *Journal of Ceramic Processing Research*, 9(4), pp.398-400.
124. Lotfabad, T., Abassi, H., Ahmadkhaniha, R., Roostaazad, R., Masoomi, F., Zahiri, H.S., Ahmadian, G., Vali, H. and Noghabi, K., 2010. Structural characterisation of a rhamnolipid-type biosurfactant produced by *Pseudomonas aeruginosa MR01*: Enhancement of di-rhamnolipid proportion using gamma irradiation. *Colloids and Surfaces B: Biointerfaces*, 81(2), pp.397-405.
125. Lord, C. and Ashworth, A., 2010. Biology-driven cancer drug development: back to the future. *BMC Biology*, 8, p.38.
126. MacKintosh, F. and Safran, S., 1993. Phase separation and curvature of bilayer membranes. *Physical Review E*, 47(2), p.1180.
127. Madsen, F., Eberth, K. and Smart, J., 1998. A rheological assessment of the nature of interactions between mucoadhesive polymers and a homogenised mucus gel. *Biomaterials*, 19(11), pp.1083-1092.
128. Magalhães, L. and Nitschke, M., 2013. Anti-microbial activity of rhamnolipids against *Listeria monocytogenes* and their synergistic interaction with nisin. *Food Control*, 29(1), pp.138-142.
129. Maingault, M., Institut Francais Du Petrole, 1999. Utilisation of sophorolipids as therapeutically active substances or cosmetic products, in particular for the treatment of the skin. U.S. Patent 5,981,497.
130. Manconi, M., Sinico, C., Valenti, D., Loy, G. and Fadda, A., 2002. Niosomes as carriers for tretinoin. I. Preparation and properties. *International Journal of Pharmaceutics*, 234(1), pp.237-248.
131. Manivasagan P, Sivasankar P, Venkatesan J, Sivakumar K. and Kim S.K. 2014. Optimisation, production and characterisation of glycolipid biosurfactant from the marine *Actinobacterium, Streptomyces sp. MAB36*, 37(5), 783-797.
132. Mansour, O., Cattoz, B., Heenan, R., King, S. and Griffiths, P., 2015. Probing competitive interactions in quaternary formulations. *Journal of Colloid and Interface Science*, 454, pp.35-43.
133. Marwa, A., Omaima, S., Hanaa, E. and Mohammed, A., 2013. Preparation and *in vitro* evaluation of diclofenac sodium niosomal formulations. *International Journal of Pharmaceutical Sciences and Research*, 4(5), pp.1757-1765.
134. Mathieu, D., Linke, J. and Wattel, F., 2006. Non-healing wounds. *Handbook on Hyperbaric Medicine*, pp.401-428.

135. Matthews, K., Stevens, H., Auffret, A., Humphrey, M. and Eccleston, G., 2005. Lyophilised wafers as a drug delivery system for wound healing containing methylcellulose as a viscosity modifier. *International Journal of Pharmaceutics*, 289(1), pp.51-62.
136. Matthews, K., Stevens, H., Auffret, A., Humphrey, M. and Eccleston, G., 2006. Gamma-irradiation of lyophilised wound healing wafers. *International Journal of Pharmaceutics*, 313(1), pp.78-86.
137. McClure, C. and Schiller, N., 1996. Inhibition of macrophage phagocytosis by *Pseudomonas aeruginosa* rhamnolipids *in vitro* and *in vivo*. *Current Microbiology*, 33(2), pp.109-117.
138. McLaughlin-Drubin, M. and Munger, K., 2008. Viruses associated with human cancer. *Biochimica et Biophysica Acta*, 1782(3), pp.127-150.
139. Mendonça, R. and Coutinho-Netto, J., 2009. Cellular aspects of wound healing. *Brazilian Annal Dermatologia*, 84(3), pp.257-262.
140. Meyer, T., Devanathan, S., Woo, T., Getzoff, E., Tollin, G. and Cusanovich, M., 2003. Site-specific mutations provide new insights into the origin of pH effects and alternative spectral forms in the photoactive yellow protein from *Halorhodospira halophila*. *Biochemistry*, 42(11), pp.3319-3325.
141. Mills, R., Taylor, K., Podshivalova, K., McKay, D. and Jameson, J., 2008. Defects in skin $\gamma\delta$ T cell function contribute to delayed wound repair in rapamycin-treated mice. *The Journal of Immunology*, 181(6), pp.3974-3983.
142. Mohamadnia, Z., Zohuriaan-Mehr, M., Kabiri, K., Jamshidi, A. and Mobedi, H., 2008. Ionically cross-linked carrageenan-alginate hydrogel beads. *Journal of Biomaterials Science, Polymer Edition*, 19(1), pp.47-59.
143. Mokhtar, M., Sammour, O., Hammad, M. and Megrab, N., 2008. Effect of some formulation parameters on flurbiprofen encapsulation and release rates of niosomes prepared from proniosomes. *International Journal of Pharmaceutics*, 361(1-2), pp.104-111.
144. Momoh, F., Boateng, J., Richardson, S., Chowdhry, B. and Mitchell, J., 2015. Development and functional characterisation of alginate dressing as potential protein delivery system for wound healing. *International Journal of Biological Macromolecules*, 81, pp.137-150.
145. Monneret, C., 2001. Recent developments in the field of antitumour anthracyclines. *European Journal of Medicinal Chemistry*, 36(6), pp.483-493. Available at: <Go to ISI>://000171889800001.
146. Moore, P. and Chang, Y., 2010. Why do viruses cause cancer? Highlights of the first century of human tumour virology. *Nature reviews Cancer*, 10(12), pp.878-889. Available at: <http://dx.doi.org/10.1038/nrc2961>.

147. Mordorski, B., Rosen, J. and Friedman, A., 2015. Nanotechnology as an innovative approach for accelerating wound healing in diabetes. *Diabetes Management*, 5(5), pp.329-332.
148. Mozafari, M., Reed, C. and Rostron, C., 2007. Cytotoxicity evaluation of anionic nanoliposomes and nanolipoplexes prepared by the heating method without employing volatile solvents and detergents. *Pharmazie*, 62(3), pp.205-209.
149. Müller, R., Jacobs, C. and Kayser, O., 2001. Nanosuspensions as particulate drug formulations in therapy: rationale for development and what we can expect for the future. *Advanced Drug Delivery Reviews*, 47(1), pp.3-19.
150. Muzzalupo, R., Trombino, S., Iemma, F., Puoci, F., La Mesa, C. and Picci, N., 2005. Preparation and characterisation of bolaform surfactant vesicles. *Colloids and Surfaces B: Biointerfaces*, 46(2), pp.78-83
151. Nagarajan, R., 2002. Molecular packing parameter and surfactant self-assembly: the neglected role of the surfactant tail. *Langmuir*, 18(1), pp.31-38.
152. Nagarwal, R., Kant, S., Singh, P., Maiti, P. and Pandit, J., 2009. Polymeric nanoparticulate system: a potential approach for ocular drug delivery. *Journal of Controlled Release*, 136(1), pp.2-13.
153. Nasser, B., 2005. Effect of cholesterol and temperature on the elastic properties of niosomal membranes. *International Journal of Pharmaceutics*, 300(1), pp.95-101.
154. Nemoto, T., Kubota, R., Murasawa, Y. and Isogai, Z., 2012. Viscoelastic properties of the human dermis and other connective tissues and its relevance to tissue aging and aging-related disease. In *Viscoelasticity-From Theory to Biological Applications*. InTech.
155. Nguyen, T. and Sabatini, D., 2009. Formulating alcohol-free microemulsions using rhamnolipid biosurfactant and rhamnolipid mixtures. *Journal of Surfactants and Detergents*, 12(2), pp.109-115.
156. Nguyen, T., Edelen, A., Neighbors, B. and Sabatini, D., 2010. Biocompatible lecithin-based microemulsions with rhamnolipid and sophorolipid biosurfactants: formulation and potential applications. *Journal of Colloid and Interface Science*, 348(2), pp.498-504.
157. Nie, B., Stutzman, J. and Xie, A., 2005. A vibrational spectral marker for probing the hydrogen-bonding status of protonated Asp and Glu residues. *Biophysical Journal*, 88(4), pp.2833-2847.
158. Nigam, Y., Bexfield, A., Thomas, S. and Ratcliffe, N., 2006. Maggot therapy: The science and implication for CAM part II - Maggots combat infection. *Evidence-based Complementary and Alternative Medicine*, 3(3), pp.303-308.

159. Nitschke, M., Costa, S., Haddad, R., Gonc, L., Alves, N., Eberlin, M., Contiero, J., 2005. Oil wastes as unconventional substrates for rhamnolipid biosurfactant production by *Pseudomonas aeruginosa* LBI. *Biotechnology Progress*, 21(5), pp.1562-1566.
160. Nono, M., Durand, D. and Nicolai, T., 2012. Rheology and structure of mixtures of κ -carrageenan and sodium caseinate. *Food Hydrocolloids*, 27(1), pp.235-241.
161. Okay, O., 2009. General properties of hydrogels. In *Hydrogel sensors and actuators* (pp. 1-14). Springer Berlin Heidelberg.
162. Ortiz, A., Teruel, J., Espuny, M., Marques, A., Manresa, A. and Aranda, F., 2006. Effects of di-rhamnolipid on the structural properties of phosphatidylcholine membranes. *International Journal of Pharmaceutics*, 325, 99-107.
163. Paolino, D., Cosco, D., Muzzalupo, R., Trapasso, E., Picci, N. and Fresta, M., 2008. Innovative bola-surfactant niosomes as topical delivery systems of 5-fluorouracil for the treatment of skin cancer. *International Journal of Pharmaceutics*, 353(1), pp.233-242.
164. Parani, M., Lokhande, G., Singh, A. and Gaharwar, A., 2016. Engineered nanomaterials for infection control and healing acute and chronic wounds. *ACS Applied Materials & Interfaces*, 8(16), pp.10049-10069.
165. Pardakhty, A., Varshosaz, J. and Rouholamini, A., 2007. *In vitro* study of polyoxyethylene alkyl ether niosomes for delivery of insulin. *International Journal of Pharmaceutics*, 328(2), pp.130-141.
166. Park, H., Amiji, M. and Park, K., 1989. Mucoadhesive hydrogels effective at neutral pH. In *Proceedings of the International Symposium on Controlled Release Bioactive Materials*, 16, pp. 217-218.
167. Park, Y., Huang, R., Corti, D. and Franses, E., 2010. Colloidal dispersion stability of unilamellar DPPC vesicles in aqueous electrolyte solutions and comparisons to predictions of the DLVO theory. *Journal of Colloid and Interface Science*, 342(2), pp.300-310.
168. Parkin, D., 2006. The evolution of the population-based cancer registry. *Nature reviews. Cancer*, 6(8), pp.603-612.
169. Paşcalău, V., Popescu, V., Popescu, G., Dudescu, M., Borodi, G., Dinescu, A., Perhaița, I. and Paul, M., 2012. The alginate/ κ -carrageenan ratio's influence on the properties of the cross-linked composite films. *Journal of Alloys and Compounds*, 536, pp.S418-S423.
170. Paşcalău, V., Popescu, V., Popescu, G., Dudescu, M., Borodi, G., Dinescu, A. and Moldovan, M., 2013. Obtaining and characterising alginate/ κ -carrageenan hydrogel cross-linked with adipic dihydrazide. *Advances in Materials Science and Engineering*, 2013.
171. Pashley, R., Karaman, M. 2004. *Applied Colloid and Surface Chemistry*. 1st edition. West Sussex: John Wiley and Sons Ltd; 200.

172. Pawar, H., Boateng, J., Ayensu, I. and Tetteh, J., 2014. Multifunctional medicated lyophilised wafer dressing for effective chronic wound healing. *Journal of Pharmaceutical Sciences*, 103(6), pp.1720-1733.
173. Pecci, Y., Rivardo, F., Martinotti, M. and Allegrone, G., 2010. LC/ESI-MS/MS characterisation of lipopeptide biosurfactants produced by the *Bacillus licheniformis* V9T14 strain. *Journal of Mass Spectrometry*, 45(7), pp.772-778.
174. Pecorino, L., 2016. Molecular biology of cancer: mechanisms, targets, and therapeutics. Oxford university press.
175. Penfold, J., Chen, M., Thomas, R., Dong, C., Smyth, T., Perfumo, A., Marchant, R., Banat, I., Stevenson, P., Parry, A. and Tucker, I., 2011. Solution self-assembly of the sophorolipid biosurfactant and its mixture with anionic surfactant sodium dodecyl benzene sulfonate. *Langmuir*, 27(14), pp.8867-8877.
176. Peppas, N. and Buri, P., 1985. Surface, interfacial and molecular aspects of polymer bioadhesion on soft tissues. *Journal of Controlled Release*, 2, pp.257-275.
177. Pornsunthorntawe, O., Chavadej, S. and Rujiravanit, R., 2009. Solution properties and vesicle formation of rhamnolipid biosurfactants produced by *Pseudomonas aeruginosa* SP4. *Colloids and Surfaces B: Biointerfaces*, 72(1), pp.6-15.
178. Pornsunthorntawe, O., Chavadej, S. and Rujiravanit, R., 2011. Characterisation and encapsulation efficiency of rhamnolipid vesicles with cholesterol addition. *Journal of Bioscience and Bioengineering*, 112(1), pp.102-106.
179. Pritchard, J., Pickrell, J. and Coop, G., 2010. The genetics of human adaptation: hard sweeps, soft sweeps, and polygenic adaptation. *Current biology*, 20(4), pp.R208-R215.
180. Queen, D., Gaylor, J., Evans, J., Courtney, J. and Reid, W., 1987. The preclinical evaluation of the water vapour transmission rate through burn wound dressings. *Biomaterials*, 8(5), pp.367-371.
181. Rajput, G., Majmudar, F., Patel, J., Thakor, R. and Rajgor, N., 2010. Stomach-specific mucoadhesive microsphere as a controlled drug delivery system. *Systematic Reviews in Pharmacy*, 1(1), p.70.
182. Rashad, M., Nooman, M., Ali, M., Al-kashef, A. and Mahmoud A., 2014. Production, characterisation and anticancer activity of *Candida bombicola* sophorolipids by means of solid state fermentation of sunflower oil cake and soybean oil. *Grasas y Aceites*, 65(2), p.e017.
183. Reddy, P. and Swarnalatha, D., 2010. Recent advances in novel drug delivery systems. *International Journal of PharmTech Research*, 2(3), pp.2025-2027.
184. Regan, P., 2007. The impact of cancer and its treatment on wound healing. *Wound Essentials*, 3(2), pp.144-148.

185. Ribeiro, I., Faustino, C., Guerreiro, P., Frade, R., Bronze, M., Castro, M. and Ribeiro, M., 2015. Development of novel sophorolipids with improved cytotoxic activity toward MDA-MB-231 breast cancer cells. *Journal of Molecular Recognition*, 28-9-13, pp.155-165.
186. Rosen, M., 1978. Surfactants and Interfacial Phenomena. 1st edition. *John Wiley and Sons, Inc*; 322. Toronto.
187. Rosique, R., Rosique, M. and Farina Junior, J., 2015. Curbing inflammation in skin wound healing: A review. *International Journal of Inflammation*, 2015.
188. Sachan, N., Pushkar, S., Jha, A. and Bhattacharya, A., 2009. Sodium alginate: the wonder polymer for controlled drug delivery. *Journal of Pharmacy Research*, 2(8), pp.1191-1199.
189. Salamat-Miller, N., Chittchang, M. and Johnston, T., 2005. The use of mucoadhesive polymers in buccal drug delivery. *Advanced drug delivery reviews*, 57(11), pp.1666-1691.
190. Sambhakar, S., Singh, B., Paliwal, S. and Mishra, P., 2011. Niosomes as a potential carrier for controlled release of cefuroxime axetil. *Asian Journal of Biochemical and Pharmaceutical Research*, 1(1), pp.126-136.
191. Samyuktha, R. and Vedha, H., 2011. Niosomal Formulation of orlistat: formulation and *in vitro* evaluation. *International Journal of Drug Development Research*, 3(3), pp.300-311.
192. Sánchez, M., Aranda, F., Espuny, M., Marqués, A., Teruel, J., Manresa, Á. and Ortiz, A., 2007. Aggregation behaviour of a dirhamnolipid biosurfactant secreted by *Pseudomonas aeruginosa* in aqueous media. *Journal of Colloid and Interface Science*, 307(1), pp.246-253.
193. Scarlat, N., Dallemand, J., Monforti-Ferrario, F. and Nita, V., 2015. The role of biomass and bioenergy in a future bioeconomy: Policies and facts. *Environmental Development*, 15, 3-34.
194. Schwartz, H., and Mihic, E., 1973. Species and tissue differences in drug selectivity. In: Mihic, E. (Ed.), Drug resistance and selectivity biochemical and cellular basis, *Academic Press*, New York, pp. 413-449.
195. Seaman, S., 2006. Management of malignant fungating wounds in advanced cancer. *Seminars in Oncology Nursing*, 22(3), pp.185-193.
196. Šegota, S., 2006. Spontaneous formation of vesicles. *Advances in Colloid and Interface Science*, 121(1), pp.51-75.
197. Seydlová, G. and Svobodová, J., 2008. Review of surfactin chemical properties and the potential biomedical applications. *Open Medicine*, 3(2), pp.123-133. Available at:

<http://www.degruyter.com/view/j/med.2008.3.issue-2/s11536-008-0002-5/s11536-008-0002-5.xml>.

198. Shah, D. and Schulman, J., 1967. Influence of calcium, cholesterol, and unsaturation on lecithin monolayers. *Journal of Lipid Research*, 8(3), pp.215-226.
199. Shah, J., 2011. The history of wound care. *Journal of the American College of Certified Wound Specialists*, 3(3), pp.65-66.
200. Shao, L., Song, X., Ma, X., Li, H. and Qu, Y., 2012. Bioactivities of sophorolipid with different structures against human esophageal cancer cells. *Journal of Surgical Research*, 173(2), pp.286-291.
201. Shilpa, Srinivasan, B. and Chauhan, M., 2011. Niosomes as vesicular carriers for delivery of proteins and biologicals. *International Journal of Drug Delivery*, 3(1), pp.14-24.
202. Smith, J. and Haigh, J., 1974. The hitch-hiking effect of a favourable gene. *Genetical Research*, 23(01), pp.23-35.
203. Sotirova, A., Spasova, D., Galabova, D., Karpenko, E. and Shulga, A., 2008. rhamnolipid–biosurfactant permeabilising effects on gram-positive and gram-negative bacterial strains. *Current Microbiology*, 56(6), pp.639-644.
204. Sousa, M., Dantas, T., Feitosa, F., Alencar, A., Soares, S., Melo, V., Gonçalves, L. and Sant'ana, H., 2014. Performance of a biosurfactant produced by *Bacillus subtilis* LAMI005 on the formation of oil / biosurfactant / water emulsion: study of the phase behaviour of emulsified systems *Brazilian Journal of Chemical Engineering*, 3(3). pp. 613-623.
205. Stanley, F., Warner, A., Schneiderman, E. and Stalcup, A., 2009. Rapid determination of surfactant critical micelle concentrations using pressure-driven flow with capillary electrophoresis instrumentation. *Journal of Chromatography A*, 1216(47), pp.8431-8434.
206. Stewart, B. and Wild, C., 2014. World cancer report 2014. 2014. *Lyon CEDEX, France*.
207. Stipevic, T., Piljac, A. and Piljac, G., 2006. Enhanced healing of full-thickness burn wounds using dirhamnolipid. *Burns*, 32(1), pp.24-34.
208. Stohr, E., Bhandare, P., Peura, R. and Mendelson, Y., 1992. Quantitative FTIR spectrophotometry of cholesterol and other blood constituents and their interference with the in-vitro measurement of blood glucose. In *Bioengineering Conference, 1992., Proceedings of the 1992 Eighteenth IEEE Annual Northeast* (pp. 105-106). IEEE.
209. Szaraz, S., Oesterhelt, D. and Ormos, P., 1994. pH-induced structural changes in bacteriorhodopsin studied by Fourier transform infrared spectroscopy. *Biophysical Journal*, 67(4), pp.1706-1712.

210. Talsma, H., Van Steenberghe, M., Borchert, J. and Crommelin, D., 1994. A novel technique for the one-step preparation of liposomes and nonionic surfactant vesicles without the use of organic solvents. Liposome formation in a continuous gas stream: The 'Bubble' method. *Journal of Pharmaceutical Sciences*, 83(3), pp.276-280.
211. Tanaka, T., 1978. Collapse of gels and the critical endpoint. *Physical Review Letters*, 40(12), p.820.
212. Tang, J., Zhao, F., Gao, H., Dai, Y., Yao, Z., Hong, K., Li, J., Ye, W. and Yao, X., 2010. Characterisation and online detection of surfactin isomers based on HPLC-MSn analyses and their inhibitory effects on the overproduction of nitric oxide and the release of TNF- α and IL-6 in LPS-induced macrophages. *Marine Drugs*, 8(10), pp.2605-2618.
213. Tangri, P. and Khurana, S., 2011. Niosomes: formulation and evaluation. *International Journal*, 2229, p.7499.
214. Thanomsub, B., Pumeechockchai, W., Limtrakul, A., Arunrattiyakorn, P., Petchleelaha, W., Nitoda, T. and Kanzaki, H., 2006. Chemical structures and biological activities of rhamnolipids produced by *Pseudomonas aeruginosa* B189 isolated from milk factory waste. *Bioresource Technology*, 98(5), pp.1149-1153.
215. Thomas, S., 2000. Alginate dressings in surgery and wound management, Part 1. *Journal of Wound Care*, 9(2), pp.56-60.
216. Thomson, T., Hydrophilix, Llc, 2006. Comprising networks of open cell hydrophobic polyurethanes having pores on the surfaces and coatings of hydrophilic curable polyurethane emulsions on the surfaces. *U.S. Patent* 7, 048, 966.
217. Thorn, C., Oshiro, C., Marsh, S., Hernandez-Boussard, T., McLeod, H., Klein, T. and Altman, R., 2011. Doxorubicin pathways: pharmacodynamics and adverse effects. *Pharmacogenetics and Genomics*, 21(7), pp.440-446.
218. Toby, M., Johnson, J. and Dettmar, P., 1997. Factors affecting *in vitro* gastric mucoadhesion IV. Influence of tablet excipients, surfactants and salts on the observed mucoadhesion of polymers. *European Journal of Pharmaceutics and Biopharmaceutics*, 43(1), pp.65-71.
219. Tocco, I., Zavan, B., Bassetto, F. and Vindigni, V., 2012. Nanotechnology-based therapies for skin wound regeneration. *Journal of Nanomaterials*, 2012, p.4.
220. Tordova, K. and Lazarova, Z., 2008. Reversed micelle solvents as tools of enzyme purification and enzyme-catalysed conversion. *Biotechnology Advances*, 26(6), pp.516-532.

221. Tsai, W. and Chung, R., 2010. Viral hepatocarcinogenesis. *Oncogene*, 29(16), pp.2309-2324.
222. Uchechi, O., Ogbonna, J. and Attama, A., 2014. Nanoparticles for dermal and transdermal drug delivery. In *Application of Nanotechnology in Drug Delivery*. InTech.
223. Uchegbu, I. and Vyas, S., 1998. Non-ionic surfactant based vesicles (niosomes) in drug delivery. *International Journal of Pharmaceutics*, 172(1), pp.33-70.
224. Vandamme, T. and Brobeck, L., 2005. Poly (amidoamine) dendrimers as ophthalmic vehicles for ocular delivery of pilocarpine nitrate and tropicamide. *Journal of Controlled Release*, 102(1), pp.23-38.
225. Van der Veer, W., Niessen, F., Ferreira, J., Zwiers, P., de Jong, E., Middelkoop, E. and Molema, G., 2011. Time course of the angiogenic response during normotrophic and hypertrophic scar formation in humans. *Wound Repair and Regeneration*, 19(3), pp.292-301.
226. Van Rijswijk, L., 2006. Ingredient- based wound dressing classification: A paradigm shift that is passé and in need of replacement. *Wound Care*, 15, pp.11-14.
227. Vater, J., Barbel, K., Wilde, C., Franke, P., Mehta, N. and Cameotra, S., 2002 Matrix assisted laser desorption ionisation-time of flight mass spectrometry of lipopeptide biosurfactants in whole cells and culture filtrates of *Bacillus subtilis* C-1 isolated from petroleum sludge. *Applied and Environmental Microbiology*, 68(12), pp.6210-6219.
228. Vlachou, M., Naseef, H., Efentakis, M., Tarantili, P. and Andreopoulos, A., 2001. Swelling properties of various polymers used in controlled release systems. *Journal of Biomaterials Applications*, 16(2), pp.125-138.
229. Waddad, A., Abbad, S., Yu, F., Munyendo, W., Wang, J., Lv, H. and Zhou, J., 2013. Formulation, characterisation and pharmacokinetics of Morin hydrate niosomes prepared from various nonionic surfactants. *International Journal of Pharmaceutics*, 456(2), pp.446-458.
230. Wang, R., Zheng, S. and Zheng, Y., 2011. Polymer matrix composites and technology. Elsevier.
231. Watson, G., 2005. Pharmaceutical Analysis: A textbook for pharmacy students and pharmaceutical chemists. pp. 49–71.
232. Wartewig, S. and Neubert, R., 2005. Pharmaceutical applications of mid-IR and Raman spectroscopy. *Advanced Drug Delivery Reviews*, 57(8), pp.1144-1170.
233. World Health Organisation (WHO). Cancer global facts & figures. <http://www.who.int/topics/cancer/en/>. (Accessed in December 2016).

234. Williams, S. and Brodbelt, J., 2004. MS n characterisation of protonated cyclic peptides and metal complexes. *Journal of the American Society for Mass Spectrometry*, 15(7), pp.1039-1054.
235. Yeh, J., Du, S., Tortajada, A., Paulo, J. and Zhang, S., 2005. Peptergents: Peptide detergents that improve stability and functionality of a membrane protein, glycerol-3-phosphate dehydrogenase. *Biochemistry*, 44(51), pp.16912-16919.
236. Yoshioka, T., Sternberg, B. and Florence, A., 1994. Preparation and properties of vesicles (niosomes) of sorbitan monoesters (Span 20, 40, 60 and 80) and a sorbitan triester (Span 85). *International journal of pharmaceutics*, 105(1), pp.1-6.
237. Zhao, J., Wu, Y., Alfred, A.T., Xin, X. and Yang, S., 2013. Chemical structures and biological activities of rhamnolipid biosurfactants produced by *Pseudomonas aeruginosa* M14808. *Journal of Chemical and Pharmaceutical Research*, 5(12), pp.177-182.
238. Zouari, R., Moalla-Rekik, D., Sahnoun, Z., Rebai, T., Ellouze-Chaabouni, S. and Ghribi-Aydi, D., 2016. Evaluation of dermal wound healing and *in vitro* antioxidant efficiency of *Bacillus subtilis* SPB1 biosurfactant. *Biomedicine & Pharmacotherapy*, 84, pp.878-891
239. Zunino, F., Pratesi, G. and Perego, P., 2001. Role of the sugar moiety in the pharmacological activity of anthracyclines: Development of a novel series of disaccharide analogs. *Biochemical Pharmacology*, 61, pp.933-938.
240. zur Hausen, H., 2009. The search for infectious causes of human cancers: Where and why (Nobel Lecture). *Angewandte Chemie - International Edition*, 48(32), pp.5798-5808.

CHAPTER 9 APPENDIX

9.1 SUPPLEMENTARY INFORMATION

SUPPLEMENTARY DATA – CHAPTER 3

A3.1 *Growth curves*

In these studies MTT assay was optimised under various conditions before the commencement of dose and time dependent studies. Dose and time dependent studies involve increasing the dose and altering time intervals to identify the maximum tolerable dose at which a particular compound would not be toxic to normal cells. The impact of the four selected BSs on their cellular growth characteristics were then investigated. The cell growth curves are applied in the evaluation of the characteristics of cell growth, which shows a lag-phase immediately after culturing the cells in 96 well plates. Subsequently, the cell enters into exponential growth referred to as the log-phase, in which the cell population doubles at a characteristic rate defined as doubling time (DT) (characteristic for each cell line). Therefore, the effects of drugs and chemical agents that stimulate or inhibit cell growth can be studied. Finally, when the cell population is very dense and all the substrate has been metabolised, the cells enter into a stationary phase, where the rate of growth drops to almost zero (Freshney, 2006). There was generally a good correlation between the TB and MTT growth curves of HEK 293, although TB showed a faster log phase from 168-192 h corresponding to a more distinct rate of decay. This behaviour could not be observed in the cellular-growth curve determined by MTT assays. A possible explanation of this behaviour is the relative subjectivity of visual cell counting with the TB exclusion method. These notwithstanding, the TB method has some advantages over measurement of absorbance on spectrophotometers, the main one being its utility for observation of cell morphology and detection of culture contaminants. The TB test method is also simple and inexpensive; it provides a rapid means of assessing cell viability and allows comparison of suspension homogeneity (Graves *et al.*, 2006; Lu *et al.*, 2009).

After the first 50 h of incubation, the cellular growth began in an exponential fashion in the cell lines. THP-1 line showed the highest doubling time (DT) followed by MCF-7 and then HEK 293. From the onset of plating, THP-1 did not manifest the lag phase, however, it was the only line to demonstrate the stationary phase of cell growth, while the other cell lines only manifested the lag and log-phases. The THP-1 line, started exponential growth 4 h from the onset of plating. It is important to note that the concentration (2.5×10^5) at which THP-1 cells were seeded in comparison with 5×10^4 and 1×10^5 for HEK 293 and MCF-7 lines respectively, was responsible for the acceleration of the growth phase. It is entirely possible that changes in respective cell densities may result in growth phase variations. However, at these particular seeded densities, the lag-phase was observed for MCF-7 and HEK 293 cell lines during the first 24 h of incubation. After this period, the log-phase data

indicate that the growth is more remarkable for THP-1 and MCF-7 lines than for HEK 293, though it should be noted that the concentration at which THP-1 cells were seeded was higher than those of MCF-7 and HEK 293. Generally, the DT result could depend on three main factors: cellular system type in culture (cancerous versus non-cancerous); type of tissue and the species origin. THP-1 and MCF-7 lines registered DT values of 24 and 48 h by TB and MTT assays respectively. THP-1 cell lines are non-adherent cells therefore carrying out the optimised MTT assay was challenging. To carry out MTT in a single plate would require daily centrifugation on succeeding cells which may compromise the seeded population of cells. The alternative of plating cells in different culture plates would be equally unreliable, costly and negate the experimental data. As a result, TB was used to analyse the growth curve, however the adherent nature of THP-1 precludes the need for trypsinisation which is an added advantage.

SUPPLEMENTARY TABLES – CHAPTER 3

Table A3.1. Assignment of various molecules (functional groups) BSs based on vibrational peaks by ATR-FTIR analysis

95% Rhamnolipids (BS1a)	90% Rhamnolipids (BS1b)	Surfactin (BS2)	Sophorolipids (BS3)
3335 cm ⁻¹	3331 cm ⁻¹	3300 cm ⁻¹	3406 cm ⁻¹
2925-2855 cm ⁻¹	2926-2856 cm ⁻¹	2957-2927 cm ⁻¹	2927-2856 cm ⁻¹
1731 cm ⁻¹	1740 cm ⁻¹	1719 cm ⁻¹	1744 cm ⁻¹
1457-1380 cm ⁻¹	1445-1370 cm ⁻¹	1643 cm ⁻¹	1451 cm ⁻¹
1303-1049 cm ⁻¹	1232-1034 cm ⁻¹ (shoulder)	1232-1034 cm ⁻¹ (shoulder)	1232 cm ⁻¹
917-981 cm ⁻¹	916 cm ⁻¹	1467-1387 cm ⁻¹ (shoulder)	1166 cm ⁻¹
838 cm ⁻¹	806-838 cm ⁻¹	3300 cm ⁻¹	1071 cm ⁻¹

Table A3.2. Assignment of various molecules present in BSs molecules based on possible intermolecular interactions as analysed by ATR-FTIR analysis

95% Rhamnolipids (BS1a)	90% Rhamnolipids (BS1b)	Surfactin (BS2)	Sophorolipids (BS3)
OH due to hydrogen bonding),	OH due to hydrogen bonding),	N-H stretch due to peptide residues	OH
CH ₃ , CH ₂ and CH aliphatic bond stretch	CH ₃ , CH ₂ and CH aliphatic bond stretch	CH ₃ , CH ₂ and CH aliphatic bond stretch	CH ₃ , CH ₂ and CH methylene group stretch
C=O stretch due to the ester functional group	C=O stretch due to the ester functional group	C=O stretch due to the ester functional group	C=O stretch due to lactone ester or acids
O-H bands bending in the carboxylic acid group	O-H bands bending in the carboxylic acid group	O-H bands bending in the carboxylic acid group	C-O-H plane binding of carboxylic acids
C-O-C stretching in the rhamnose	C-O-C stretching in the rhamnose	CO-N stretch due to amide group	C=O absorption band due to acetyl esters
Pyranyl I sorption band	Pyranyl I sorption band	N-H stretch due to peptide residues	C-O of C (-O)-O-C band due to lactones
α -pyranyl II sorption	α -pyranyl II sorption	CH ₃ , CH ₂ and CH aliphatic bond stretch	C-O from C-O-H stretch from sophorose sugars

Table A3.3. Mass peaks obtained for surfactin and homologues assigned from literature

[M+H] ⁺	Orientation of surfactin homologues	References
995	C-13 β -OHFA-E-L-L-V-D-L-V	Kowall <i>et al.</i> , 1998 ; Peypoux <i>et al.</i> , 1991; Vater <i>et al.</i> , 2002,
	C-13 β -OHFA-E-I-L-V-D-L-V	Kowall <i>et al.</i> , 1998
	C-12 β -OHFA-E-I-L-V-D-L-L	Peypoux <i>et al.</i> , 1991
	C-14 β -OHFA-E-I-L-A-D-L-L	Peypoux <i>et al.</i> , 1994
1009	C-14 β -OHFA-E-L-L-V-D-L-V	Kowall <i>et al.</i> , 1998 Peypoux <i>et al.</i> , 1991
	C-16 β -OHFA-E-I-L-A-D-L-L	Peypoux <i>et al.</i> , 1994
1023	C-15 β -OHFA-E-L-L-V-D-L-V	Kowall <i>et al.</i> , 1998 Peypoux <i>et al.</i> , 1991
	C-15 β -OHFA-E-I-L-V-D-L-V	Kowall <i>et al.</i> , 1998
1037	C-14 β -OHFA-E-I-L-I-D-L-I	Grangemard <i>et al.</i> , 1997 Kowall <i>et al.</i> , 1998
	C-15 β -OHFA-E-L-L-V-D-L-L	Grangemard <i>et al.</i> , 1997
	C-15 β -OHFA-E-I-L-V-D-L-L	Kowall <i>et al.</i> , 1998
1051	C-15 β -OHFA-E-I-L-I-D-L-I	Grangemard <i>et al.</i> , 1997 Kowall <i>et al.</i> , 1998
	C-16 β -OHFA-E-I-L-V-D-L-L	Grangemard <i>et al.</i> , 1997 Kowall <i>et al.</i> , 1998

Table A3.4. Chromatogram peaks obtained for BS3 isomers

Isomers	R.T. (mins)	<i>m/z</i>
1	1.96	689, 706, 707, 711, 713
2	2.26	687, 688, 707, 709, 710
3	2.34	687, 689, with coeluting <i>m/z</i> at 706, 707, 708
4	2.73	689, 706, with coeluting <i>m/z</i> at 711, 712, and 712 and 1183
5	2.97	two coeluted <i>m/z</i> at 689, another two sodiated adducts at 711 and 712 and 1181
6	3.03	<i>m/z</i> at 689, two coeluted <i>m/z</i> at 707 and a sodiated adduct at 711
7	3.21	689, 706, 711 and 1188

SUPPLEMENTARY FIGURES - CHAPTER 3

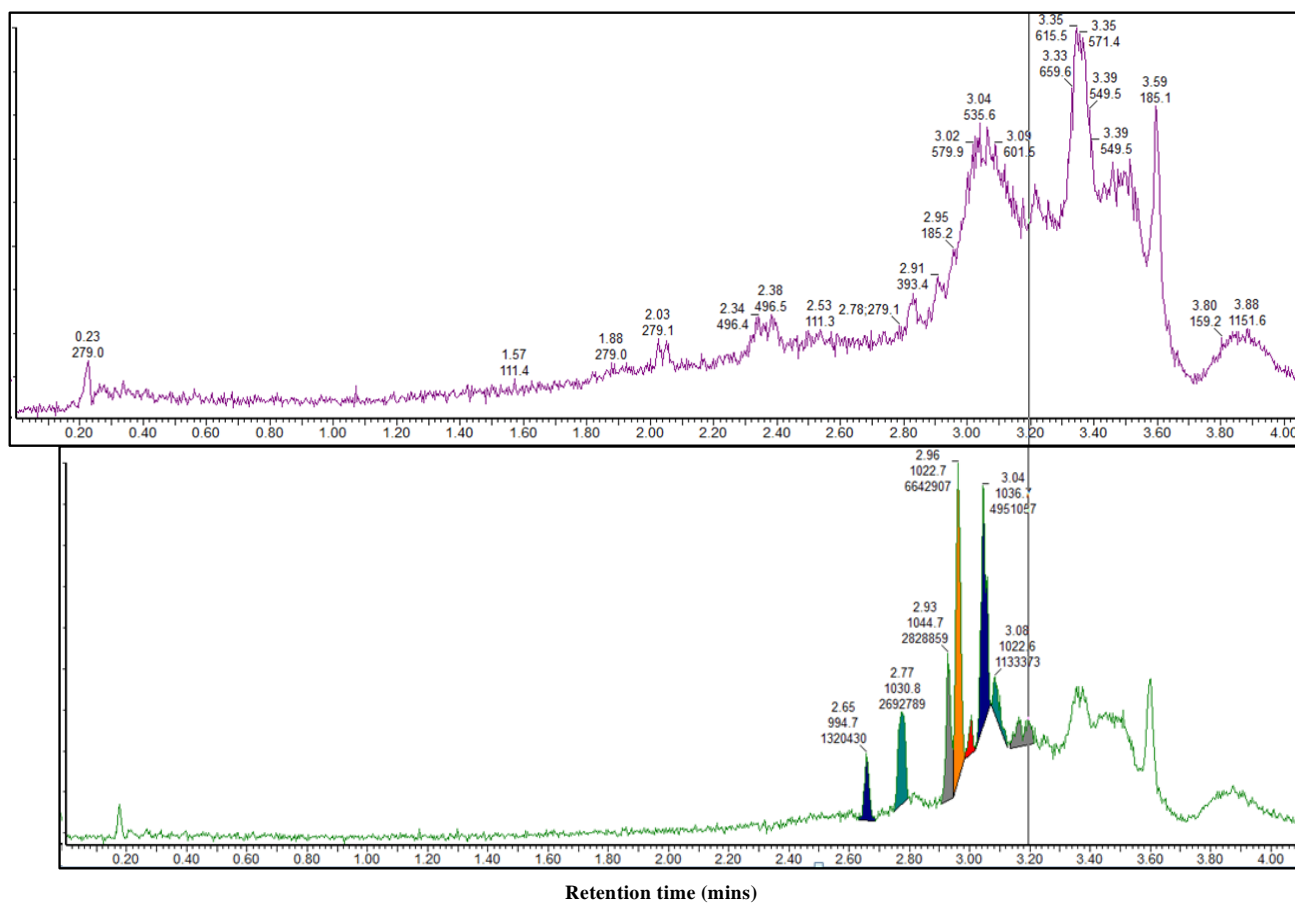


Figure A3.1. Low voltage ion chromatogram of surfactin.

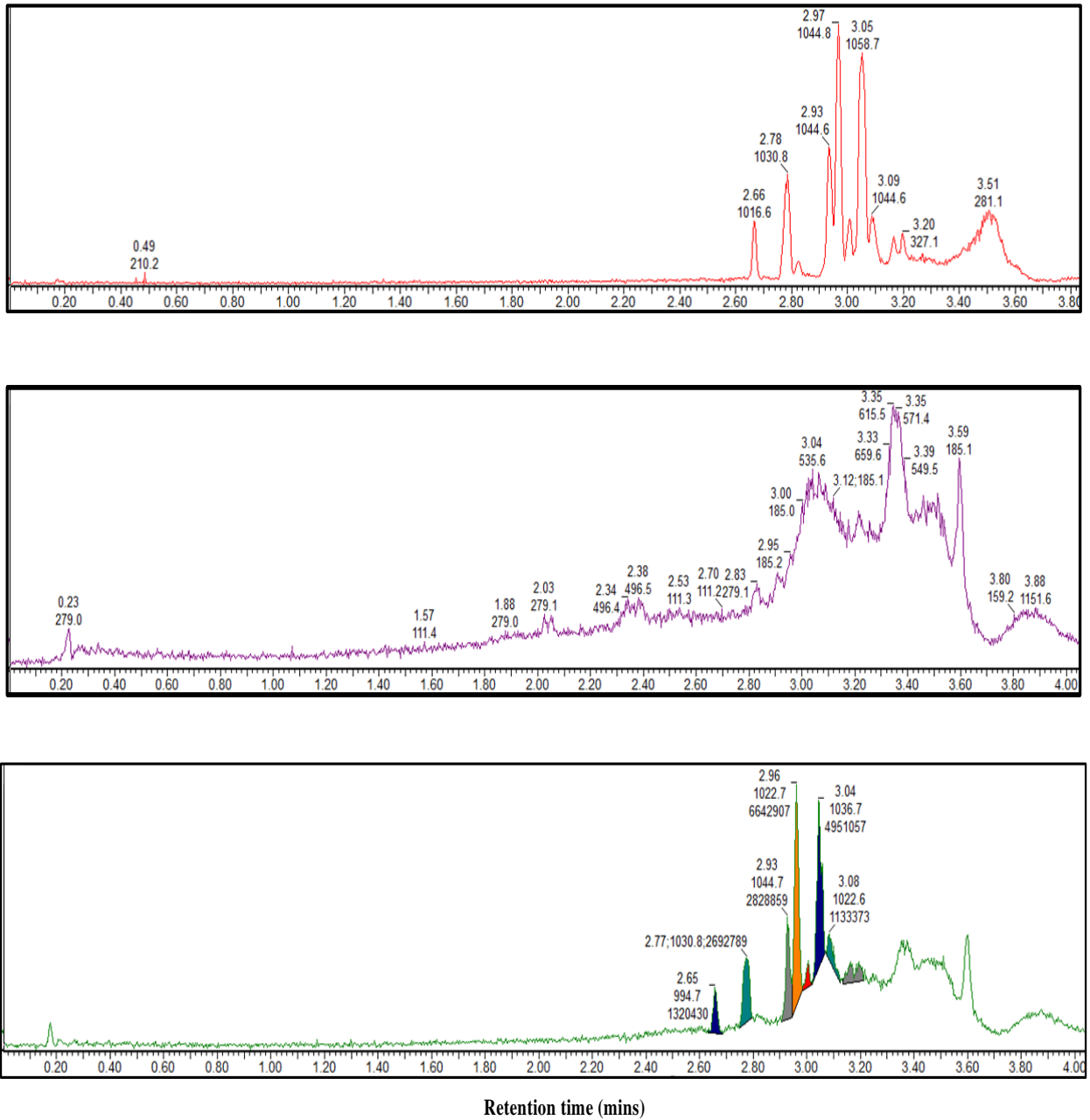
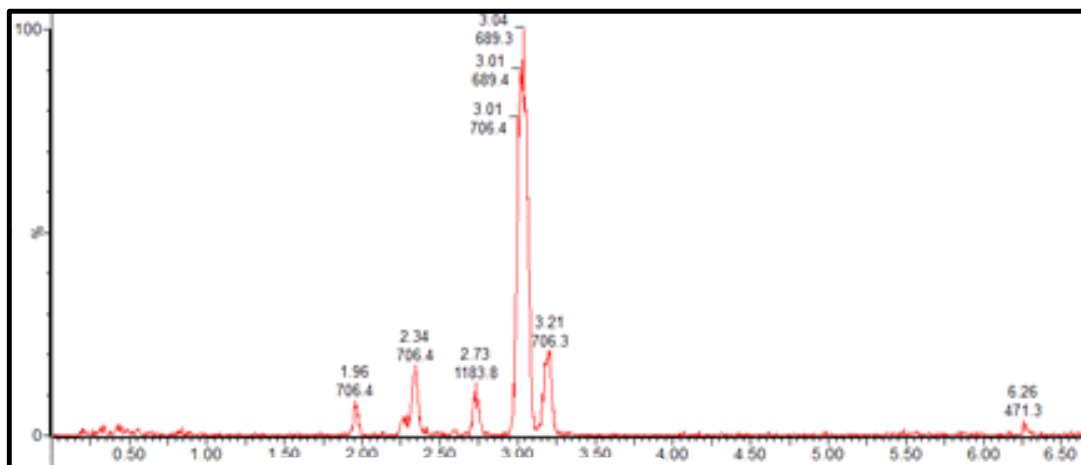
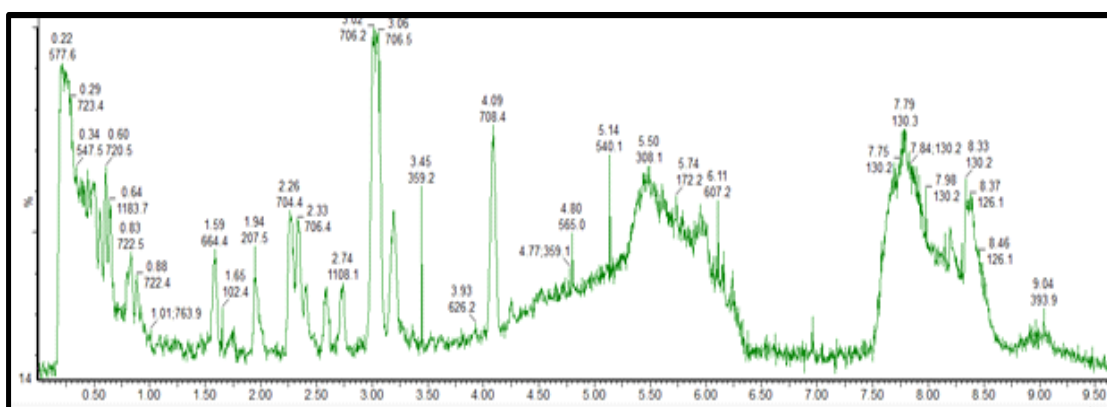


Figure A3.2. High voltage ion chromatogram of surfactin.



Retention time (mins)

(a)



Retention time (mins)

(b)

Figure A3.3: (a) LC-MS chromatogram for BS3 and (b) total ion chromatogram for BS3.

SUPPLEMENTARY TABLES - CHAPTER 4

Table A4.1. Effect of temperature on particle size intensities of 1', 4''-sophorolactone 6', 6''-diacetate loaded niosomes $n = 3$

BS3:S60:C HL (mM)	60°C			70°C			80°C		
	Peak 1 (%)	Peak 2 (%)	Peak 3 (%)	Peak 1 (%)	Peak 2 (%)	Peak 3 (%)	Peak 1 (%)	Peak 2 (%)	Peak 3 (%)
0:10:0	87.0 (±9)	13 (±6)	-	98 (±1)	2 (±1)	-	100	-	-
0:10:10	100	-	-	100	-	-	-	-	-
0:10:20	100 (±0)	-	-	89 (±5)	11 (±5)	-	91 (±9)	9 (±1)	5 (±3)
7.8:2.5:0	100	-	-	-	-	-	79 (±3)	19 (±1)	6
7.8:2.5:10	100 (±0)	-	-	-	-	-	87 (±10)	12 (±9)	1.5
7.8:2.5:20	85 (±2)	15 (±2)	-	-	-	-	93 (±7)	11 (±4)	-
5:5:0	88 (±4)	12 (±4)	-	83 (±8)	17 (±8)	-	67 (±3)	31 (±0)	5
5:5:10	92 (±5)	8	-	91 (±9)	23 (±19)	-	88 (±2)	10 (±1)	2
5:5:20	100	-	-	84.1 (±8)	16 (±8)	-	89 (±14)	17 (±15)	-
10:0:0	100	-	-	98 (±3)	6	-	91.4	9	-
10:0:10	78	22	-	73 (±18)	27 (±18)	-	96 (±6)	8	-
10:0:20	100	-	-	85 (±16)	15 (±16)	-	73 (±19)	27 (±19)	-

Table A4.2. Effect of longer duration of sonication (40 min) on the zeta potential of selected 1', 4''-sophorolactone 6', 6''-diacetate loaded niosomes at 60°C *n* = 3

BS3:S60:CHL	Unsonicated	Zeta potential (mV) 40 min (sonication)
00:10:00	-	-25.9 (\pm 4.68)
00:10:10	-	-61.81 (\pm 7.81)
00:10:20	-	-66.7 (\pm 7.31)
7.8:2.5:0	-35.5 (\pm 5.57)	-35.5 (\pm 5.57)
7.8:2.5:10	-	-1.10 (\pm 3.51)
7.8:2.5:20	-	-58.8 (\pm 11.1)
5.0:5.0:0	-	-41.1 (\pm 6.85)
5.0:5.0:10	-	-48.0 (\pm 7.77)
5.0:5.0:20	-	-54.2 (\pm 7.66)

Table A4.3. Comparison of the Zeta potential of buffer based biosurfactant loaded niosomes *n* = 3

BSs loading (mg/l)	BS1c niosomes (mV)	BS1c vesicles (mV)	BS4a niosomes (mV)	BS4b niosomes (mV)	BS2 niosomes (mV)	BS3 niosomes (mV)
8.0 x 10 ⁻²	-33.23 (\pm 1.07)	-	-34.17 (\pm 4.3)	-0.01 (\pm 0.0)	-0.01 (\pm 0.0)	-
1.0 x 10 ⁻¹	-34.40 (\pm 2.2)	-14.27 (\pm 3.7)	-32.37 (\pm 1.2)	-34.57 (\pm 1.0)	-32.70 (\pm 2.6)	-34.13 (\pm 1.9)
1.65 x 10 ⁻¹	-	-	-	-	0.00 (\pm 0.0)	-
2.0 x 10 ⁻¹	-35.27 (\pm 3.1)	-15.37 (\pm 4.02)	-32.43 (\pm 1.6)	-34.20 (\pm 2.5)	-33.33 (\pm 2.8)	-
3.0 x 10 ⁻¹	-31.63 (\pm 3.2)	-19.57 (\pm 8.4)	-0.03 (\pm 0.0)	-34.67 (\pm 1.8)	0.00 (\pm 0.0)	-
4.0 x 10 ⁻¹	-34.23 (\pm 3.6)	-7.16 (\pm 0.8)	-	-33.37 (\pm 1.7)	-	-35.53 (\pm 0.8)
6.0 x 10 ⁻¹	-33.90 (\pm 2.69)	-	-33.2 (\pm 3.2)	-39.40 (\pm 4.5)	-12.33 (\pm 11.69)	-34.50 (\pm 1.0)

Table A4.4. Effect of temperature on conductivity (by conductivity meter) of undiluted 1', 4''-sophorolactone 6', 6''-diacetate loaded niosomes $n = 3$

BS3:S60:CHL	Conductivity ($\mu\text{S/cm}$)				Temperature trend ($^{\circ}\text{C}$)
	60 $^{\circ}\text{C}$	70 $^{\circ}\text{C}$	80 $^{\circ}\text{C}$		
0:10:10	16.28 (± 3.95) $\times 10^{-3}$	17.47 (± 2.74) $\times 10^{-3}$	26.83 (± 2.55) $\times 10^{-3}$		60<70<80
5.0:5.0:10	26.57 (± 1.18) $\times 10^{-3}$	19.69 (± 1.39) $\times 10^{-3}$	78.95 (± 0.78) $\times 10^{-3}$		70<60<80
7.8:2.5:10	32.57 (± 2.14) $\times 10^{-3}$	27.23 (± 2.04) $\times 10^{-3}$	89.03 (± 1.70) $\times 10^{-3}$		70<60<80
10:0:0	40.00 (± 1.31) $\times 10^{-3}$	31.17 (± 1.18) $\times 10^{-3}$	38.10 (± 1.41) $\times 10^{-3}$		70<80<60

Table A4.5. Effect of sonication on the conductivity (by DLS) of selected 1', 4''-sophorolactone 6', 6''-diacetate loaded niosomes at 60 $^{\circ}\text{C}$ and 80 $^{\circ}\text{C}$ $n = 3$

BS3:S60:CHL	60 $^{\circ}\text{C}$	60 $^{\circ}\text{C}$	60 $^{\circ}\text{C}$	80 $^{\circ}\text{C}$
	Unsonicated	3 min sonication	40 min sonication	3 min sonication
0:10:0	-	6.71 (± 4.04) $\times 10^{-3}$	-	-
0:10:10	2.05 (± 0.25) $\times 10^{-3}$	8.43 (± 1.30) $\times 10^{-3}$	-	7.73 (± 0.23) $\times 10^{-3}$
0:10:20	-	4.98 (± 3.39) $\times 10^{-3}$	-	-
7.8:2.5:0	-	3.83 (± 0.78) $\times 10^{-3}$	-	-
7.8:2.5:10	-	5.98 (± 1.18) $\times 10^{-3}$	9.147 (± 4.68) $\times 10^{-3}$	10.38 (± 9.56) $\times 10^{-3}$
7.8:2.5:20	-	7.78 (± 0.66) $\times 10^{-3}$	-	-
5.0:5.0:0	4.67 (± 6.96) $\times 10^{-3}$	7.49 (± 8.75) $\times 10^{-3}$	-	-
5.0:5.0:10	-	8.33 (± 6.99) $\times 10^{-3}$	-	8.92 (± 9.08) $\times 10^{-3}$
5.0:5.0:20	-	9.10 (± 12.03) $\times 10^{-3}$	-	-
10.0:0:0	-	10.75 (± 11.59) $\times 10^{-3}$	-	-
10.0:0:10	-	17.50 (± 7.88) $\times 10^{-3}$	-	9.72 (± 4.00) $\times 10^{-3}$
10.0:0:20	-	10.48 (± 12.14) $\times 10^{-3}$	-	-

Table A4.6. Comparison of the DLS conductivities of biosurfactant loaded niosomes $n = 3$

Concentration of BSs	BS1c niosomes (mS/cm)	BS1c vesicles (mS/cm)	BS4a niosomes (mS/cm)	BS4b niosomes (mS/cm)	BS2 niosomes (mS/cm)	BS3 niosomes (mS/cm)
8.0×10^{-2}	3.12×10^{-3} (± 0.01)	-	23.63 (± 2.68)	2.0×10^{-3} (± 0.00)	3.0×10^{-3} (± 0.00)	-
1.0×10^{-1}	19.40 (± 1.93)	21.73 (± 1.70)	19.67 (± 1.95)	20.07 (± 1.71)	24.33 (± 2.49)	21.93 (± 2.76)
2.0×10^{-1}	23.33 (± 2.25)	22.37 (± 2.36)	19.53 (± 1.86)	19.47 (± 1.81)	24.97 (± 2.72)	-
3.0×10^{-1}	22.57 (± 2.17)	20.10 (± 1.57)	6.0×10^{-3} (± 0.01)	19.63 (± 1.78)	2.0 (± 0.00)	-
4.0×10^{-1}	23.07 (± 2.42)	19.83 (± 1.97)	19.87 (± 1.81)	19.93 (± 1.97)	-	21.43 (± 2.04)
6.0×10^{-1}	24.93 (± 2.51)	-	24.27 (± 2.48)	19.07 (± 1.80)	23.07 (± 2.33)	22 (± 1.66)

Table A4.7. Effect of different concentrations of rhamnolipids (BS1c) loaded in four component niosomes analysed by ATR-FTIR

Peak number	8.0 x 10 ⁻² mg/l	1.0 x 10 ⁻¹ mg/l	2.0 x 10 ⁻¹ mg/l	3.0 x 10 ⁻¹ mg/l	4.0 x 10 ⁻¹ mg/l	6.0 x 10 ⁻¹ mg/l
1	3363	3370	3358	3371	3397	3390
2	-	-	-	-	2956	-
3	2918	2918	2918	2918	2917	2918
4	2850	2850	2850	2850	2850	2850
5	1736	1736	1736	1736	1736	1737
6	1467	1467	1467	1467	1467	1467
7	1378	1378	1378	1378	1378	1378
8	1163	1163	1163	1165	1167	1176
9	1057	1057	1058	1057	1057	1056
10	952	954	953	953	952	-
11	859	860	860	860	860	840
12	-	-	-	-	800	-
13	721	721	721	721	721	721
14	521	517	519	522	521	529

Table A4.8. Effect of different concentrations of rewoferm SL ONE (BS4a) loaded in four component niosomes analysed by ATR-FTIR

Peak number	8.0 x 10 ⁻² mg/l	1.0 x 10 ⁻¹ mg/l	2.0 x 10 ⁻¹ mg/l	3.0 x 10 ⁻¹ mg/l	4.0 x 10 ⁻¹ mg/l	6.0 x 10 ⁻¹ mg/l
1	3391	3398	3398	3398	3393	3398
2	2956	-	-	-	-	-
3	2917	2917	2917	2917	2917	2917
4	2850	2850	2850	2850	2850	2850
5	1737	1736	1736	1737	1736	1737
6	1467	1467	1467	1467	1467	1467
7	1378	1378	1378	1378	1378	1378
8	1168	1168	1168	1167	1164	1166
9	1057	1057	1057	1057	1057	1057
10	953	953	953	953	952	952
11	859	860	860	860	859	859
12	800	-	-	-	-	-
13	721	721	721	721	721	721
14	520	522	522	521	518	519

Table A4.9. Effect of different concentrations of rewoferm SL 446 (BS4b) loaded in four component niosomes analysed by ATR-FTIR

Peak number	8.0 x 10 ⁻² mg/l	1.0 x 10 ⁻¹ mg/l	2.0 x 10 ⁻¹ mg/l	3.0 x 10 ⁻¹ mg/l	4.0 x 10 ⁻¹ mg/l	6.0 x 10 ⁻¹ mg/l
1	3393		-	3361	3391	3371
2	2918		2917	2918	2917	2918
3	2850		2850	2850	2850	2850
4	1737		1735	1738	1737	1737
5	1467		1467	1467	1467	1467
6	1378		1379	1379	1378	1378
7	1164		1159	-	1163	-
8	1057		1059	1059	1057	1058
9	952		953	953	953	
10	859		858	859	859	864
11	800		-	-	800	
	721		721	721	721	721
12	-		-	-	-	
13	545		-		532	
14	517		516	518	-	513

Table A4.10. Effect of different concentrations of surfactin (BS2) mg/l loaded in four component niosomes analysed by ATR-FTIR

Peak number	8.0 x 10 ⁻² mg/l	1.0 x 10 ⁻² mg/l	1.65 x 10 ⁻¹ mg/l	2.0 x 10 ⁻¹ mg/l	3.0 x 10 ⁻¹ mg/l	6.0 x 10 ⁻¹ mg/l
1	3371	3386	3382	3392	3398	-
2	2917	2918	2918	2917	2918	2920
3	2850	2850	2850	2850	2850	2851
4	1737	1736	1735	1736	1737	1736
5	1467	1467	1467	1467	1467	1465
6	1378	1378	1378	1378	1378	-
7	1169	1168	1162	1168	1167	-
8	1059	1057	1057	1056	1057	1055
9	953	953	952	953	953	-
10	859	859	858	860	860	-
11	800	800	-	800	800	-
12	721	721	721	721	721	-
13	521	523	544	545	545	-
14	-	-	518	520	522	-

Table A4.11. Comparison of components (BS, S60, CHL, DCP) effect on 1.0×10^{-1} mg/l BS4a standard loaded in four and three component niosomes analysed by ATR-FTIR

Peak number	BS4a STD	1.0×10^{-1} mg/l BS4a 4CN	1.0×10^{-1} mg/l BS4a 3CN
1	3368	3398	3365
2	2928	2917	2918
3	2855	2850	2850
4	-	1736	1737
5	1641	-	-
6	1553	-	-
7	-	1467	1467
8	1415	-	-
9	-	1378	1378
10	1369	-	-
11	1247	-	-
12	1170	1168	-
13	1077	-	-
14	-	1057	1057
15	1034	-	-
16	-	953	985
17	-	860	863
18	-	721	721
19	-	522	524

Table A4.12. Comparison of components (BS, S60, CHL, DCP) effect on 1.0×10^{-1} mg/l BS2 standard loaded in four and three component niosomes analysed by ATR-FTIR

Peak number	BS2 STD	6.0×10^{-1} mg/l BS2 4CN	6.0×10^{-1} mg/l BS2 3CN
1	3300	-	3355
2	2957	-	-
3	2927	2920	2918
4	-	2851	2850
5	1719	1736	1734
6	1643	-	-
7	1467	1465	1467
8	1387	-	1378
9	1232	-	-
10	1034	1055	1058
11	-	-	983
12	-	-	863
13	-	-	721
14	-	-	523

Table A4.13. Composition of crystalline and amorphous phases of niosome formulation standards

STDs	Crystal phase (%)	Amorphous phase (%)	Trend
S60	71.18	28.82	DCP>CHL>S60
CHL	88.43	11.57	
DCP	96.3	3.7	
BS1a	95.95	4.05	
BS1b	95.32	4.66	
BS1c	36.36	63.64	
BS2	79.1	20.9	
BS3	74.85	25.15	BS1a/b>BS2>BS3

Table A4.14. Effect of temperature on the crystalline and amorphous phases of BS3 loaded niosomes

BS:S60:CH L (mM)	60°C	70°C	80°C	60°C	70°C	80°C	°C
	Crystal phase (%)	Crystal phase (%)	Crystal phase (%)	Amorphou s phase (%)	Amorphou s phase (%)	Amorphou s phase (%)	Crystallinit y Trend
0:10:0	77.44	-	69.36	22.56	-	30.64	70<60
0:10:10	88.33	76.55	75.07	11.67	23.45	24.93	80<70<60
0:10:20	77.08	90.29	86.05	22.92	9.71	13.95	60<80<70
5:5:00	72.14	74.37	70.25	27.86	25.63	29.77	80<60<70
5:5:10	84.7	76.39	78.16	15.3	23.61	21.84	70<80<60
5:5:20	74.61	79.62	82.68	25.39	20.39	17.32	60<70<80
7.8:2.5:0	68.05	74.07	70.25	31.95	25.93	29.75	60<80<70
7.8:2.5:10	76.35	72.82	72.49	23.65	27.18	27.51	80<70<60
7.8:2.5:20	83.99	82.54	82.43	16.01	17.46	17.57	80<70<60
10:0:00	71.25	71.49	69.48	28.75	28.51	30.52	80<60<70
10:0:10	77.55	80.7	75.84	22.45	19.3	24.16	80<60<70
10:0:20	80.4	86.38	76.56	19.6	13.62	23.44	80<60<70

Table A4.15. Effect of different types of biosurfactants on the crystalline and amorphous phases of BSs:NIO-DCP

Crystal phase (%)	8.0 x 10 ⁻² mg/l	1.0 x 10 ⁻¹ mg/l	1.65 x 10 ⁻¹ mg/l	2.0 x 10 ⁻¹ mg/l	3.0 x 10 ⁻¹ mg/l	4.0 x 10 ⁻¹ mg/l	6.0 x 10 ⁻¹ mg/l
BS1c	72.46	88.35	-	75.00	76.58	78.93	73.80
BS4a	75.65	84.77	-	74.37	75.81	76.17	78.01
BS4b	73.24	88.15	-	78.93	79.30	77.13	81.10
BS2	71.35	76.35	78.77	84.83	74.58	-	84.48
Amorphous phase (%)							
BS1c	27.53	11.65	-	25.00	23.42	21.07	26.20
BS4a	24.35	15.23	-	25.63	24.19	23.83	21.99
BS4b	26.77	11.85	-	21.07	20.7	22.87	18.90
BS2	28.65	23.66	21.23	15.17	25.42	-	15.52

SUPPLEMENTARY FIGURES – CHAPTER 4

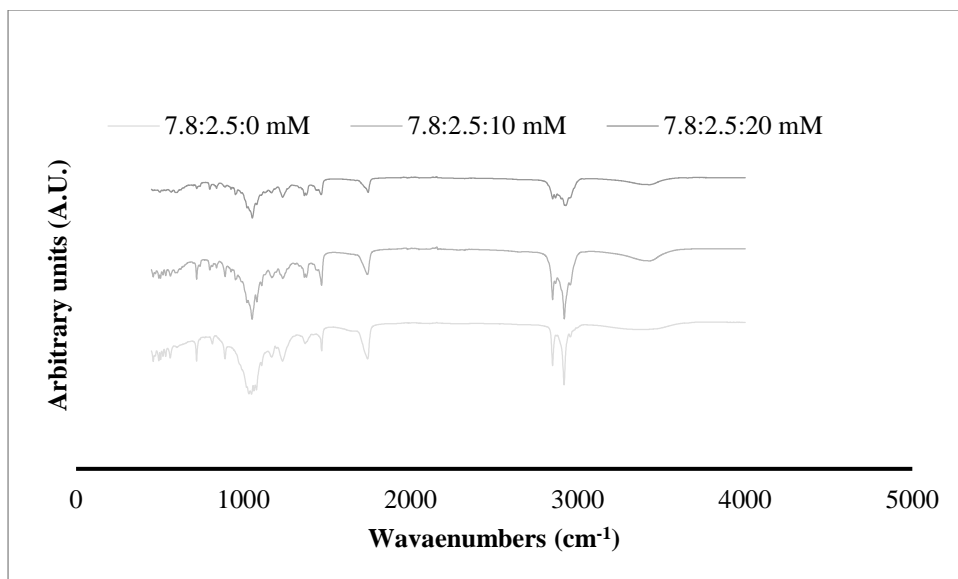


Figure A4.1. Effect of cholesterol ratios on representative ATR-FTIR spectra of BS3(7.8):S60(2.5):CHL(0-20) mM niosome formulated at 60°C.

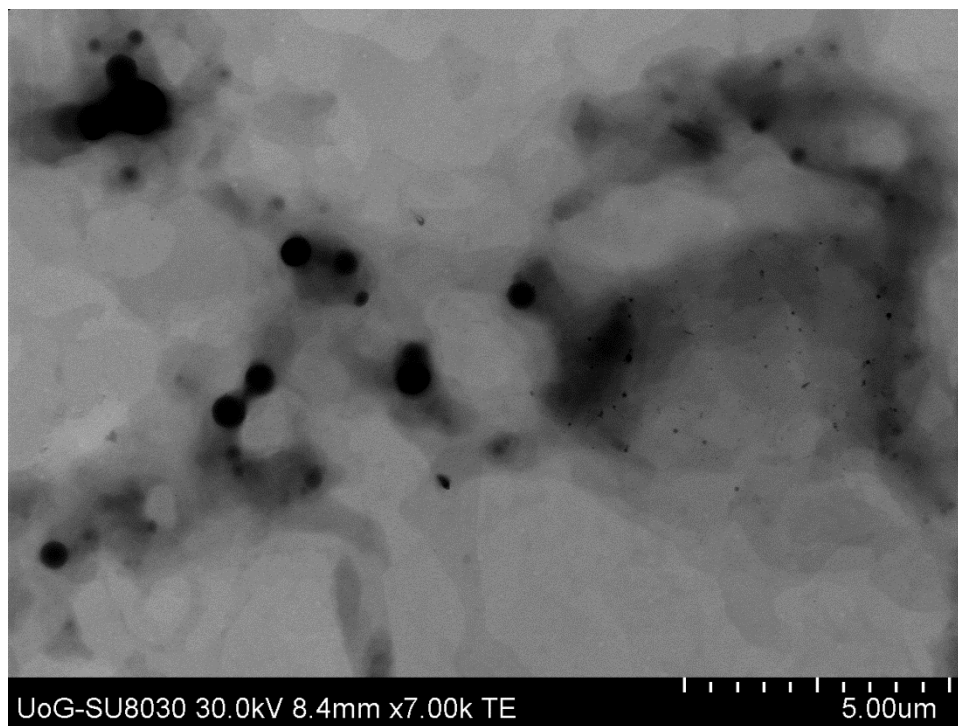


Figure A4.2. STEM images of unsonicated blank S60 with CHL niosomes BS3:S60:CHL 0:10:10 mM.

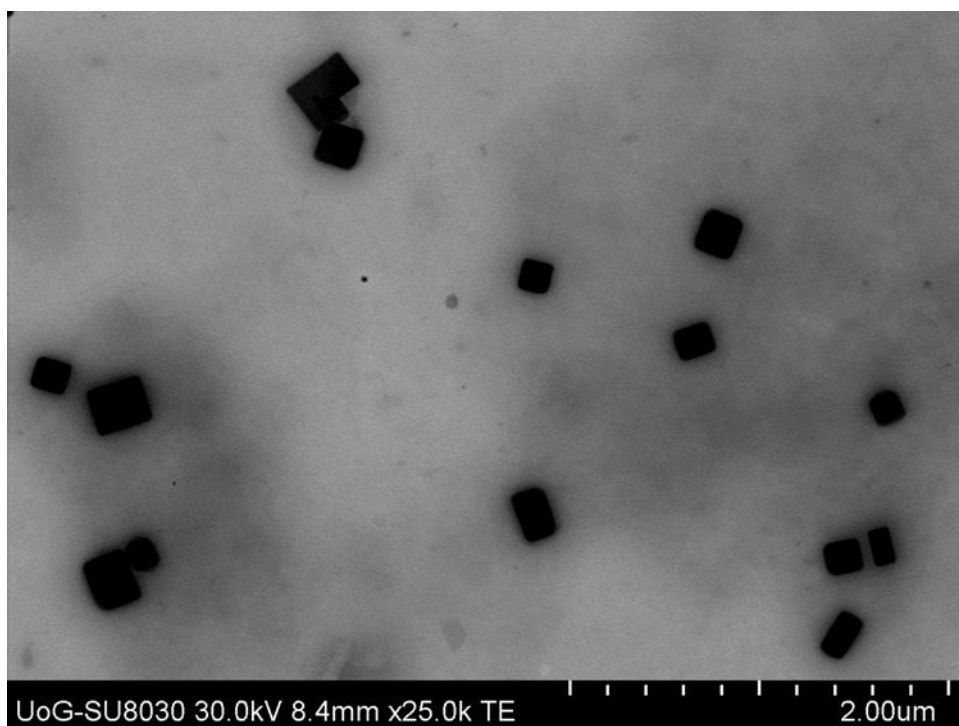


Figure A4.3. STEM images of BS3:S60:CHL 7.8:2.5:0 mM unsonicated niosomes.

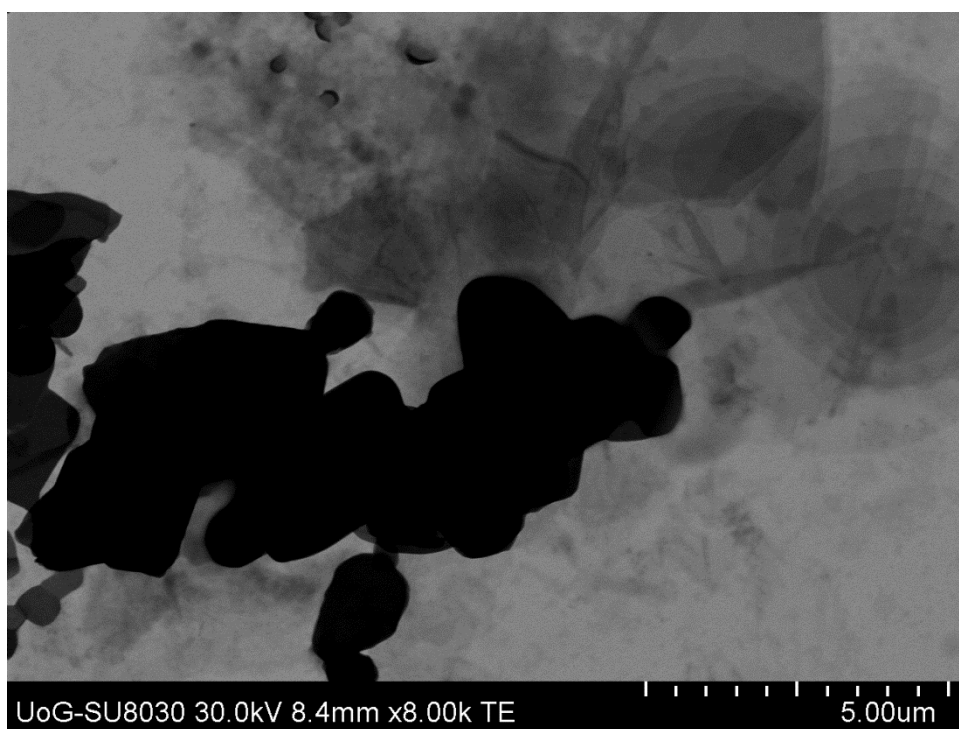


Figure A4.4. STEM images of BS3:S60:CHL 7.8:2.5:0 niosomes sonicated for 40 min.

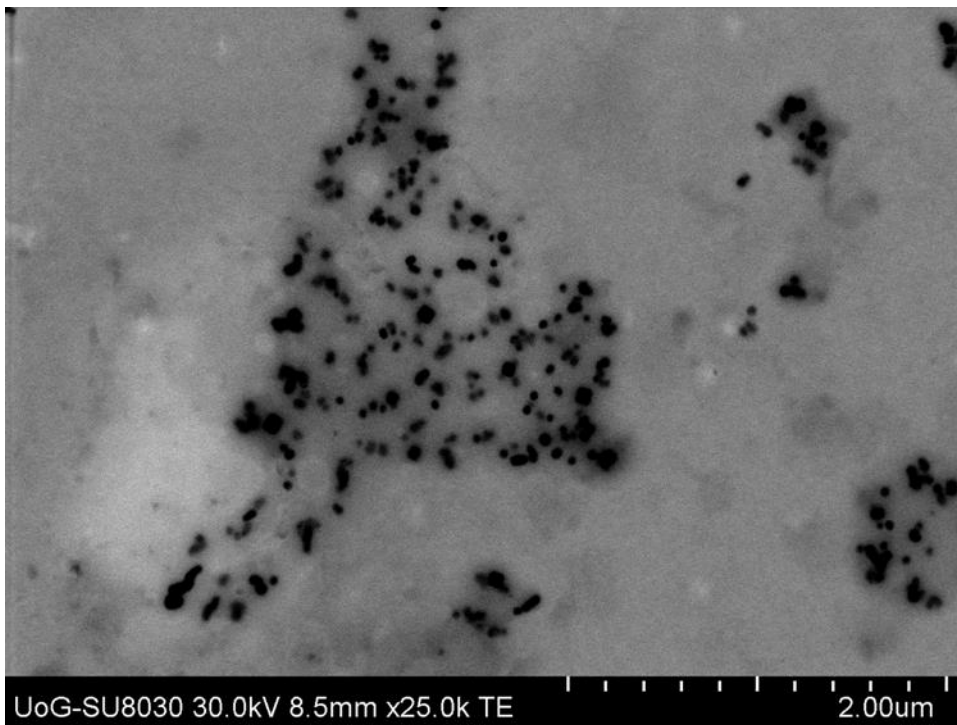


Figure A4.5. STEM images of unsonicated BS3:S60:CHL 7.8:2.5:10 mM niosomes.

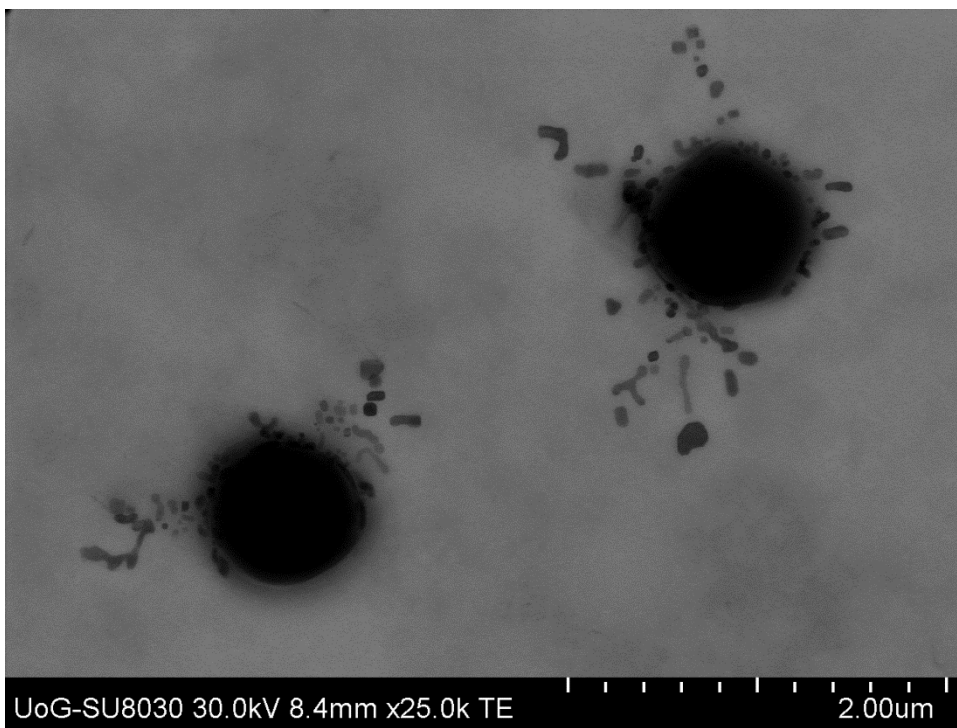


Figure A4.6. STEM images of unsonicated BS3:S60:CHL 5.0:5.0:0 mM niosomes.

SUPPLEMENTARY TABLES – CHAPTER 5

Table A5.1. Crystalline and amorphous phases of single, composite and BSs loaded wafers

1 (%, w/w)	1:0	0:1	1:1	1:2	1:3	2:1	3:1
Crystal phase	59.77	33.84	42.87	50.04	34.63	58.11	57.45
Amorphous phase	40.23	66.16	57.13	49.96	65.37	41.89	42.55
1.5 (%, w/w)							
Crystal phase	67.40	31.70	43.79	51.04	27.03	51.16	55.72
Amorphous phase	32.60	68.30	56.21	48.96	72.97	48.84	44.28
2 (%, w/w)							
Crystal phase	60.67	32.08	24.30	38.95	19.66	46.06	39.41
Amorphous phase	39.33	67.92	75.70	61.05	80.34	53.94	60.59
2.5%(1:0)							
Crystal phase	49.85	-	-	-	-	-	-
Amorphous phase	50.15	-	-	-	-	-	-
3 (%, w/w)							
Crystal phase	46.80	-	-	-	-	-	-
Amorphous phase	53.20	-	-	-	-	-	-
1.5%(1:3)	0.1% BS1c	0.2% BS1c	0.1% BS4a	5% BS4a	0.1% BS2		
Crystal phase	28.85	33.83	24.23	18.06	-	-	-
Amorphous phase	71.15	66.17	75.77	81.94	-	-	-
2%(1:2)							
Crystal phase	20.64	27.97	19.97	17.66	21.56	-	-
Amorphous phase	79.36	72.03	80.03	82.34	78.44	-	-

Table A5.2. Assignment of various functional groups present in pure CARR standard and 1 – 3%(1:0) CARR:SA wafers based on possible intermolecular/intramolecular interactions analysed by ATR-FTIR analysis

Peak number	Functional groups	Pure CARR standard	1%(1:0)	1.5%(1:0)	2%(1:0)	2.5%(1:0)	3%(1:0)
1	O-H stretching	3373	3367	3368	3370	3368	3369
2	Sulphates stretching			1373	1356	1374	1374
3	Sulphate ester	1221	1224	1224	1224	1224	1225
4	C-O stretching of pyranose ring		1157	1156	1155	1156	1156
5	3, 6 anhydrogalactose residue	925	926	925	925	925	925
6	Galactose 4-sulphate)	844	844	844	845	844	844

Table A5.3. Assignment of various functional groups present in pure SA standard and 1 – 2%(0:1) CARR:SA wafers based on possible intermolecular interactions as analysed by ATR-FTIR analysis

Peak number	Functional groups	Pure SA standard	1%(0:1)	1.5%(0:1)	2%(0:1)
1	O-H stretching	3244	3252	3252	3251
2	COO ⁻ asymmetric stretching	1595	1599	1598	1598
3	C-OH deformation vibration symmetric	1407	1408	1408	1408
4	C-O stretching		1084	1083	1083
5	C-C stretching	1025	1028	1028	1028

Table A5.4. Assignment of various functional groups present in 1 – 3%(1:1) CARR:SA wafers based on possible intermolecular interactions as analysed by ATR-FTIR analysis

Peak number	Functional groups	1%(1;1)	1.5%(1;1)	2%(1;1)
1	O-H stretching	3350	3350	3350
2	COO ⁻ asymmetric stretching	1602	1602	1602
3	C-OH deformation vibration symmetric	1415	1413	1413
4	Sulphate ester	1232	1235	1234
5	C-C stretching	1032	1030	1030
6	3, 6 anhydrogalactose residue	928	928	928
7	Galactose 4-sulphate	846	846	846

Table A5.5. Assignment of various functional groups present in 1 – 2%(1:2) CARR:SA wafers based on possible intermolecular interactions as analysed by ATR-FTIR analysis

Peak number	Functional groups	1%(1:2)	1.5%(1:2)	2%(1:2)
1	O-H stretching	3282	3351	3340
2	COO ⁻ asymmetric stretching	1599	1604	1600
3	C-OH deformation vibration symmetric	1411	1417	1412
4	Sulphate ester	1255	1232	1254
5	C-O stretching		1065	
6	C-C stretching	1029	1035	1029
7	3, 6 anhydrogalactose residue	931	927	930
8	Galactose 4-sulphate)		845	846

Table A5.6. Assignment of various functional groups present in 1 – 2%(1:3) CARR:SA wafers based on possible intermolecular interactions as analysed by ATR-FTIR analysis

Peak number	Functional groups	1%(1:3)	1.5%(1:3)	2%(1:3)
1	O-H stretching	3339	3337	3265
2	COO ⁻ asymmetric stretching	1601	1599	1599
3	C-OH deformation vibration symmetric	1412	1410	1409
4	Sulphate ester	1258	1255	1255
5	C-C stretching	1029	1029	1027
6	3, 6 anhydrogalactose residue	932	931	931

Table A5.7. Assignment of various functional groups present in 1 – 2%(2:1) CARR:SA wafers based on possible intermolecular interactions as analysed by ATR-FTIR analysis

Peak number	Functional groups	1%(2:1)	1.5%(2:1)	2%(2:1)
1	O-H stretching	3351	3340	3367
2	COO ⁻ asymmetric stretching	1603	1599	1603
3	C-OH deformation vibration symmetric	1417	1412	1417
4	Sulphate ester	1232	1253	1231
5	C-O stretching of pyranose ring			1156
6	C-O stretching			1065
7	C-C stretching	1029	1030	1034
8	3, 6 anhydrogalactose residue	927	929	926
9	Galactose 4-sulphate	845	846	845

Table A5.8. Assignment of various functional groups present in 1 – 2%(3:1) CARR:SA wafers based on possible intermolecular interactions as analysed by ATR-FTIR analysis

Peak number	Functional groups	1%(3:1)	1.5%(3:1)	2%(3:1)
1	O-H stretching	3368	3351	3369
2	Asymmetric -COO ⁻ stretching	1606	1603	1610
3	C-OH deformation vibration symmetric	1420	1417	1420
4	Sulphate ester	1231	1231	1230
5	C-O stretching of pyranose ring	1156	1154	1156
6	C-O stretching	1066		1064
7	C-C stretching	1035	1029	1037
8	3, 6 anhydrogalactose residue	926	927	927
9	Galactose-4-sulphate	845	844	845

SUPPLEMENTARY FIGURES – CHAPTER 5

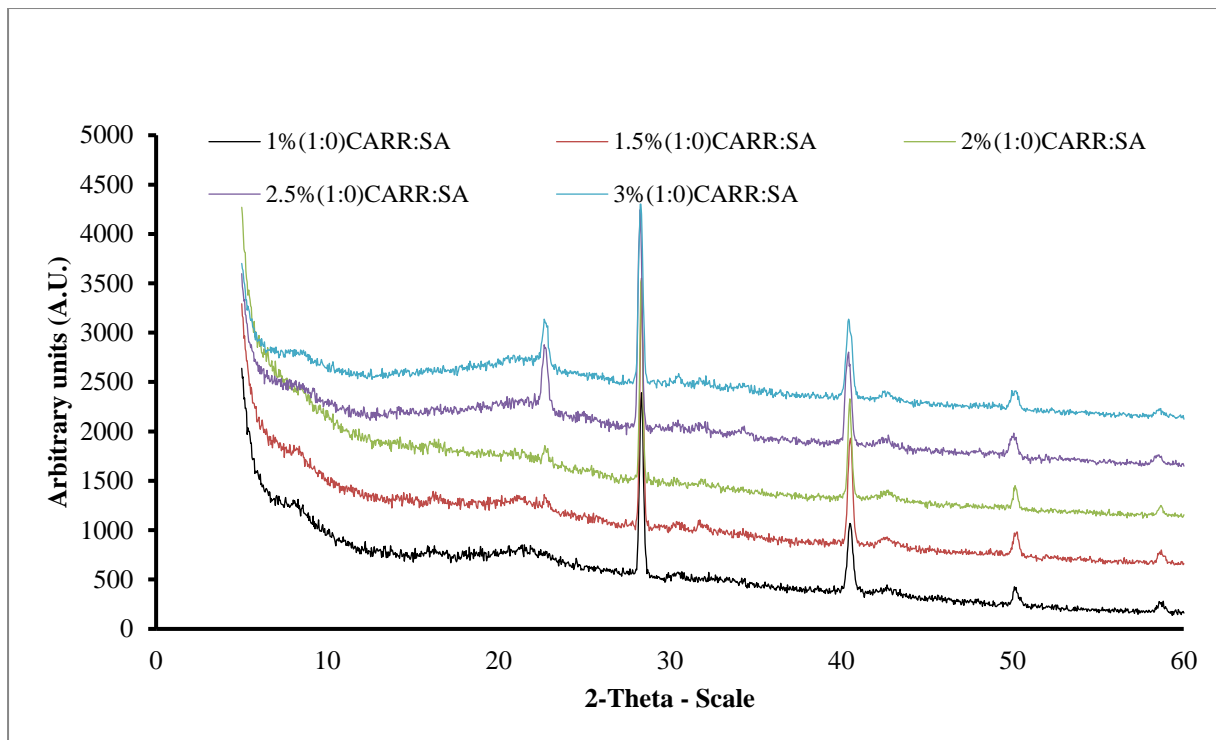


Figure A5.1. XRD diffractograms of 1 - 3%(1:0) CARR:SA.

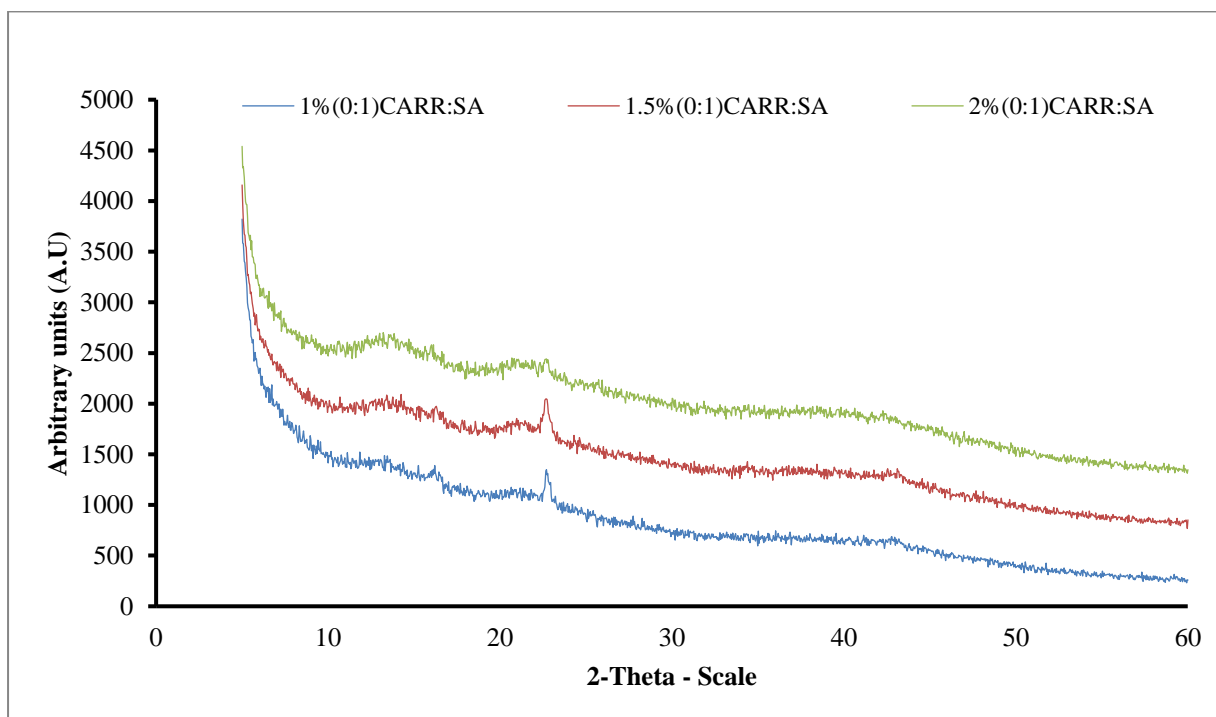


Figure A5.2. XRD diffractograms of 1 - 2%(0:1) CARR:SA.

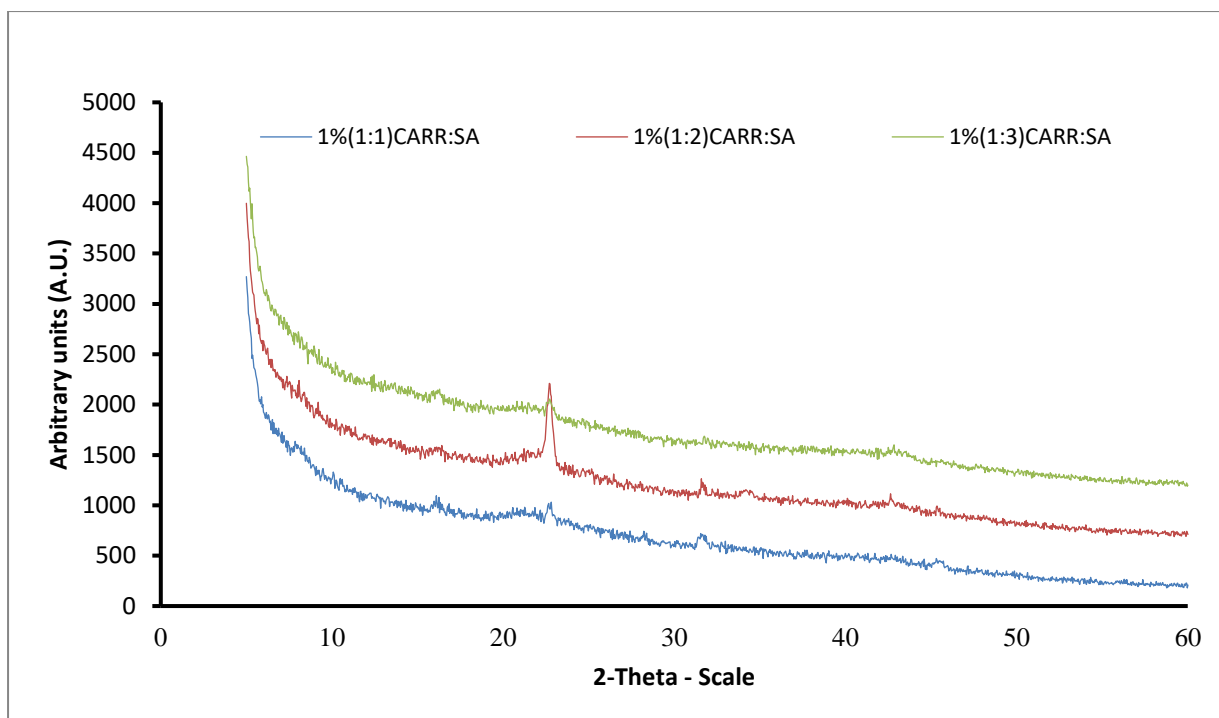


Figure A5.3. XRD diffractograms of 1%(1:1,1:2 and 1:3) CARR:SA.

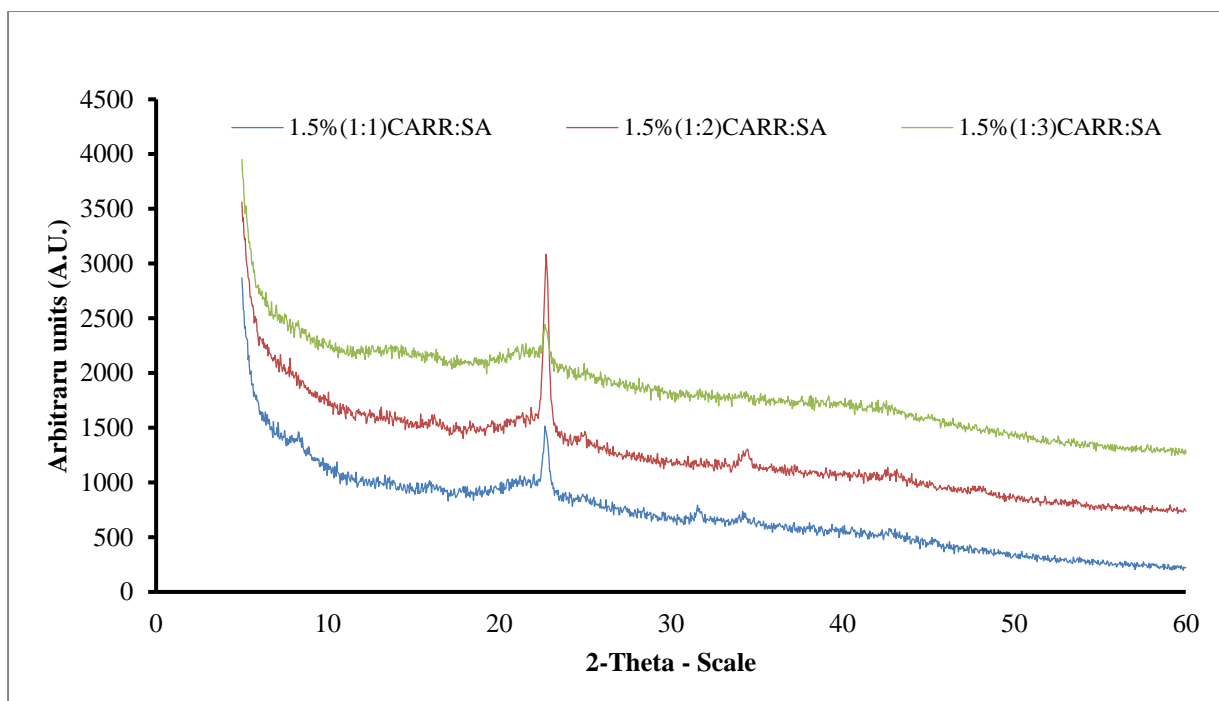


Figure A5.4. XRD diffractograms of 1.5%(1:1, 1:2 and 1:3) CARR:SA.

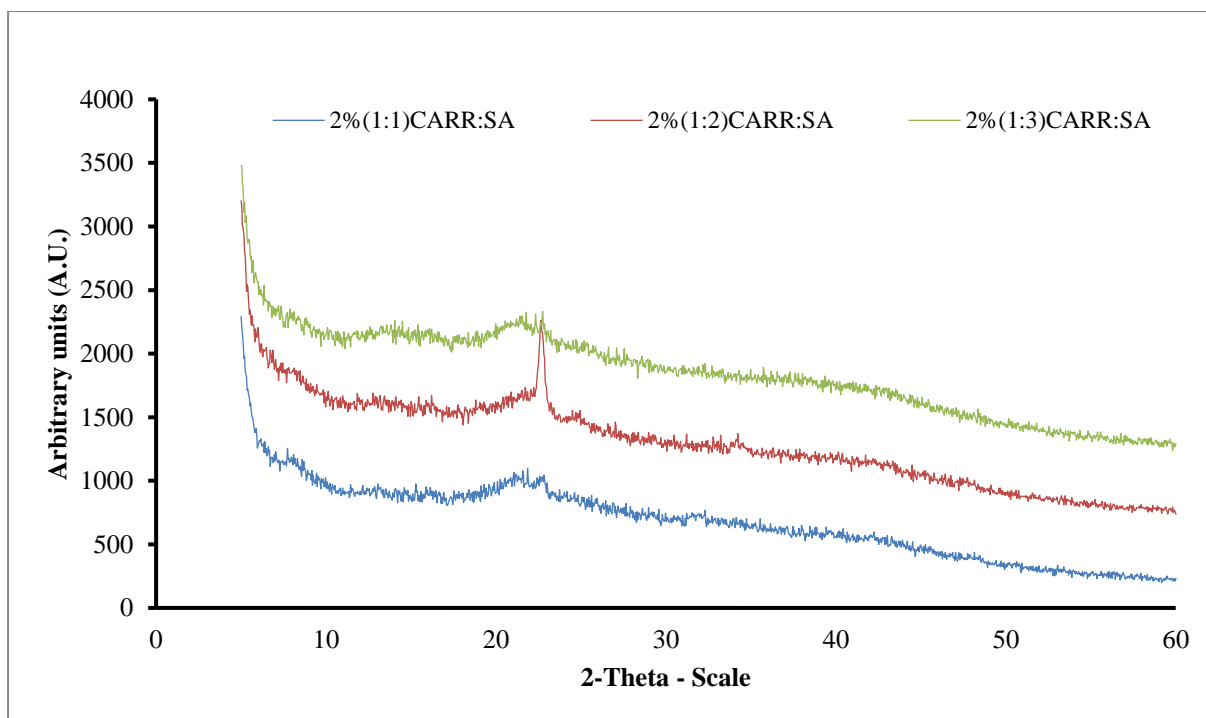


Figure A5.5. XRD diffractograms of 2%(1:1, 1:2 and 1:3) CARR:SA.

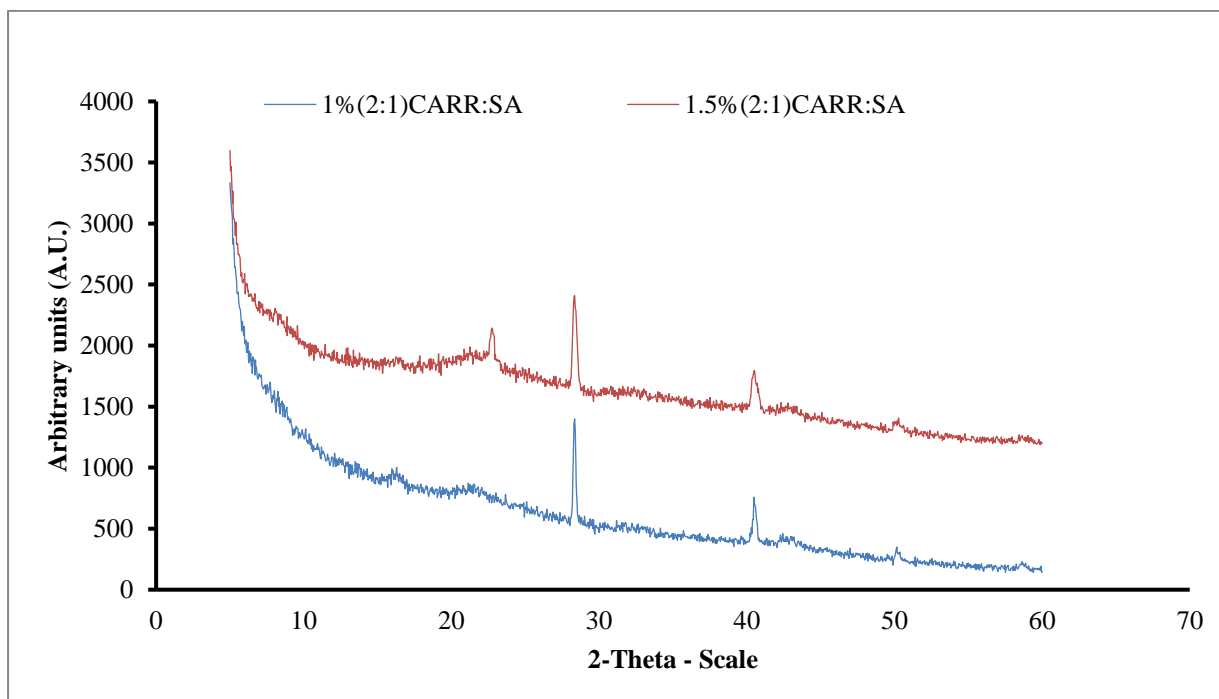


Figure A5.6. XRD diffractograms of 1%(2:1) and 1.5%(2:1) CARR:SA.

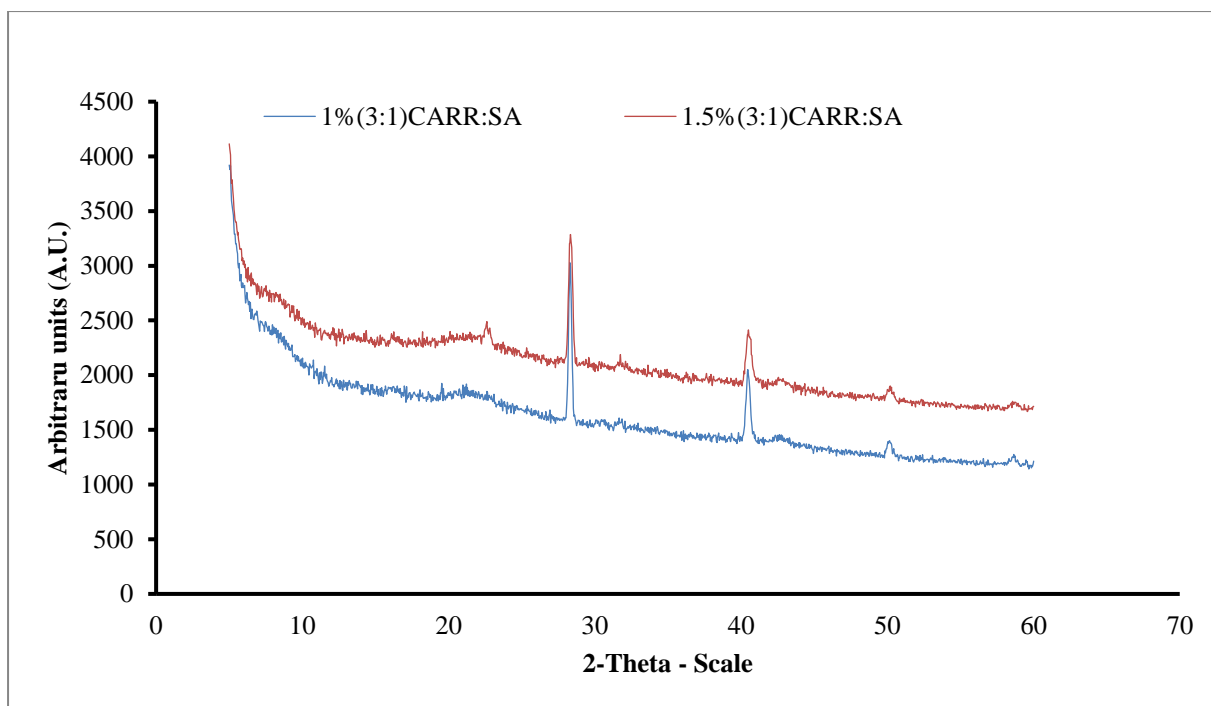


Figure A5.7. XRD diffractograms of 1%(3:1) and 1.5%(3:1) CARR:SA.

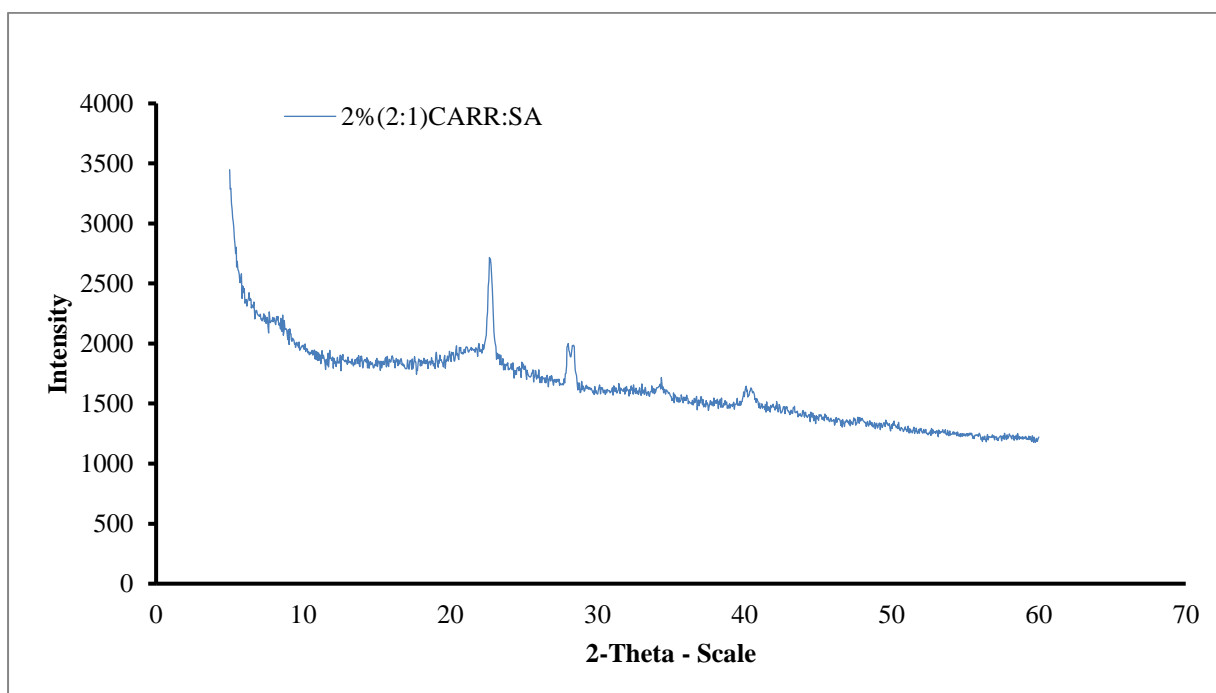


Figure A5.8. XRD diffractogram of 2%(2:1) CARR:SA.

Journal of Colloid and Interface Science 479 (2016) 221–233

Contents lists available at ScienceDirect



Journal of Colloid and Interface Science

journal homepage: www.elsevier.com/locate/jcis



Regular Article

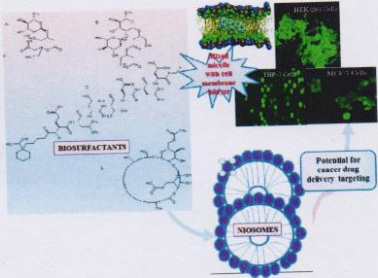
Systematic comparison of the functional physico-chemical characteristics and biocidal activity of microbial derived biosurfactants on blood-derived and breast cancer cells

Olufunke Akiyode, Daliya George, Giulia Getti, Joshua Boateng*

Faculty of Engineering and Science, University of Greenwich, Medway, Kent ME4 4TB, UK

 CrossMark

GRAPHICAL ABSTRACT



ARTICLE INFO

Article history:
 Received 13 May 2016
 Revised 12 June 2016
 Accepted 21 June 2016
 Available online 22 June 2016

Keywords:
 Biosurfactants
 Cancer chemotherapy
 Critical micelle concentration
 Cytotoxicity
 HEK 293
 MCF-7
 Rhamnolipid
 Sophorolipid
 Surfactin
 THP-1

ABSTRACT

Hypothesis: The cytotoxicity of biosurfactants on cell membranes may be influenced by composition of their hydrophilic head and hydrophobic tails. It is hypothesised that they form mixed micelles which exert a detergent-like effect that disrupts the plasma membrane. The functional physico-chemical and biocidal characteristics of four biosurfactants were concurrently investigated to determine which of their structural characteristics may be tuned for greater efficacy.

Experiments: Rhamnolipid-95, rhamnolipid-90, surfactin and sophorolipid were characterised using FTIR, LC-MS, HPLC, surface tension and critical micelle concentration. Their biocidal activity against HEK 293, MCF-7 and THP-1 cell lines were investigated by MTT assay, using doxorubicin as cytotoxic control. Growth curves were established for all cell lines using trypan blue (TB) and MTT assays, corresponding doubling time (DT) and growth rate were obtained and compared.

Findings: HEK 293 cell-line had the highest growth rate amongst the three cell lines. For TB assay, growth of HEK 293 > THP-1 and for MTT, HEK 293 > MCF-7 while the DT was in the order of THP-1 > MCF-7 > HEK 293. Sophorolipid showed anti-proliferative activity comparable to doxorubicin on THP-1 > MCF-7 > HEK 293. THP-1 showed high sensitivity to sophorolipid with IC_{50} of 10.50, 25.58 and 6.78 ($\mu\text{g/ml}$) after 24, 48 and 72 h respectively. However, sophorolipid was cytotoxic from 24 to 72 h on HEK 293 cell lines with IC_{50} of 21.53, 40.57 and 27.53 $\mu\text{g/ml}$ respectively. Although, doxorubicin showed higher anti-proliferative activity than all biosurfactants, it had poorer selectivity index for the same time durations

* Corresponding author.
 E-mail addresses: j.s.boateng@gre.ac.uk, joshboat40@gmail.com (J. Boateng).

<http://dx.doi.org/10.1016/j.jcis.2016.06.051>
 0021-9797/© 2016 Elsevier Inc. All rights reserved.

b. Conference abstracts and posters

TAT Conference Abstract

TARGETED CYTOTOXIC EFFECTS OF BIOSURFACTANTS IN BREAST AND BLOOD DERIVED CANCER CELLS

Olufunke Akiyode, Daliya George, Joshua Boateng, Giulia Getti

Faculty of Engineering and Science, University of Greenwich, Medway, Kent, UK
ME4 4TB

Introduction; Microbial biosurfactants (BSs) are amphiphilic compounds that exist as families of congeners and isomers identified as possible anti-cancer agents. The aim of this study is to investigate the anticancer activity of BSs on breast and blood derived cancers.

Materials and methods; Four biosurfactants (BSs) 95% rhamnolipid (BS1a), 90% rhamnolipid (BS1b), surfactin (BS2), sophorolipid (BS3) and a positive control Doxorubicin hydrochloride (DOX) were tested at concentrations ranging from 3.13-100µg/ml and 1.25-25µM for the BSs and DOX respectively. Cytotoxicity was obtained via MTT assay following cell line-specific optimization at intervals of 24, 48 and 72 hours from treatment on non-cancerous human embryo kidney (HEK293), human caucasian breast adenocarcinoma (MCF7) and human leukaemia monocyte (THP-1) cell lines.

Results; BS3 showed the greatest potency against all cell lines with IC₅₀ of 18, 16 and 15 µg/ml at 24, 48 and 72 hours respectively against THP-1 cells and IC₅₀ ranging between 20 and 30µg/ml against HEK293 and MCF7 after the same treatment times. The effect of BS2 and BS1b were variable with lower IC₅₀ in cancerous cell lines at late stages of treatment (68 and 18 µg/ml for MCF7 and THP-1 at 72 hours treatment) when compared with IC₅₀ of over 100µg/ml in HEK293. Finally BS1a showed no activity (IC₅₀>100µg/ml) against all cell lines tested independently from the incubation time used.

Conclusion; Although BS1a and BS1b have almost identical mass spectra, BS1b showed a higher amount of potency. BS2 and BS1b showed considerable potential as possible therapeutic agents in breast and blood derived cancer research. Future work will investigate identification of the specific congeners/isomers responsible for the observed activities.

Application of Biosurfactants in Cancer Therapy

Abstract code:P6.04

Olufunke Akiyode, Daliya George, Joshua Boateng, Giulia Getti

Faculty of Engineering and Science, University of Greenwich, Kent, UK, ME4 4TB

Corresponding author: ao37@gre.ac.uk



INTRODUCTION

Microbial biosurfactants (BSs) are amphiphilic compounds that exist as families of congeners and isomers identified as possible anti-cancer agents [1]. They exist as low and high molecular weight compounds which are sub-divided into glycolipids, lipopeptides, (fatty acids, phospholipids and neutral lipids) and polymeric biosurfactants) respectively.

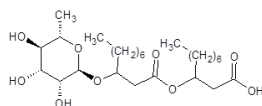


Fig 1. Glycolipid congener (Rha-C₁₆-C₁₆)

AIMS

The aim of this study is to investigate the anticancer activity of BSs on breast and blood derived cancers.

MATERIALS & METHODS

Biosurfactants were obtained from Sigma Aldrich and tested on three human cell lines: a non cancerogenic human embryo kidney (HEK293, ECACC 85120602), human caucasian breast adenocarcinoma (MCF7 ECACC number 86012803) and human leukemic monocyte (THP1, ECACC number 88081201). HEK293 and MCF7 were subcultured in Dulbecco's modified eagles medium (DMEM), while THP-1 was grown in RPMI 1640 medium respectively, supplemented with 10% heat inactivated foetal bovine serum and 1% penicillin/streptomycin.

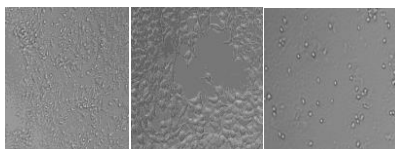


Fig 2. HEK293 cells Fig 3. MCF7 cells Fig 4. THP-1

Cytotoxicity was detected via MTT assay following cell line-specific optimisation. Briefly, HEK293 and MCF7 cells were plated at a concentration of 1x10⁶cells/well while THP-1 cells were seeded 5x10⁶cells/well and allowed to adhere for 24 hrs. Serial dilutions of each BSs was then applied and viability read at 24, 48, and 72 hrs.

CHARACTERISATION

Four biosurfactants (BSs) 95% rhamnolipid (BS1a), 90% rhamnolipid (BS1b), surfactin (BS2), sophorolipid (BS3) and a positive control doxorubicin hydrochloride (DOX) were tested against the cell lines at concentrations ranging from 3.13-100µg/ml and 1.25-25µM for the BSs and DOX respectively.

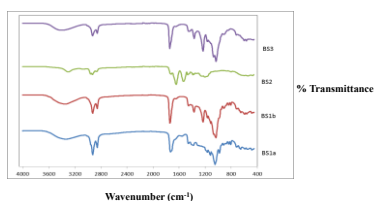


Fig 5. ATR-FTIR spectra of BS1a, BS1b, BS2 and BS3

RESULTS & DISCUSSION

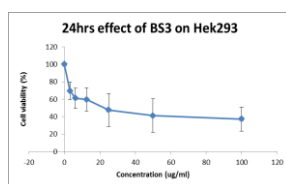


Fig 6. HEK293 cells starting concentration 1x10⁶cells/well

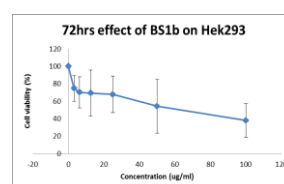


Fig 7. HEK293 cells starting concentration 1x10⁶cells/well

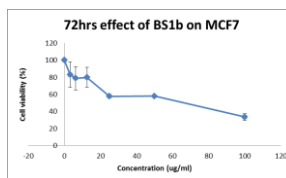


Fig 8. MCF7 cells starting concentration 1x10⁶cells/well

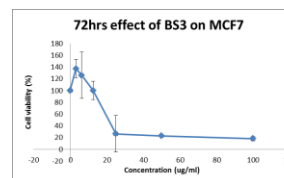


Fig 9. MCF7 cells starting concentration 1x10⁶cells/well

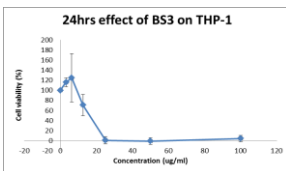


Fig 10. THP-1 cells starting concentration 5x10⁶cells/well

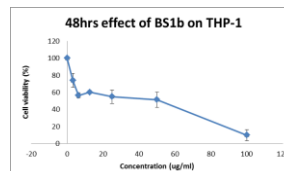


Fig 11. THP-1 cells starting concentration 5x10⁶cells/well

In contrast to previously reported data where BS3 was reported to have no activity on MCF7 [2], BS3 showed the highest potency against all cell lines with IC₅₀ of 18, 16 and 15 µg/ml at 24, 48 and 72 hrs respectively against THP-1 cells and IC₅₀ ranging between 20 and 30µg/ml against HEK293 and MCF7 after the same treatment times. A possible explanation of this apparent contradiction is that BS3 was synthesized and extracted with 3 types of extractants while that used for this study is a commercial standard. Additionally the presented testings has been carried out at a greater range of concentrations and intervals.

The effect of BS2 and BS1b were variable with lower IC₅₀ in cancerous cell lines at late stages of treatment (68 and 18 µg/ml for MCF7 and THP-1 at 72 hrs) when compared with IC₅₀ of over 100µg/ml in HEK293. Finally BS1a showed no activity (IC₅₀>100µg/ml) against all cell lines tested independently of the incubation time used.

CONCLUSIONS & FUTURE WORK

Although BS1a and BS1b have almost identical FTIR spectra, BS1b showed a higher level of potency. BS2 and BS1b showed considerable potential as possible therapeutic agents in breast and blood derived cancer research. Future work will investigate identification of the specific congeners/isomers responsible for the observed activities

REFERENCES

- [1] Gudina, E., Rangarajan, V., Sen, R. and Rodrigues, L. (2013). Potential therapeutic applications of biosurfactants. *Trends in Pharmaceutical Sciences* xxx:1-9.
- [2] Rashad, M., Nooman, M., Ali, M., Al-kashef, A. and Mahmoud, A. (2014). Production, characterization and anticancer activity of *Candida bombicola*sophorolipids by means of solid state fermentation of sunflower oil cake and soybean oil. *Grassay Acetes* 65(2).

Formulation and Functional Characterization of Lactonic Sophorolipid Biosurfactant and Span 60 Based Niosomes

O.A. Akiyode, G.G. Getti, D.A. George, J.S. Boateng*

Faculty of Engineering and Science, University of Greenwich, Medway, Kent, UK ME4 4TB.

j.s.boateng@gre.ac.uk

INTRODUCTION

Niosomes are drug delivery vesicles (nano – micro metre sized) composed mainly of hydrated non-ionic surfactants with or without cholesterol (CHL) or its derivatives. Microbial biosurfactants are amphiphilic compounds derived from microorganisms. Lactonic sophorolipids are glycolipid biosurfactants (BS) that exist as a result of an internal esterification of a carboxylic acid group to a lactone ring. Sophorolipids have been formulated into microemulsions, micelles and nanoparticles [1], however, their formulation in niosomes combined with span 60 (S60) is a novel concept.

MATERIALS AND METHODS

Niosome vesicles were prepared from sophorolipid BS, S60, and their mixtures with and without CHL in different molar ratios (table 1), in the presence of 8.2 mg dicetyl phosphate (DCP) using the thin film hydration method [2]. Hydration time of the surfactant lipid film varied from 45 – 60 mins. The vesicles formed were subjected to sonication from 3-40 mins. The resulting niosomes were characterized using dynamic-light scattering (DLS), (ATR-FTIR) and scanning electron microscopy in transmission mode (STEM). The effect of BS:S60:CHL ratios, hydration and sonication times on vesicle formation was investigated.

RESULTS AND DISCUSSION

All BS incorporated niosomes appear to have a high polydispersity index (PDI) of > 0.6 compared to the S60 only vesicles. This could be the result of the temperature at which hydration was carried out (60°C). S60 has a transition temperature of 53°C, and it's reported that sophorolipids melt at 123°C and undergo glass transition at 61°C [1]. It is therefore possible that preparation temperature affects the PDI and particle size in general.

Table 1 DLS Characterisation of niosomal dispersions.

Formulation	Molar ratio	Particle size (d.nm)	PDI	Zeta potential (mV)
BS:S60:CHL	0:1:0	701	0.55	-26
BS:S60:CHL	0:1:1	1170	0.33	-62
BS:S60:CHL	0:1:2	1195	0.25	-66
BS:S60:CHL	0.75:0.25:0	2071	1.00	-35
BS:S60:CHL	0.75:0.25:1	670	0.78	-1
BS:S60:CHL	0.75:0.25:2	1853	0.82	-59
BS:S60:CHL	0:50:0.50:0	968	0.68	-41
BS:S60:CHL	0:50:0.50:1	2083	1.00	-48
BS:S60:CHL	0:50:0.50:2	1566	0.66	-54

For example, it has been reported that particle size of sophorolipids used as capping agents for cobalt nanoparticles decreased with increasing temperature and longer time is needed at lower temperatures to obtain complete particle formation and growth [3]. Particle size of sonicated niosomes was reduced from 2083 to 670 nm and STEM study showed spherical and closed vesicular structure in the size range 805 to 4230 nm (Fig 1). The characteristic ATR-FTIR peaks of BS, S60 and DCP were completely masked by water hydrated in the niosomes as a result of their low concentrations or complete absence due to their encapsulation to form niosomes.

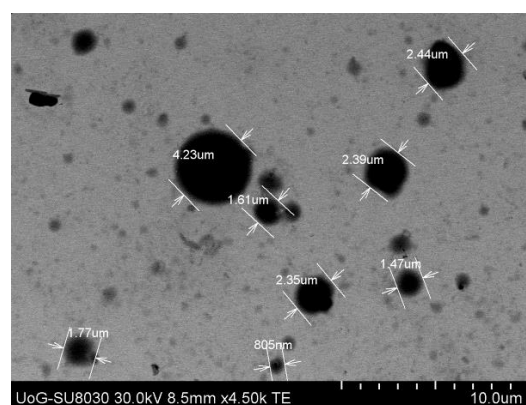


Fig. 1. Representative STEM image of BS:S60:CHL in 0.75:0.25:1 formulation, 60 mins hydration and 3 mins sonication.

CONCLUSIONS

BS and S60 show great potential for use in niosome delivery systems. Future work will involve optimizing the formulation to obtain a monodisperse formulation before cell testing for biological activity.

REFERENCES

- [1]. E. Delbeke, M. Movsisyan, K. Geem, and C. Stevens. "Chemical and enzymatic modification of sophorolipids" *Green Chem.*, **18** (2016) 76.
- [2]. P. Balakrishnan, A. Shanmugam, W. Seok Lee, W. Mo Lee, J. Oh Kim, D. Hoon Oh, D. Kim, J. Kim, B. Kyu Yoo, H. Choi, J. Soo Woo and C. Soon Yong. "Formulation and in vitro assessment of minoxidil niosomes for enhanced skin delivery particles for inhalation" *Int. J. Pharm.*, **377** (2008) 1 – 8.
- [3]. M. Kasture, S. Singh, P. Patel, P. Joy, A. Prabhune, C. Ramana, C. Ramana, and B. Prasad, "Multi-utility sophorolipids as nanoparticle capping agents: synthesis of stable and water dispersible Co nanoparticles" *Langmuir.*, **23** (2007) 11409-11412.

INTRODUCTION

Niosomes are drug delivery vesicles (nano – micro metre sized) composed mainly of hydrated non-ionic surfactants with or without cholesterol (CHL) or its derivatives [1]. Microbial biosurfactants are amphiphilic compounds derived from microorganisms. Lactonic sophorolipids are glycolipid biosurfactants (BS) that exist as a result of an internal esterification of a carboxylic acid group to a lactone ring. Sophorolipids have been formulated into microemulsions, micelles and nanoparticles [2], however, their formulation in niosomes combined with span 60 (S60) is a novel concept.

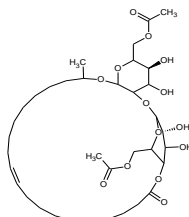


Figure 1. Chemical structure of sophorolipid (BS).

MATERIALS & METHODS

Niosome vesicles were prepared from BS, S60, and their mixtures with and without CHL in different molar ratios (Table 1), in the presence of 8.2 mg dicetyl phosphate (DCP) using the thin film hydration method (Fig 2) [3]. Hydration time of the surfactant lipid film varied from 45 – 60 mins.

The vesicles formed were subjected to sonication from 3-40 mins. The resulting niosomes were characterised using dynamic-light scattering (DLS), ATR-FTIR and scanning electron microscopy in transmission mode (STEM). The effect of BS:S60:CHL ratios, hydration and sonication times on vesicle formation was investigated.

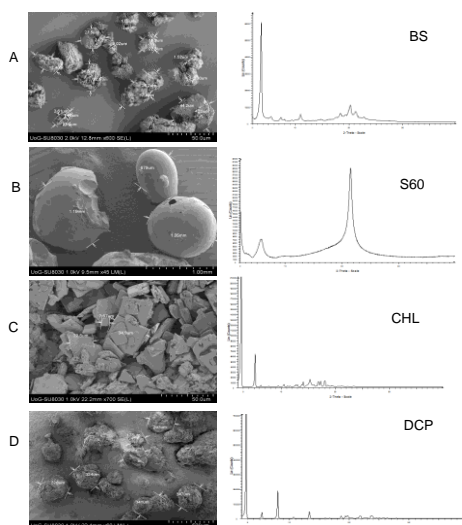


Figure 2. SEM and corresponding XRD diffractograms of pure: (A) sophorolipids, (B) Span 60, (C) cholesterol, (D) dicetyl phosphate

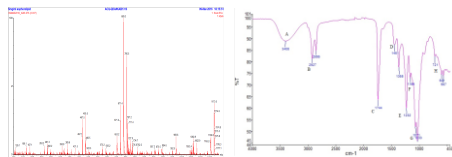


Figure 3. Representative LCMS and ATR-FTIR profiles of pure sophorolipid.

ACKNOWLEDGEMENTS

The authors are grateful to Mr Andrew Hurt for his help with STEM, SEM and XRD analysis, Dr Cris Laphom and Dr Iain Goodall for their help with LC-MS analysis

RESULTS & DISCUSSION

S60 has a transition temperature of 53° C, and it's reported that BS melt at 123° C and undergo glass transition at 61° C [2]. It is therefore possible that preparation temperature affects the polydispersity index (PDI) and particle size in general. For example, it has been reported that particle size of BS used as capping agents for cobalt nanoparticles decreased with increasing temperature [4]. Therefore the effect of temperature was investigated at 60, 70 and 80° C. Niosomes formed at the higher temperature were observed to predominantly have reduced size as well as possessed a lower polydispersity index (PDI) compared to those formed at a lower temperature. All niosomal dispersions had a milky appearance with those containing cholesterol exhibiting more turbidity. Particle size of sonicated niosomes was reduced from 2083 to 670 nm and STEM study showed spherical and closed vesicular structure in the size range 805 to 4230 nm. XRD diffractograms show that higher amounts of CHL and absence of DCP increases the amorphous nature of formulations (Figs 5A and 5B).

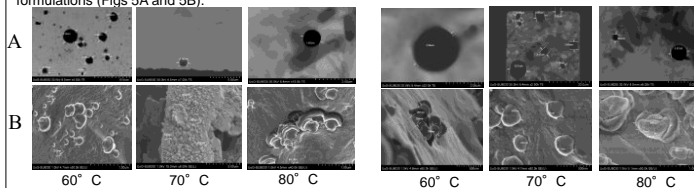


Figure 4. Representative (A) STEM of niosomal dispersions and (B) corresponding SEM of freeze dried BS:S60:CHL in 0.75:0.25:1 and 0:1:1 formulations with 60 mins hydration and 3 mins sonication.

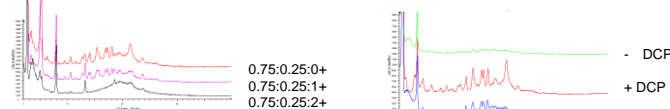


Figure 5 XRD diffractograms showing (A) effect of cholesterol on BS:S60 in 0.75:0.25:1 formulation at 60° C and (B) effect of DCP on BS:S60:CHL in 0.75:0.25:1 formulation at 70° C.

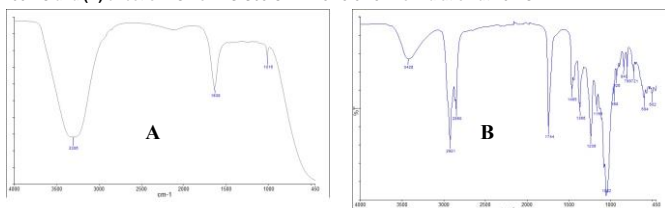


Figure 6 ATR-FTIR spectra of (A) BS:S60 in 0.75:0.25:1 niosomal dispersion formulation at 60° C; and (B) freeze dried niosomes. The characteristic ATR-FTIR peaks of BS, S60 and DCP were completely masked by water hydrated in the niosomes as a result of their low concentrations or complete absence due to their encapsulation to form niosomes but some peaks were visible after freeze drying.

Table 1 DLS Characterisation of niosomal dispersions.

Formulation	Molar ratio	Particle size (d, nm)	PDI	Zeta Potential (mV)
BS:S60:CHL	0:1:0	701	0.55	-26
BS:S60:CHL	0:1:1	1170	0.33	-62
BS:S60:CHL	0:1:2	1195	0.25	-66
BS:S60:CHL	0.75:0.25:0	2071	1.00	-35
BS:S60:CHL	0.75:0.25:1	670	0.78	-1
BS:S60:CHL	0.75:0.25:2	1853	0.82	-59
BS:S60:CHL	0:50:0.50:0	968	0.68	-41
BS:S60:CHL	0:50:0.50:1	2083	1.00	-48
BS:S60:CHL	0:50:0.50:2	1566	0.66	-54

Table 2 pH of selected 4 final formulations

Temp (°C)	0:1:1	0.75:0.25:1	0:50:0.50:1	1:0:0
60	5.1	4.3	4.3	4.1
70	4.9	4.1	4.2	4.3
80	4.0	3.4	3.4	3.8

CONCLUSIONS & FUTURE WORK

BS and S60 show great potential for use in niosome delivery systems. Future work will involve optimising the formulation to obtain a monodisperse formulation and cell testing for biological activity.

REFERENCES

[1]. I. Uchegbu, and S. Vyas. "Non-ionic surfactant based (niosomes) in drug delivery" *Int. J. Pharm.*, **172** (1998) 33 – 70.
 [2]. E. Delbeke, M. Movsisyan, K. Geem, and C. Stevens. "Chemical and enzymatic modification of sophorolipids" *Green Chem.*, **18** (2016) 76.
 [3]. P. Balakrishnan, A. Shanmugam, W. Seok Lee, W. Mo Lee, J. Oh Kim, D. Hoon Oh, D. Kim, J. Kim, B. Kyu Yoo, H. Choi, J. Soo Woo, and C. Soon Yong. "Formulation and in vitro assessment of minoxidil niosomes for enhanced skin delivery particles for inhalation" *Int. J. Pharm.*, **377** (2008) 1 – 8.
 [4]. M. Kasture, S. Singh, P. Patel, P. Joy, A. Prabhune, C. Ramana, C. Ramana, and B. Prasad. "Multi-utility sophorolipids as nanoparticle capping agents: synthesis of stable and water dispersible Co nanoparticles" *Langmuir*, **23** (2007) 11409-11412.